

Università degli Studi di Napoli Federico II

Dottorato di Ricerca in Ingegneria Strutturale, Geotecnica e Rischio Sismico

THESIS FOR THE DEGREE OF DOCTOR OF PHILOSOPHY

Performance-based approach for bridges fire fragility assessment

by

Marco Gallo

Advisor: Prof. Emidio Nigro

Co-advisor: Dr. Donatella de Silva

2024



SCUOLA POLITECNICA E DELLE SCIENZE DI BASE

DIPARTIMENTO D STRUTTURE PER L'INGEGNERIA E L'ARCHITETTURA

A Massimo,

Con la Speranza che, nel posto in cui ti trovi adesso,

tu stia vivendo la felicità

che non hai potuto vivere nel posto in cui mi trovo io



Performance-based approach for bridges fire fragility assessment

Ph.D. Thesis presented

for the fulfillment of the Degree of Doctor of Philosophy in Ingegneria Strutturale, Geotecnica e Rischio Sismico

by

Marco Gallo

October 2024



Approved as to style and content by	y
-------------------------------------	---

Drof Emidia Niana Advisor

Prof. Emidio Nigro, Advisor

Dr. Donatella de Silva, Co-advisor

Università degli Studi di Napoli Federico II

Ph.D. Program in Ingegneria Strutturale, Geotecnica e Rischio Sismico XXXVI cycle - Chairman: Prof. Iunio Iervolino



www.dist.unina.it/dottorati-di-ricerca/dottorati

Candidate's declaration

I hereby declare that this thesis submitted to obtain the academic degree of Philosophiæ Doctor (Ph.D.) in Ingegneria Strutturale, Geotecnica e Rischio Sismico is my own unaided work, that have not used other than the sources indicated, and that all direct and indirect sources are acknowledged as references.

Parts of this dissertation have been published in international journals and/or conference proceedings (see list of the author's publications at the end of the thesis).

Napoli, October 1, 2024

Margall

Marco Gallo

Abstract

This Ph.D. thesis, starting from an in-depth study of the scientific literature on fire engineering, proposes a methodological evolution in the field of performance approach for the assessment of fire vulnerability of infrastructure such as bridges and viaducts and subsequent retrofit.

Criteria for assessing vulnerability to thermal and mechanical actions induced by fire events are standardized only in the case of buildings with specific uses. In addition, prescriptions are often lacking in performance-based approach, preferring verifications in prescriptive approach, which is easier to apply and provides conservative results. In the case of infrastructures, on the other hand, such criteria are not explicitly defined by the relevant technical standards although experience shows how the action due to fire can have impactful consequences on the functionality of the infrastructure. Referring to the relevant technical literature, one methodology was proposed by Kodur, that prescribes the performance criteria of infrastructures according to their "level of importance".

This thesis work extends the definition of the criteria by proposing four performance levels that the viaduct must satisfy according to its level of importance. The proposed approach aims at the utilization of Fire-Safety Engineering (FSE) principles by highlighting how this approach, although a higher computational burden, provides non-negligible performance differences. Finally, fragility curves are provided, using the Cloud linear regression method, based on different fire scenarios whose temperature curves were evaluated through a CFD analysis, for two levels of performance varying the static scheme and the initial utilization factor.

Keywords: Fire Engineering, Thermo-mechanical Analysis, CFD Analysis, Fire Vulnerability, Infrastructures, Fragility Curves.

Sintesi in lingua italiana

La presente tesi di Dottorato, a partire da un approfondito studio della letteratura scientifica in materia di ingegneria del fuoco, propone una evoluzione metodologica nel campo dell'approccio prestazionale per la valutazione di vulnerabilità al fuoco e di opere infrastrutturali quali ponti e viadotti e conseguente retrofit. I criteri di valutazione della vulnerabilità nei confronti delle azioni termiche e meccaniche indotte dagli eventi di incendio sono normati solo nel caso di edifici con specifiche destinazioni d'uso. Inoltre, le prescrizioni sono spesso carenti per quanto concerne l'approccio prestazionale, prediligendo verifiche in approccio prescrittivo, che risulta di più semplice applicabilità e fornisce risultati anche conservativi. Nel caso delle infrastrutture, però, tali criteri non sono espressamente definiti dalle norme tecniche di settore sebbene l'esperienza passata dimostri come l'azione dovuta all'incendio possa avere conseguenze impattanti sulla funzionalità delle opere. Rifacendosi alla letteratura tecnica in materia si possono trovare delle metodologie proposte, soprattutto dal Kodur, che prescrivono i criteri prestazionali di una infrastruttura in funzione del suo "livello di importanza". Il lavoro di tesi estende la definizione dei criteri proponendo quattro livelli di prestazione che il viadotto dovrà soddisfare in funzione del proprio livello di importanza. L'approccio proposto mira all'utilizzazione dei principi della Fire Safety Engineering (FSE), mettendo, tra l'altro, in evidenza come tale approccio, a fronte di un onere computazionale maggiore, fornisce differenze di performance non trascurabili. Infine, sono fornite le curve di fragilità, con il metodo Cloud, sulla base di diversi scenari di incendio le cui curve di temperature sono state valutate con un'analisi CFD, per due livelli di prestazione al variare dello schema statico e del fattore di utilizzazione iniziale.

Parole chiave: Ingegneria antincendio, Analisi termo-meccaniche, Analisi termo-fluido-dinamica, Vulnerabilità al fuoco, Infrastrutture, Curve di fragilità.

Contents

Abs	stract	
Sint	tesi in lingua italiana	i
Con	ntents	ii
List	of Acronyms	vii
List	of Figures	X
List	of Tables	xxi
List	of Symbols	XXV
1	Introduction	1
1.1	Fire events in transport infrastructures	1
1.2	Bridges performance in case of fire	6
1.3	Thesis objectives	9
2	Assessment of structural vulnerability in case of fire	12
2.1	Design and vulnerability assessment approaches in case of fire	14
2.2	Materials behaviour in fire conditions	15

	2.2.1	Mechanical properties				
	2.2.2	Thermal properties				
2.3	Fire m	odelling				
	2.3.1	Nominal fire curves				
	2.3.2	Parametric fire curves				
	2.3.3	Natural fire curves, CFD method				
2.4	Therm	al analysis				
	2.4.1	Theoretical background				
	2.4.2	FE method				
2.5	5 Verification approach					
2.6	Mecha	Mechanical analysis for bridges in fire				
2.7	State o	te of the art for Structural fire design and assessment of bridges				
2.8	Fire fra	agility assessment: literature review				
2.9	Propos	ed approach				
3	Fire risk	c assessment of bridges: parametric advanced analysis and vulnerability mitigation	ı.			
3.1		sk assessment of bridge infrastructures				
3.2	Fire de	esign and safety check of bridges				
3.3	Advanced fire safety check – parametric analysis					
	3.3.1	Prescriptive-based approach				
	3.3.2	Performance-based approach				
3.4	Design	of fire vulnerability mitigation				
3.5	Results	s comparison and discussion				

3.6	Evoluti	on of performance level for bridges
4	Steel bri	dges fire fragility91
4.1	Case str	ady: modelling and validation
	4.1.1	Description
	4.1.2	Gravity load assessment
	4.1.3	Structural modelling and validation
	4.1.4	Verification
4.2	Fire sce	enarios
	4.2.1	Definition of Heat Release Rate curves
	4.2.2	CFD analyses
4.3	Thermo	-mechanical analyses
	4.3.1	Thermal analyses
	4.3.2	Mechanical analyses
4.4	Develo	oment of fragility curves
	4.4.1	Linear regression Cloud Procedure
	4.4.2	Fragility curves
5	Conclusi	ons
6	Bibliogra	aphy
Autl	nor's publ	ications
App	endix A –	Procedure for resistance and buckling domain in cold and fire conditions evaluation
App	endix B –	CFD analyses results
App	endix C –	Fragility curves

ppendix D –Structural mode	l code	. 19)(
----------------------------	--------	------	----



List of Acronyms

The following acronyms are used throughout the thesis.

EEC European Economic Community

PA Prescriptive approach

PBA Performance-based approach

IF Importance Factor

PL Performance level

CFD Computational fluid dynamic



List of Figures

Figure 1.1. Fire event on "Ponte di Ferro" in Rome, Italy, 2021 [4]2
Figure 1.2. Massive fire causing collapse of an overpass on Interstate 85 in Atlanta, US, 2017 [5]
Figure 1.3. I95 collapse in Philadelphia after tanker fire, US, 2023 [6]3
Figure 1.4. Massive fire ignited from train derailment in Arizona [7]4
Figure 1.5. Piazza Ottocalli in Naples, revisited from [8]
Figure 2.1. Safety in case of fire according to Directive 89/106/EEC [11]13
Figure 2.2. Stress-strain relationship for carbon steel at elevated temperature [13]16
Figure 2.3. Reduction factors for the stress-strain relationship of carbon steel at elevated temperature
Figure 2.4. Stress-strain relationship for concrete a elevated temperature [12]18
Figure 2.5. Reduction factor for the stress-strain relationship of concrete at elevated temperature
Figure 2.6. Specific heat of a carbon steel as a function of the temperature [13]20
Figure 2.7. Thermal conductivity of carbon steel as a function of the temperature [13]
Figure 2.8. Specific heat, $c_p(\theta)$, by weight for siliceous concrete [12]22
Figure 2.9. Thermal conductivity of concrete as a function of the temperature [12]
Figure 2.10. Fire event phases scheme [11]
Figure 2.11 Nominal fire curves 25

Figure 2.12. Comparison between ISO834 and parametric fire curve	.27
Figure 2.13. Cross-section of the bridge [16]	.37
Figure 2.14. Temperatures in cross-section for t=7200s	.38
Figure 2.15. Lower bulb temperatures for t=7200s	.38
Figure 2.16. Key characteristics affecting fire risk in a bridge	. 44
Figure 2.17. Steps of the proposed approach for mitigating fire hazard in bridges	3 47
Figure 3.1. Key features influencing fire risk in bridges [25]	.56
Figure 3.2. 3D model used for a thermal analysis	.61
Figure 3.3. Comparison between the temperatures from SAFIR and from experimental test	
Figure 3.4. Cross-section of a typological steel-concrete fully composite bridge.	. 62
Figure 3.5. Temperature in the steel profile under hydrocarbon fire	. 62
Figure 3.6. Temperature in the steel profile under hydrocarbon fire	.63
Figure 3.7. Bending moment under hydrocarbon fire systems 1 and 2	. 64
Figure 3.8. Bending moment under hydrocarbon fire systems 3a and 3b	.65
Figure 3.9. Displacement in the four systems under hydrocarbon fire	.65
Figure 3.10. (a) FDS model (b) CFAST model	. 68
Figure 3.11. HRR curve of a bus	. 68
Figure 3.12. Comparison between average temperatures in FDS and CFAST	. 69
Figure 3.13. HRR curve of the five vehicles	.71
Figure 3.14. (a) Thermo-couples layout (b) discretization in 10 zones	.72
Figure 3.15. Temperatures recorded by ten thermocouples in Scenario 1	.73
Figure 3.16. Maximum temperature in the steel profile in the five scenarios	74

Figure 3.17. Temperatures in the steel profile (Scenario 1 – zone 5)
Figure 3.18. maximum deflection Scenario 1
Figure 3.19. Bending moment Scenario 1
Figure 3.20. maximum deflection Scenario 3
Figure 3.21. Bending moment Scenario 3
Figure 3.22. Nomogram for Hydrocarbon fire curve
Figure 3.23. Temperature in the steel profile with 8mm SFRM under hydrocarbor fire
Figure 3.24. Temperature in the steel profile with 16mm SFRM under hydrocarbor fire
Figure 3.25. Maximum deflection in the considered structural schemes under hydrocarbon fire
Figure 3.26. Temperatures in the steel profile protected with 16mm of SFRM (S.1 - Zone 5)
Figure 3.27. Deflection of protected an unprotected beam (Scenario 1)84
Figure 4.1. Flowchart of structural-fire fragility curve development
Figure 4.2. W36x300 Cross-section geometric properties
Figure 4.3. Bridge Cross-Section, adapted from [52]
Figure 4.4. Gap restraint model: (a) at rest; (b) partially opened; (c) fully closed .95
Figure 4.5. Node-line definition in SAFIR software
Figure 4.6. Girder shell model, barycentric restraints
Figure 4.7. Barycentric bearings (a) Vertical displacement; (b) Stress in shel

Figure 4.8. Eccentric bearings (a) Vertical displacement; (b) Stress in shell elements
Figure 4.9. SAFIR results in terms of displacement for t=1s98
Figure 4.10. SAFIR results in terms of bending moment for t=1s98
Figure 4.11. Color map of temperatures in cross-section for t=660s99
Figure 4.12. Comparison between fire curve and temperature in different part of cross-section
Figure 4.13. Horizontal support displacement and Middle span vertical displacement
Figure 4.14. Truss axial force
Figure 4.15. Cold and fire conditions resistance and buckling domain
Figure 4.16. HRR Curves for selected scenarios
Figure 4.17. Viaduct CFD model
Figure 4.18. Fire scenario S1-1
Figure 4.19. Temperatures recorded in thermocouples for each fire scenario 107
Figure 4.20. Comparison between the THCP1 temperatures in each scenario 108
Figure 4.21. Cross-section color map temperature Scenario S1-1 for t=900s and web temperatures vs time
Figure 4.22. Cross-section color map temperature Scenario S1-2 for t=900s and web temperatures vs time
Figure 4.23. Cross-section color map temperature Scenario S1-3 for t=900s and web temperatures vs time
Figure 4.24. Cross-section color map temperature Scenario S1-4 for t=900s and web

Figure 4.25. Cross-section color map temperature Scenario S1-5 for t=900s and web
temperatures vs time
Figure 4.26. Cross-section color map temperature Scenario S2-1 for t=3000s and
web temperatures vs time
Figure 4.27. Cross-section color map temperature Scenario S2-2 for t=3000s and
web temperatures vs time
Figure 4.28. Cross-section color map temperature Scenario S2-3 for t=3000s and
web temperatures vs time
Figure 4.29. Cross-section color map temperature Scenario S3-1 for t=1500s and
web temperatures vs time
Figure 4.30. Cross-section color map temperature Scenario S3-2 for t=1800s and
web temperatures vs time
Figure 4.31. Cross-section color map temperature Scenario S4 for t=2400s and web
temperatures vs time
Figure 4.32. Cross-section color map temperature Scenario S5-1 for t=1800s and
web temperatures vs time
Figure 4.33. Cross-section color map temperature Scenario S5-2 for t=1800s and
web temperatures vs time
Figure 4.34. Cross-section color map temperature Scenario S6 for t=1500s and web
temperatures vs time
Figure 4.35. Temperature comparison for each fire scenario
Figure 4.36. Linear regression for PLIII and PLIV in terms of HRR peak and Q in
case of simply-supported beams and μ_0 =0.28
Figure 4.37. Linear regression for PLIII and PLIV in terms of HRR peak and Q in
case of simply supported beams and u ₀ =0.42

Figure 4.38. Linear regression for PLIII and PLIV in terms of HRR peak and Q in case of simply supported beams and μ_0 =0.56
Figure 4.39. Linear regression for PLIII and PLIV in terms of HRR peak and Q in case of simply-supported beams and μ_0 =0.28 – Maximum and residual displacement
Figure 4.40. Linear regression for PLIII and PLIV in terms of HRR peak and Q in case of simply-supported beams and μ_0 =0.42 – Maximum and residual displacement
Figure 4.41. Linear regression for PLIII and PLIV in terms of HRR peak and Q in case of simply-supported beams and μ_0 =0.56 – Maximum and residual displacement
Figure 4.42. Linear regression for PLIV in terms of HRR peak and Q in case of hyperstatic beams and μ_0 =0.28
Figure 4.43. Linear regression for PLIV in terms of HRR peak and Q in case of hyperstatic beams and μ_0 =0.42
Figure 4.44. Linear regression for PLIV in terms of HRR peak and Q in case of hyperstatic beams and μ_0 =0.56
Figure 4.45. Comparison between fragility curves built for simply supported beam and PLIII verification, maximum displacement as a function of HRR peak.
Figure 4.46. Comparison between fragility curves built for simply supported beam and PLIII verification, maximum displacement as a function of Q132
Figure 4.47. Comparison between fragility curves built for simply supported beam and PLIV verification, maximum displacement as a function of HRR peak.

Figure 4.48. Comparison between fragility curves built for simply supported beam and PLIV verification, maximum displacement as a function of Q
Figure 4.49. Comparison between fragility curves built for simply supported beam and PLIII verification, maximum and residual displacement as a function of HRR peak.
Figure 4.50. Comparison between fragility curves built for simply supported beam and PLIII verification, maximum and residual displacement as a function of Q
Figure 4.51. Comparison between fragility curves built for simply supported beam and PLIV verification, maximum and residual displacement as a function of HRR peak.
Figure 4.52. Comparison between fragility curves built for simply supported beam and PLIV verification, maximum and residual displacement as a function of Q
Figure 4.53. Comparison between fragility curves built for hyperstatic beam and PLIII verification, maximum and residual displacement and compressive verification of bottom flange at support as a function of HRR peak136
Figure 4.54. Comparison between fragility curves built for hyperstatic beam and PLIII verification, maximum and residual displacement and compressive verification of bottom flange at support as a function of Q
Figure 4.55. Comparison between fragility curves built for hyperstatic beam and PLIV verification, maximum and residual displacement and compressive verification of bottom flange at support as a function of HRR peak137
Figure 4.56. Comparison between fragility curves built for hyperstatic beam and PLIV verification, maximum and residual displacement and compressive verification of bottom flange at support as a function of Q

Figure 4.57. Comparison between fragility curves built for PLIII verification,
maximum and residual displacement and compressive verification of bottom
flange at support as a function of HRR (MW) varying the static scheme 139
Figure 4.58. Comparison between fragility curves built for PLIV verification,
maximum and residual displacement and compressive verification of bottom
flange at support as a function of HRR (MW) varying the static scheme 139
Figure 4.59. Comparison between fragility curves built for PLIII and PLIV
verification, maximum displacement in Case 1 as a function of HRR (MW)
140
Figure 4.60. Comparison between fragility curves built for PLIII and PLIV
verification, maximum and residual displacement in Case 2 as a function of
HRR (MW)140
Figure 4.61. Comparison between fragility curves built for PLIII and PLIV
verification, maximum and residual displacement and compressive
verification of bottom flange at support in Case 3 as a function of HRR (MW)
141
Figure C.1. Fragility curve for PLIII for HRR $-\mu_0$ =0.28 $-$ Simply-supported 178
Figure C.2. Fragility curve for PLIII for $Q - \mu_0 = 0.28$ – Simply-supported 178
Figure C.3. Fragility curve for PLIV for HRR– μ_0 =0.28 – Simply-supported 179
Figure C.4. Fragility curve for PLIV for Q $-\mu_0$ =0.28 $-$ Simply-supported 179
Figure C.5. Fragility curve for PLIII for HRR– μ_0 =0.42 – Simply-supported 180
Figure C.6. Fragility curve for PLIII for Q $-\mu_0$ =0.42 $-$ Simply-supported180
Figure C.7. Fragility curve for PLIV for HRR $-\mu_0$ =0.42 $-$ Simply-supported 181
Figure C.8. Fragility curve for PLIV for Q $-\mu_0$ =0.42 $-$ Simply-supported181
Figure C.9. Fragility curve for PLIII for HRR $-\mu_0$ =0.56 $-$ Simply-supported 182

Figure C.10. Fragility curve for PLIII for Q $-\mu_0\!\!=\!\!0.56-Simply\!$ -supported 182
Figure C.11. Fragility curve for PLIV for HRR $-\mu_0 = 0.56 - Simply\text{-supported}183$
Figure C.12. Fragility curve for PLIV for Q $-\mu_0\!\!=\!\!0.56$ – Simply-supported183
Figure C.13. Fragility curve for PLIII for HRR $-\mu_0\!\!=\!\!0.28$ – Simply-supported184
Figure C.14. Fragility curve for PLIII for Q $-\mu_0$ = 0.28 $-$ Simply-supported 184
Figure C.15. Fragility curve for PLIV for HRR $-\mu_0 = 0.28$ – Simply-supported 185
Figure C.16. Fragility curve for PLIV for Q $-\mu_0\!\!=\!\!0.28$ – Simply-supported185
Figure C.17. Fragility curve for PLIII for HRR $-\mu_0 = 0.42 - Simply-supported$ 186
Figure C.18. Fragility curve for PLIII for Q $-\mu_0$ = 0.42 $-$ Simply-supported186
Figure C.19. Fragility curve for PLIV for HRR $-\mu_0 \!\!=\!\! 0.42 - Simply-supported$ 187
Figure C.20. Fragility curve for PLIV for Q $-\mu_0\!\!=\!\!0.42$ – Simply-supported 187
Figure C.21. Fragility curve for PLIII for HRR $-\mu_0 = 0.56 - Simply-supported$ 188
Figure C.22. Fragility curve for PLIII for Q $ \mu_0\text{=}0.56$ $-$ Simply-supported 188
Figure C.23. Fragility curve for PLIV for HRR $-\mu_0 \!\!=\!\! 0.56 - Simply\text{-supported} 189$
Figure C.24. Fragility curve for PLIV for Q $-\mu_0\!\!=\!\!0.56$ – Simply-supported189
Figure C.25. Fragility curve for PLIII for HRR $-\mu_0\!\!=\!\!0.28$ – Hyperstatic190
Figure C.26. Fragility curve for PLIII for Q $-\mu_0$ =0.28 $-$ Hyperstatic190
Figure C.27. Fragility curve for PLIV for HRR $-\mu_0$ = 0.28 $-$ Hyperstatic
Figure C.28. Fragility curve for PLIV for Q $-\mu_0\!\!=\!\!0.28$ – Hyperstatic191
Figure C.29. Fragility curve for PLIII for HRR $-\mu_0\!\!=\!\!0.42$ – Hyperstatic192
Figure C.30. Fragility curve for PLIII for $Q - \mu_0 = 0.42$ – Hyperstatic

Figure C.31. Fragility curve for PLIV for HRR $-\mu_0$ =0.42 $-$ Hyperstatic	193
Figure C.32. Fragility curve for PLIV for Q $-\mu_0$ =0.42 $-$ Hyperstatic	193
Figure C.33. Fragility curve for PLIII for HRR $-\mu_0$ =0.56 $-$ Hyperstatic	194
Figure C.34. Fragility curve for PLIII for Q $-\mu_0$ =0.56 $-$ Hyperstatic	194
Figure C.35. Fragility curve for PLIV for HRR $-\mu_0$ =0.56 $-$ Hyperstatic	195
Figure C.36. Fragility curve for PLIV for $Q - \mu_0 = 0.56$ – Hyperstatic	195



List of Tables

Table 2.1. Steel stress-strain at elevated temperature functions [13]16
Table 2.2. Reduction factors for stress-strain relationship of carbon steel at elevated temperature [13]
Table 2.3. Concrete stress-strain at elevated temperature functions [12]
Table 2.4. Values for the main parameters of the stress-strain relationship of normal weight concrete with siliceous or calcareous aggregates concrete at elevated temperature [12]
Table 2.5. Critical temperature $\theta_{a,cr}$ for values of the utilization factor μ_0
Table 2.6. Risk grades and associated IF [25]
Table 2.7. Description and recommendations for the risk categories [25]
Table 2.8. Performance levels for buildings
Table 3.1. Risk grades and associated IF [25]
Table 3.2. Description and recommendations for the risk categories [25]
Table 3.3. Proposed performance levels for bridges
Table 3.4. Collapse times and times at which L/30 is reached
Table 3.5. Result of safety check in fire conditions
Table 3.6. Five fire scenarios analyzed
Table 3.7. Thermocouples and zones geometric features
Table 3.8. Proposed fire mitigation strategies [47]
Table 3.9. Protection thicknesses designed
Table 3.10. Failure times recorded in SAFIR in the four structural system

Table 3.11. Failure times recorded in SAFIR in the four structural system82
Table 3.12. Failure times recorded in SAFIR in the four structural system82
Table 3.13. Results obtained in prescriptive approach analyses
Table 3.14. Results obtained in performance-based approach (Scheme 3a)
Table 3.15. Proposed performance levels for bridges
Table 4.1. Geometric properties of Girder Cross-Section
Table 4.2. Cross-section properties
Table 4.3. Mechanical material properties
Table 4.4. Input data
Table 4.5. HRR parameters for occupancy selected
Table 4.6. Fire scenario characteristics
Table 4.7. DCR for isostatic model and μ_0 =0.28
Table 4.8. DCR for isostatic model and μ_0 =0.42
Table 4.9. DCR for isostatic model and μ_0 =0.56
Table 4.10. DCR for hyperstatic model and μ_0 =0.28
Table 4.11. DCR for hyperstatic model and μ_0 =0.42
Table 4.12. DCR for hyperstatic model and μ_0 =0.56





List of Symbols

The following symbols are used within the thesis

E	effect of action;
E_{a}	the modulus of elasticity of steel for normal temperature design;
$E_{a,\theta}$	the slope of the linear elastic range for steel at elevated temperature $\boldsymbol{\theta}_{a};$
$E_{c,eff} \\$	effective modulus of elasticity of concrete;
$E_{cd} \\$	design value of modulus of elasticity of concrete;
E_{cm}	secant modulus of elasticity of concrete;
E _c (t)	tangent modulus of elasticity of normal weight concrete at a stress of σ_c = 0 and at time t;
$E_{\rm fi,d}$	the design effect of actions for the fire situation, determined in accordance with EN 1991-1-2, including the effects of thermal expansions and deformations;
E_{p}	design value of modulus of elasticity of prestressing steel;
E_s	design value of modulus of elasticity of reinforcing steel;
G_{k}	the characteristic value of a permanent action;
$M_{b, fi, t, Rd} \\$	the design buckling resistance moment at time t;
$M_{\mathrm{fi},t,Rd}$	the design moment resistance at time t;
$M_{\mathrm{fi},\theta,Rd}$	the design moment resistance of the cross-section for a uniform temperature θ_a which is equal to the uniform temperature θ_a at time t in a cross-section which is not thermally influenced by the supports;

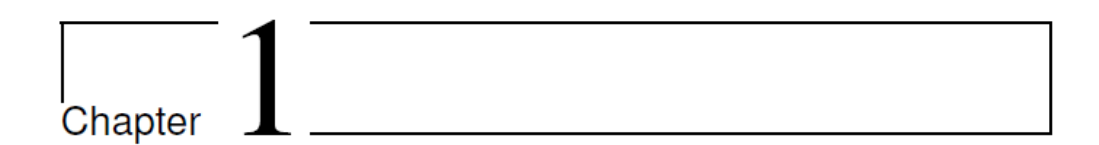
the plastic moment resistance of the gross cross-section M_{pl,Rd} M_{Rd} for normal temperature design; the elastic moment resistance of the gross cross-section M_{el,Rd} for normal temperature design; the design buckling resistance at time t of a compression $N_{b,fi,t,Rd}$ member; the design resistance of the cross-section Npl,Rd for normal N_{Rd} temperature design, according to EN 1993-1-1; the design resistance of a tension member a uniform temperature $N_{\mathrm{fi},\theta,Rd}$ θ_a ; the design resistance at time t of a tension member with a non- $N_{\text{fi,t,Rd}}$ uniform temperature distribution across the cross-section; the principal variable load; $Q_{k,1}$ K_{sh} section factor; b configuration factor; specific heat; С specific heat of steel; c_a specific heat of concrete; c_{c} effective yield strength; $f_{y,\theta}$ $f_{p,\theta}$ proportional limit; $f_{c,\theta}$ compressive strength; reduction factor for concrete compressive strength; $k_{c,\theta}$ reduction factor for yield strength; $k_{y,\theta}$ the reduction factor for the slope of the linear elastic range; $k_{E,\theta}$ coefficient of heat transfer by convection; $\alpha_{\rm c}$ $\epsilon_{p,\theta}$ strain at the proportional limit;

yield strain; $\epsilon_{y,\theta}$ limiting strain for yield strength; $\epsilon_{t,\theta}$ ultimate strain; $\epsilon_{u,\theta}$ strain corresponding to compressive strength; $\epsilon_{c1,\theta}$ relative emissivity; εr emissivity of flame, of the fire; ϵ_{f} surface emissivity of the element; ϵ_{m} thermal conductivity; λ

Stephan Boltzmann constant;

σ





1 Introduction

1.1 Fire events in transport infrastructures

Fire can represent a critical risk to structures and especially to transportation infrastructures. For the latter, the probability of fire occurrence is increasing through time due to significant urbanization and an intensification of vehicles that daily use such infrastructures, of which trucks transporting chemical materials with high combustion potential are part. [1]

Most fire events involving transportation infrastructure are caused by crashes of one or more vehicles or collisions with structural elements. Although the effects on structures of these events are often catastrophic causing partial or total collapses of the invested structures resulting in significant loss of life and economic losses to society, there is a widespread lack of recommendations about the performance that de structures may have under fire conditions in national and international technical regulations. For these reasons, most of the currently used transportation infrastructures has not been designed, nor verified, against fire conditions and, therefore, may be highly vulnerable. Furthermore, the collapse or loss of functionality of these structures can result in major consequences for society by severely limiting the proper functioning of national and international road networks. [2] [3]

Fires caused by vehicles are explosive in nature since fuels are highly flammable and have a low ignition point. Another cause of fire, which is quite common especially in the case of railroad bridges, is of natural origin, which are forest fires and lightning fires. Railroad bridges are typically located in wilderness areas and far from population centers, which is why reporting and response times can be much longer due to this distance from fire stations and the poor accessibility of the works. In these cases, forest fires can grow and spread freely over larger areas, causing damage to the environment as well as to rail infrastructure. All this affects the definition of risk. The Figure 1.1, Figure 1.2, Figure 1.3 and Figure 1.4 show some fire event causing collapse for bridges or viaducts.



Figure 1.1. Fire event on "Ponte di Ferro" in Rome, Italy, 2021 [4]



Figure 1.2. Massive fire causing collapse of an overpass on Interstate 85 in Atlanta, US, 2017 [5]



Figure 1.3. I95 collapse in Philadelphia after tanker fire, US, 2023 [6]



Figure 1.4. Massive fire ignited from train derailment in Arizona [7]

Therefore, the fire scenarios typically used in infrastructure fire vulnerability assessments and, therefore, in retrofit design, are scenarios based on typical thermal release curves of different vehicles, single or multiple. However, these types of scenarios are not the only ones that should be considered, since the space under bridges is often subject to various urbanization works with different uses. In addition, there are frequent urban areas where housing, which is organized in apartment blocks, is mixed with infrastructure works, and this happens more in the suburbs. From the point of view of the architecture of urban spaces in these suburban areas, the space under bridges can be exploited for urbanization works due to the limited availability of space in heavily populated contexts. [8]



Figure 1.5. Piazza Ottocalli in Naples, revisited from [8]

It is clear, therefore, that very intense events can induce temperatures in structural elements high enough to result in reductions in strength and stiffness so significant as to cause partial or total collapse of structures. Even in the case of less intense fire events, investigations and inspections are nescessary to plan any maintenance or rehabilitation of structures. Under these conditions, infrastructures should still be interdicted, and closure results in traffic reorganization with detours to other routes with consequent increases in travel time and, therefore, generalized discomfort.

Fire risk, as well as risk in general, is defined by the combination of several aspects, such as:

1. *Intrinsic vulnerability of the structure*: this is related to structural characteristics such as, among others, length of spans, static scheme, material composing the main elements. I n addition to the structural characteristics that describe the individual artifacts, it should be emphasized that for the proper assessment of vulnerability to fire, it should be duly taken into account in the analyses the nonlinear properties of materials varying with temperature and to the possible hyperstatic effects that are related to the static scheme, as well as considering the need to carry out analyses and evaluations in large displacements and, therefore, abandon the classical assumptions of structural analysis widely, and correctly, used in cases of design for static and dynamic loads. Moreover, there is a deep interaction between the structure and the

- acting loads, such as wind load (wind-structure interaction) and with the boundary conditions (soil-structure interaction).
- 2. Probability of occurrence of the event: This is related to the amount and type of vehicles using the particular structure. In fact, the issue of the probability of occurrence of a fire in the proximity of a bridge has also been variously discussed in the scientific literature, and it can be deduced how this is non-negligible and, in any case increases together with the percentage of heavy vehicles using it out of the total traffic volume. In addition, developed fire events are consequent, as mentioned, to accidents or natural events, and the absence of warning systems together with the timing of intervention means that the fire can develop freely and uninterrupted in its initial stages.
- 3. Exposed value: all possible economic losses resulting from an event should be included in the exposed value. These losses should be estimated not only by considering the costs necessary for the rehabilitation (minor damage) or reconstruction of the bridge (partial or total collapses) such as costs related to investigations and inspections, engineering design fees, and costs related to the demolition and reconstruction site, but must also consider all indirect costs related to replacement transportation services for example, as well as the social impact of the resulting inconvenience.

1.2 Bridges performance in case of fire

The fire performance of a bridge is affected by some key factors discussed below:

- 1. Fire bridges vulnerability
 - 1.1. Geometric features: The geometry and size of structural elements can have an important impact on defining the global vulnerability of the structure. In fact, if we consider, for example, steel girder bridges usually have high slenderness and local or element (flexural-flexural-torsional) buckling phenomena can limit considerably the maximum exposure time to high

- temperatures. In other cases, such as in prestressed girder bridges in CAP, the thickness of concrete cover passively protects the prestressing reinforcement from high temperatures by slowing the phenomenon of strength degradation.
- 1.2. Materials Utilized: the performance of bridges exposed to fire is highly dependent on the thermophysical and mechanical properties of the materials that constitute the structural elements. In current practice, steel is widely used in bridge construction because of its strength, ductility, ease of installation and cost-effectiveness. However, because of its high thermal conductivity (about 50 times higher than that of concrete), its low specific heat and the slenderness of the elements, temperature rises very rapidly in exposed elements. Since the strength and modulus of elasticity of steel are very sensitive to high temperatures, increased temperature in steel elements causes very rapid degradation of strength and stiffness. This implies that structural steelwork elements can lose their load-bearing capacity within the first few minutes of fire exposure. Therefore, steel elements have generally lower fire resistance than concrete structural elements, which experience slower temperature growth in cross sections due to lower thermal conductivity and higher specific heat, as well as slower loss of strength and stiffness as temperature increases. This implies that steel bridges are more vulnerable to fire-induced collapse than ordinary or prestressed concrete bridges. In contrary to concrete and steel, wood is a combustible material and loses strength and stiffness at relatively lower temperatures. [1]
- 1.3. Loading and restraint conditions: Loading conditions can significantly affect the fire vulnerability of structures because the time to collapse is related to the initial static utilization level, i.e., the initial relationship between demand and capacity. A bridge with a lower initial static utilization level will have a greater availability of strength to be degraded under fire

- conditions. This is a priority issue for bridges that are isostatic and remain so during exposure. In fact, in the event that the restraint conditions change during the event (i.e., in the case of expansion joints) hyperstatic effects can induce an increase in demand and, therefore, increase the vulnerability.
- 1.4. Fire intensity: fire intensity and duration have a significant impact on the performance of structural elements. Fire intensity and duration depend on the type and amount of fuel, as well as ventilation characteristics. Fires in buildings tend to develop with lower intensity and progress more slowly than fires involving bridges, due to limited ventilation (oxygen availability), the presence of active and passive protection systems, and fuels consisting mainly of cellulose-based materials. In contrast, bridges are open structures with an unlimited supply of oxygen and for which active and passive fire protection measures are typically lacking, and the presence of highly flammable hydrocarbon products can accelerate the rate of fire growth, producing high-intensity fires. [9]

2. Bridges criticalities

- 2.1. Bridge site: the strategic importance of a structure is directly related to its location in the transportation network. If the bridge is located at an intersection crossing natural obstacles (such as valleys or rivers) and if there are no alternative routes available any closure will force a disruption of traffic.
- 2.2. Traffic volume: the importance of the bridge is also related to the volume of traffic handled daily, so all other factors being equal, a bridge with a higher traffic volume will have a higher related fire risk.
- 2.3. Probability: It is worth noting that the occurrence of a fire on a bridge (or in a tunnel) is a rare event, and not all fires reach significant temperatures. Kodur and Naser have shown that the annual probability of a fire on a bridge is about 3 percent, thus much lower than the annual probability of a fire in a building (about 29 percent). Despite this low probability, recent incidents

have shown that high intensity fires that start near a bridge or tunnel can cause significant damage to structural elements, including collapse, which in turn can lead to severe traffic delays, detours, and costly repairs. Even in the case of minor fires, a rapid rise in temperature can still develop high thermal gradients that can produce localized failure modes, such as concrete spalling or temperature-induced local buckling in steel members.

1.3 Thesis objectives

Starting from the study of the state of the art, both national and international technical regulations and scientific literature, this thesis work aims to analyze the fire risk for bridges with particular reference to the definition of the vulnerability of structures and the probability of occurrence of fire events.

Therefore, special emphasis will be placed on the analysis of the available methodologies for the definition of such vulnerability, comparing the results and identifying technically most suitable procedures depending on the work analyzed and its "importance." The vulnerability of a work may be expressed in terms of collapse times, i.e., the time that a work can withstand a given fire curve by not exceeding strength or stability requirements.

On the other hand, with respect to the probability of occurrence, a parametric and comparative analysis will be carried out on the effect of uncertainty in defining the input parameters of the fire load.

Main objectives are reported in the following bullet points:

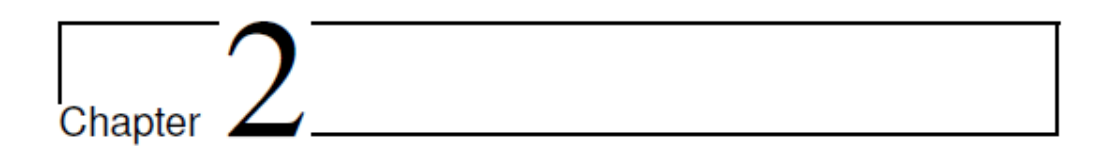
- Provide an overview of the state of the art in infrastructure fire vulnerability;
- Define fire performance levels for bridges based on simple and parametric case studies;

 Construct fragility curves in case of fire using the performance levels previously defined on a real case study;

The Thesis is structured as follows:

- Chapter 1 Introduction: It presents an overview of fire vulnerability for structures and in particular for infrastructure. The concept and basic parameters of bridges performance in the event of fire are introduced. In addition, B-Road fire scenarios, the ones due to the proximity of infrastructure to structures with a high fire ignition potential, are described.
- Chapter 2: provides an overview of the state of the art in scientific literature and technical regulations in the field of fire vulnerability assessment of structures and infrastructure, fire models, and methods of analysis and verification under fire conditions.
- Chapter 3: provides an evolution in the definition of performance levels
 that a bridge should meet in case of fire and, by analyzing a parametric
 case study, highlights the differences between the prescriptive approach
 and the performance-based approach.
- Chapter 4: sets out the complete procedure for constructing fragility curves in the event of fire, based on the previously defined performance levels, for a viaduct simply supported with steel girders and a non-collaborating concrete slab.
- Chapter 5: Conclusions are drawn from the work done by emphasizing key concepts on both thermo-structural modelling and the performance level approach. Some developments are also proposed.





2 Assessment of structural vulnerability in case of fire

The structural safety in case of fire of a building was formally defined by the Construction Product Directive 89/106/EEC in 1988 which states the safety basic requirements a building may have in case of fire, such as mechanical resistance, stability and safety under fire condition.

The cited Directive, thus, gives the definition to the safety in case of fire: (also see Figure 2.1) "The construction works must be designed and built in such a way that in the event of an outbreak of fire:

- The load-bearing capacity of the construction can be assumed for a specific period of time;
- The generation and spread of fire and smoke within the works is limited;
- The spread of fire to neighboring construction works is limited;
- Occupants can leave the works or be rescued by other means;
- The safety of rescue teams is takes into consideration." [10]

Following the Directive, the Interpretative Document No. 2 "Safety in case of fire" [10] defines a strategy organized as:

- Minimize the probability of a fire event (fire prevention);

- Assess the safety of occupants and decide in which case it may be improved by the utilization of fire detection systems and alarm (active protection systems);
- Identify a suitable level of compartmentation in order to prevent the spread of fire within the construction works;
- Prevent the spread of fire to neighboring buildings;
- Ensure safety conditions for the intervention of rescue team;

It is, thus, clear how the structural resistance and stability during a fire event is a crucial factor in order to ensure the safety according to the strategy discussed.

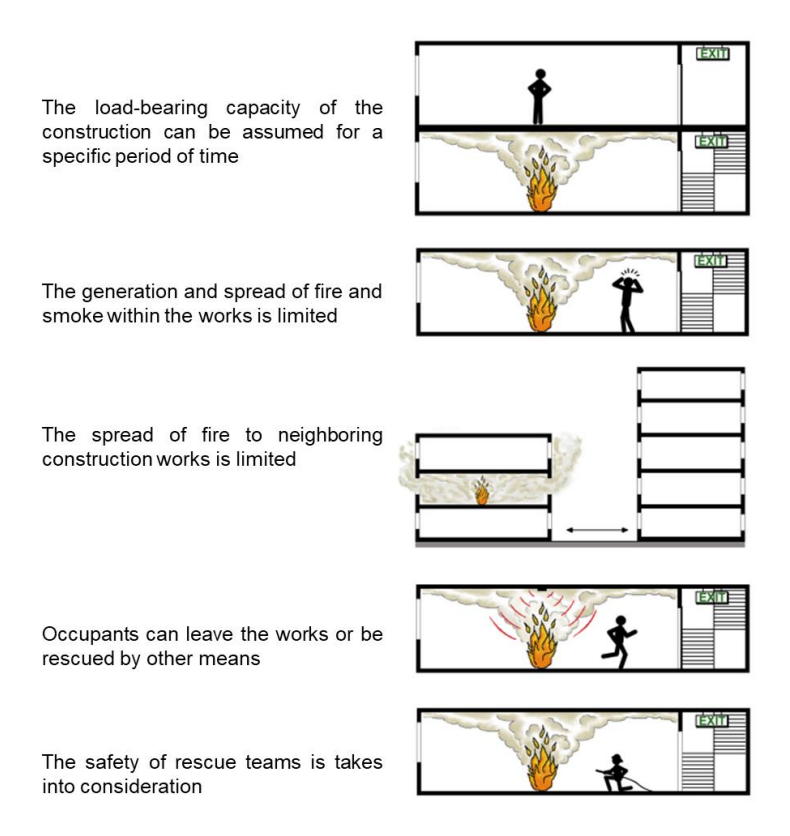


Figure 2.1. Safety in case of fire according to Directive 89/106/EEC [11]

In order to assess the structural resistance in case of fire the designer needs to analyze the structure or the infrastructure using an organic set of rules that define the action (applied loads, thermal loads, load combinations) and the resistance (evaluation of the resistance in a specific time during the fire event) and, then, the verification criteria to figure out whether the structure can ensure a minimum performance in case of fire.

This set of rules basically depend on which approach is used for the fire vulnerability assessment.

2.1 Design and vulnerability assessment approaches in case of fire

In order design a construction work under fire condition or assess the fire vulnerability two approaches are useful, mainly, the prescriptive approach (PA) and the performance-based approach (PBA). The main difference between the prescriptive and the performance-based approaches is that the first one is based on standard fire resistance tests or empirical calculation methods, using nominal fire curves. In particular, the codes provide three types of conventional fire curves (standard ISO834, hydrocarbon, and external nominal curve), selected according to the nature of the combustible materials in the compartment. On the other hand, the PBA considers the complexity of structures and the inter-relationship between the various fire safety measures and systems, using specific natural fire curves, generally obtained by advanced thermo-fluid-dynamic analyses. The first step of the PBA design consists of the thermal input assessment through the selection of design fire scenarios, which represent qualitative description of the fire development, based on key aspects that characterize the real fire (compartment dimension, ventilation, fire loads, etc.). About the verification criteria, the PA approach provides a verification in terms of minimum fire resistance in the time domain, classifying the structures in a discrete number of classes (R30, R60, etc.). All these aspects about the fire resistance of construction works cannot be directly applied to infrastructures like

bridges, as many differences have to be underlined. In the case of buildings, the fire occurs in a compartment and the natural fire curve is influenced by the oxygen available as a function of the openings. In case of bridges, it is not possible to define a confined compartment, so the standard fire curves do not represent the real fires adequately. A better way to define the fire curve in the case of bridges is the computational fluid dynamic (CFD) analysis that allows to model the fire propagation near the bridge structure. These analyses also allow to model different fire scenarios in order to take into account the most severe fire event location for the structural bridge verification. Even if the performance-based approach seems to be the best way to design and verify bridges in case of fire, no defined criteria are provided in technical references.

2.2 Materials behaviour in fire conditions

Fire events induce high temperature in exposed structural elements, those are dependent on the intensity of fire and on the thermal properties of materials such as thermal conductivity (λ) and specific heat (c). High temperatures cause variation in thermal properties as well as the mechanical properties (resistance and stiffness) degrading the latter and making the structure progressively weal to applied loads. The following sections describe the relationship for the main thermal and mechanical properties of steel and concrete as a function of the temperature according to Eurocode 2 Part 1-2 [12] and Eurocode 3 Part 1-2. [13]

2.2.1 Mechanical properties

Steel

The steel stress-strain relationship for a given temperature θ is shown in Figure 2.2, it is divides into four parts: rising linear for $0 \le \epsilon \le \epsilon_{p,\theta}$, elliptical for $\epsilon_{p,\theta} \le \epsilon$

 $\leq \epsilon_{y,\theta} \text{, flat for } \epsilon_{y,\theta} \leq \epsilon \leq \epsilon_{t,\theta} \text{ and then descending linear for } \epsilon_{t,\theta} \leq \epsilon \leq \epsilon_{u,\theta} \text{. The functions}$ describing the stress-strain relationship are shown in

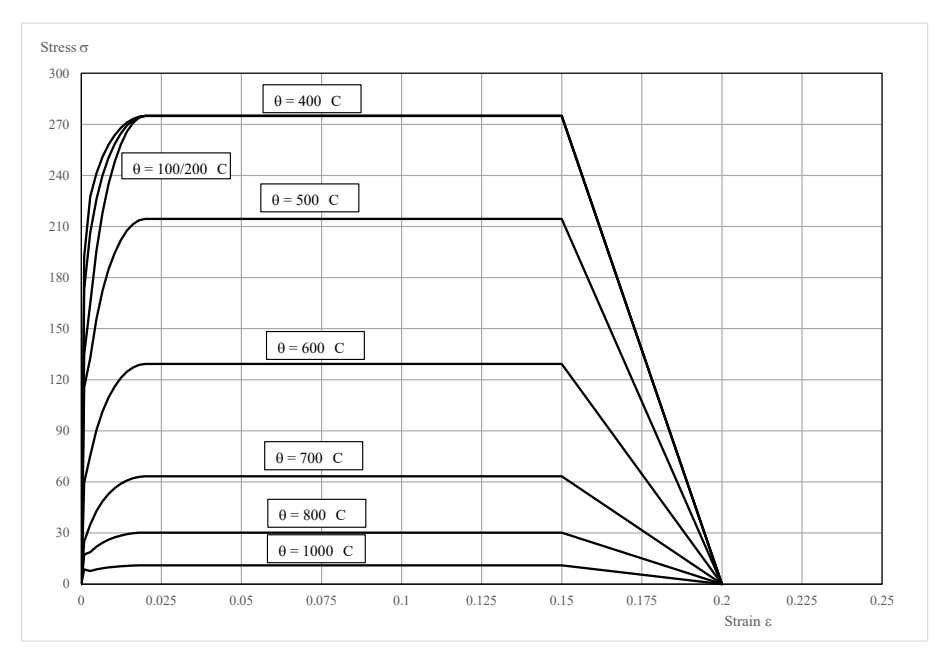


Figure 2.2. Stress-strain relationship for carbon steel at elevated temperature [13]

Table 2.1. Steel stress-strain at elevated temperature functions [13]

Strain range	Stress σ	Tangent modulus
$\varepsilon \leq \varepsilon_{p,\vartheta}$	$arepsilon E_{a,artheta}$	$E_{a,\vartheta}$
$\varepsilon_{p,\vartheta} \le \varepsilon \le \varepsilon_{y,\vartheta}$	$f_{p,\vartheta} - c + \left(\frac{b}{a}\right) \left[a^2 - \left(\varepsilon_{y,\vartheta} - \varepsilon\right)^2\right]^{0.5}$	$\frac{b(\varepsilon_{y,\vartheta} - \varepsilon)}{a \left[a^2 - \left(\varepsilon_{y,\vartheta} - \varepsilon\right)^2\right]^{0.5}}$
$\varepsilon_{y,\vartheta} \le \varepsilon \le \varepsilon_{t,\vartheta}$	$f_{\mathcal{Y}, artheta}$	0
$\varepsilon_{t,\vartheta} \le \varepsilon \le \varepsilon_{u,\vartheta}$	$f_{y,\vartheta}\left[1 - \frac{\varepsilon - \varepsilon_{t,\vartheta}}{\varepsilon_{u,\vartheta} - \varepsilon_{t,\vartheta}}\right]$	-
$\varepsilon = \varepsilon_{u,\vartheta}$	0.00	-
Parameters	$arepsilon_{p,artheta} = rac{f_{p,artheta}}{E_{a,artheta}} \;\; arepsilon_{y,artheta} = 0.02$	$\varepsilon_{t,\vartheta} = 0.15$ $\varepsilon_{u,\vartheta} = 0.20$
Functions	$a^{2} = (\varepsilon_{y,\theta} - \varepsilon_{p,\theta}) \left(\varepsilon_{y,\theta} - \varepsilon_{p,\theta} + \frac{c}{E_{a,\theta}} \right)$ $b^{2} = c(\varepsilon_{y,\theta} - \varepsilon_{p,\theta}) E_{a,\theta} + c^{2}$ $c^{2} = \frac{\left(f_{y,\theta} - f_{p,\theta} \right)^{2}}{\left(\varepsilon_{y,\theta} - \varepsilon_{p,\theta} \right) E_{a,\theta} - 2 \left(f_{y,\theta} - f_{p,\theta} \right)}$	

The reduction factors for effective yield stress f_y , proportional limit f_p and for the slope of the linear elastic range are shown in Table 2.2 and Figure 2.3.

Table 2.2. Reduction factors for stress-strain relationship of carbon steel at elevated temperature [13]

	Reduction factors at ter	Reduction factors at temperature θ_a relative to the value of f_y or E_a at 20 °C				
Steel Temperature θ _a	Reduction factor (relative to f_y) for effective yield strength $k_{y,\theta} = f_{y,\theta}/f_y$	Reduction factor (relative to f_y) for proportional limit $k_{p,\theta} = f_{p,\theta}/f_y$	Reduction factor (relative to E _a) for the slope of the linear elastic range $k_{E,\vartheta} = E_{a,\vartheta}/E_a$			
20 °C	1.000	1.000	1.000			
100 °C	1.000	1.000	1.000			
200 °C	1.000	0.807	0.900			
300 °C	1.000	0.613	0.800			
400 °C	1.000	0.420	0.700			
500 °C	0.780	0.360	0.600			
600 °C	0.470	0.180	0.310			
700 °C	0.230	0.075	0.130			
800 °C	0.110	0.050	0.090			
900 °C	0.060	0.0375	0.0675			
1000 °C	0.040	0.0250	0.0450			
1100 °C	0.020	0.0125	0.0225			
1200 °C	0.000	0.0000	0.0000			

NOTE: For intermediate values of the steel temperature, linear interpolation may be used.

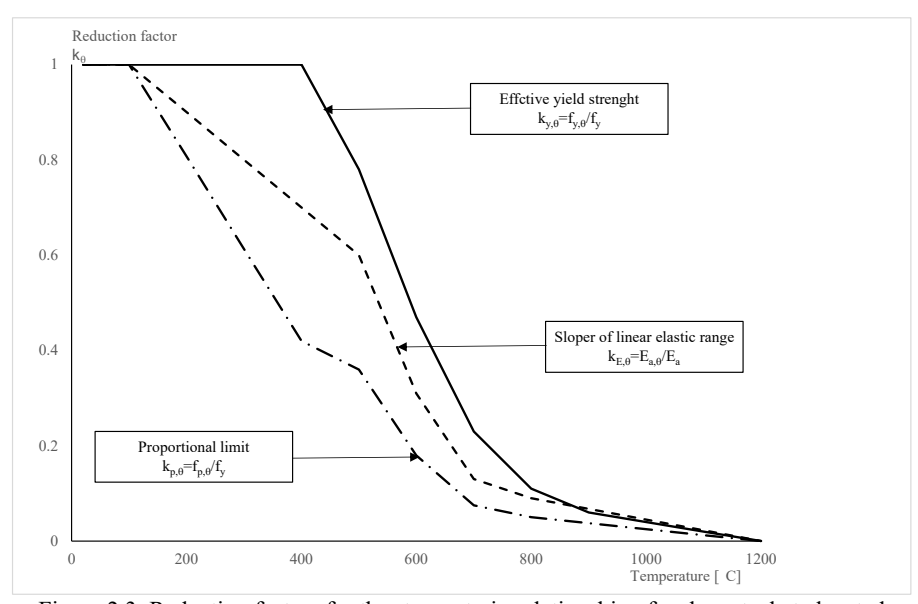


Figure 2.3. Reduction factors for the stress-strain relationship of carbon steel at elevated temperature

Concrete

The concrete stress-strain relationship at elevated temperature is shown in Figure 2.4. This is defined by two parameters: The compressive strength $f_{c,\theta}$ and the strain $\epsilon_{c1,\theta}$ corresponding to $f_{c,\theta}$. The function describing the increasing branch are given in Table 2.3, a descending one, linear or non-linear, should be used for a numerical purpose, indeed.

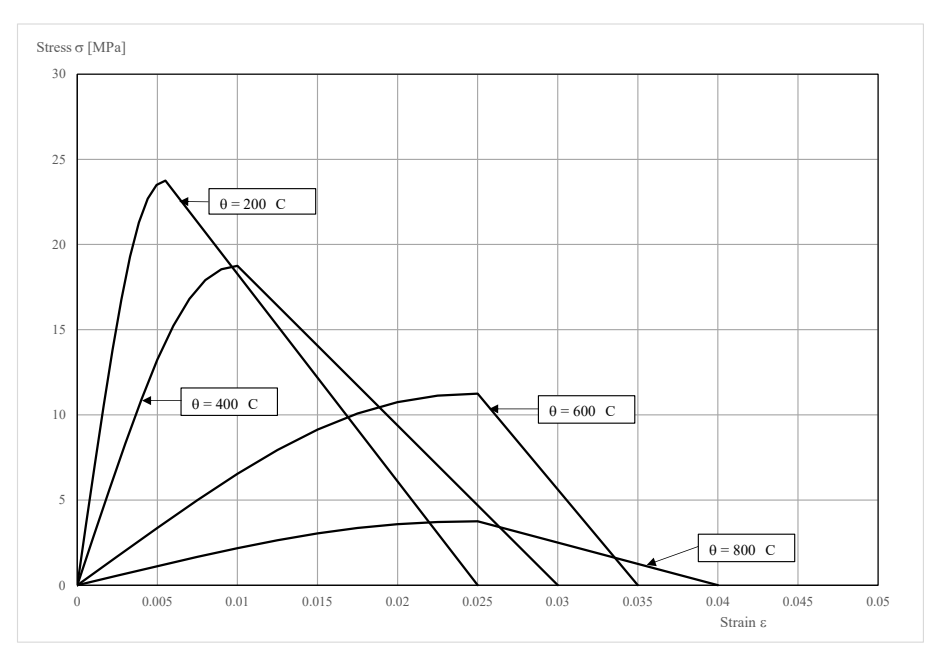


Figure 2.4. Stress-strain relationship for concrete a elevated temperature [12]

Table 2.3. Concrete stress-strain at elevated temperature functions [12]

Strain range	Stress $\sigma(\theta)$	
$\varepsilon \leq \varepsilon_{c1,\vartheta}$	$\frac{3\varepsilon f_{c,\vartheta}}{\varepsilon_{c1,\vartheta}\left(2+\left(\frac{\varepsilon}{\varepsilon_{c1,\vartheta}}\right)^3\right)}$	
$\varepsilon_{c1,\vartheta} \le \varepsilon \le \varepsilon_{cu1,\vartheta}$	For a numerical purpose a descending branch should be adopted. Linear or non-linear models are permitted.	

The reduction factor $k_{c,\theta}$ and the values of strain defining the limit of descending branch and the ultimate strain are reported in Figure 2.5 and Table 2.4. The parameters may be used for a normal weight concrete with siliceous and calcareous aggregates.

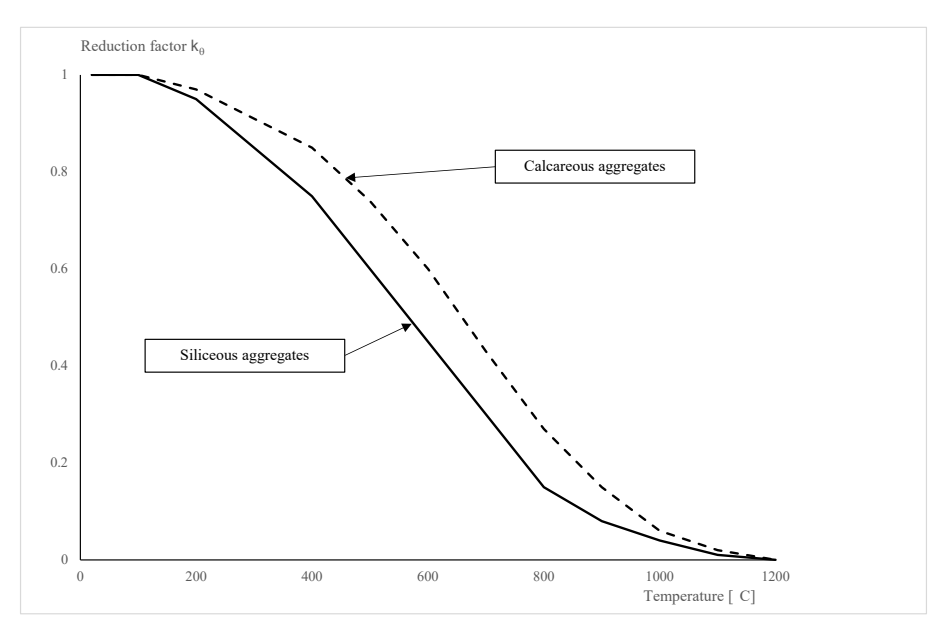


Figure 2.5. Reduction factor for the stress-strain relationship of concrete at elevated temperature

Table 2.4. Values for the main parameters of the stress-strain relationship of normal weight concrete with siliceous or calcareous aggregates concrete at elevated temperature [12]

Concrete	Siliceous aggregates		Calcareous aggregates			
Temperature θ_a	$f_{c,\vartheta}/f_{c,k}$	$\varepsilon_{c1,\vartheta}$	$arepsilon_{cu1,artheta}$	$f_{c,\vartheta}/f_{c,k}$	$arepsilon_{c1,artheta}$	$\varepsilon_{cu1,\vartheta}$
20 °C	1.00	0.0025	0.0200	1.00	0.0025	0.0200
100 °C	1.00	0.0040	0.0225	1.00	0.0040	0.0225
200 °C	0.95	0.0055	0.0250	0.97	0.0055	0.0250
300 °C	0.85	0.0070	0.0275	0.97	0.0070	0.0275
400 °C	0.75	0.0100	0.0300	0.85	0.0100	0.0300
500 °C	0.60	0.0150	0.0325	0.74	0.0150	0.0325
600 °C	0.45	0.0250	0.0350	0.60	0.0250	0.0350
700 °C	0.30	0.0250	0.0375	0.43	0.0250	0.0375
800 °C	0.15	0.0250	0.0400	0.27	0.0250	0.0400
900 °C	0.08	0.0250	0.0425	0.15	0.0250	0.0425
1000 °C	0.04	0.0250	0.0450	0.06	0.0250	0.0450
1100 °C	0.01	0.0250	0.0475	0.02	0.0250	0.0475
1200 °C	0.00	-	-	0.00	-	-

2.2.2 Thermal properties

Steel

The relations defining the value of specific heat and thermal conductivity for carbon steel at elevated temperature are following summarized according to Eurocode 3 part 1-2. [13]

- for
$$20^{\circ}C \leq \vartheta < 600^{\circ}C$$

$$c_a = 425 + 7.73x10^{-1}\vartheta_a - 1.69x10^{-3}\vartheta_a^2$$
 Eq. 2.1
$$+ 2.22x10^{-6}\vartheta_a^3 \ J/kgK$$

- for $600^{\circ}C \leq \vartheta < 735^{\circ}C$

$$c_a = 666 + \frac{13002}{738 - \vartheta_a} J/kgK$$
 Eq. 2.2

- for $735^{\circ}C \leq \vartheta < 900^{\circ}C$

$$c_a = 545 + \frac{17820}{\vartheta_a - 731} J/kgK$$
 Eq. 2.3

- for $900^{\circ}C \leq \vartheta \leq 1200^{\circ}C$

$$c_a = 650 J/kgK$$
 Eq. 2.4

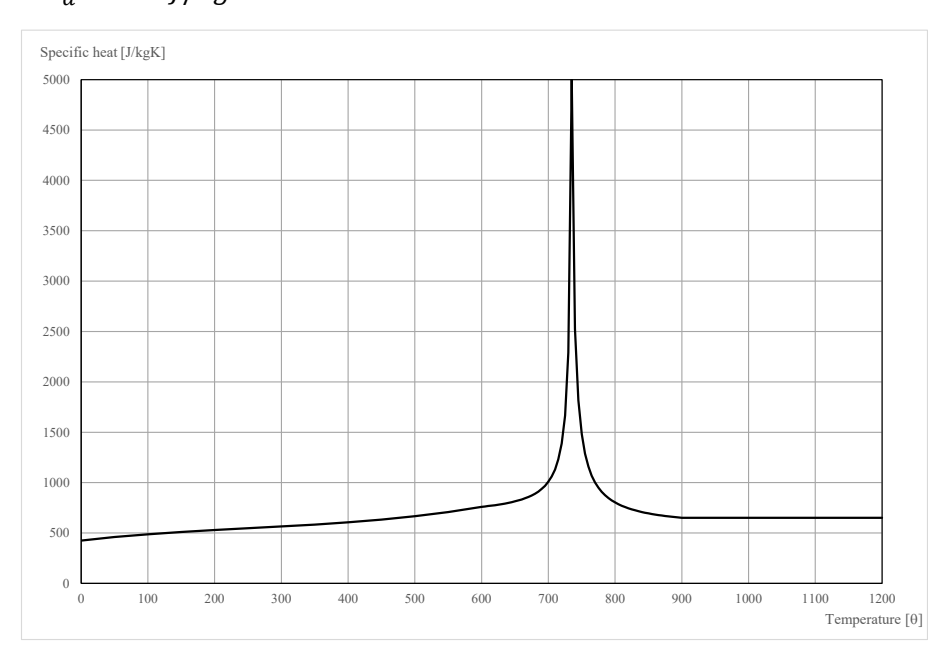


Figure 2.6. Specific heat of a carbon steel as a function of the temperature [13]

$$- \quad \text{for } 20^{\circ}C \leq \vartheta < 800^{\circ}C$$

$$\lambda_a = 54 - 3.33x10^{-2}\vartheta_a \, W/mK$$

$$- \quad \text{for } 800^{\circ}C \leq \vartheta < 1200^{\circ}C$$

$$\lambda_a = 27.3 \, W/mK$$
 Eq. 2.6

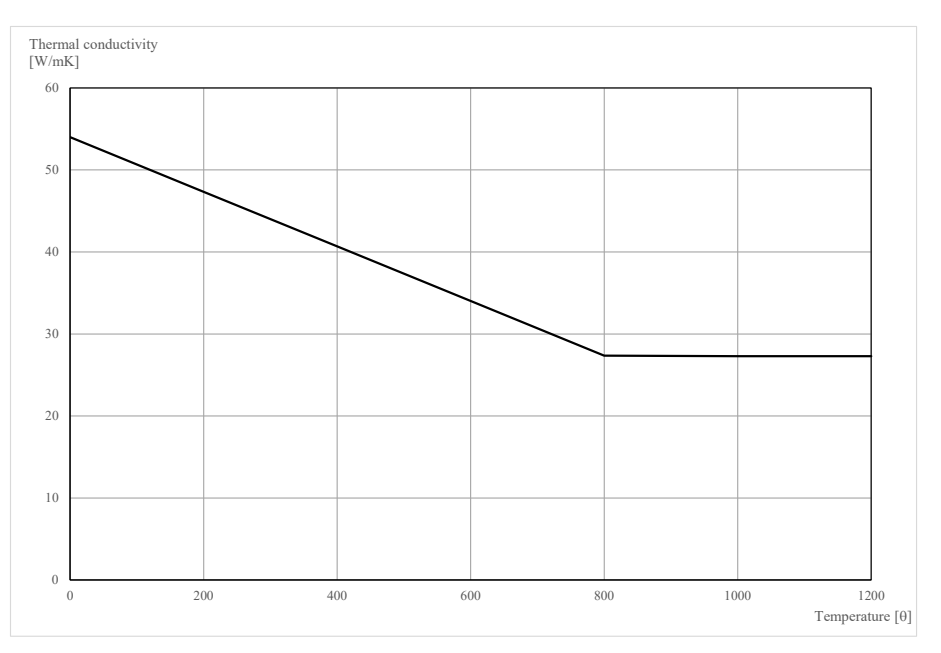


Figure 2.7. Thermal conductivity of carbon steel as a function of the temperature [13]

Concrete

The relations defining the value of specific heat and thermal conductivity for concrete with siliceous and calcareous aggregates at elevated temperature, for dry concrete case, are following summarized according to Eurocode 2 part 1-2. [12]

$$- \quad \text{for } 20^{\circ}C \leq \vartheta < 100^{\circ}C$$

$$c_p(\vartheta) = 900 J/kgK$$

$$- \quad \text{for } 100^{\circ}C \leq \vartheta < 200^{\circ}C$$

$$c_p(\vartheta) = 900 + (\vartheta - 100) J/kgK$$

$$- \quad \text{for } 200^{\circ}C \leq \vartheta < 400^{\circ}C$$
 Eq. 2.8

$$c_p(\vartheta)=1000+(\vartheta-200)/2J/kgK$$
 Eq. 2.9
$$-\text{ for }400^{\circ}C\leq\vartheta\leq1200^{\circ}C$$

$$c_p(\vartheta)=1100J/kgK$$
 Eq. 2.10

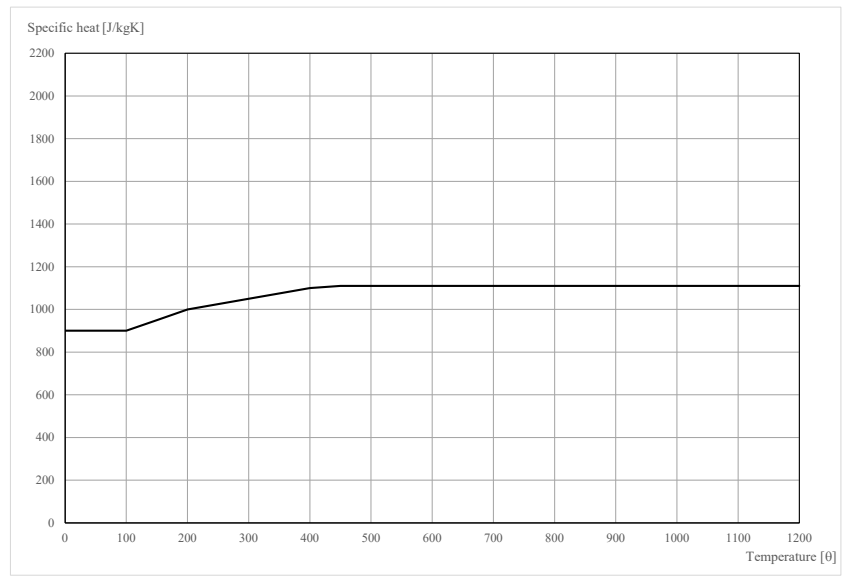


Figure 2.8. Specific heat, $c_p(\theta)$, by weight for siliceous concrete [12]

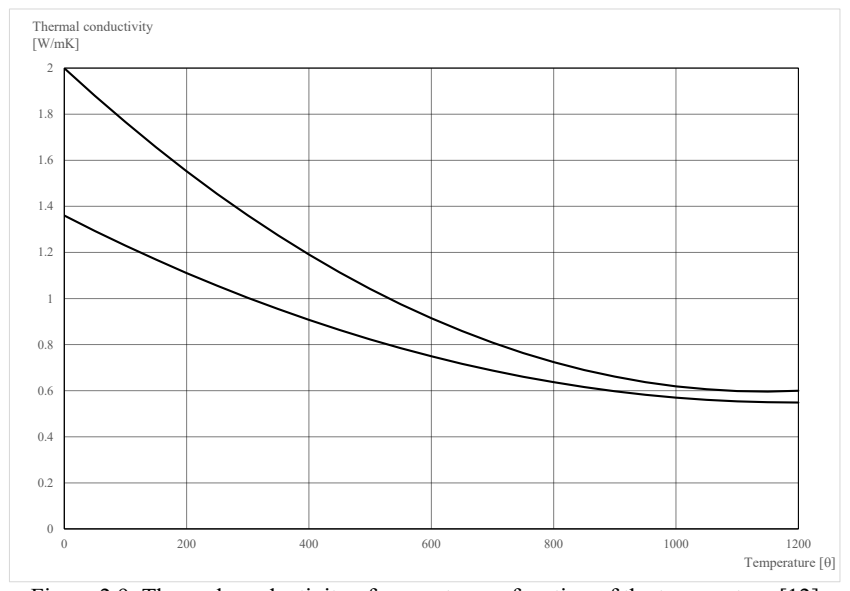


Figure 2.9. Thermal conductivity of concrete as a function of the temperature [12]

- Upper limit

$$\lambda_c = 2 - 0.2451 \left(\frac{\vartheta}{100}\right) + 0.0107 \left(\frac{\vartheta}{100}\right)^2 W/mK$$
 Eq. 2.11

Lower limit

$$\lambda_c = 1.36 - 0.136 \left(\frac{\vartheta}{100}\right) + 0.0057 \left(\frac{\vartheta}{100}\right)^2 W/mK$$
 Eq. 2.12

2.3 Fire modelling

In order to understand the mathematical model of fire event a foreword about the physical phenomenon of a fire event. A fire event is generally split into four main phases: ignition phase, propagation phase, fully developed fire phase and extinguishing fire phase. In the very first phase, ignition, one or more flammable stuff (combustible) keep contact with a heat source (ignition energy) and, being available oxygen (comburent), a fire is triggered. This phase is characterized by a huge difference in the compartment temperatures and the flames are localized in a small spot. Then, in the case of there is no limitation to ventilation and combustible materials in the compartment, the fire propagates and the flames quickly expand interesting the most part of the compartment, so-called flashover. After this the fire became a fully developed event and the temperature is uniform throughout the compartment. At the end, when the oxygen or combustible limit the combustion, the fire extinguish and temperature are descending in the compartment.

To the real physical phenomena, a mathematical model can be related. The simplest way to do that is to describe a fire event by a time-temperature curve also call fire curve.

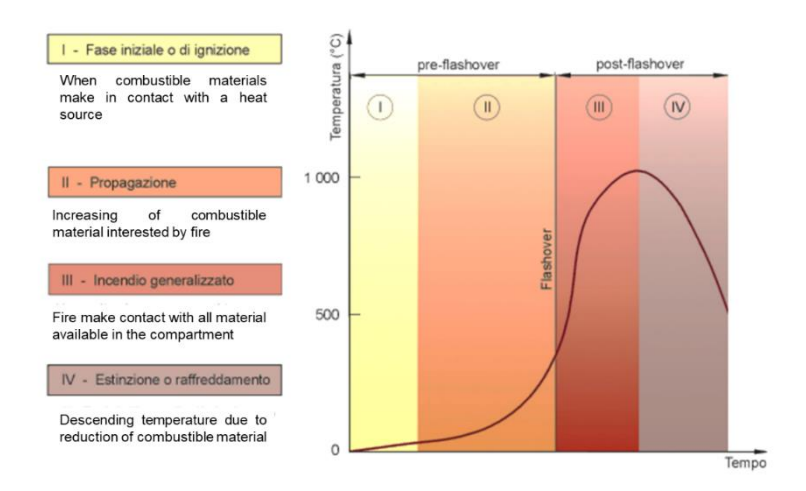


Figure 2.10. Fire event phases scheme [11]

2.3.1 Nominal fire curves

Thermal actions in fire structural resistance assessment can be evaluated by using nominal or natura fire curves. Nominal fire curves are simple temperature-time relations not dependent on any boundary conditions. The standard ISO834 fire curve, which is typically used to describe fire in buildings, provides for a monotonic increase in temperature with the exposing time. This characteristic is typical of any nominal fire curve and clearly leads to overestimate temperature in structural elements due that the fire cooling phase is not taken into account. ISO834 fire curve is based on cellulosic material fire which have a rate of combustion lower than other material such as gasoline and other chemical products. For this reason, Eurocode 1 part 1-2 [14] provides for the hydrocarbon fire curve.

The hydrocarbon curve is the most widely used for fires on bridges and is applicable where small oil fires might occur, i.e. contained in the tanks of cars, tankers, etc. In fact, although the hydrocarbon curve is based on a standard type of fire standard, there are numerous fire types associated with combustible petrochemicals. The intensity of a deck fire depends on the characteristics of the fuel and ventilation. Since bridges are generally located in open areas, there is no shortage

of oxygen to fuel the fire. The scenario of fire in a bridge, therefore, is mainly controlled by the load of fuel of the vehicles involved in the accident and can be represented by a hydrocarbon fire curve, applicable for gasoline fires in large open spaces. Hydrocarbon fires are much more severe than fires in buildings and are characterized by high heating rates.

Hydrocarbon fire temperatures can exceed 1000°C within the first few minutes of the fire. Because of the unlimited availability of oxygen, the hydrocarbon curve has no cooling phase and, therefore, the fire is theoretically infinite. The use of the hydrocarbon curve instead of the standard ISO 834 curve is justified because the latter represents a fire that is completely developed in a compartment and, therefore, is suitable for fires in buildings but does not reflect conditions for fires on bridges.

ISO834
$$\vartheta = \vartheta_0 + 345 \log_{10}(8t+1)$$
 Eq. 2.13
Hydrocarbon $\vartheta = 1080(1 - 0.325e^{-0.167t} - 0.675e^{-2.5t}) + \vartheta_0$ Eq. 2.14
External $\vartheta = 660(1 - 0.687e^{-0.32t} - 0.313e^{-3.8t}) + \vartheta_0$ Eq. 2.15

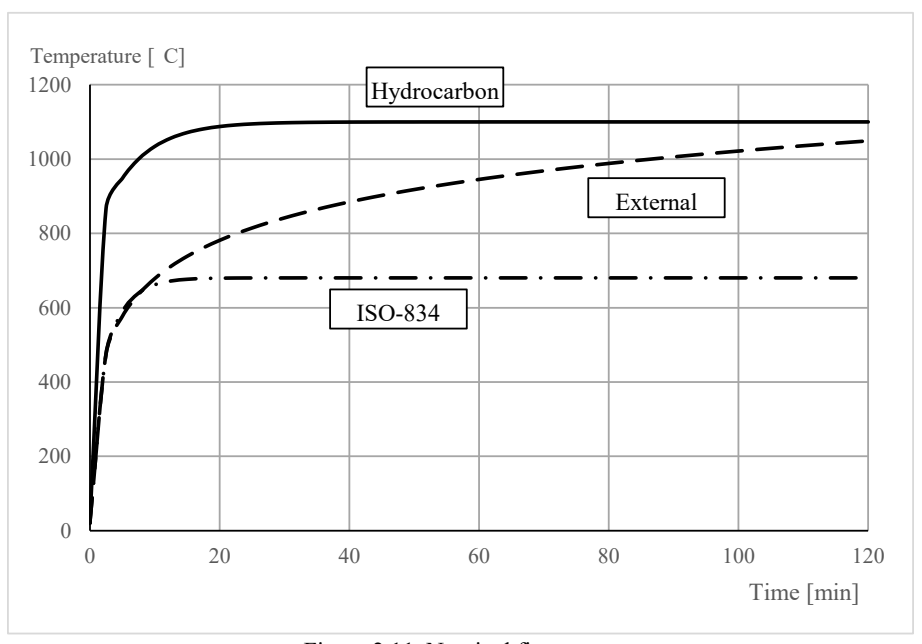


Figure 2.11. Nominal fire curves

2.3.2 Parametric fire curves

This type of curve is used to represent fully developed fires, when pressure and temperature conditions are uniform in the compartment. Some limitation may be taken into account to apply this fire model:

- Maximum compartment surface 500 m²;
- Maximum compartment heigh 4 m;
- Ventilation factor $0.02 \le O \le 0.2$.

The following equation describe the gas temperature-time curve in the compartment.

$$\vartheta_g = 20 + 1325(1 - 0.324e^{-0.2t^*} - 0.204e^{-1.7t^*} - 0.472e^{-19t^*})$$
 Eq. 2.16

Compartment is a volume bounded by structural or non-structural elements able to limit the heat transfer to the external. The boundary of these structures have thermal characteristics that strongly influence the development of a fire, as it is subject to heat exchange between the internal and external environment. These characteristics are the specific heat c and thermal conductivity λ , which are dependent on temperature, and density ρ , which is independent of it. These three parameters are used in combination with each other and define the thermal inertia of a material b:

$$b = \sqrt{\lambda \rho c}$$
 Eq. 2.17

The ventilation factor O take into account the openings of the compartment.

$$O = \frac{A_v \sqrt{h_{eq}}}{A_t}$$
 Eq. 2.18

Being:

- A_v openings surface;
- At total surface of the compartment walls, including openings;

- h_{eq} equivalent height of openings.

$$h_{eq} = \frac{\sum_{i} A_{vi} h_i}{\sum_{i} A_{vi}}$$
 Eq. 2.19

The following Figure 2.12 shows a comparison between the ISO834 nominal fire curve and an example of a parametric curve. It is clear how there is a good overlap between the increasing temperature phase of the both curves. However, the parametric curve, once the peak temperature is reached, exhibit a linear descending branch which allow to model the real behavior of a fire event due that the temperature may be decreasing when all the combustible material available is burned.

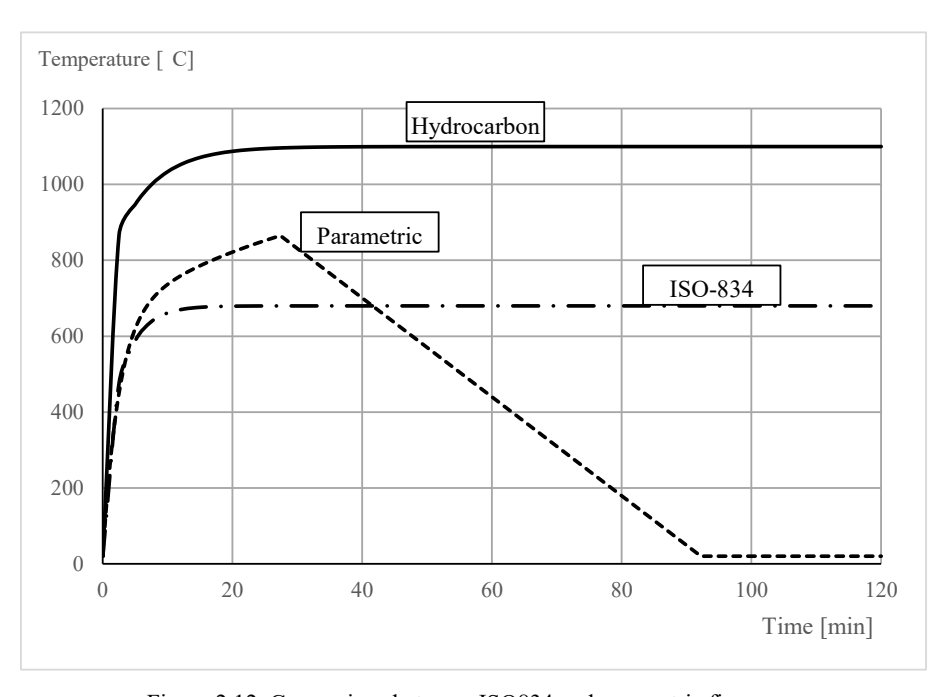


Figure 2.12. Comparison between ISO834 and parametric fire curve

2.3.3 Natural fire curves, CFD method

This Computational Fluid Dynamics (CFD) plays a crucial role in analyzing fire scenarios, providing detailed insights into the complex behavior of fire and smoke within built environments. By simulating the flow of gases, heat transfer, and combustion processes, CFD allows engineers and researchers to predict the spread

of fire, assess the effectiveness of fire suppression systems, and optimize evacuation strategies.

In fire safety engineering, CFD models simulate the interaction between fire, smoke, and the surrounding environment, considering factors such as ventilation, building geometry, and material properties. These simulations help in identifying potential fire hazards, designing smoke control systems, and evaluating the thermal conditions that occupants may experience during a fire event.

Key parameters analyzed through CFD include temperature distribution, velocity profiles of gases, smoke movement patterns, and the concentration of toxic gases. These insights enable engineers to enhance building designs for better fire safety performance, ensuring compliance with regulatory standards and minimizing risks to life and property.

Moreover, CFD analysis supports the development of effective fire protection strategies by simulating different fire scenarios and validating the performance of fire protection measures, such as sprinkler systems, fire barriers, and compartmentation.

In conclusion, the application of CFD in fire scenario analysis continues to advance our understanding of fire dynamics and contributes significantly to improving fire safety measures in buildings and other infrastructures.

2.4 Thermal analysis

Once material thermal and mechanical properties are defined, as well as the variability as a function of the temperature, the thermal analysis may be carried out in order evaluate the temperature reached in the cross-section as a function of the exposing time. Following theoretical background and finite element method are discussed.

2.4.1 Theoretical background

Thermal action can be assumed as the net heat flux, \dot{h}_{net} , transferred to the structural elements and it is the sum of two contributions, the one due to the convection, $\dot{h}_{net,c}$, and irradiation one, $\dot{h}_{net,r}$.

$$\dot{h}_{net} = \dot{h}_{net,c} + \dot{h}_{net,r}$$
 Eq. 2.20

Convective part of heat flux is given by:

$$\dot{h}_{net,c} = \alpha_c (\vartheta_q - \vartheta_m)$$
 Eq. 2.21

Being:

- α_c coefficient of heat transfer by convection (W/m²K);
- θ_g gas temperature;
- θ_m structural element temperature.

The coefficient of heat transfer by convection depends on the fire model utilized and is provided form Eurocode 1 part 1-2.

The net heat flux to unit surface area due to radiation is given by the following:

$$\dot{h}_{net,r} = \phi \varepsilon_r \sigma \left[\left(\vartheta_g \right)^4 - \left(\vartheta_m \right)^4 \right]$$
 Eq. 2.22

Being:

- φ configuration factor;
- ε_r relative emissivity;
- σ Stephan Boltzmann constant;
- θ_g gas temperature;
- θ_m structural element temperature.

Relative emissivity is given by the product of surface emissivity of the member ε_m and emissivity of flames, of the fire, ε_f :

$$\varepsilon_r = \varepsilon_m \varepsilon_f$$
 Eq. 2.23

Eurocodes provide for emissivity values for steel and concrete equal to 0.7, for emissivity of flames a value of 1 may be assumed. In the case of steel structural elements heat transfer due to convection can be neglected due the material thermal conductivity and the small thickness of plate which normally a steel frame exhibits.

In this conditions the temperature in steel element cross-section can be assumed as uniform so the value of the increment in temperature $\Delta\theta_{a,t}$ in the period of time Δt can be assumed equal to the resultant of the net heat flux trough the surface In the same period of time.

$$\dot{h}_{net} A_{m,i} \Delta t = \rho_a c_a V_i \Delta \vartheta_{a,t}$$
 Eq. 2.24

$$\Delta \vartheta_{a,t} = K_{sh} \frac{A_{m,i} / V_i}{c_a \rho_a} \dot{h}_{net} \Delta t$$
 Eq. 2.25

Being:

- K_{sh} shadow effect factor;
- A_{m,i}/V_i section factor;
- A_{m,i} surface exposed;
- V_i structural element volume;
- c_a steel specific heat;
- ρ_a steel weight density;
- \dot{h}_{net} net heat flux;
- Δt period of time.

The temperature reached in specific time t, can be evaluated by the sum of any increment $\Delta\theta_{a,t}$.

$$\vartheta_a(t) = \sum_{i=1}^n \Delta \vartheta_{ai},$$
 Eq. 2.26

2.4.2 FE method

The heat transfer problem governing equation is the Fourier equation:

$$\frac{\partial}{\partial x} \left(k \frac{\partial T}{\partial x} \right) + \frac{\partial}{\partial y} \left(k \frac{\partial T}{\partial y} \right) + \frac{\partial}{\partial z} \left(k \frac{\partial T}{\partial z} \right) + Q = c\rho \frac{\partial T}{\partial t}$$
 Eq. 2.27

The FE formulation of governing Fourier equation and boundary condition, according to Robert D. Cook [15], is given by:

$$\{\partial\}^T([k]\{T_{\partial}\}) + Q - c\rho\dot{T} = 0$$
 Eq. 2.28
 $f_B = \{\mu\}^T[k]\{T_{\partial}\}$ Eq. 2.29

Where:

$$\{\partial\} = \begin{cases} \partial/\partial x \\ \partial/\partial y \\ \partial/\partial z \end{cases} \qquad \{T_{\partial}\} = \begin{cases} T_x \\ T_y \\ T_z \end{cases} \qquad \{\mu\} = \begin{cases} l \\ m \\ n \end{cases}$$

 μ is the vector of direction cosines, ∂ the vector of partial derivation and T the partial derivation in (x, y, z) direction of temperature vector, f_B the boundary heat flux, k the vector for thermal conductivity. The functional is:

$$\Pi = \int \left(\frac{1}{2} [T_{\partial}]^T [k] [T_{\partial}] - QT + c\rho T \dot{T}\right) dV$$

$$- \int \left(f_B T + h T_{fl} T - \frac{1}{2} h T^2\right) dS$$
Eq. 2.30

From this the FE equation can be evaluated from $\partial \Pi/\partial T = 0$, in which assembled arrays are denoted by upper case letters.

$$[C]\{\dot{T}\} + [K_T]\{T\} = \{R_T\}$$
 Eq. 2.31

Where [KT] is the sum of [K] assembled conductivity matrix and [H] assembled boundary convection matrix and $\{R_T\}$ is the sum of $\{R_B\}$ heat flux vector, $\{R_h\}$ boundary convection vector and $\{R_Q\}$ is the heat generation vector.

A time-varying solution may be obtained by the modal method or by direct integration. The choice is guided by the same considerations that apply in structural mechanics. If the problem is linear and if the solution is dominated by lower eigenmodes and is required over an appreciable time span, the modal method is favored. If the problem is nonlinear and sharp transient must be represented in the solution, direct integration is favored. [15]

Modal method

It is firstly needed to solve the eigenproblem:

$$([K_T] - \lambda[C])\{\bar{T}\} = \{0\}$$
 Eq. 2.32

Let $[\phi]$ be the square modal matric, then:

$$[\phi]^T[C][\phi] = [I]$$
 Eq. 2.33

$$[\phi]^T[K_T][\phi] = [\lambda]$$
 Eq. 2.34

Where [I] is a unit matrix and $[\lambda]$ is the diagonal spectral matrix. Nodal temperatures $\{T\}$ are related to generalized temperature $\{Z\}$:

$$\{T\} = [\phi][Z]$$
 Eq. 2.35

Where Z_i in $\{Z\}$ state the fraction of each normalized eigenvector that contributes to $\{T\}$. Thus, for an n-by-n system obtain n uncoupled equations, each having form:

$$\dot{Z}_i + \lambda_i Z_i = p_i$$
 Eq. 2.36

$$p_i = \{\phi\}_i^T \{R_T\}$$
 Eq. 2.37

After Eq. 2.36 is integrated with respect to time for each i used, $\{Z\}=\{Z(t)\}$ is known and Eq. 2.35 provides for $\{T\}=\{T(t)\}$.

2.5 Verification approach

Verification under fire conditions, for structures and infrastructures, can be carried out in three different domains:

- Time domain: typical in the case of prescriptive approach in which it is verified whether the resistance and stability are guaranteed for a specific period of time. Following the verification equation:

$$t_{fi.Rd} \ge t_{fi.Ed}$$
 Eq. 2.38

- Temperature domain: the temperature reached at a specific time may be lower than a critical temperature which measure the performance of the structural element. This is specifically effective for steel frame structures; the critical temperature is strongly influenced by the degree of utilization. Following the verification equation:

$$\theta_{d,t} \le \theta_{dc,r}$$
 Eq. 2.39

- Resistance domain: consisting in the evaluation of the resistance for a specific time and compare it to the stresses with the respect to the same time. It is particularly effective for isostatic structures for which stresses do not vary as a function of time. Following the verification equation:

$$R_{fi,d,t} \ge E_{fi,d,t}$$
 Eq. 2.40

Temperature domain

According to Eurocode 2 part 1-2, the verification may be carried out in the temperature domain. Except when considering deformation criteria or when instability phenomena must be taken into account the critical temperature, of a carbon steel element, is given by:

$$\vartheta_{a,cr} = 39.19 \ln \left(\frac{1}{0.9674 \mu_0^{3.833}} - 1 \right) + 482$$

Where μ_0 is the degree of utilization in cold conditions (t=0), given by:

$$\mu_0 = E_{fi,d}/R_{fi,d}$$
 Eq. 2.42

The values of critical temperature are shown in Figure 2.13 and Table 2.5.

 $\theta_{\underline{a},cr}$ $\theta_{\underline{a},cr}$ $\theta_{a,cr}$ μ_0 0.22 711 0.42 612 0.62 549 0.24 698 0.44 605 0.64 543 0.26 685 0.46 598 537 0.66 0.28 674 0.48 591 0.68 531 0.30 0.50 585 0.70 526 664 520 0.32 654 0.52 578 0.72 0.34 645 0.54 572 0.74514 0.36 636 0.56 0.76 508 566 0.38 628 0.58 560 0.78 502 0.80496 0.40 620 0.60 554

Table 2.5. Critical temperature $\theta_{a,cr}$ for values of the utilization factor μ_0

Resistance domain

According to Eurocode 2 part 1-2, design buckling resistance at time e of a compression member is given by:

$$N_{b,fi,t,Rd} = \chi_{fi} A k_{y,\vartheta} \frac{f_y}{\gamma_{M,fi}}$$
 Eq. 2.43

Where:

- $\chi_{\rm fi}$ is the reduction factor for flexural buckling in the fire design situation;
- $k_{y,\theta}$ is the reduction factor for the yield strength of steel at elevated temperature.

The value of χ_{fi} is given by:

$$\chi_{fi} = \frac{1}{\varphi_{\vartheta} + \sqrt{\varphi_{\vartheta}^2 - \bar{\lambda}_{\vartheta}^2}}$$
 Eq. 2.44

With:

$$\varphi_{\vartheta} = \frac{1}{2} \left[1 + \alpha \bar{\lambda}_{\vartheta} + \bar{\lambda}_{\vartheta}^{2} \right]$$

$$\alpha = 0.65 \sqrt{\frac{235}{f_{y}}}$$

$$\bar{\lambda}_{\vartheta} = \bar{\lambda} \left[\frac{k_{y,\vartheta}}{k_{F,\vartheta}} \right]^{0.5}$$
Eq. 2.47

The design moment resistance with a uniform temperature should be determined from:

$$M_{fi,\vartheta,Rd} = k_{y,\vartheta} \left[\frac{\gamma_{M,0}}{\gamma_{M,fi}} \right] M_{Rd}$$
 Eq. 2.48

Where:

- M_{Rd} is the plastic moment resistance of the cross-section for normal temperature design;
- $k_{y,\theta}$ is the reduction factor for yield strength of steel at elevated temperature.

The design moment resistance at time t for non-uniform temperature distribution across the cross-section may be determined from:

$$M_{fi,t,Rd} = \sum_{i=1}^{n} A_i z_i k_{y,\vartheta,i} \frac{f_{y,i}}{\gamma_{M,fi}}$$
 Eq. 2.49

Where:

 z_i is the distance from the plastic neutral axis to the centroid of the elemental area A_i; - $f_{y,i}$ is the nominal yield strength f_y for the elemental area A_i .

The design buckling resistance at time t of a member subjected to combined bending and axial compression should be verified by satisfying the following:

$$\frac{N_{fi,Ed}}{\chi_{min,fi}Ak_{y,\vartheta}\frac{f_{y}}{\gamma_{M,fi}}} + \frac{k_{y}M_{y,fi,Ed}}{W_{pl,y}k_{y,\vartheta}\frac{f_{y}}{\gamma_{M,fi}}} + \frac{k_{z}M_{z,fi,Ed}}{W_{pl,z}k_{y,\vartheta}\frac{f_{y}}{\gamma_{M,fi}}} \le 1$$
Eq. 2.50

$$\frac{N_{fi,Ed}}{\chi_{z,fi}Ak_{y,\vartheta}\frac{f_y}{\gamma_{M,fi}}} + \frac{k_{LT}M_{y,fi,Ed}}{\chi_{LT,fi}W_{pl,y}k_{y,\vartheta}\frac{f_y}{\gamma_{M,fi}}} + \frac{k_zM_{z,fi,Ed}}{W_{pl,z}k_{y,\vartheta}\frac{f_y}{\gamma_{M,fi}}} \le 1$$
 Eq. 2.51

2.6 Mechanical analysis for bridges in fire

Thermo-mechanical analysis for structures may consider the reduction in load-bearing capacity of structural elements according to reduction factors previously discussed. In a performance-based approach, in the case of an advanced FE model is used to perform the analysis, the hyperstatic effect can be properly considered in stress and strain analysis output. This approach has no limitation as it may be applied for structures and infrastructures. FE method provides for output as a function of time, this way the main result in terms of displacements, bending moments, axial forces, shear forces are known in span time of exposing to fire. As an example, starting from the case study examined in [16] [17] following some result of a thermo-mechanical analyses performed for a viaduct with simply supported prestressed concrete beams (see Figure 2.13). According to the procedures explained in previous sections, and according to [18], it is firstly needed to evaluate the cold resistance of the beam and the degree of utilization related to the quasi-permanent load combination with a combination factor for the traffic load equal to zero.

$$y_c = \frac{A_{sp}f_{ptd}}{0.8bf_{cd}} = 209.14 \ mm$$
 Eq. 2.52

$$M_{Rd,0} = A_{sp} f_{ptd} (h - c - 0.4 y_c) = 31066 \, kNm$$
 Eq. 2.53

$$q_{Ed,fi} = g_{1k} + g_{2k} = 41.25 \, kN/m$$
 Eq. 2.54

$$M_{Ed,0} = \frac{q_{Ed,fi}L^2}{8} = 8531 \, kNm$$
 Eq. 2.55

$$\mu_0 = \frac{M_{Ed,0}}{M_{Rd,0}} = 0.27$$
 Eq. 2.56

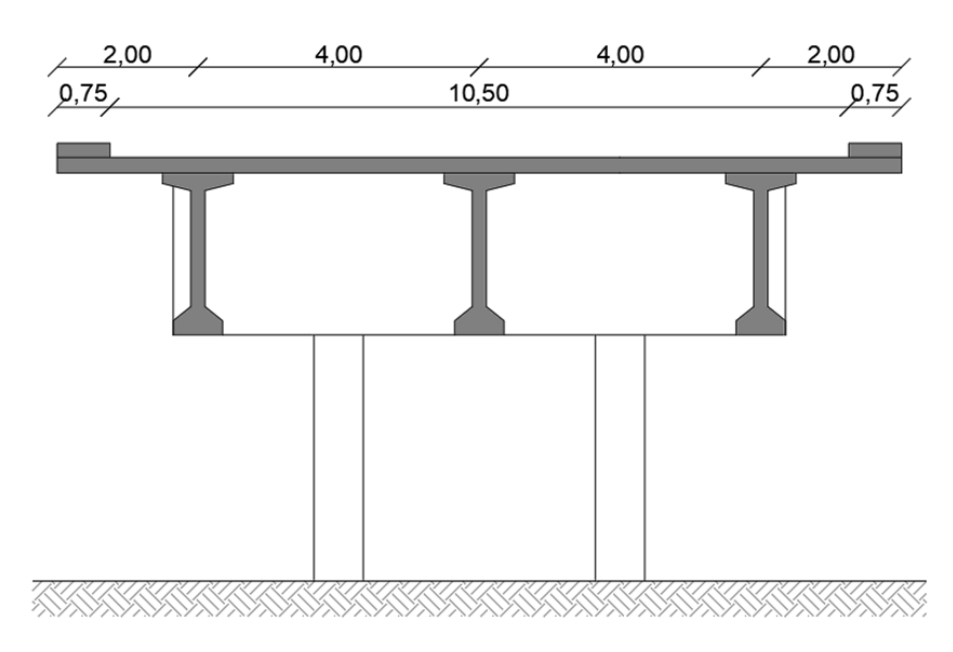


Figure 2.13. Cross-section of the bridge [16]

Next, the thermal analysis of the section of the single deck beam can be performed. The mapping of temperatures reached within the section when it is exposed to the standard hydrocarbon fire curve is shown below in Figure 2.14.

From the thermal analysis, it can be seen, first, that the temperature in the slab, and especially in the compressed part at SLU equilibrium, are low and compatible with a unit strength reduction factor. Secondly, making a focus on the lower bulb, the concrete offers good protection to the prestressing reinforcement, in fact, as can

be seen from Figure 2.15, after two hours of exposure to the standard hydrocarbon fire the temperature in the cables draws the value of about $400\,^{\circ}\text{C}$.

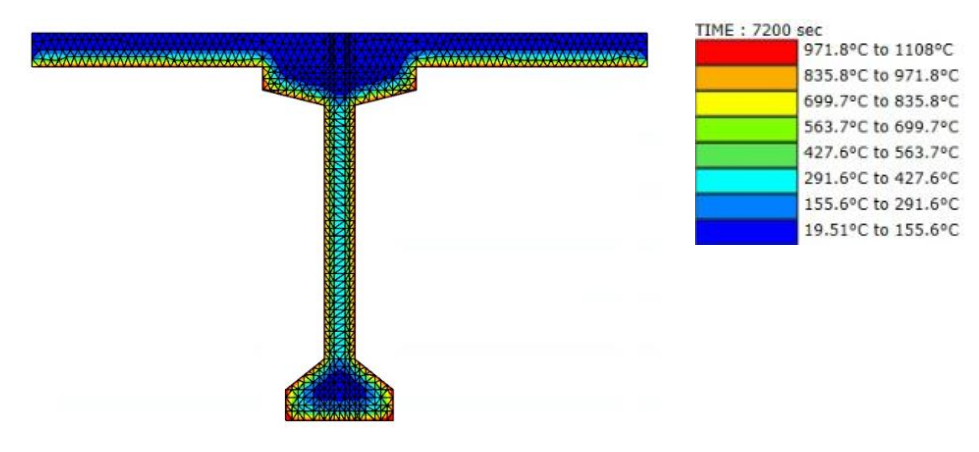


Figure 2.14. Temperatures in cross-section for t=7200s

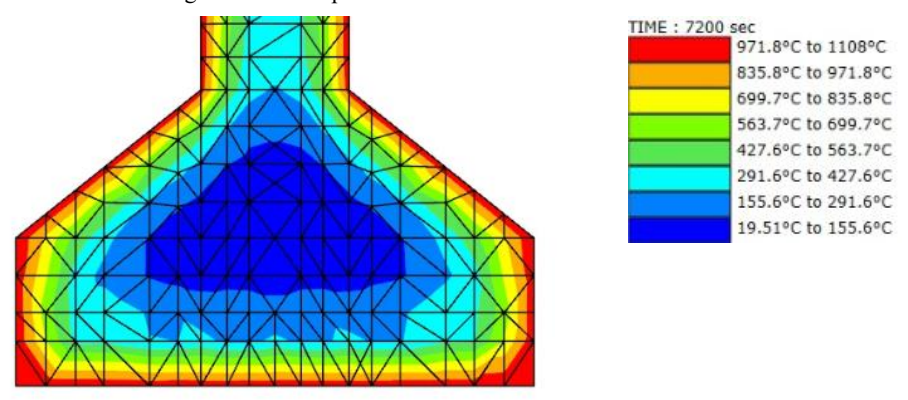


Figure 2.15. Lower bulb temperatures for t=7200s

Given the temperature, the design stress reduction factor of the compressive reinforcement can be estimated. For a temperature θ =400 °C, a factor $f_{py,\theta}$ =0.5 is derived. On the other hand, as mentioned above, the concrete slab exhibits relatively low temperatures, so the resistant moment of the hot section can be evaluated again. Moreover, for strength verification, the stressing moment can be considered constant during the thermal transient since the analyzed structure is isostatic.

$$y_{c,fi} = \frac{k_{py,\vartheta} A_{sp} f_{ptd}}{0.8 b f_{cd}} = 104.17 \ mm$$
 Eq. 2.57

$$M_{Rd,fi} = k_{py,\vartheta} A_{sp} f_{ptd} (h - c - 0.4y_c) = 15809 \, kNm$$
 Eq. 2.58

$$\left(\frac{D}{C}\right)_{fi} = \frac{M_{Ed,fi}}{M_{Rd,fi}} = 0.54$$
 Eq. 2.59

2.7 State of the art for Structural fire design and assessment of bridges

The literature review clearly indicated that there is very few information about the bridge fires occurred over time. Only the major fire accidents are well documented, and the data about the causes of fires, the traffic status at the fire beginning, the duration of the fire, the bridge features, etc. vary significantly from one source to another. Even in the cases where data are available, there is a lack of statistical models that represent the interaction between the different parameters, linking them to the probability of fire-induced collapse. However, based on available statistical data, an estimation of the probability of a bridge fire and the of the structural collapse can be obtained thanks to some assumptions that simplify the above-mentioned complex relationship between the parameters, using reliable information on the number of accidents and on losses associated with fires. This approach is based on assumptions like those used by other researchers to estimate the probability of building fires. According to the National Fire Protection Association (NFPA) [19], there were 195,600 vehicle fire accidents on all US roadways in 2011. Based on the data collected, applying the principles of the Poisson distribution, the probability of a vehicle fire occurring each year estimated by the NFPA is P=37%.

In addition, assuming that 5% of the total traffic crashes occur near bridges, the probability of a bridge fire is estimated to be 2.27%. According to NFPA [20], a hazard having the probability between 0.1% and 10% is classified as "probable". In

addition, Wardhana and Hadipriono [21] published statistical data on the total number of highway bridges and on the number of collapsed bridges in the United States over an 11-year period (1989-2000). They also reported that in those years the total number of highway bridges was 691,060 and the one of collapsed bridges, due to various extreme loading conditions, was 503 and 16 of these collapses were caused by fires.

The assessed probability is 4.9% in agreement with the value of 3.2% estimated by Scheer [22]. Using the same procedure again, the probability of at least one bridge collapsing due to fire over a 10- and 50-year period is 27.3% and 79.8%, respectively. This clearly shows that there is a high probability of collapse induced by fire in a bridge considering a period of 50 year. In order to compare the magnitude of the fire in bridges with the one in buildings, the Poisson distribution is also applied to analyze the fires in buildings. In 2006, there were 118 million buildings in United States. In 2012, approximately 480,500 fires in buildings occurred and about 1,375,000 fires were reported in total estimating a building fire probability of occurrence equal to 29.5%.

Although there is no reliable data on the total number of buildings that collapsed in 2002, Wardhana and Hadipriono reported that the total number of collapses from various catastrophic events, including fire, was 225. Thus, the probability of a fire-induced building collapse is 12.1%. The above statistical data clearly show that the probability that a fire occurs in a building, as well as the probability of a fire-induced collapse in the building, is much higher than that of bridges. In addition, the U.S. Department of Homeland Security [23] and Eldukair and Ayyub [24] estimated that the economic consequences of residential building and bridge fires were \$7199 and \$959 million, respectively.

The consequences of fire risk in buildings are reported in current codes and, therefore, structural elements in buildings must be designed according to fire resistance requirements, since occupant safety is paramount. On the other hand, even

if the fire risk assessment of infrastructures is becoming crucial there are no requirements for design or verification of bridges in the current codes and standards. For this reason, this paper aims to investigate the structural behavior of bridges in fire conditions to propose a systematic methodology for the identification of the most vulnerable bridges to fire and for the rational fire design of them.

The statistical studies show that considering fire risk for infrastructure in a similar way to earthquake risk would lead to major economic disadvantages. However, the fire risk cannot be neglected altogether because of the consequences in terms of costs of repairing or replacing structures and the indirect economic and social costs induced by service interruption could be significant. Kodur and Naser [25] developed a methodology for determining an IF for the classification of bridges, according to the fire risk.

Even if this factor was specifically developed for bridges, the principles of this approach can be extended to develop a similar IF for the classification of tunnels. This IF considers the vulnerability to fire of the bridge structural elements, as well as the criticality of the bridge to traffic flow. The fire vulnerability of a bridge depends on the geometric dimensions, material properties, design features of its structural elements and the probability of fire nearby. Based on past bridge real fires, these aspects have been found the main factors contributing to the state of fire bridge vulnerability. The key features that define the importance of a bridge, such as fire vulnerability and critical nature, are grouped into five classes as shown in Figure 2.16.

Each class covers various parameters of influence that contribute to the calculation of the IF, which is evaluated through a weighted factors approach. Within each parameter there are various sub-parameters that determine the condition of a specific bridge [25]. Based on engineering judgment and recommendations from previous studies [22], [26], [27], [28] weightage factors are assigned to the different sub-parameters. The weightage factors, assigned on a scale of 1 to 5, carry subscripts

that define the relevant class and parameter. The overall class coefficient λ is used to assign the fire risk grade to the bridge under consideration. This is done by comparing the value of λ with the numerical scores reported in Table 2.6 [25], thus

determining the IF. The fire risk associated with bridges can be grouped into four

risk grades: low, medium, high, and critical.

Table 2.6. Risk grades and associated IF [25]

Risk grade	Overall class coefficient (λ)	IF
Critical	≥0.95	1.5
High	0.51-0.94	1.2
Medium	0.20-0.50	1.0
Low	< 0.20	0.8

The IF indicates the susceptibility of a bridge to fire hazard. For example, a bridge with an IF of 1.5 represents the most critical bridge related to fire hazard and, therefore, requires a certain level of fire protection measures to mitigate the negative impact of the fire. The weightage factors described before, were obtained by considering different types of bridges (highway, rail, etc.). Generally, the weightage factors are assigned in ascending numerical order and the largest value indicates the highest risk of fire. In the following, the criteria for assigning these factors to the sub-parameters of each class are described:

- Class I Geometrical features, material properties, design characteristics: these factors that contribute to a bridge vulnerability arise from the type of structural system, material type, girder span, number of lanes, age, bridge category and special features of service.
- 2. Class II Hazard fire likelihood: the likelihood of fire occurrence is another key factor affecting the vulnerability of bridges. Fires can occur due to accidental or human-induced fires. The hazard likelihood is primarily influenced by four parameters: response time, historical/architectural importance, threat perception and possible fire scenario.

- 3. Class III Traffic demand: traffic demand is a key factor governing the importance of a bridge from the perspective of traffic flow in the region. Two main parameters are identified, namely the Average Daily Traffic (ADT) and the facility location.
- 4. Class IV Economical impact: because of a fire event, both the structural integrity of the bridge and the efficiency of the traffic network are compromised. For example, after a fire, the damaged bridge must be closed for inspection and necessary repairs. This requires traffic deviation to nearby roads, leading to additional delays in travel times and delivery of goods, which can impact business operations. On the contrary, economic consequences can be minimal in the event of fire on bridges located in remote areas, serving very low traffic volumes, or that may have multiple alternate routes.
- 5. Class V Expected fire losses: in case of fire there are not only human and material losses, but also considerable environmental damage. However, it should be noted that statistical data on human/material losses, as well as environmental damage, are sometimes available, therefore, a qualitative assessment and technical engineering judgment may be helpful.

Table 2.7 quantifies the impacts of the fire on bridges in terms of structural damage, traffic disruption and human casualties, also describing the recommended fire resistance requirements for different fire risk categories. For example, severe fires expected to occur on bridges classified with the "high" risk rating, are expected to cause significant damage to the bridge structural elements (partial/total collapse), partial stop of operation and possible injuries/victims. Therefore, it is recommended that the structural elements of these bridges have at least one hour of fire resistance. If, on the other hand, the fire risk grade is "critical" it may result in the immediate collapse of the structure with complete loss of functionality. Further expected

consequences are human casualties and permanent closure of the bridge. In this case, the structural elements must guarantee from 1 to 2 hours of fire resistance.

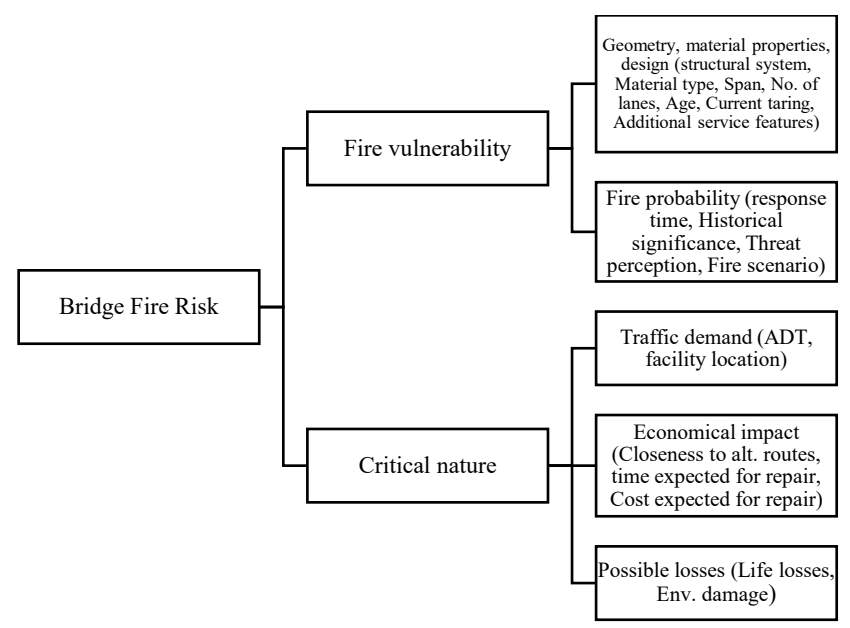


Figure 2.16. Key characteristics affecting fire risk in a bridge

Table 2.7. Description and recommendations for the risk categories [25]

Fire risk category	(IF)	Impact of fire on bridge	Recommended fireproofing to structural members
Low	1.5	Negligible impact on integrity of bridge or operation of facility, with no human losses.	No need of fireproofing
Medium	1.2	Minor impact on structural member of bridge and operation with no human losses. No investments are necessary to restore bridge following fire incident.	No need of fireproofing
High	1.0	Significant impact on structural members of bridge with partial/complete collapse of main structural elements, partial shutdown of operation with possible human injuries/losses.	At least one hour fire proofing should be provided to main structural elements
Critical	0.8	Immediate/severe impact on bridge (loss of carrying load capacity and total collapse) and complete loss of operation. Expected human casualties and permanent closure of highway/bridge.	One-to-two hour(s) fireproofing should be provided to main structural elements

2.8 Fire fragility assessment: literature review

The study of the fragility of structures is a well-established topic in academia and extensively treated in the scientific literature. This is particularly true with regard to fragility against earthquake actions. In the domain of this type of analysis, there are several works dealing with the subject of building fragility curves for existing reinforced concrete buildings [29] [30] [31], steel buildings [32] and also masonry buildings [33]. Although the cited papers do not constitute an exhaustive literature search on the subject, they are an example of how much the topic of seismic fragility of buildings is present in scientific fields. Fragility curves are obtained by methods that may sometimes differ, but nevertheless lead to consistent results. Also in the case of bridges and viaducts, the literature is extensive in the field of seismic fragility and in fact several works are available for bridges with different static schemes [34] [35].

In the field of fragility analysis of actions due to fire events, some research work in the literature is available in relation to buildings, especially steel-framed buildings. [36] [37] [38]. In the case of buildings, the performance levels to be considered for the construction of fragility curves (damage states) can be found in the Italian national standards [39] and the relevant Eurocodes.

The same is not true in the case of infrastructures, and viaducts in particular, so this thesis work aims to define novel performance levels to be considered in the design of infrastructures with respect to fire actions or vulnerability analysis and fragility assessment.

2.9 Proposed approach

The steps to be followed in the proposed approach to mitigate fire risk in bridges are shown in Figure 2.17. In the first step, the fire risk grade is quantified for the

considered bridge through the evaluation of its IF. In order to do that, relevant data on the characteristics of the bridge must be collected and analyzed. Based on the value of the IF, the fire risk associated with bridges is grouped into four risk grades (low, medium, high, and critical). If the bridge under consideration falls under a "low" or "medium" risk rating, such as a concrete bridge located in rural areas that serves a low volume of traffic, then it is considered that the bridge is less susceptible to fire damage or collapse and, therefore, additional measures may not be necessary to improve the fire safety. However, if the bridge falls under a "high" or "critical" risk rating, such as in the case of a steel suspension bridge that serves a large volume of traffic and is located above a river, then the bridge is considered a bit or very susceptible to damage/collapse caused by fire and, therefore, additional measures are required to minimize the fire risk on that bridge. In general, structural elements in steel bridges that are classified with "high" or "critical" risk grade often have an intrinsic fire resistance of much less than 45 minutes. Therefore, appropriate strategies must be developed to reduce the fire risk of these bridges to "medium" or, better, "low." This can be done through the development of relevant strategies to improve the fire resistance (FR) of main bridge structural elements. One useful strategy is the application of fire protection (insulation) to main structural elements of a steel bridge. The applied fire protection should provide $60 \div 120$ minutes of fire resistance to the selected bridge structural elements, significantly reducing the risk of damage/collapse of the bridge. Also, several mitigation strategies can be implemented to improve fire performance and reduce the effects of fire. These measures are, generally, planned during the design phase of a bridge or implemented during maintenance. The effect of mitigation strategies on the fire risk can be quantified by evaluating again the IF. Specifically, these measures can be accounted through Class VI and the reduction in the IF value is a function of the number and type of mitigation strategies implemented for the bridge. The different mitigation strategies are grouped under three main parameters:

- security: monitoring systems, guards, restricted access zones, fire detection systems.
- laws and regulation: provide distinguished exits for large fuel tanker, limit operation timings, limit vehicle speed, limit transport size (20.000l).
- fire protection and insulation features: on site firefighting equipment, use
 of flooding agents and/or foam deluge systems, 1 or 2 hours of insulation
 to main structural members, implementing structural fire design of
 bridge.

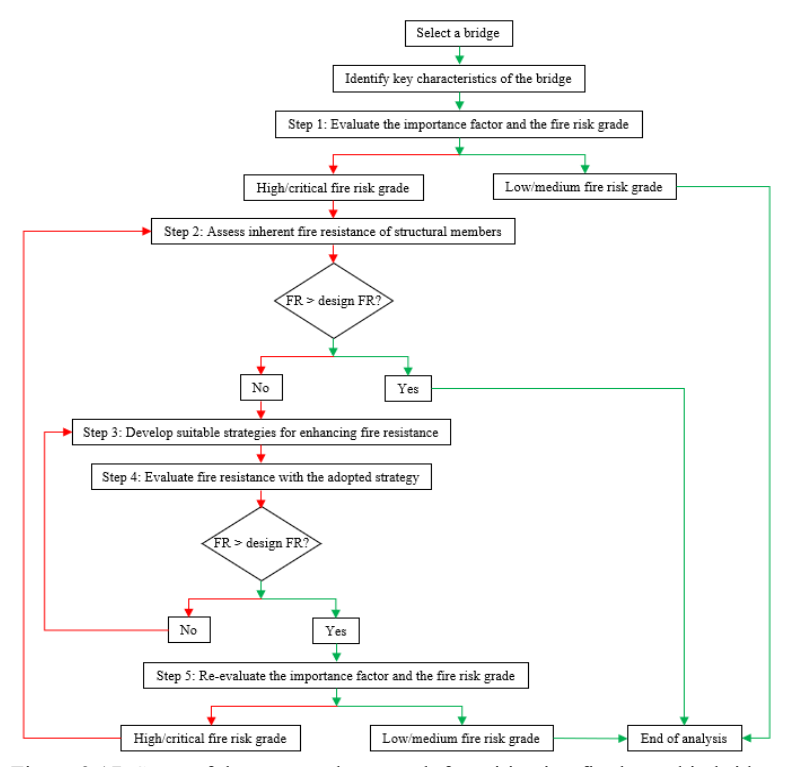


Figure 2.17. Steps of the proposed approach for mitigating fire hazard in bridges

In the case of structures, the performances required to the structural elements can be classified into five performance levels (see Table 2.8), which are valid whether a prescriptive or a performance approach is chosen. The performance level that must be ensured depending on the intended use of the buildings, thus the new national code [39] allows to select one of the following possible approaches:

- compliant solutions: i.e. prescriptive approach. No further technical evaluation is required, and it is an indirect verification because each level of performance must be linked to a REI/R requirement. This means that the load-bearing capacity (R), integrity (E) and insulation (I) requirements must be guaranteed for a fixed period of time;
- alternative solutions: i.e. performance approach. In this case the
 performance level is assigned to the examined structure by evaluating
 resistance and displacement during the fire event.

Performance
Level (PL)

I No external consequences for structural collapse

II Maintaining the fire resistance requirements for a period sufficient for the evacuation of occupants

III Maintaining the fire resistance requirements for the whole fire duration

IV Limited damage of the structure after fire duration

V Complete serviceability of the structure after fire exposure

Table 2.8. Performance levels for buildings

For structures included in performance level I, no fire resistance performance is required, except, however, verifying the presence of an appropriate separation distance on open space towards other constructions. Structures with performance level II must comply with what is defined for the performance level I and maintain, in addition, the fire resistance requirements for a period sufficient to allow the evacuation of occupants to safe zone. This period of time, in the case of a prescriptive approach, is equal to 30 minutes. The performance level III consists of the satisfaction of a resistance verification in fire conditions:

$$E_{fi,d,t} < R_{fi,d,t}$$
 Eq. 2.60

where $E_{fi,d,t}$ and $R_{fi,d,t}$ are the design value of the relevant effects of actions and the design value of the resistance of the member in the fire situation at time t, respectively. Following the performance-based approach, in order to achieve the performance level III, the structure must satisfy this verification throughout the entire duration of the fire while, according to the prescriptive approach, the verification must be satisfied for a fixed period of time. This performance level can be considered adequate for all constructions intended for activities subject to the control of the Fire Department, except those for which levels IV are required explicitly.

For levels IV and V, on the other hand, performances are required that guarantee a limited damage to the structures, maintaining the total functionality of them during and after fire (i.e. hospitals). These levels imply the satisfaction of deformability verifications at serviceability limit state:

$$f_{fi,d,t} < f_{\text{lim,t}}$$
 Eq. 2.61

where $f_{fi,d,t}$ is the design value of the deflection in the fire situation at time t and $f_{lim,t}$ is the maximum acceptable deflection value according to the required performance level. In particular, performance level IV corresponds to a limited damage of the structure, i.e. a limiting deflection of L/100, while level V implies no damage, i.e. a limiting displacement at L/250, where L is the length of the structural element.

These values of limiting displacements should be compared with the values of displacements recorded at the end of the fire, in the case of the performance approach, or at a fixed time (which is the time for which the load-bearing capacity must be guaranteed), in the case of a prescriptive approach.

Starting from these considerations, in the following sections, criteria of performance levels proposed for bridge, will be discussed.



Fire risk assessment of bridges: parametric advanced analysis and vulnerability mitigation.



3 Fire risk assessment of bridges: parametric advanced analysis and vulnerability mitigation.

According to the current international literature, the number of fires involving transportation facilities is rapidly growing in recent years due to the huge urbanization and the increased transportation of fuel and chemical material. [3] The consequences of these fires can be very significant, endangering the lives of users and causing slowdowns of traffic flow, economic losses, and partial or total collapse of facilities. Refurbishing or replacing these structures after fires would cause a high financial investment and this implies that, in the short-term, the only available choice is to extend their service life. In order to do this, it is necessary to recognize and assess the fire risk in bridges, reducing their vulnerability to fire through appropriate strategies.

Most of these fires occurred due to the collision of vehicles, e.g., tankers, freight trucks, and cars, with other vehicles or with structural components, generating fuel spills. In addition, these facilities are easily accessible and open to public, with minimal or any security, and therefore they are susceptible to fires caused by vandalism. [25]

Some of these fires caused significant economic and human losses, nevertheless, a lack of appropriate fire safety requirements in codes and standards is evident and

the transportation facilities are designed without specific fire mitigation strategies. Thus, in case of fire, these facilities can be particularly vulnerable to fire-induced damage even to collapse, affecting the performance of the transport network and causing prolonged interruptions of the traffic flow. [2]

Fires involving transportation facilities are, typically, very intense and explosive nature. This is due to the collisions that can occur at high speeds causing rapid ignition of highly flammable gasoline-based fuels, which have low flash points, in an open environment. This fuel burning produces very high temperatures (about 800 \div 900°C) within the first minutes of fire ignition and the temperature peak can exceed 1200°C.

In many cases, fires in transportation facilities are quickly extinguished by the fire rescue team. However, in some scenarios, very intense fires can induce significant degradation of the load-bearing capacity of structural elements, due to the loss of strength and stiffness of the structure, resulting in possible collapse, as in the case of some recent fires on important bridges in the United States and in European tunnels. [40] After a fire, even in the case of minor events, a proper investigation, inspection and eventually maintenance of the structure before reopening it to the public, are required. The closure of a bridge or tunnel for maintenance requires traffic deviations on alternative routes, causing significant traffic delays in the affected region.

However, as mentioned before, there is a lack of the specific guidelines for the designing of fire risk mitigation of these infrastructures. In some critical fire scenarios, where fire protection of infrastructures is necessary, designers tend to extend the fire protection requirements used for buildings to transportation structures, despite the huge differences between the types of structures. Therefore, these requirements may not be directly applicable to transportation facilities because of significant differences of the fire scenarios (fire load properties, geometry, structural parameters, etc.), producing inappropriate fire safety measures for

infrastructures. For example, combustible materials found in buildings are, typically, cellulose-based and, therefore, produce less intense fires than those occurring in bridges or tunnels, which are mainly hydrocarbon-based. The fires from cellulosic materials, represented through the standard ISO 834 fire curve, [41] reaches a temperature of about 1000°C in two hours. While, the hydrocarbon fires, typically associated to bridges, can reach a temperature of 1050°C in the first 5 ÷ 10 minutes. Another key difference is the ventilation conditions between buildings and bridges. Indeed, buildings are often designed with compartment features, having a limited availability of oxygen and fuels. Bridges, on the other hand, are in wide and open spaces, providing an unlimited amount of oxygen. When combined with many combustible materials existing in vehicles, the result is the optimal condition for rapid combustion and fire spread. In addition, for economic considerations, slender structural members are typically chosen in bridges, while class 1 elements are generally chosen for buildings. These slender elements, even if they can provide the correct strength and stiffness, are more vulnerable to fire. [9]

In general, the fire protection required for structural members can be achieved on the basis of conventional prescriptive or performance-based approaches. However, most prescriptive approaches are based on fire tests conducted in accordance with the standard fire curve, which is applicable to structural elements of buildings, since fires in buildings are mostly cellulosic in origin. [41] Thus, the use of instructions based on prescriptive approaches and derived from the ISO 834 fire, may not be appropriate for bridges structures. For example, one hour of fire resistance evaluated using ISO 834 curve may be equivalent to less than one hour of exposure to a hydrocarbon fire. On the other hand, the implementation of performance-based design methods can provide designers with efficient and cost-effective solutions. Indeed, these methods are based on rational and engineering principles to achieve specific solutions for high-risk fire bridges.

The purpose of this thesis is to provide the base of a strategy for the design and verification of bridges under fire conditions, in the context of performance-based approach. In particular, as also mentioned in section 2, the focus is on the identification of fire performance levels for bridges, giving information also about the selection and modelling of bridges fire scenarios, according to the performance-based approach principles. The proposed approach can be useful both for designers and industrial categories to assess the bridge performances in fire, not only according to prescriptive approach but also considering the performance-based one.

3.1 Fire risk assessment of bridge infrastructures

Fire exposure effects are typically neglected in structures and infrastructures design, even though they could determinate their failure. Indeed, high temperatures can reduce mechanical material properties and they can also produce redundant stresses in structural elements, therefore, to evaluate the fire risk of bridges is a crucial aspect. As a general discussion, the risk is a combination between several factors that are the probability of the event occurrence, the vulnerability and the exposed value. In terms of probability of occurrence, the technical literature provides statistical analyses of national polls about the occurrence of fire events: a comparison between the fire probability of occurrence in buildings and bridges shows that in the first case the probability is 29.5% against the 2.3% of bridges. [20]

Thus, considering these probabilities, it seems that the fire risk on bridges is not particularly relevant. However, comparing the failure probability of buildings and bridges in case of fire the same conclusion cannot be confirmed. Indeed, these probabilities of failure become more similar to each other, so the bridges intrinsic fire vulnerability leads to a common structural collapse. [24] [23]

Even if the probability of bridge fires is not particularly high, their consequences can be significant, so to design and verify bridge structures in case of fire is necessary. For this reason, a general method that allows to identify which bridges should be designed or verified in fire situation can be useful. In this regard, Kodur&Naser proposed the IF (IF) of bridges [25] for the classification of their fire vulnerability. Bridges can be classified in four classes according to the IF value, corresponding to different risk levels from low to critical. The evaluation of this factor is based on the bridge's vulnerability and their critical nature (Figure 3.2).

In particular, the bridges vulnerability is described by considering its structural features, such as the structural system, the materials, the length spans, the lanes number, etc. The critical nature measures the value exposed to the risk and, in general, this value includes all the economic losses consequent to the bridge failure (such as the costs to repair or rebuild the infrastructure), the social damage caused by the stopped viability, the ADT (vehicles/day), the economic impact, the historical importance, etc. The combination of all these factors leads to the IF evaluation that measures the fire risk grade of each bridge. The IF can be classified according to fire risk, that can vary from low to critical, as shown in Table 3.1.

Table 3.1. Risk grades and associated IF [25]

Risk grade	Overall class coefficient (l)	IF
Critical	≥0.95	1.5
High	0.51-0.94	1.2
Medium	0.20-0.50	1.0
Low	< 0.20	0.8

The method proposed by Kodur also provides the verification criteria, as shown in Table 3.2 For low fire risk, no verification of the bridges has to be performed. While, the method proposes a fire verification in the time domain by monitoring the maximum displacement, which has to be lower than L/30 (where L is the length of the bridge span) for one hour in case of high risk level or two hours in case of critical one. This verification must be led by using the hydrocarbon fire curve, in order to take into account the most probable fire nature in bridges.

3. Fire risk assessment of bridges: parametric advanced analysis and vulnerability mitigation.

Table 3.2. Description and recommendations for the risk categories [25]

Fire risk category (IF)	(IF)	Impact of fire on bridge	Recommended fireproofing to
category			structural members
Low	Low 1.5	Negligible impact on integrity of bridge or	No need of
Low	1.5	operation of facility, with no human losses.	fireproofing
		Minor impact on structural member of	
Medium	1.2	bridge and operation with no human losses.	No need of
Medium	1.2	No investments are necessary to restore	fireproofing
		bridge following fire incident.	
High	1.0	Significant impact on structural members of bridge with partial/complete collapse of main structural elements, partial shutdown of operation with possible human injuries/losses.	At least one-hour fireproofing should be provided to main structural elements
Critical	0.8	Immediate/severe impact on bridge (loss of carrying load capacity and total collapse) and complete loss of operation. Expected human casualties and permanent closure of highway/bridge.	One-to-two hour(s) fireproofing should be provided to main structural elements

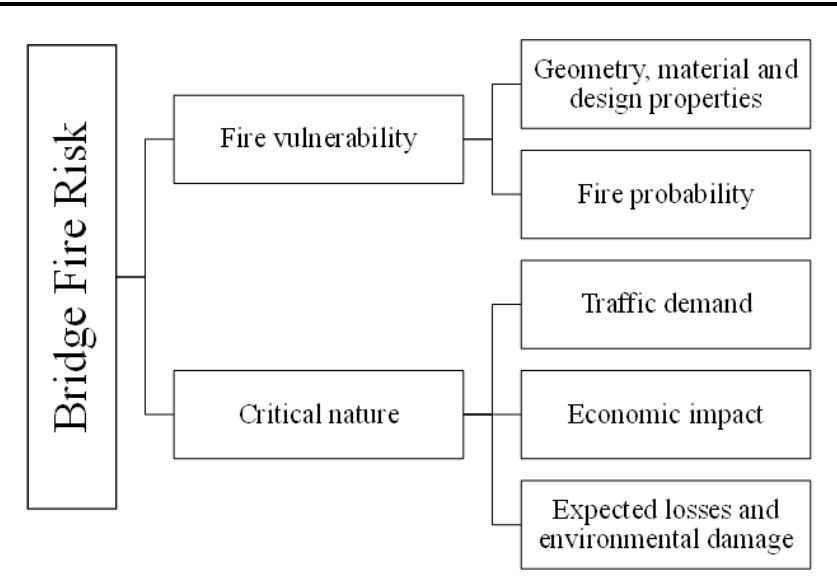


Figure 3.1. Key features influencing fire risk in bridges [25]

3.2 Fire design and safety check of bridges

In the context of the modern technical codes, as the new Italian Technical Code on Fire Prevention, [39] the fire resistance is defined as a passive fire protection measure to guarantee load-bearing and compartmentation capabilities of structures according to performance levels, selected by the designer in order to achieve the defined fire safety objectives.

The Italian code, in accordance with European ones, defines five performance levels (PL), described in previous section, depending on the importance of the building.

In order to satisfy the fixed performance level, different design solutions according to prescriptive or performance-based approaches can be chosen. The main difference between the prescriptive (PA) and the performance-based (PBA) approaches is that the first one is based on standard fire resistance tests or empirical calculation methods, using nominal fire curves. In particular, the code provides three types of conventional fire curves (standard ISO834, hydrocarbon, and external nominal curve), selected according to the nature of the combustible materials in the compartment. On the other hand, the PBA considers the complexity of structures and the inter-relationship between the various fire safety measures and systems, using specific natural fire curves, generally obtained by advanced thermo-fluid-dynamic analyses. The first step of the PBA design consists of the thermal input assessment through the selection of design fire scenarios, which represent qualitative description of the fire development, based on key aspects that characterize the real fire (e.g. compartment dimension, ventilation, fire loads, etc.).

About the verification criteria, the PA approach provides a verification in terms of minimum fire resistance in the time domain, classifying the structures in a discrete number of classes (R30, R60, etc.). All these aspects about the fire resistance of buildings cannot be directly applied to infrastructures like bridges, as many

differences have to be underlined. As also described before, in the case of buildings, the fire occurs in a compartment and the natural fire curve is influenced by the oxygen available as a function of the openings. In case of bridges, it is not possible to define a confined compartment, so the standard fire curves do not represent the real fires adequately. A better way to define the fire curve in the case of bridges is the computational fluid dynamic (CFD) analysis that allows to model the fire propagation near the bridge structure. These analyses also allow to model different fire scenarios in order to take into account the most severe fire event location for the structural bridge verification. Even if the performance-based approach seems to be the best way to design and verify bridges in case of fire, no defined criteria are provided in technical references.

Starting from the performance levels for the buildings reported in Table 2.8, the ones related to infrastructures can be defined, taking into account the IF proposed by Kodur as a measure of the fire risk of any bridges. In this work, four fire performance levels are defined (Table 3.3). The first two can be related to low and medium fire risk grades and correspond to the satisfaction of resistance criteria. The other two can be related to high and critical risk grades and, therefore, require an improved performance that can be achieved by limiting displacements. In this way the IF also sets the performance level that must be achieved in bridges.

Table 3.3. Proposed performance levels for bridges

Performance Level (PL)	Description	IF	Fire risk grade
I	The bridge must hold for the time required for evacuation	0.8	Low
II	The bridge must withstand the duration of the fire	1.0	Medium
III	Displacements should be limited to L/100 for the duration of the fire	1.2	High
IV	Displacements should be limited to L/250 for the duration of the fire	1.5	Critical

If the prescriptive based approach is used, this PLs have to be linked to a certain fire-resistant class. In particular, PLI considers a required fire resistance time (t_I)

equal to the minimum between 15 min and $2t_{\rm evac}$, where $t_{\rm evac}$ is the time to evacuate the bridge. For PLII the required time can be fixed equal to 60 min ($t_{\rm II}$), also considering the Italian regulation suggestions [21], in which this time is obtained as a function of the specific design fire load $q_{\rm f,d}$. For the bridges, the specific design fire load was considered equal to 900 MJ/m² [2]. For the satisfaction of PLIII, the structure has to preserve its bearing capacity for the time required by level II (i.e., 60 minutes) and the damage recorded at the same time $\Delta t_{\rm II}$ has to be limited to L/100. While, for the PLIV, no damage must be recorded, meaning that after 60 minutes a maximum deflection of L/250 is accepted.

3.3 Advanced fire safety check – parametric analysis

To validate the proposed performance levels and to better quantify their limits, the response of a typical steel-concrete fully composite bridge exposed to fire was investigated, by performing parametric thermo-mechanical analyses, using the FEM software SAFIR. [42] These analyses were carried out following both the prescriptive and the performance-based approach, to highlight the main differences between the two approaches and to identify how to optimize the fire design of bridges. For the first one, the hydrocarbon fire curve was chosen and the analyses were carried out on four different structural systems, variable for constraint conditions and exposure to fire. According to the performance-based approach, natural fire curves have been obtained using the software CFAST, [43] considering five fire scenarios. All the details are described below.

3.3.1 Prescriptive-based approach

Thermo-mechanical analyses were performed using the FEM software SAFIR, [42] simulating a fire close to a typical steel-concrete composite bridge. Their results allowed investigating several aspects of fire vulnerability of road bridges. In thermal analyses different emissivity values were considered to take into account the shadow

effect offered by the lower flange to the rest of the profile. According to Kodur and Aziz suggestions, [44] an emissivity value of 0.7 was chosen for the lateral and lower parts of the bottom flange, a value of 0.5 was used for the remaining part of the bottom flange and for the web, while 0.3 was chosen for the upper flange. Furthermore, according to the Eurocode 1 – Part 1-2, [14] convection coefficients $\alpha_c = 50 \frac{W}{m^2} {}^{\circ}C$ and $\alpha_c = 35 \frac{W}{m^2} {}^{\circ}C$ were used for the thermal analyses carried out with the hydrocarbon curve and with the natural fire curve, respectively. The thermal properties of steel and concrete (conductivity, specific heat, thermal expansion) vary with temperature according to Eurocodes [12] [13]. The temperatures reached in the elements of the composite beam (slab, web and flanges) were obtained as average of temperatures recorded in several nodes of each element. To study the response of a bridge under fire, only dead loads were considered applied to the structure, neglecting live loads, according to the Eurocode 1. Furthermore, Paya-Zaforteza & Garlock [45] carried out mechanical analyses considering four different load combinations and they observed that the amount of live load does not have a strong influence on both time and type of failure. Thus, live loads can be neglected. To validate the thermo-mechanical model performed with SAFIR, the experimental results of a composite beam exposed to fire was simulated. The experimental test was carried out by the British Steel Technical and Sweden Laboratories. [46] The steel profile, simply supported with a 4.5 m span, is not insulated, and was exposed to ISO 834 fire curve. The tested steel beam has a height of 357 mm and a width of 171 mm, while the concrete slab has a thickness of 126 mm. The 3D thermal analysis model is shown in Figure 3.2, while a comparison between the temperatures predicted by the FEM model and the ones measured in the fire test is shown in Figure 3.3. The upper flange of the beam has lower temperatures compared with the bottom one, due to the effect of the concrete slab which dissipates heating in the top flange.

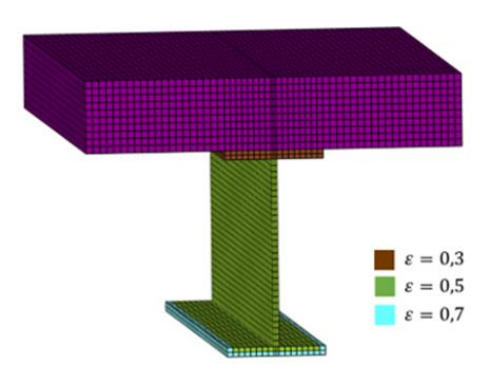


Figure 3.2. 3D model used for a thermal analysis

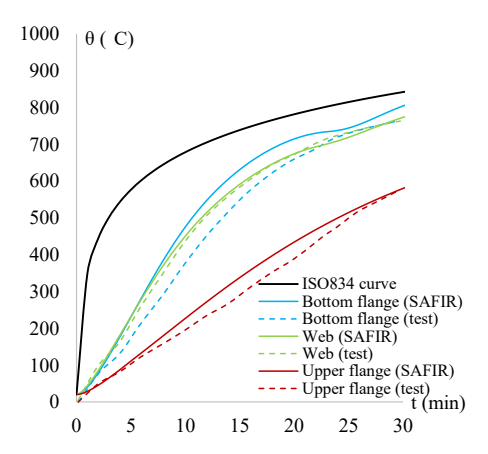


Figure 3.3. Comparison between the temperatures from SAFIR and from the experimental test

The predicted theoretical temperatures are in a very good agreement with the experimental data and the slight difference can be due to the variation in the heat-transfer parameters, such as emissivity and convection coefficients, used in the analysis compared with the real values inside the furnace.

After the SAFIR thermal analysis validation, a typological fully-composite bridge was analysed. In particular, several parametric analyses were performed, varying the constraint conditions, fire scenarios and fire protection. The cross section of the analysed bridge is shown in Figure 3.4 and the structural materials are C25/30 concrete and S355 steel. In order to understand the fire effect on this type of bridges,

Fire risk assessment of bridges: parametric advanced analysis and vulnerability mitigation.

both the prescriptive and performance-based approaches were used; all the details are described below.

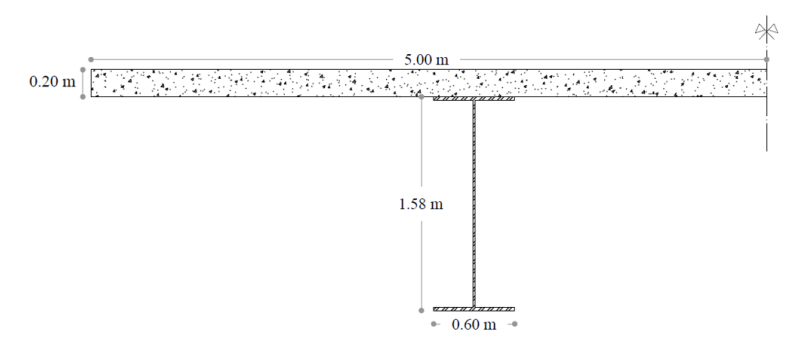


Figure 3.4. Cross-section of a typological steel-concrete fully composite bridge

Considering this typical steel-concrete bridge located in an urban area, according to the Kodur classification [15], it has an IF of 1.2 so its structural members have to guarantee a fire resistance of 60 minutes under the hydrocarbon fire curve. For this reason, it is necessary to carry out thermo-mechanical analyses for evaluating the behaviour of the bridge in fire conditions and to determine whether the bridge can guarantee one hour of fire resistance. The first step was to perform thermal analyses of the composite steel-concrete section; the resulting temperatures are shown in Figure 3.5.

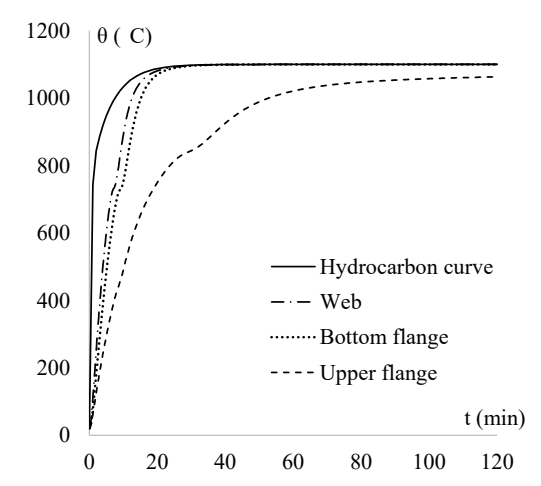


Figure 3.5. Temperature in the steel profile under hydrocarbon fire

3. Fire risk assessment of bridges: parametric advanced analysis and vulnerability mitigation.

After the thermal analyses, the mechanical ones were carried out considering different structural systems, to evaluate the failure time of the bridge as the constraint and exposure conditions vary. In particular, four systems were considered: (1) simply supported beam constrained with a hinge and a spin, (2) simply supported beam constrained with two hinges, (3a) continuous beam with two spans exposed only on the left span and system (3b) where both the spans are exposed to fire (Figure 3.6).

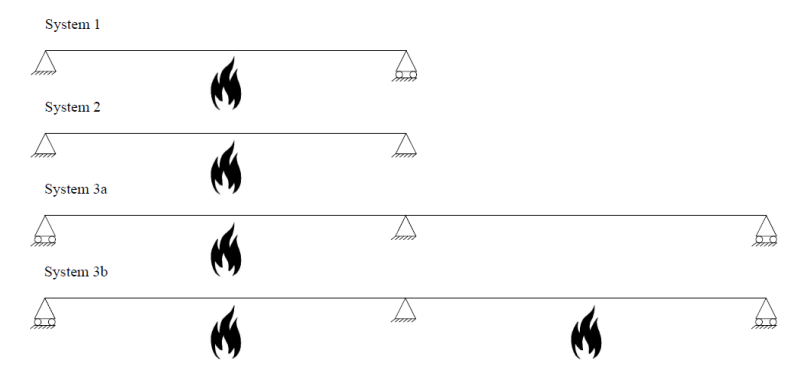


Figure 3.6. Temperature in the steel profile under hydrocarbon fire

Each span is 27.5 m long and the applied load is equal to 62 kN/m, corresponding to the structural loads (concrete slab and steel profile) and the not structural ones (road surface) of half section, for symmetry. These conditions in system 1 lead to utilization factors of 0.35 (flexural) and 0.19 (shear). The failure time (t_{R,SAFIR}) obtained with SAFIR mechanical analysis for system 1 is 414 seconds, because the bridge structural section reaches the resistant moment Mrd in the middle of the span (Fig. 6a). The decrease of the beam stiffness, due to high temperatures, leads to a consequent increase in displacements (Figure 3.9). In system 2, due to the structural redundancy and the constrained thermal expansions, the axial force increases during the first part of fire exposure, leading to an increase of bending moment Med (II-order effects) and displacements, whereas in the second part of fire exposure a tension axial force develops allowing the so-called "chain effect": the chain effect in this case is beneficial, as it avoids the flexural failure of the beam, which after almost

3. Fire risk assessment of bridges: parametric advanced analysis and vulnerability mitigation.

16 minutes reaches the maximum resistance tensile force inside the steel profile (Figure 3.7).

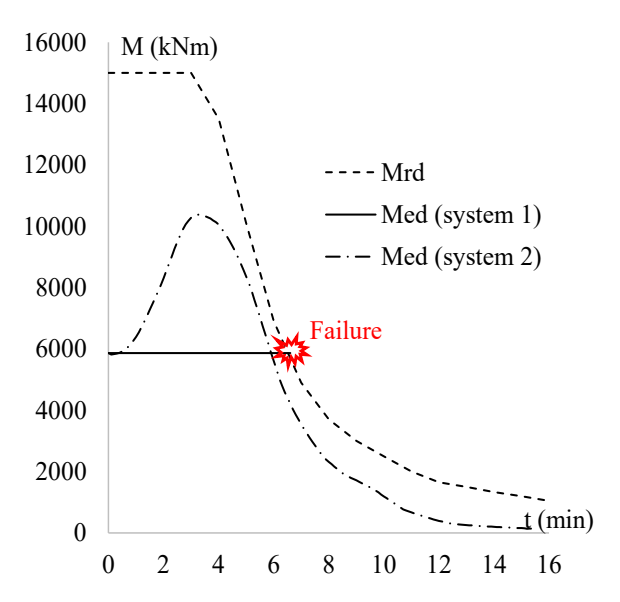


Figure 3.7. Bending moment under hydrocarbon fire systems 1 and 2

The maximum negative Med– and positive Med+ bending moments recorded in systems 3a and 3b are shown in Figure 3.8: they vary during fire exposure due to flexural redundancy and the constrained thermal deformations. The failure behaviour of the two structural systems are similar to each other: in both cases, after about 5 minutes a plastic hinge is generated on the central support, where the negative resistant moment is reached. Once the ductility is exhausted, the formation of an additional plastic hinge is not expected and positive moment is always lower than the resistant one. The trends of displacements (Δ_{max}) over time in the four structural systems are shown in Figure 3.9, where it can be seen that redundant systems guarantee much lower deformation levels.

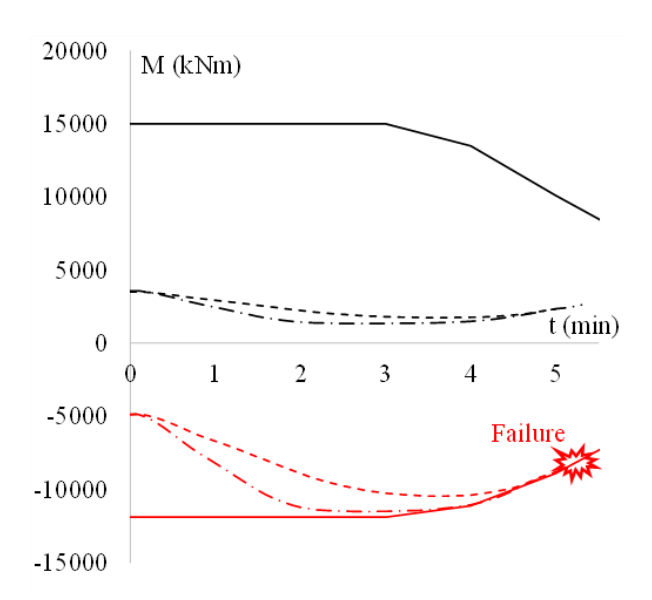


Figure 3.8. Bending moment under hydrocarbon fire systems 3a and 3b

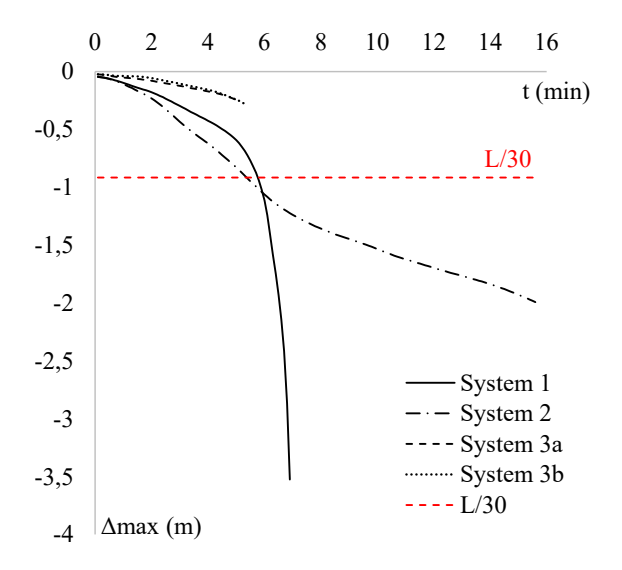


Figure 3.9. Displacement in the four systems under hydrocarbon fire

The failure times $t_{R,SAFIR}$ and the time at which the maximum displacement L/30 is reached $t_{L/30}$ in the four systems are represented in the following Table 3.4.

According to structural checks proposed by Kodur [25] for a high fire risk, the maximum displacement must be less than L/30 for at least one hour. In this case, the limit displacement L/30=0.92 m is reached at 5.8 minutes in system 1 and at 5.4 minutes in system 2, respectively. In the two continuous beam system, SAFIR does not record the L/30 displacement.

Table 3.4. Collapse times and times at which L/30 is reached

System	t _{R,SAFIR} (min)	t _{L/30} (min)
System 1	6.9	5.8
System 2	15.6	5.4
System 3a	5.0	-
System 3b	5.1	-

The L/30 limitation can be seen as a different way to interpret the collapse. This value of deflection is not particularly restrictive, and it does not allow to preserve the functionality of the structure: indeed, after this displacement value the bridge is out of service and it has to be repaired. So, considering the proposed performance level for bridges (see paragraph 3), this criterion corresponds to a performance level II; if levels III or IV are required, it is necessary to add a more severe limitation on deflections and on operation after fire. Then, in general, the failure time can be seen as the minimum value between the time at which L/30 is reached and the failure time recorded by SAFIR.

In Table 3.5, the outcome of safety checks in fire conditions is shown for each structural system, depending on the IF value. If the risk grade is low or medium, there is no need of fireproofing (NFP). If, on the other hand, the risk grade is high or critical, a fire resistance of at least one hour or between one and two hours is required, respectively.

In conclusion, performing prescriptive-based analyses, all the considered systems were not verified (NV) in fire conditions if the risk grade is high or critical.

Fire risk assessment of bridges: parametric advanced analysis and vulnerability mitigation.

Following these criteria, regardless of the constraint and exposure conditions, the application of fire mitigation strategies is required in order to reduce the IF.

Table 3.5. Result of safety check in fire conditions

System	Low (IF=0.8)	Medium (IF=1.0)	High (IF=1.2)	Critical (IF=1.5)
System 1	NFP	NFP	NV	NV
System 2	NFP	NFP	NV	NV
System 3a	NFP	NFP	NV	NV
System 3b	NFP	NFP	NV	NV

3.3.2 Performance-based approach

One of the novelties of this paper is the application of the Fire Safety Engineering (FSE) criteria to the bridges, demonstrating the satisfaction of the different fire performance levels of bridges, according to the fire risk classification proposed by Kodur. [25] In particular, to simulate fire scenarios more realistic for road bridges, natural fire curves have been obtained through fluid-dynamic analyses in CFAST [43] and the fire performance was assessed according to FSE, considering the performance levels for bridges, proposed in previous paragraph.

Fire scenarios and CFD modelling

The volume below the bridge was modelled in CFAST with two closed faces, the ceiling and the floor, while the other faces were completely opened, in order to simulate the real ventilation condition. The fire was modelled by choosing the location of the ignition point and inserting the heat release rate (HRR) curve of the vehicle subject to fire. The gas temperatures were recorded by thermocouples located at different positions, to investigate the temperature evolution at which the bridge was subjected. This model was validated with the results of advanced modelling in FDS [47] performed by Wright et al. [48] in which 14 simulations of bridge fires were presented, varying the type of vehicle (bus, HGV, 1/2 HGV and tanker) and the position of the fire (in the middle of the central span or

3. Fire risk assessment of bridges: parametric advanced analysis and vulnerability mitigation.

longitudinally/transversely translated). The studied steel-concrete composite bridge has 3 spans: the central one 35.8 m long and the two lateral ones of 25 m. To validate the model in CFAST, Case A (which corresponds to the fire of a bus located in the middle of the bridge central span) has been reproduced in CFAST, as shown in Figure 3.10. The HRR curve related to the bus fire used in the reference project is shown in Figure 3.11 and corresponds to a released thermal energy of 51250.5 MJ.

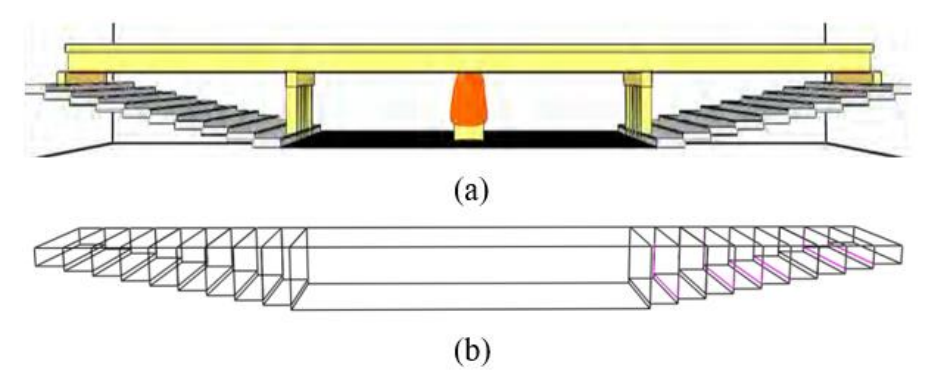


Figure 3.10. (a) FDS model (b) CFAST model

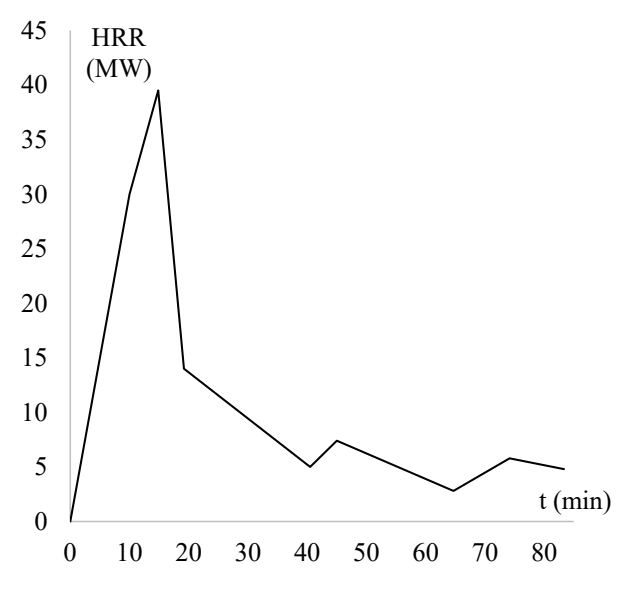


Figure 3.11. HRR curve of a bus

In the report [48], for each studied case, Wright et Al. provide the average temperature recorded in axis of the fire. Therefore, to obtain the same result, 11 thermocouples have been placed in CFAST, spaced 30 cm from each other above the fire ignition plane.

The CFAST results in terms of average temperature recorded by each thermocouple are in a very good agreement with FDS results (Figure 3.12), especially in the growing phase, while a higher temperature was simulated by CFAST in the cooling phase.

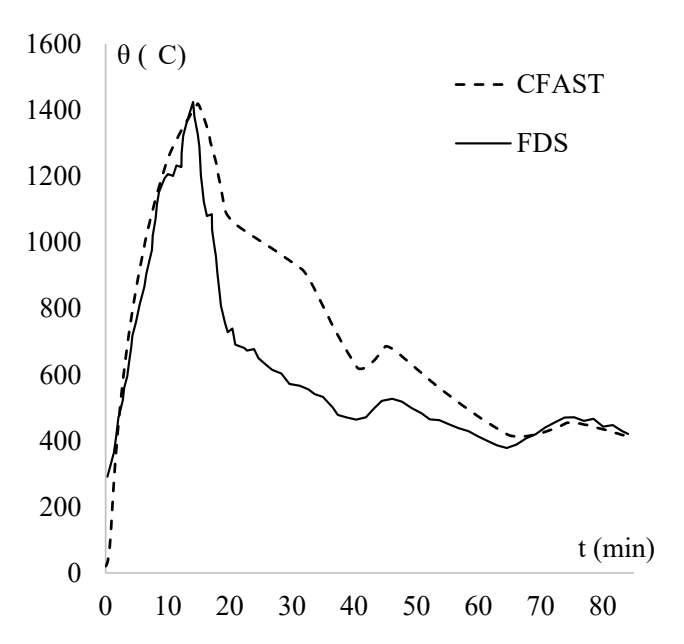


Figure 3.12. Comparison between average temperatures in FDS and CFAST

This result is justified by the fact that a zone model, being more simplified, can often achieve higher temperature than FDS ones [43]. In [48], the same analysis was carried out with other types of vehicles and other fire locations, concluding that the fire in the middle of the span is the most critical for the structure.

For this reason, all the fire scenarios analysed below will involve the fire of different vehicles located in the middle of the span.

Fire risk assessment of bridges: parametric advanced analysis and vulnerability mitigation.

After the CFAST model validation and since the good agreement between the CFAST and FDS results, the following parametric analyses were carried out with CFAST, which has a lower computational burden than FDS. The volume below the bridge was modelled in CFAST as explained above: it is a volume 55 m long, 10 m wide and 6.5 m high, corresponding to two bridge spans of equal size, which is the same previously analysed (Figure 3.6, system 3a).

Five fluid-dynamic analyses were carried out corresponding to the fire of five different vehicles: an HGV, a truck, a school bus, a car with an internal combustion engine (ICE) and an electric car (see Figure 3.13). In all these scenarios the vehicles was located in the most critical position, i.e., in the middle of the left span of the bridge.

Table 3.6. Five fire scenarios analyzed

#Scenario	Involved vehicle	Total HR (MJ)
Scenario 1	HGV	247.983
Scenario 2	Truck	100.680
Scenario 3	Schoolbus	41.432
Scenario 4	Internal combustion engine car	11.188
Scenario 5	Electric car	9.326

The HRR curves corresponding to the fires of the five vehicles are selected from literature ([29],[30],[31],[32]) and they are shown in Figure 3.13.

Fire risk assessment of bridges: parametric advanced analysis and vulnerability mitigation.

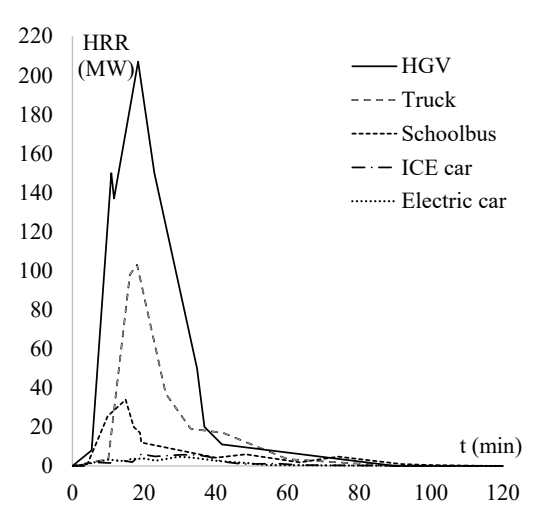


Figure 3.13. HRR curve of the five vehicles

The temperatures were recorded by 10 thermocouples arranged along the longitudinal development of the beam at a height of 4.92 m, corresponding to the lower flanges of the steel profiles. The thermocouples layout and the 10 zones in which the volume below the bridge was divided are shown in Figure 3.14. The position of each thermocouple and the dimensions of each zone are explained in detail in Table 3.7.

The volume below the left span of the bridge has been divided into nine zones of equal length (3 m) except zone 5, where the fire is located, which is 3.5 long in order to consider the maximum temperature in a larger area. The right span has been schematized as a single zone 27.5 m long, considering for safety reasons that the temperature in the whole zone was the one recorded by the thermocouple T10. The temperatures θ recorded in scenario 1 in each zone are shown in Figure 3.15, indicating that the maximum temperatures were recorded in the thermocouples T5, T4 and T6, which are the closest to fire ignition; while, in the other thermocouples the temperature rapidly decreases due to the full ventilated conditions.

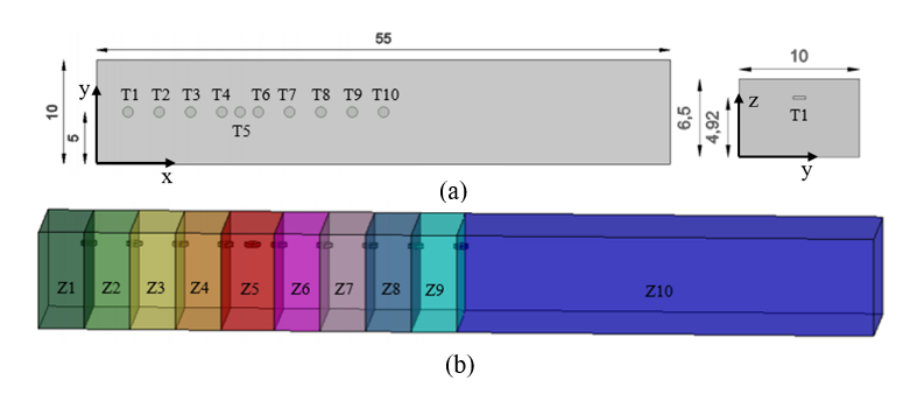


Figure 3.14. (a) Thermo-couples layout (b) discretization in 10 zones

Table 3.7. Thermocouples and zones geometric features

TC	7	Thermoc	Thermocouples coordinates			nes dimensio	ons
TC	Zone	X (m)	Y (m)	Z (m)	Length (m)	Width (m)	Height (m)
1	1	3.00			3.00		
2	2	6.00	•		3.00	•	
3	3	9.00	•		3.00	•	
4	4	12.00			3.00		
5	5	13.75	•		3.00	•	
6	6	15.50	5.00	4.92	3.00	10	6.50
7	7	18.5	•		3.00	•	
8	8	21.50			3.00	•	
9	9	24.50	•		3.00	•	
10	10	27.50			27.50	•	

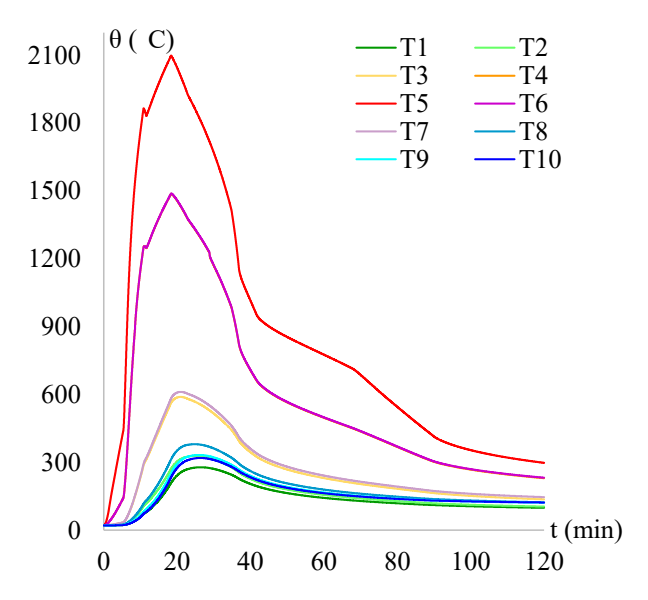


Figure 3.15. Temperatures recorded by ten thermocouples in Scenario 1

Thermo-mechanical analysis

After obtaining the natural fire curves in the fire scenarios explained in the previous paragraph, advanced thermo-mechanical analyses were carried out following the performance-based approach. As explained before, the bridge was divided in 10 zones (see Figure 3.14), in which different temperatures were recorded during the fluid-dynamic analyses; these temperature curves were used as input in the thermo-mechanical analyses. The first step was to perform thermal analyses of the bridge sections, varying the fire scenarios; Figure 3.16 represents the maximum steel temperatures $\theta_{a,max}$ reached in the profile; these temperature evolutions vary according to the ambient temperature, indeed moving away from the fire, they rapidly decrease due to the elevated ventilation. Focusing on the scenario 1-zone 5, where the maximum temperatures are reached, Figure 3.17 shows the temperature trends in the steel profile, founding that in the web and in the lower flange the temperatures are very similar to each other, both in the heating and in the cooling phases. The heating rate in the upper flange is slower, thanks to the shadow effect offered by the lower flange and to the presence of the concrete slab.

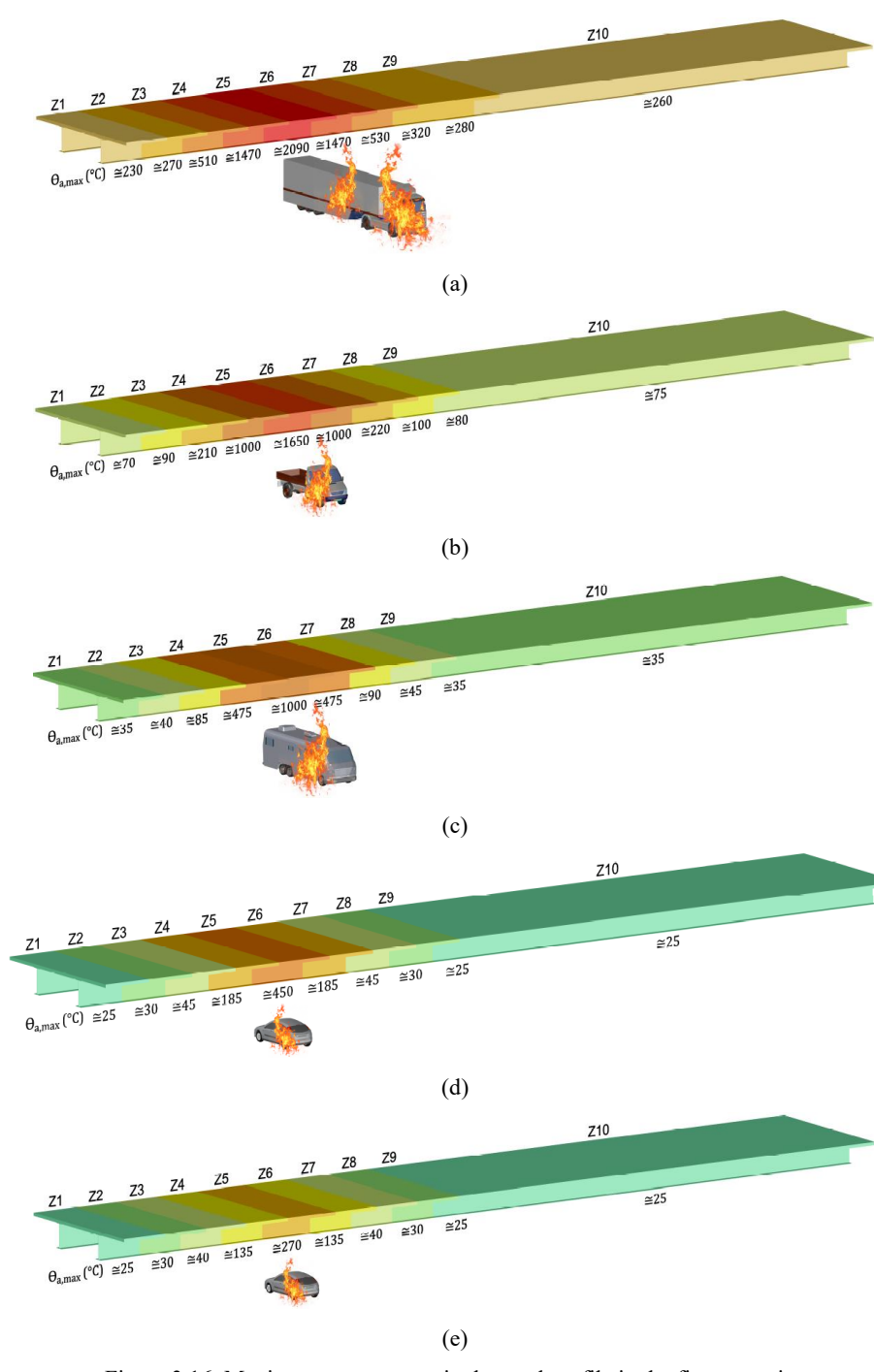


Figure 3.16. Maximum temperature in the steel profile in the five scenarios

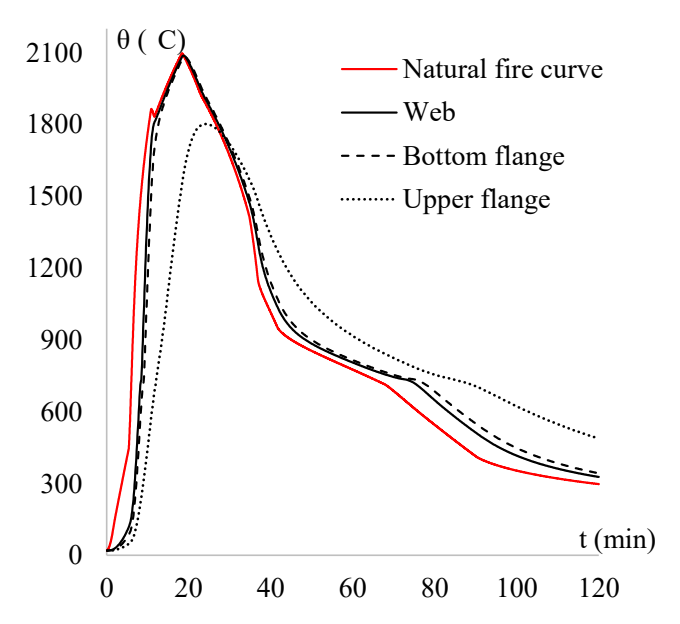


Figure 3.17. Temperatures in the steel profile (Scenario 1 – zone 5)

Known the temperatures in the steel profile, mechanical analyses were carried out to evaluate the structural behaviour of the bridge under natural fire conditions. As a result, the bridge in scenario 1 fails in about 9 minutes (Figure 3.18 and Figure 3.19). In every scenario, near the central support, where the negative moment Medis maximum, temperatures are less than 400° C (see Figure 3.16) and so no reduction in resistant bending moment $M_{Rd}^{(-)}$ is considered. On the contrary, in the section of maximum positive moment $M_{Ed}^{(+)}$, the resistant moment $M_{Rd}^{(+)}$ starts to decrease after about 7 minutes due to the high temperatures reached, since it is located very close to the fire axis. As can be seen from Figure 3.19, in about 9 minutes the resistant bending moments are reached both in the middle of the span and in the central support and, therefore, a collapse mechanism is generated with a consequent failure of the beam. A similar behaviour was recorded in Scenario 2, in which the bridge was subjected to the fire of a truck in the same position and the failure occurred in about 15 minutes. In Scenarios 3, 4 and 5 (school bus, ICE car and electric car) significantly lower temperatures are recorded and therefore the bridge does not fail

for the entire duration of the fires. For example, Figure 3.20 and Figure 3.21 shows the maximum deflection and bending moments trends in Scenario 3. It can be seen that, after the temperature peak, there is a decrease in displacements and stresses thanks to the progressive cooling of the section.

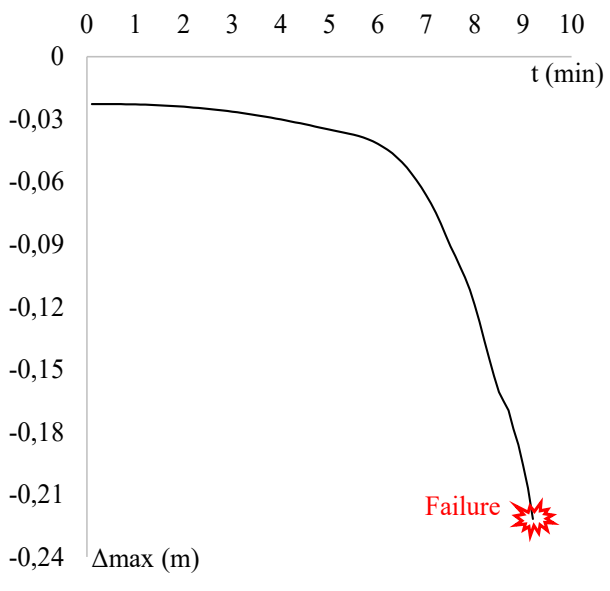


Figure 3.18. maximum deflection Scenario 1

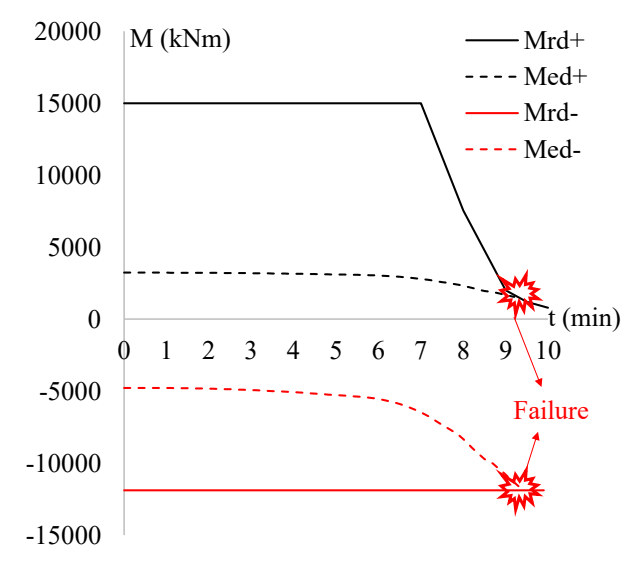


Figure 3.19. Bending moment Scenario 1

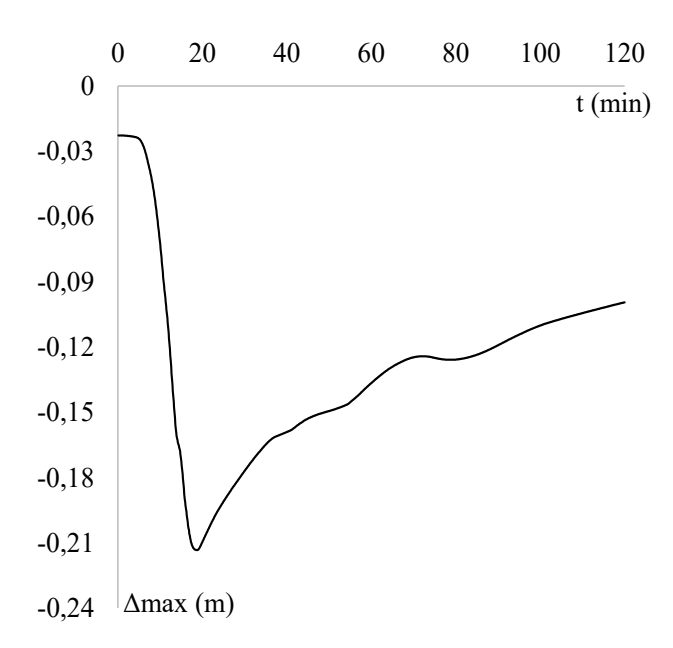


Figure 3.20. maximum deflection Scenario 3

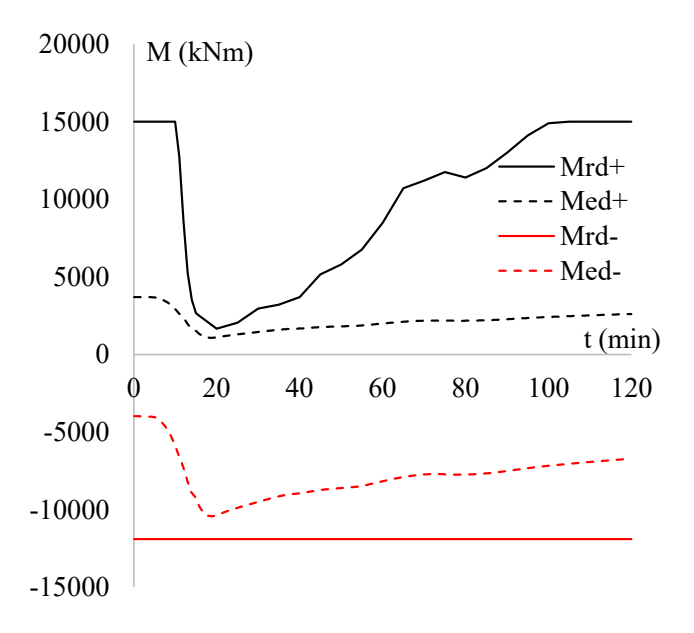


Figure 3.21. Bending moment Scenario 3

In conclusion, analysing the results of the previous analyses, the most critical situation is reached in Scenarios 1 and 2, where the fire of a HGV and a truck was

simulated. These scenarios are the most critical both from failure and displacements point of view, so, designing a fire mitigation strategy is necessary to avoid the structural failure (performance level II) or to limit the recorded damage (performance level III or IV). In case of light vehicles fires (Scenarios 3, 4 and 5) designing a fire protection is not necessary, since the bridge does not fail during the fire, showing generally limited damages (displacement amounts).

3.4 Design of fire vulnerability mitigation

Fire mitigation strategies can be implemented to prevent or reduce fire effects in structures and infrastructures. According to the concepts described in par. 2, the fire mitigation strategies affect the fire risk of a bridge and so their effect can be quantified by re-evaluating the IF. The common fire mitigation features of bridges are grouped in three main parameters: (I) security, (II) laws and regulation and (III) fire protection and insulation features, as shown in Table 3.8.

Table 3.8. Proposed fire mitigation strategies [47]

Parameter	Sub-parameter		
	Monitoring systems		
Security	Guards		
Security	Restricted access zones		
	Fire detection systems		
	Provide distinguished exits for large fuel tankers		
Layra and regulations	Limit operation timings		
Laws and regulations	Limit vehicle speed		
	Limit transport size (20.000 l)		
	On site firefighting equipment		
	Use of flooding agents and/or foam deluge systems		
Fire protection and insulation features	1h insulation to main structural members		
	2h insulation to main structural members		
	Implementing structural fire design for bridge		

In order to increase the fire performance of the analysed bridge, a passive protection with a spray applied fire resistive material (SFRM) was designed. The nomogram [49] can be used to design the protection thicknesses needed to guarantee the prescriptive requirements. For this purpose, the nomogram showing temperatures

of protected and unprotected steel sections exposed to hydrocarbon fire curve was calculated (Figure 3.22).

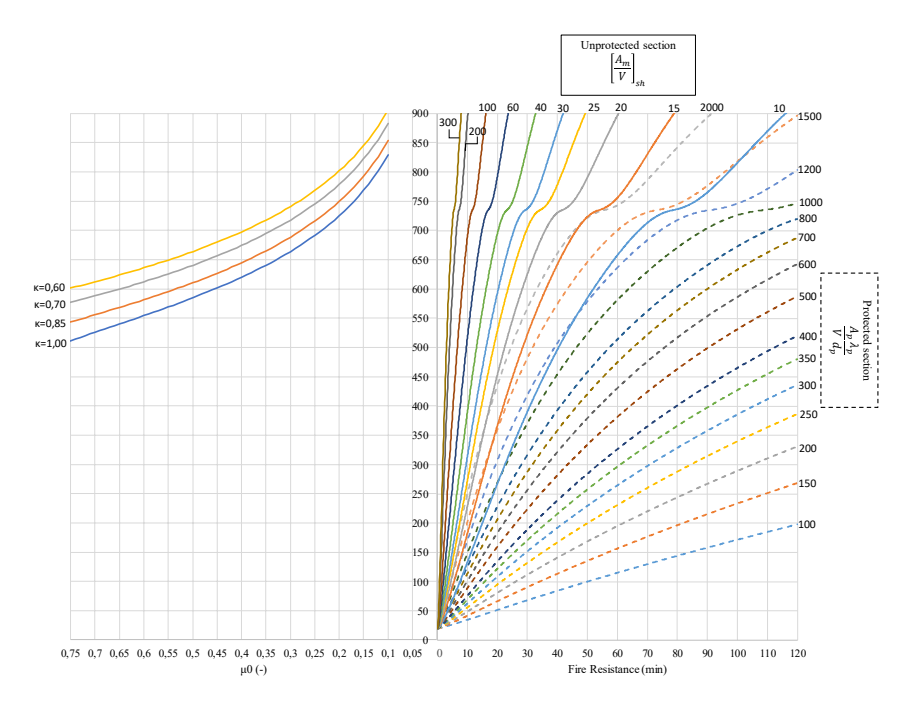


Figure 3.22. Nomogram for Hydrocarbon fire curve

Regarding the design utilization factor of system 1 (simply supported beam constrained with a hinge and a spin), the needed protection thicknesses depending on the IF are shown in Table 3.9.

Table 3.9. Protection thicknesses designed

•	IF = 0.8	IF = 1.0	IF = 1.2	IF = 1.5
	IF - 0.8	1F - 1.0	$(t_{R,req} = 60 \text{ min})$	$(t_{R,req} = 120 \text{ min})$
Protection thickness (mm)	-	-	8	16

In case of low and medium risk grade, the application of fire protection is not required. IFs of 1.2 and 1.5 (high and critical risk grades) correspond to fire resistance requirements $t_{R,req}$ of R60 and R120, respectively. These requirements are guaranteed with the application of 8 mm and 16 mm of SFRM. Temperatures in the steel profile protected with 8 mm and 16 mm of SFRM are shown in Figure 3.23;

the effect of the higher thickness protection is evident both for reaching lower steel temperatures and for reducing the heating rate in the profile (Figure 3.24).

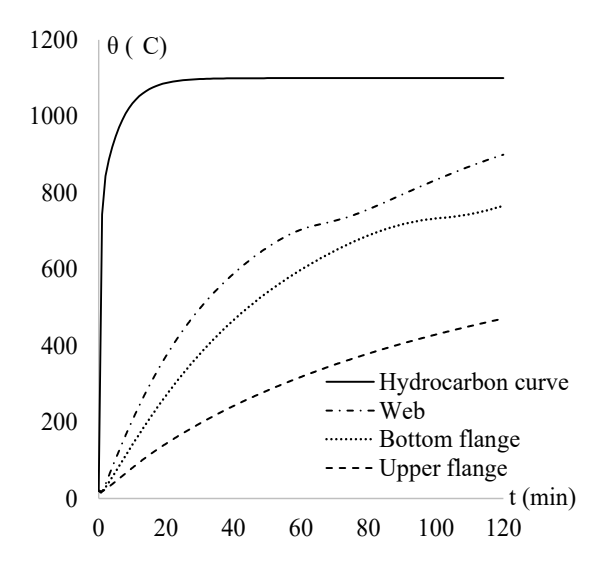


Figure 3.23. Temperature in the steel profile with 8mm SFRM under hydrocarbon fire

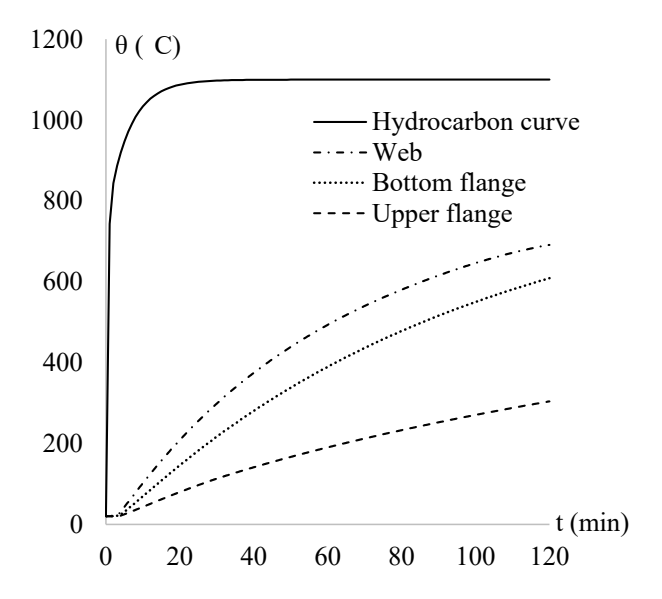


Figure 3.24. Temperature in the steel profile with 16mm SFRM under hydrocarbon fire

The results of the thermo-mechanical analyses of the protected bridges, in terms of failure time $t_{R,SAFIR}$, are shown in Table 3.10.

Table 3.10. Failure times recorded in SAFIR in the four structural system

		t _{R,SAFIR} (min)		
#System	Unprotected	8 mm (R60)	16 mm (R120)	22 mm
System 1	6.9	71.3	>120	>120
System 2	15.6	>120	>120	>120
System 3a	5.0	46.6	91.0	>120
System 3b	5.1	45.7	89.0	>120

The fire protection thickness was firstly calculated according to the utilization factor of system 1 and it is used for all the analyses listed in Table 3.10. From the same table, it can be observed that the System 1 always satisfy the required fire performance time, varying the thicknesses protection. Also, the System 2, thanks to the chain effect, is able to satisfy the fire resistance requirements. Systems 3a and 3b, on the other hand, with the same protection thicknesses do not guarantee the design resistance requirements, since the values and the distribution of the internal forces in systems 3a and 3b are very different from the ones of system 1, also for the presence of the redundant actions and their variation during the fire exposure due to the constrained thermal deformations. Therefore, for these systems, greater fire protection thicknesses have to be provided. In particular, thicknesses of 16 and 22 mm of SFRM have to be chosen for satisfying the R60 and R120 requirements (Table 3.10). As for unprotected structures, the collapse was interpreted also checking the deflection of the bridges and comparing it with the limit of L/30. The Table 3.11 shows that L/30 is reached in the systems 1 and 2, varying the protective thickness, while in systems 3a and 3b, even with protections, the structural failure occurs before reaching the displacement of L/30.

Remembering that, according to the criterion introduced in par. 2, the displacement has to be less than L/30 for 60 and 120 min if the risk grade is high or

critical, the systems 1 and 2 protected with thicknesses equal to 8 mm and 16 mm do not satisfy these requirements. A protection thickness equal to 22 mm is sufficient for system 1 to satisfy the R120 requirement, while a greater thickness would be required for system 2 because it collapse at 115 min. Therefore, for the structural schemes 1 and 2 this design criterion is more restrictive than the nomogram one.

Table 3.11. Failure times recorded in SAFIR in the four structural system

	t _{L/30} (min)					
#System	8 mm (R60)	16 mm (R120)	22 mm			
System 1	54.3	106.7	>120			
System 2	44.5	84.6	115			
System 3a	-	-	-			
System 3b	-	-	-			

Figure 3.25 represents the deflections trends in the four structural schemes varying protected systems (i.e., the protection thickness), showing that as the protection thickness increases, the structural deflection decreases; observing these figures, it is evident that for systems 3a and 3b the structural failure occurs before reaching a deflection of L/30. Finally, the risk grades and the IFs for the four structural schemes varying the protection system were re-evaluated. Table 3.12 shows that, for 8 mm of fire protection, low beneficial effects are provided and there is no reduction of the risk grade, for 16 mm beneficial effects are evident only for the systems 3a and 3b, while with 22 mm for all the systems the risk is reduced except for system 2 which is again the most critical one.

Table 3.12. Failure times recorded in SAFIR in the four structural system

-		Fire risk grade		
#System	No protection	8 mm (R60)	16 mm (R120)	22 mm
System 1			High	Medium
System 2	Hiah	High	High	High
System 3a	System 3a High		Medium	Medium
System 3b			Medium	Medium

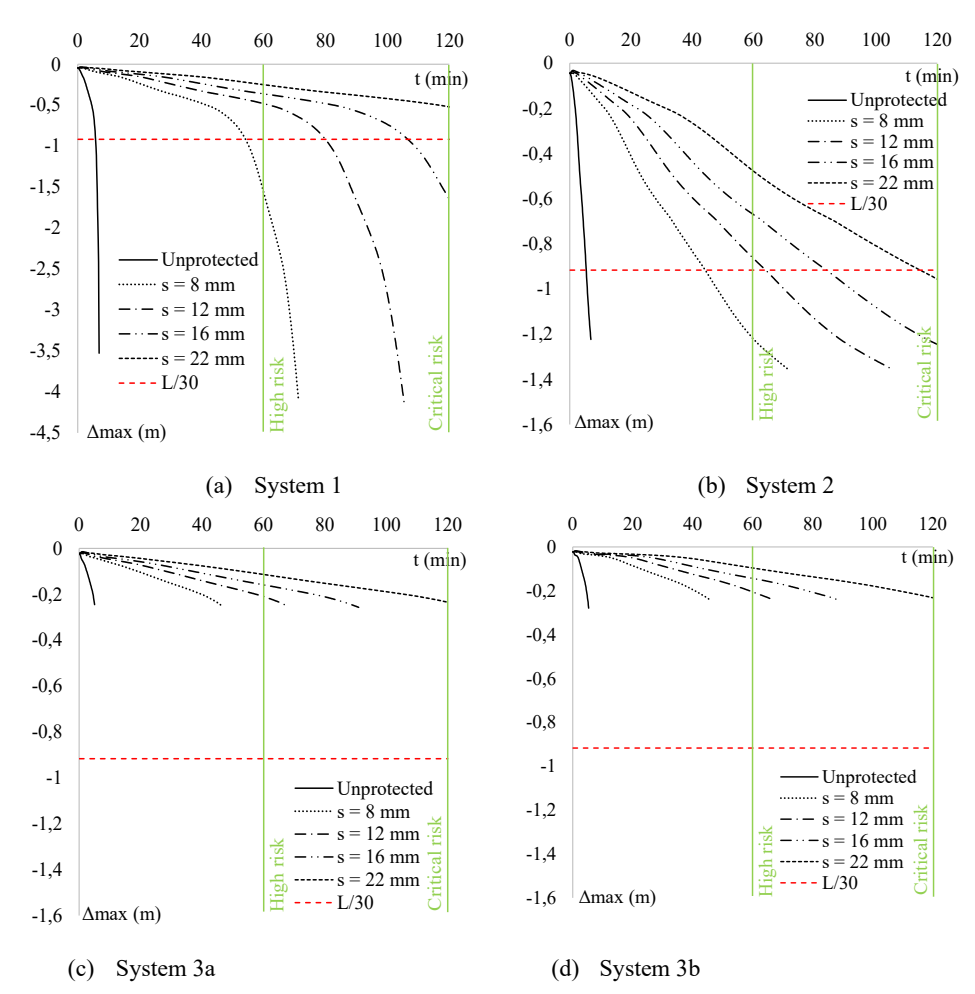


Figure 3.25. Maximum deflection in the considered structural schemes under hydrocarbon fire

Considering the analyses according to the performance-based approach, the most critical fire scenarios 1 and 2 require the application of a fire protection and so, a SFRM with a thickness of 16 mm was chosen, with a consequent reduction in steel temperatures (see Figure 3.26).

Decreasing temperatures, the bridge does not fail for the entire duration of the most critical fire scenario, with a maximum deflection of 11.3 cm recorded after 91 minutes (Figure 3.27).

Therefore, considering a fire protection of 16mm, allows to reduce the steel temperatures and also the stresses and displacements, giving to the bridge the possibility to satisfy PLIII or PLIV.

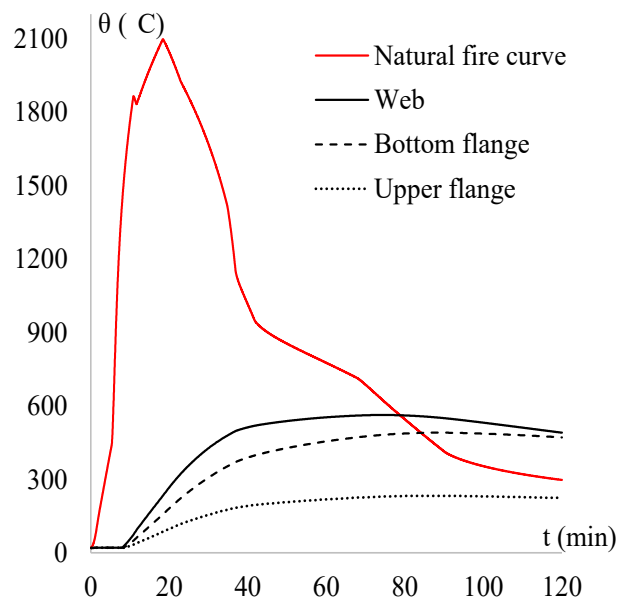


Figure 3.26. Temperatures in the steel profile protected with 16mm of SFRM (S.1 – Zone 5)

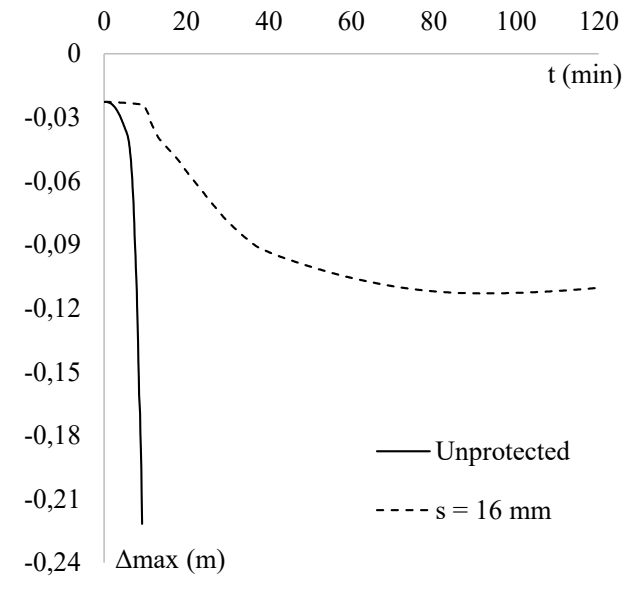


Figure 3.27. Deflection of protected an unprotected beam (Scenario 1)

3.5 Results comparison and discussion

In order to compare all the performed analyses, a benchmark between all the results is discussed in the following. The Table 3.13summarized all the results of the thermo-mechanical parametric analyses with the prescriptive approach.

The considered failure time t_{failure} is the minimum between the time at which failure is achieved in SAFIR and the one at which the limit deflection L/30 is recorded. In particular, under the hydrocarbon fire curve, the four systems failed in about 5 minutes if the beam was unprotected, not satisfying any performance level.

By considering a passive protection with an applied spray fire resistive material (SFRM) thickness of 16 mm, it is possible to verify the achievement of performance level II, III or IV, varying the structural system. To verify performance level III or IV, it is necessary to evaluate the displacement recorded at t_{II}=60 min, checking that it does not exceed L/100 or L/250 for PLIII or PLIV.

Table 3.13. Results obtained in prescriptive approach analyses

#System	Fire curve	Protection thickness (mm)	t _{failure} (min)	$\Delta_{t_{II}}$ (m)	$\Delta_{t_{11}}/L$ (-)	PL
		-	$5.8 < t_{I}$	∞	∞	-
System 1	Hydrocarbon	16	$106.7 > t_{II}$	0.36	$\frac{1}{86} \ge \left(\frac{\Delta}{L}\right)_{III}$	II
		-	$5.4 < t_{\rm I}$	∞	∞	-
System 2	Hydrocarbon	16	$84.6 > t_{II}$	0.67	$\frac{1}{41} \ge \left(\frac{\Delta}{L}\right)_{III}$	II
		-	$5.0 < t_{\rm I}$	∞	∞	-
System 3a	Hydrocarbon	16	$91.0 > t_{II}$	0.16	$\left(\frac{\Delta}{L}\right)_{IV} \le \frac{1}{172} \le \left(\frac{\Delta}{L}\right)_{III}$	III
		-	$5.1 < t_{\rm I}$	∞	00	-
System 3b	Hydrocarbon	16	$89.0 > t_{II}$	0.14	$\left(\frac{\Delta}{L}\right)_{IV} \le \frac{1}{196} \le \left(\frac{\Delta}{L}\right)_{III}$	III

The systems 1 and 2, protected with 16 mm of SFRM fails at about 107 min and 85 min respectively, so only the requirement of PLII is satisfied. The systems 3a and 3b are able to satisfy also PLIII, being the maximum displacement less than L/110

for 60 min. Table 3.14 summarizes the results of the five fire scenarios analysed with the performance-based approach. In this case, the PL verification is direct, indeed it is not necessary to define a time to evaluate the performance, but the entire duration of the fire is considered.

The system 3a was subjected to several fire scenarios, finding that the analyzed bridge, without passive fire protection, fails only in the case of HGV and truck fires, satisfying only the PLI in the truck case. In both Scenario 1 and 2 a fire protection with SFRM (thickness 16 mm) is applied, avoiding failure and giving the possibility of reaching PLIII and PLIV because the displacements are less than L/100 or L/250, respectively.

Considering the fire scenarios 3,4 and 5 the failure doesn't occur for the unprotected structure, satisfying PLII. If PLIII is required, any fire protection is still necessary, while, in the case of PLIV, only the school bus fire need a fire protection for limiting the displacement at L/250.

Table 3.14. Results obtained in performance-based approach (Scheme 3a)

#Scenario	Total HR (MJ)	Protection thickness (mm)	$\begin{array}{c} \Delta_{max} \\ (m) \end{array}$	$\Delta_{ m max}/L$ (-)	Failure	PL
Scenario 1	247.983	-	∞	œ	YES (9.2 min)	-
(HGV)	247.983	16	0.113	$\left(\frac{\Delta}{L}\right)_{IV} \le \frac{1}{243} \le \left(\frac{\Delta}{L}\right)_{III}$	NO	III
Scenario 2	100.680	-	∞	∞	YES (15.2 min)	I
(Truck)	100.080	16	0.095	$\frac{1}{290} \le \left(\frac{\Delta}{L}\right)_{IV}$	NO	IV
Scenario 3 (School bus)	41.432	-	0.211	$\left(\frac{\Delta}{L}\right)_{IV} \le \frac{1}{130} \le \left(\frac{\Delta}{L}\right)_{III}$	NO	III
Scenario 4 (ICE car)	11.188	-	0.088	$\frac{1}{313} \le \left(\frac{\Delta}{L}\right)_{IV}$	NO	IV
Scenario 5 (Electric car)	9.326	-	0.064	$\frac{1}{430} \le \left(\frac{\Delta}{L}\right)_{IV}$	NO	IV

From the comparison between the results obtained with the two approaches, it is evident that carrying out an advanced analysis following a performance-based approach allows to consider less sever and more realistic fire conditions, thanks to the use of natural fire curves, which lead to an optimization in protections design.

In performance-based analyses, a protective layer of 16 mm is enough to ensure that the bridge does not fail for the entire duration of the fire, recording limited deflections even in case of very serious fires such as the HGV or truck ones. Furthermore, in case of the most common fires, i.e., those of light vehicles, it is not necessary to provide a fire protection to the bridge, being able to satisfy performance levels III or IV.

3.6 Evolution of performance level for bridges

Following the analyses and considerations made in the previous and the current chapter, further gaps in the defined verification criteria become evident. In particular, as a general principle, in performance levels I and II, the structure must ensure non-collapse for two distinct specified periods of time. In the case of the two higher performance levels, III and IV, the criteria aim to ensure the functionality of the work even after the fire event. For this reason, along with the verification of maximum displacements, it was decided to add an additional verification of residual displacements at the end of the event, as these indicate the level of plastic deformation that occurred during the fire. Furthermore, to generalize the criteria by extending them to the cases of hyperstatic structures, it is emphasized that resistance verifications are always necessary even against the hyperstatic actions that arise during the thermal transient.

The proposed approach, nevertheless, is defined in the performance-based approach domain. Therefore, the safety assessment is carried out by considering as input a natural fire curve. The natural fire curves, as further explained below, can be evaluated based on the heat release curves by performing a CFD analysis. The performance levels reported in Table 3.15 link the definition of the importance of

the manufacts (IF) with the expected performance of the bridge. In particular, PL I and II provides for ULS performance as the criteria A, explained in the following, aims to prevent the collapse of the bridge with no prescription about the serviceability after the fire event. PL III and IV provide for SLS performance as the criteria B, also explained below, aims to ensure the that the bridge exhibits a limit damage or a complete serviceability.

Performance Level (PL)	Description	IF	Criteria
I	The bridge must hold for the time required for evacuation	0.8	A1
II	The bridge must withstand the duration of the fire	1.0	A2
III	Limited damage of the bridge after fire duration	1.2	B1-B2-B5
IV	Complete serviceability of the bridge after fire exposure	1.5	B3-B4-B5

Table 3.15. Proposed performance levels for bridges

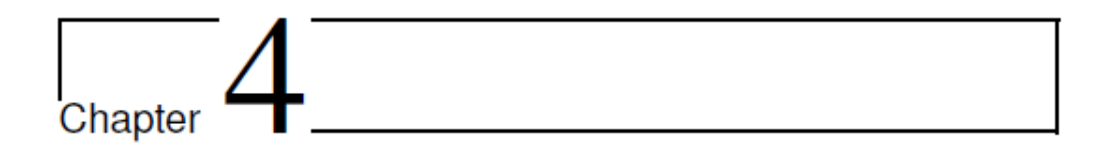
Herein the verification criteria are:

- Oriteria A: the expected performance is relative to a ULS performance as the bridge must not collapse for two different time in case of PL I or II. For these reasons no verification is needed in terms of displacement and plastic strain eventually developed into the elements. Then:
 - 1. Required fire resistance time (t_I) is the minimum between 15 min and $2t_{evac}$, where t_{evac} is the time needed to evacuate the carriage way;
 - 2. Required fire resistance (t_{II}) is set equal to the duration of the fire event.
- o Criteria B: the expected performance is relative to a SLS performance as maximum displacement the bridge develops during the event must be limited as following specified. In any case, resistance verification cannot be neglected in the case of the structure which are not statically determined. In fact, even if the structure is stressed with a fire load which

force an increasing of the displacement consistent with the limit imposed, the eventual hyperstatic stress can arise local or global failure. Then:

- Maximum displacement developed during fire event should be limited to L/100;
- 2. The net residual displacement (Δ_{fin} Δ_{in}) should be limited to 0.5 Δ_{in} , where Δ_{in} is the displacement a t=0;
- Maximum displacement developed during fire event should be limited to L/250;
- 4. The net residual displacement (Δ_{fin} Δ_{in}) should be limited to 0.2 Δ_{in} , where Din is the displacement a t=0;
- 5. Eventual resistance verification.





4 Steel bridges fire fragility

Based on the results obtained in the previous sections, another steel bridges as analyzed in this chapter. In particular, the structural-fire fragility of a viaduct with simply supported steel girder by using the performance level previously defined was assessed. The procedure to evaluate the structural-fire fragility of a bridge is shown below in Figure 4.1 which is a simplified explanation of what has been done in scientific literature [50] [51], more detailed are provided in following sections.

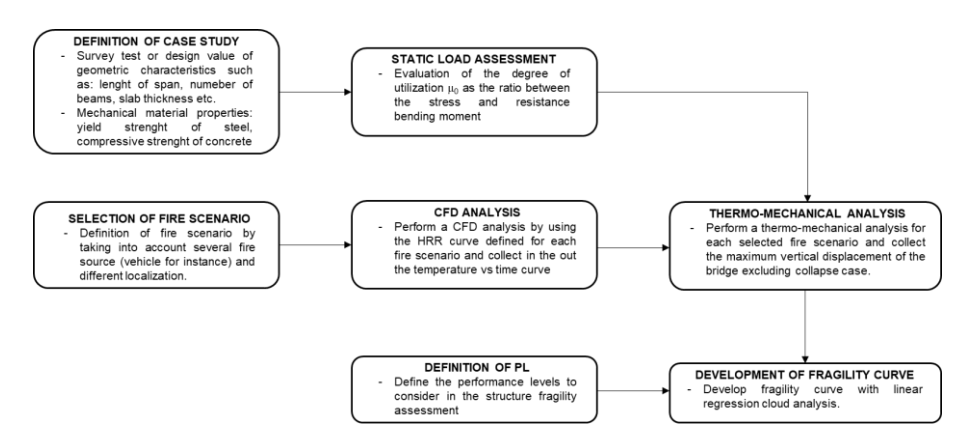


Figure 4.1. Flowchart of structural-fire fragility curve development

4.1 Case study: modelling and validation

4.1.1 Description

The bridge analyzed is a simply supported overpass, the single span is 21 m long. The deck has five hot rolled steel girder of type W36x300 (see Figure 4.2 and Table

4.1) supporting a reinforced concrete slab of 20cm thickness which has no specifically designed connection with girder, therefore no composite action can be taken into account into resistance assessment. The deck is supported by two concrete abutments with a vertical clearance of 5m. Finally, the deck is supposed to be globally simply supported, in any case out of the ten bearings one need to be fix and restraints the displacement in the longitudinal and transverse direction and one need to be unilateral restraining the displacement in the transverse direction. In addition, the structural behavior could become hyperstatic under fire condition as the deck has two expansions joints with a width of 3.8 cm. The yield strength of steel is assumed to be 250 MPa relative to A36 steel Table 4.1. Geometric properties of Girder Cross-Section

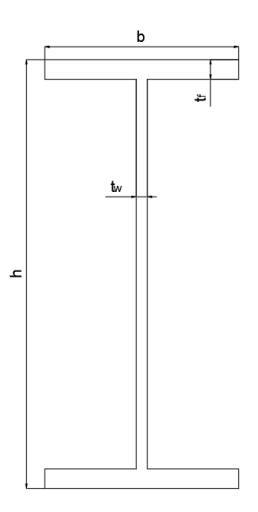


Figure 4.2. W36x300 Cross-section geometric properties

Table 4.1. Geometric properties of Girder Cross-Section

h	b	t_{f}	t_{w}	I_x	A
[mm]	[mm]	[mm]	[mm]	[cm ⁴]	[cm ²]
933.2	423.2	42.7	24.1	844949	570

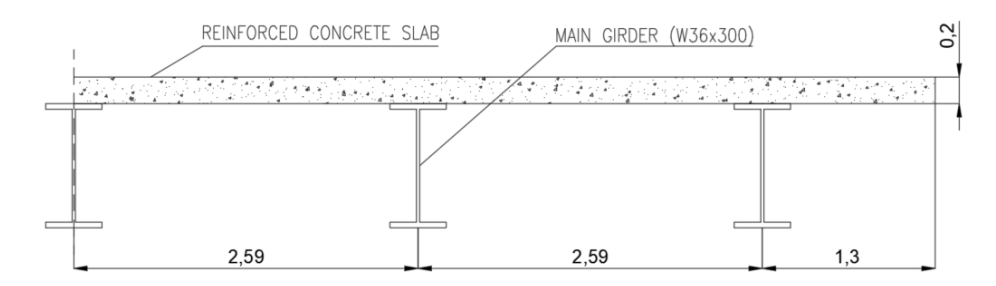


Figure 4.3. Bridge Cross-Section, adapted from [52]

4.1.2 Gravity load assessment

The gravity load considered for the evaluation of the initial degree of utilization are the following:

- Self-weight of steel girder: 4.5 kN/m;

- Weight of reinforced concrete slab: 12.9 kN/m;

- Weight of pavement: 8.6 kN/m.

The total load in the fire load combination is then assumed equal to 26 kN/m. The initial degree of utilization evaluation is shown in the following.

$$M_{Ed,fi,t,0} = \frac{q_{Ed}L^2}{8} = 1433 \ kNm$$
 Eq. 4.1

$$M_{Rd,fi,t,0} = W_{pl}f_{yk} = 5105 \, kNm$$
 Eq. 4.2

$$\mu_0 = \frac{M_{Ed,fi,t,0}}{M_{Rd,fi,t,0}} = 0.28$$
 Eq. 4.3

It is worth to underline that even if the initial degree of utilization has a huge impact on the structural-fire vulnerability assessment, for the following evaluation, and in particular for the development of the fire fragility curve, its value is basically useful only for the correct interpretation and comparison between different fragility curve obtained starting from different initial degree of utilization.

4.1.3 Structural modelling and validation

The structural modelling has been done by using SAFIR software [53]. SAFIR is a FEM software allowing to perform analysis in case of fire by considering the mechanical material properties degradation at elevated temperature and eventually the hyperstatic effect. However, the thermal condition is not mandatory as the structural analysis can also be performed in "cold" conditions thus the validation of model could be done both in "cold" conditions and at elevated temperatures. For the specific purpose of the present PhD thesis the validation process assumes an even more important phase as the case study selected exhibit some structural modelling particularity. In fact, usually simply supported steel girder viaducts has an unnegligible distance between the gravity center of the girder cross-section and the bearings. Generally, in case of isostatic scheme this condition does not produce any effect on the structural behavior in fire condition as no hyperstatic stress are transferred from the bearing to the deck. In this case, the deck has two expansion joints allowing a maximum longitudinal displacement of 3.8 cm. Then, having assumed that at least one of the bearings must restraint all the translational degree of freedom the thermal expansion of the deck is allowed only in one line of bearing and basically only in the longitudinal direction. This means that once the maximum displacement is reached the deck become hyperstatic and the bearings react with a horizontal force in the longitudinal direction.

This force produces a negative bending moment at the extremal point of the beam. The model, then, must respect two fundamental conditions, the first one is the bilinear behavior of the unilateral bearing, and the eventual reaction must be eccentrically transferred to the girder.

The bilinear behavior of the bearings is generally dealt via "gap" restraint in other FE software, anyway this solution is not available in SAFIR software and for these reasons a different approach has been adopted in order to model the "gap" restraint

in SAFIR by only using element available in software library. In the following is reported how the system works (also see [54] for more information).

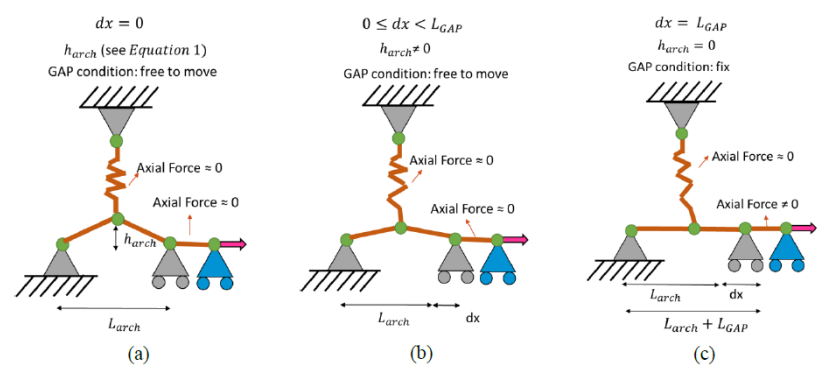


Figure 4.4. Gap restraint model: (a) at rest; (b) partially opened; (c) fully closed Adapted from [54]

$$h_{arch} = \sqrt{\frac{L_{GAP}}{2} \left(L_{arch} + \frac{L_{GAP}}{2} \right)} = 43.6 cm$$
 Eq. 4.4

The eccentricity in between the gravity center of the girder and bearings is generally modelled via rigid link in FE software, this could have allowed to take into account hyperstatic effect of the expansion joints by modelling the barycentric fiber of the girder. Anyway, in SAFIR software this is not possible, but the analyst can modify the "node-line" position. In SAFIR software the "node-line" is the node of the modelled fiber and all the action or reaction transferred to the beam are not applied on the barycentric node but in the defined "node-line".

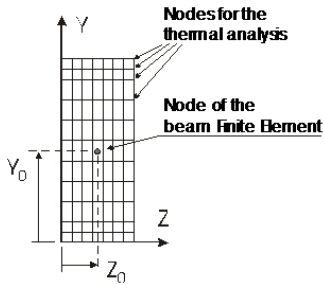


Figure 4.5. Node-line definition in SAFIR software

Modelling a different fiber respect the barycentric one makes necessary some discussion about the results provided from the Software. For correctly understand that let build a shell model of a girder with a rectangular cross-section, the beams is simply-supported and the restraints are barycentric.

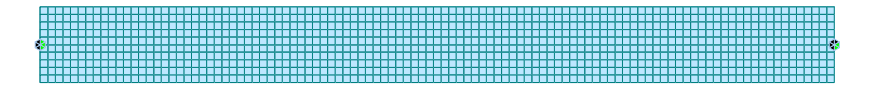


Figure 4.6. Girder shell model, barycentric restraints

Looking at Figure 4.7 it is clear that the model provides results exactly overlapped with the manual calculation as the displacement at the support is exactly zero and the stress are comparable with an emi-symmetric Navier stress distribution under self-weight.

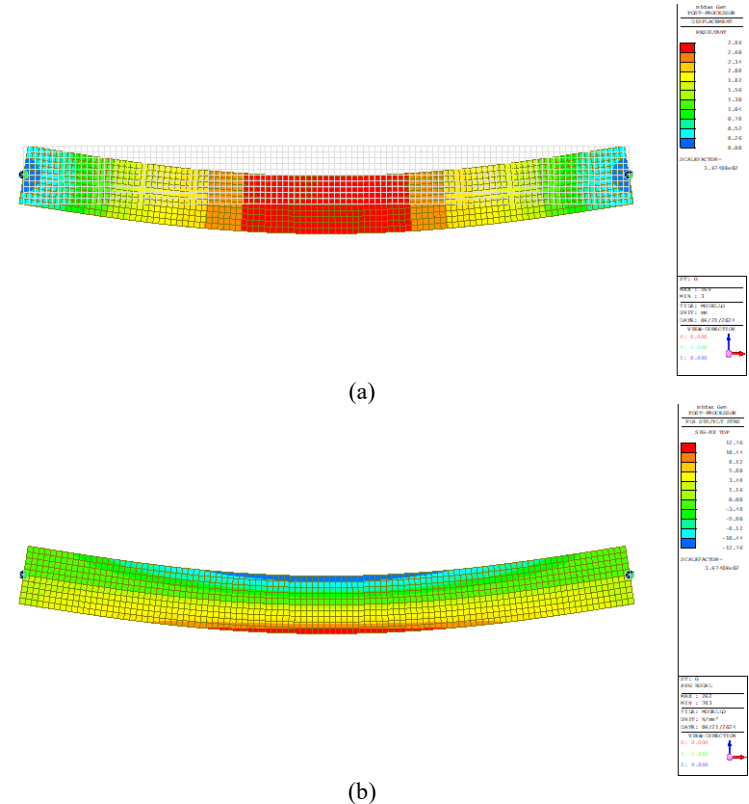


Figure 4.7. Barycentric bearings (a) Vertical displacement; (b) Stress in shell elements

Differently, model with eccentric supports Figure 4.8, coherently with the real position of the bearings for the typological viaducts analyzed in the present thesis work, the displacement and rotation at the support are correctly affected from the supports position. This suggest that the horizontal displacement of the support is the sum of the static displacement induced from the vertical load and the elongation provided from the thermal expansion in case of fire. It is, then, possible to model the structure in SAFIR software and validate its result for cold condition and in fire condition as reported below. In Figure 4.9 are reported the results in terms of displacement in x and y direction and rotation about the z axis for t=1s meaning "cold conditions"

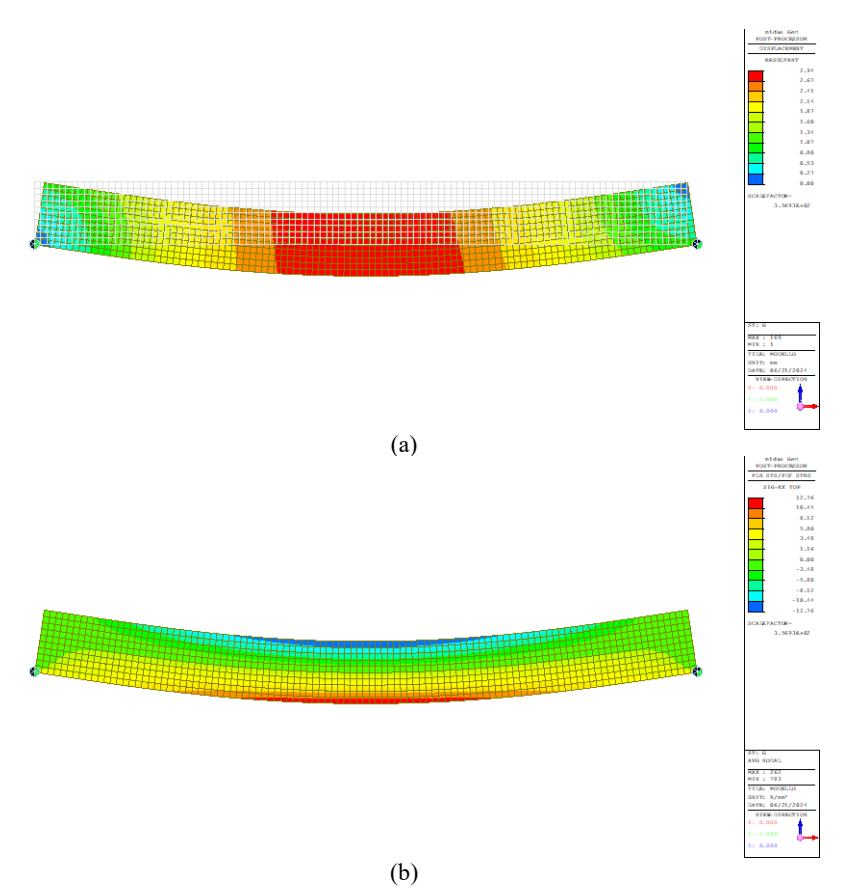
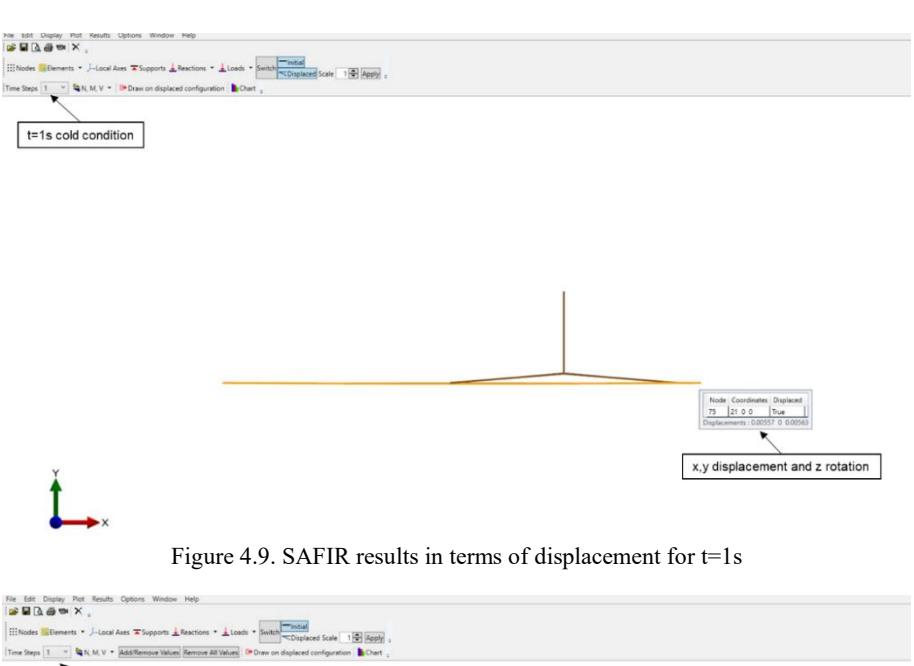


Figure 4.8. Eccentric bearings (a) Vertical displacement; (b) Stress in shell elements

The results displacement at the support are:

- δ_x =0.00557 m, longitudinal displacement;
- δ_y =0 m, vertical displacement of the support;
- φ_z =0.000563, rotation about z axis.

Displacement in x direction and z rotation can be easily evaluated by manual calculations the same also for the initial bending moment at the middle-span.



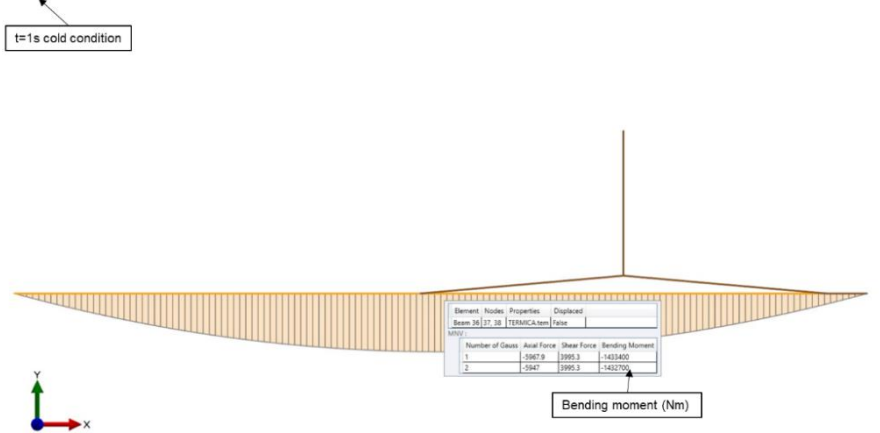


Figure 4.10. SAFIR results in terms of bending moment for t=1s

$$\varphi_z = \frac{q_{Ed}L^3}{24E_sI_x} = 0.00569$$
 Eq. 4.5

$$\delta_{x't0} = 2\varphi \frac{h}{2} = 0.00531 \, m$$
 Eq. 4.6

$$M_{Ed} = \frac{q_{Ed}L^2}{8} = 1433 \ kNm$$
 Eq. 4.7

For the model validation in case of fire a thermos-mechanical analysis was performed by considering the standard hydrocarbon fire curve as thermal input. According to SAFIR workflow it is firstly needed to perform the thermal analysis of the cross-section which leads to the color map of temperature for t=660 s reported in Figure 4.11.

It is worth nothing that the reinforced concrete slab is modelled in thermal analysis even if it is not connected to the steel girder as it effects hugely the temperature propagation through the cross-section. In any case, it is not considered in mechanical analysis as better explained in the latter.

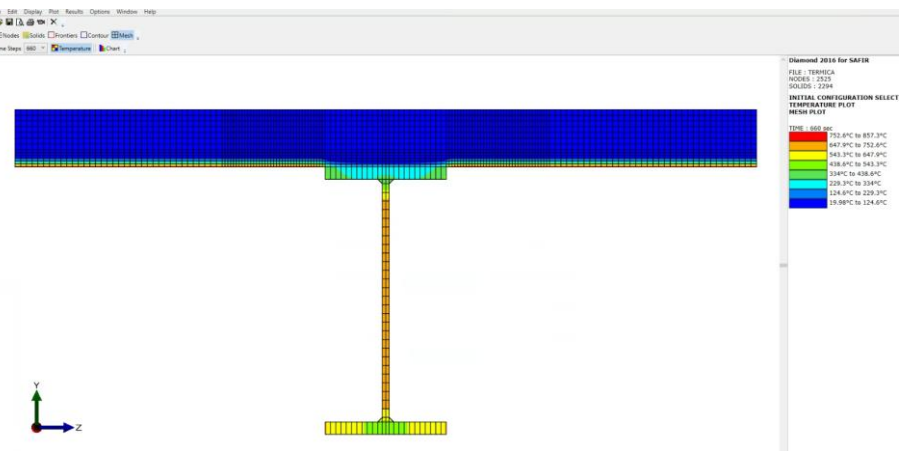


Figure 4.11. Color map of temperatures in cross-section for t=660s

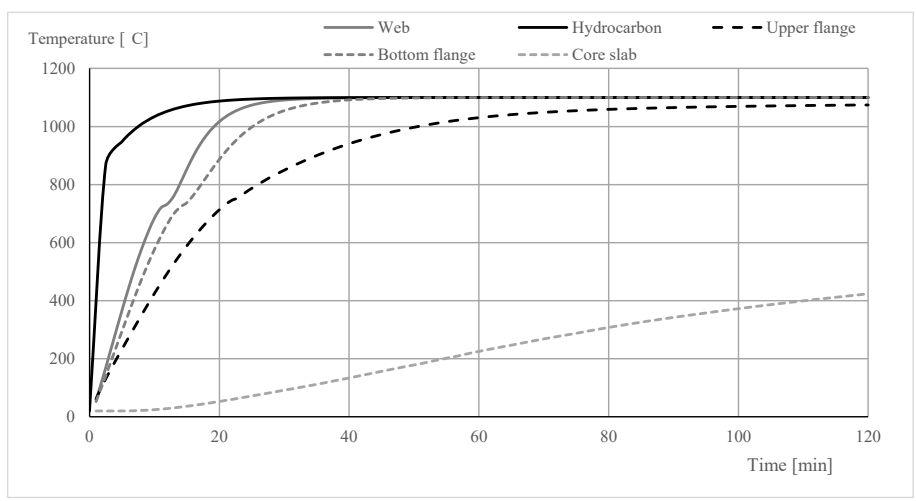


Figure 4.12. Comparison between fire curve and temperature in different part of cross-section

Validation for model behavior in case of fire is needed to ensure the gap model is correctly working in the thermal transient. To do that it is possible to plot the horizontal displacement of the support and the vertical displacement in the middle span.

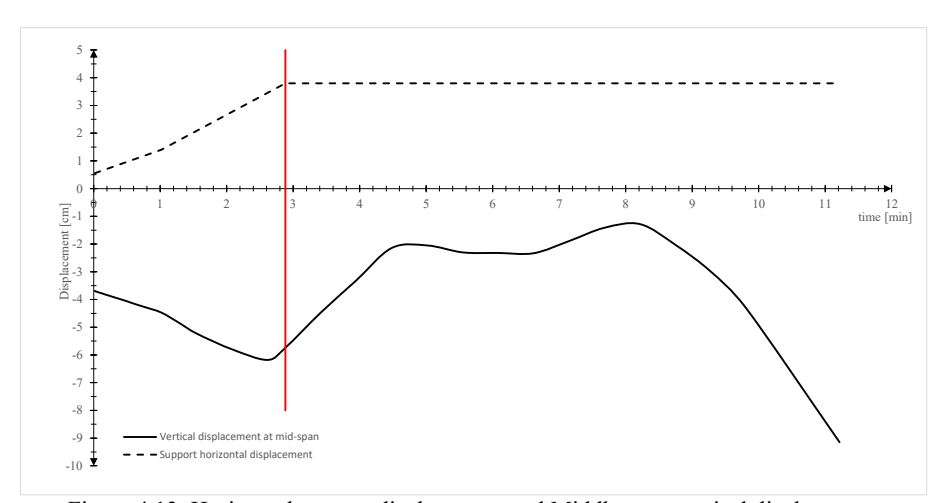


Figure 4.13. Horizontal support displacement and Middle span vertical displacement

It is correctly provided in results that the horizontal displacement of the support keeps increasing until it reaches the value of 3.8 cm equal to the gap dimension, for t = 173 s, after that it remains constant till the endo of analysis otherwise up to the collapse of the girder. At the same time, vertical displacement in the middle span

increases up to 173 s and then reduces because of the negative bending moment transferred by the hyperstatic reaction. In fact, looking at the value of the axial force in the trusses used in gap model it is also possible to detect its activation at 173 s.

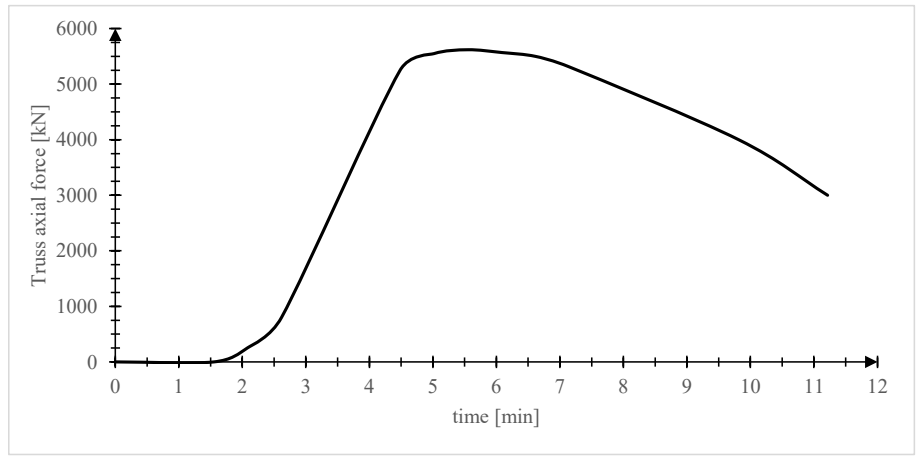


Figure 4.14. Truss axial force

4.1.4 Verification

This section aims to demonstrate that the model correctly provides for a collapse after 693s. For the purpose it has been applied the EC approach for verification in case of fire by considering a mean temperature θ =500°C.

Table 4.2. Cross-section properties

h=	933.2	mm
b=	423.3	mm
$t_w=$	24.1	mm
t _f =	42.7	mm
$h_i=$	847.9	mm
d=	799.6	mm
r=	24.1	mm

Table 4.3. Mechanical material properties

$f_y=$	250	MPa
$E_s=$	210	GPa
G_s =	81	GPa
ν=	0.3	-

Table 4.4. Input data

21	m
26	kN/m
0	kN
2987	kN
	21 26 0 2987

In the following the results of a code for the validation of this specific case study which has a general applicability are reported (for the details see Appendix A).

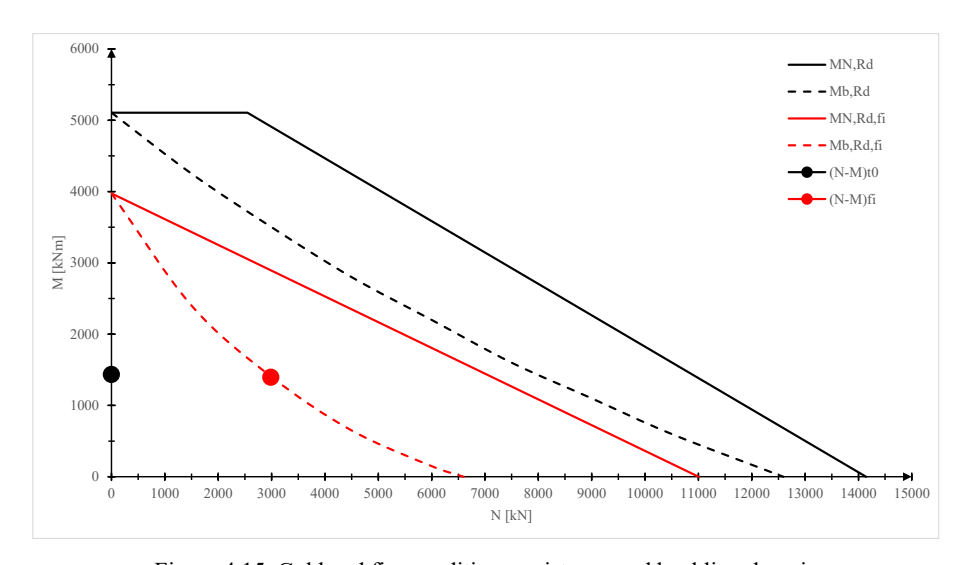


Figure 4.15. Cold and fire conditions resistance and buckling domain

The code reported provides for the resistance and stability domain in cold and fire conditions, the stress point cross the stability domain built for the mean temperature. All these considerations allow to validate the thermos-structural model.

4.2 Fire scenarios

4.2.1 Definition of Heat Release Rate curves

The Heat Release Rate curves Q (HRR) of different fire scenarios is evaluated according [12]. In particular, the following equation is provided in code:

$$Q = 10^6 \left(\frac{t}{t_\alpha}\right)^2$$
 Eq. 4.8

Where:

- Q is the rate of heat release in [W];
- t is the time in [s];

 t_{α} is the time needed to reach a rate release of 1 MW. The following Table 4.5 reports the HRR parameters of occupancy of the scenario selected for the analyses. These scenarios are selected both on the hypothesis that the place under the bridge could be subjected to an intervention of neofunctionalization and has its original functionality. These occupancies, and consequently their relative HRR parameter, are used to build different fire scenarios of which area involved in fire, HRR peak and fire load are reported in following table.

Table 4.5. HRR parameters for occupancy selected

Occupancy	Fire growth rate	ta [s]	HRR _f [kW/m ²]	$q_f [MJ/m^2]$
Parking	Really fast	75	250	200
Waste disposal site	Fast	150	250	800
Vertical farming	Medium	300	250	200
Theatre	Fast	150	500	300
Vehicle	Really fast	75	1000	2000
Truck	Really fast	75	2500	2000

Table 4.6. Fire scenario characteristics

Scenario	A _{fi} [m ²]	HRR _f [kW/m ²]	$q_f [MJ/m^2]$	HRR Peak [kW]	Q [GJ]
S1-1	10	250	200	2500	2
S1-2	20	250	200	5000	4
S1-3	40	250	200	10000	8
S1-4	120	250	200	30000	24
S1-5	200	250	200	50000	40
S2-1	20	250	800	5000	16
S2-2	100	250	800	25000	80
S2-3	200	250	800	50000	160
S3-1	20	250	200	5000	4
S3-2	100	250	200	25000	20
S4	200	500	300	100000	60
S5-1	10	1000	2000	10000	20
S5-2	48	1000	2000	48000	96
S6	48	2500	2000	120000	96

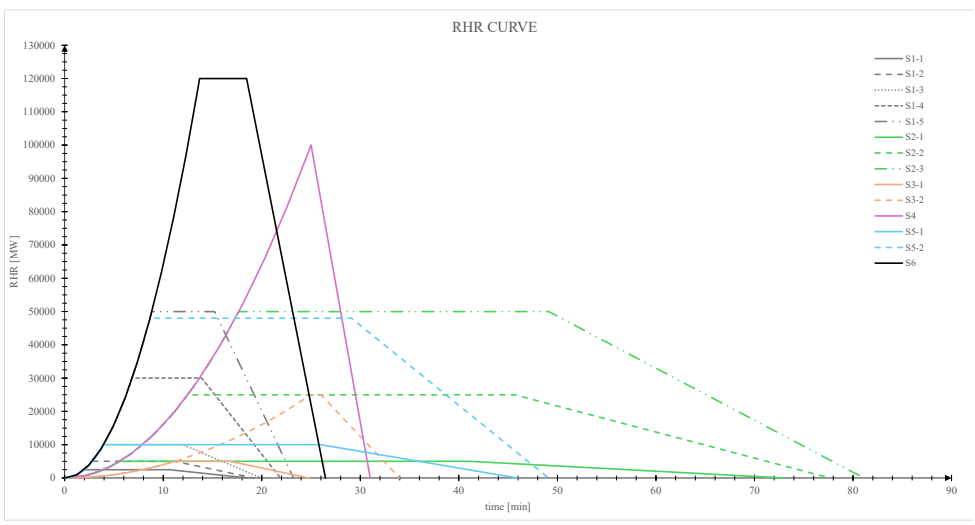


Figure 4.16. HRR Curves for selected scenarios

4.2.2 CFD analyses

In present section major result of CFD analyses is reported. The use of these advanced models was considered necessary because the zone models are too limited to the evaluation of temperature in some scenarios (i.e. when the HRR has significant peak). The analyses were performed using PyroSim software [55] which is a graphical user interface for the Fire Dynamic Simulator (FDS) [56]. The model was built accordingly to the global geometry of the viaduct and the abutments. The fire source was modelled by applying the HRR curve on the top surface of a solid of which dimensions are the one related to the specific fire scenario previously defined.

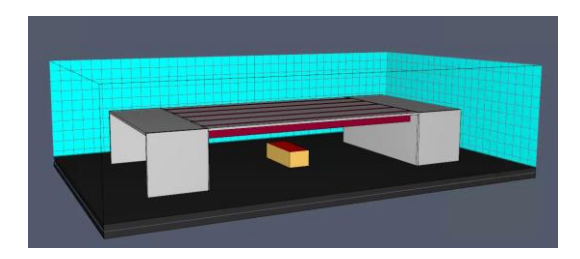


Figure 4.17. Viaduct CFD model

In the following are reported graphical results of the CFD analysis where it can be seen the dimensions of fire source, temperature propagation around the viaduct and the comparison between the HRR input and output as validation.

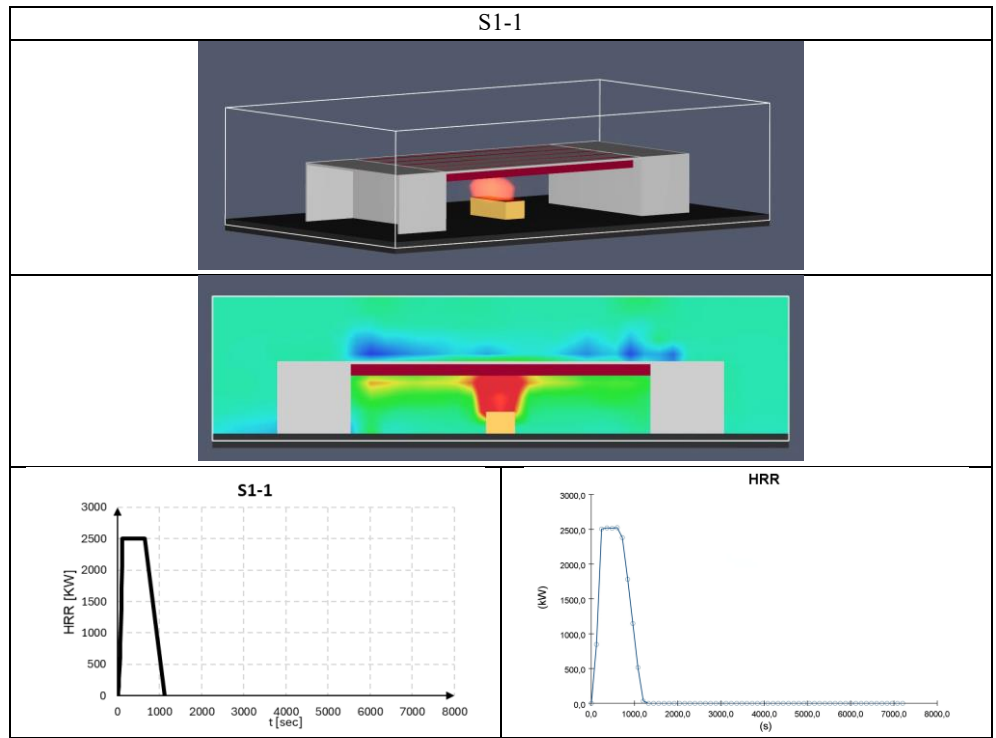
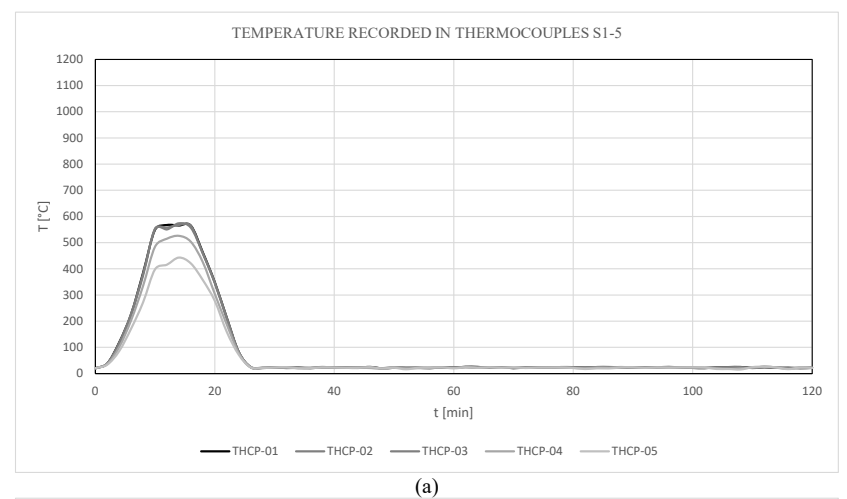
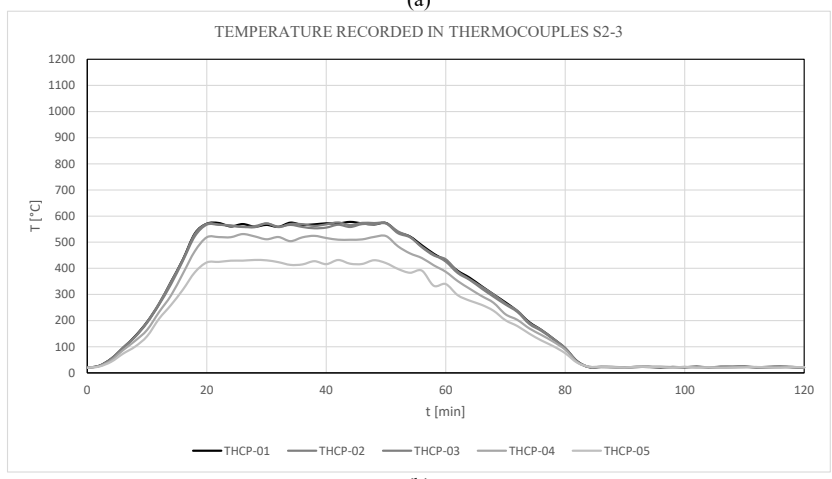
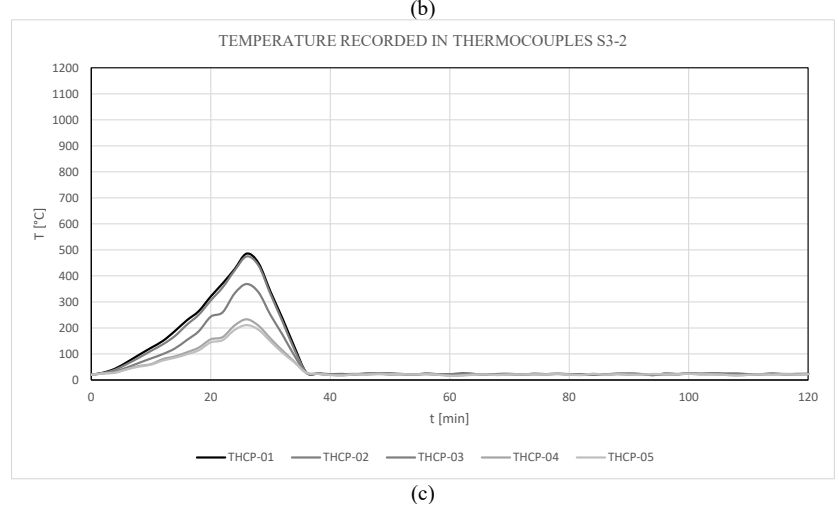


Figure 4.18. Fire scenario S1-1

See Appendix B for all other fire scenarios results. The volume below the span of the bridge has been divided into nine zones of equal length (2.25 m) except middle zone, where the fire is located, which is 3.0 m long to consider the maximum temperature in a larger area. The temperatures θ recorded in each zone, and for each scenario are shown in the following figure, indicating that the maximum temperatures were recorded in the thermocouples T1, T2, T3, T4 and T5.







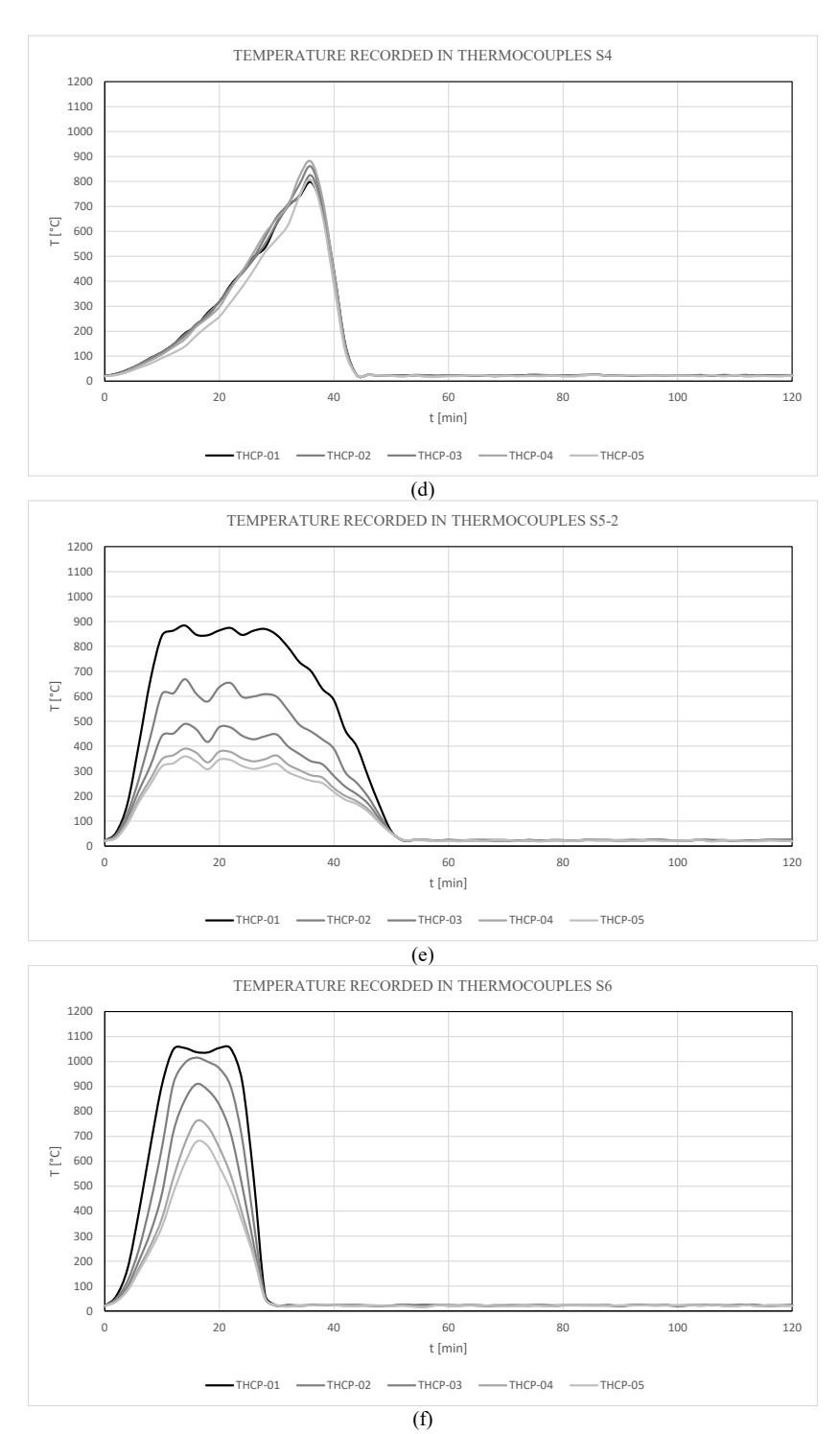


Figure 4.19. Temperatures recorded in thermocouples for each fire scenario

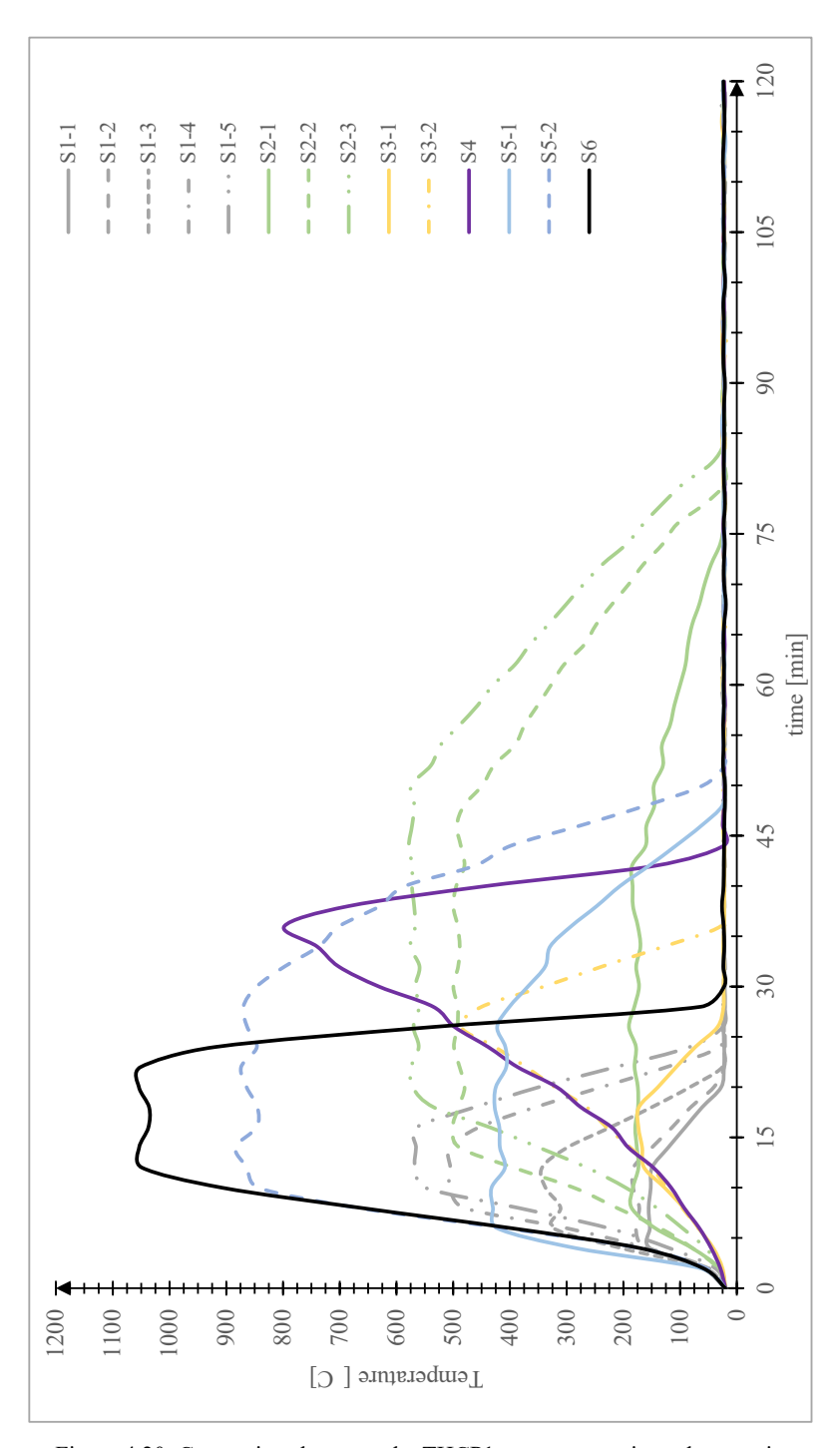
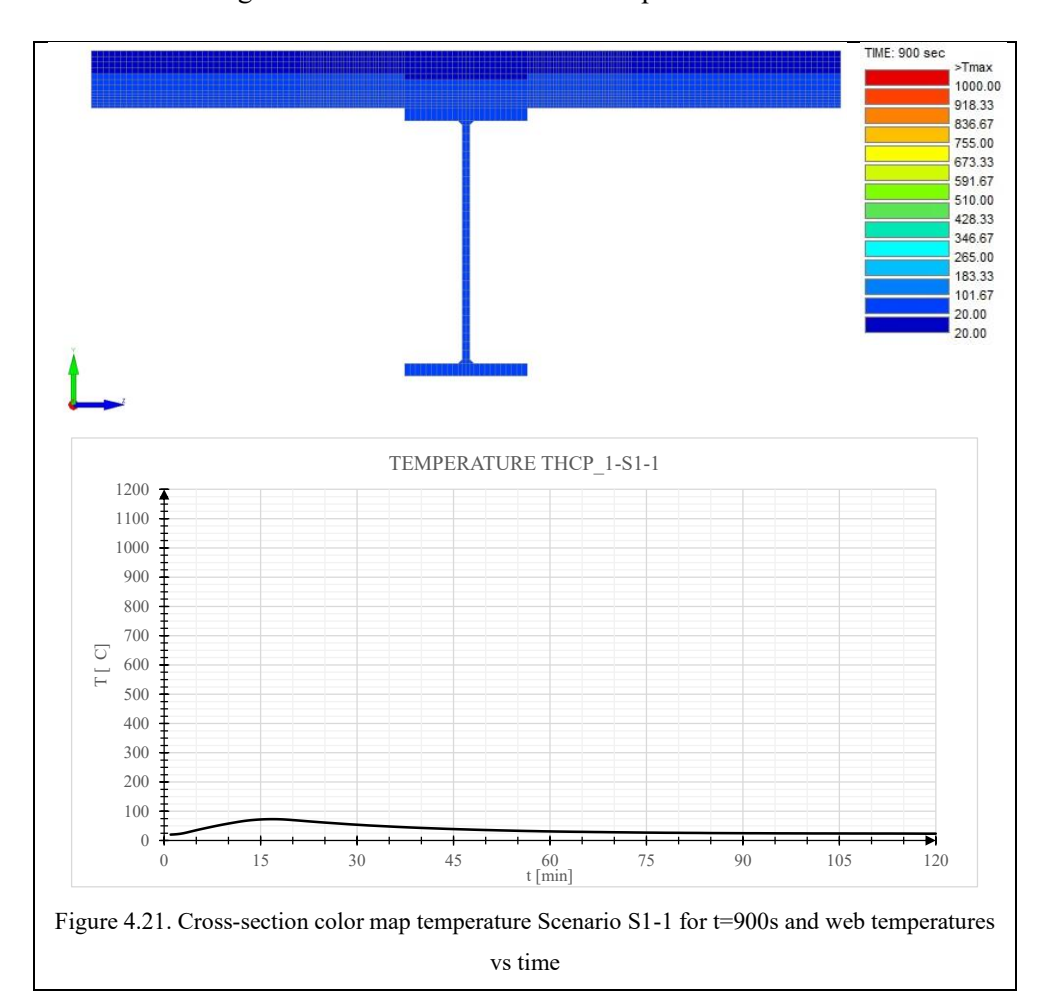


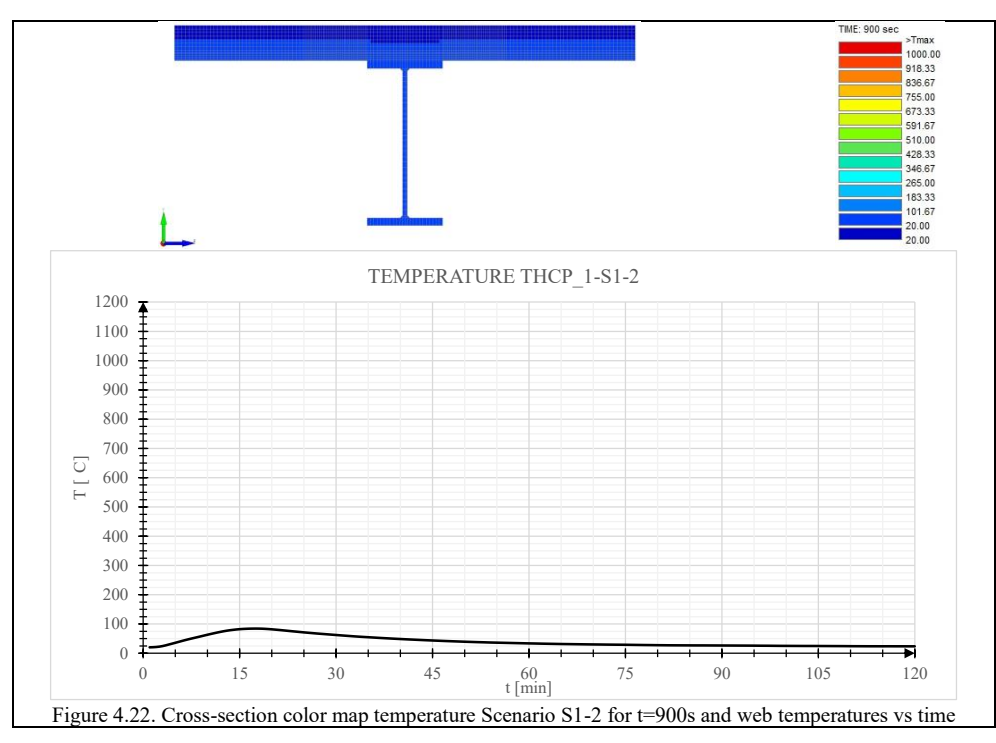
Figure 4.20. Comparison between the THCP1 temperatures in each scenario

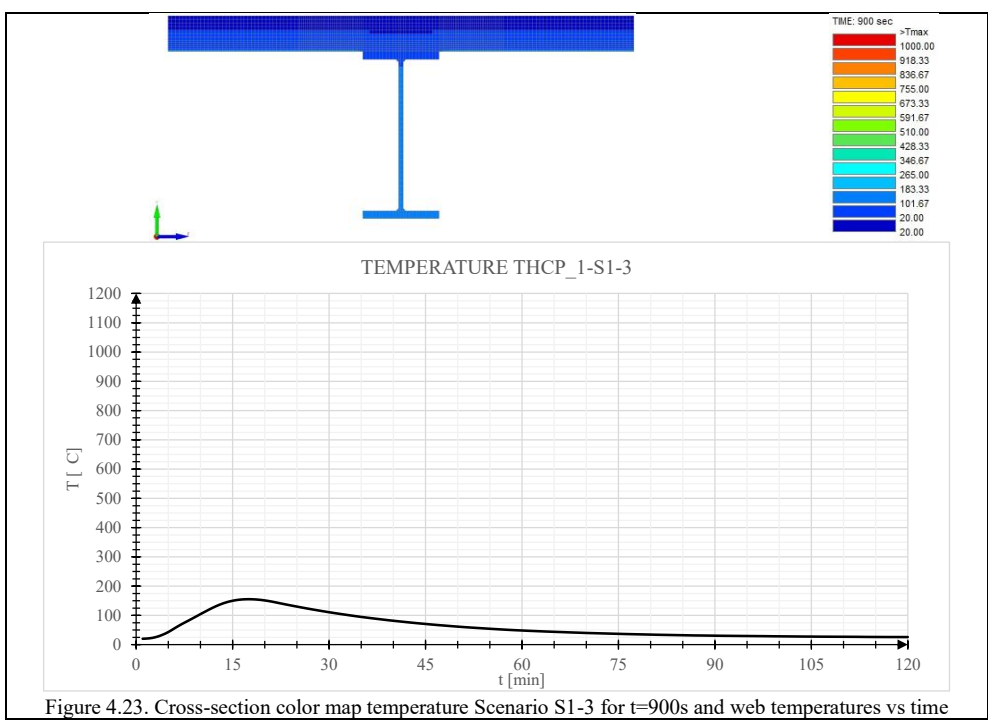
4.3 Thermo-mechanical analyses

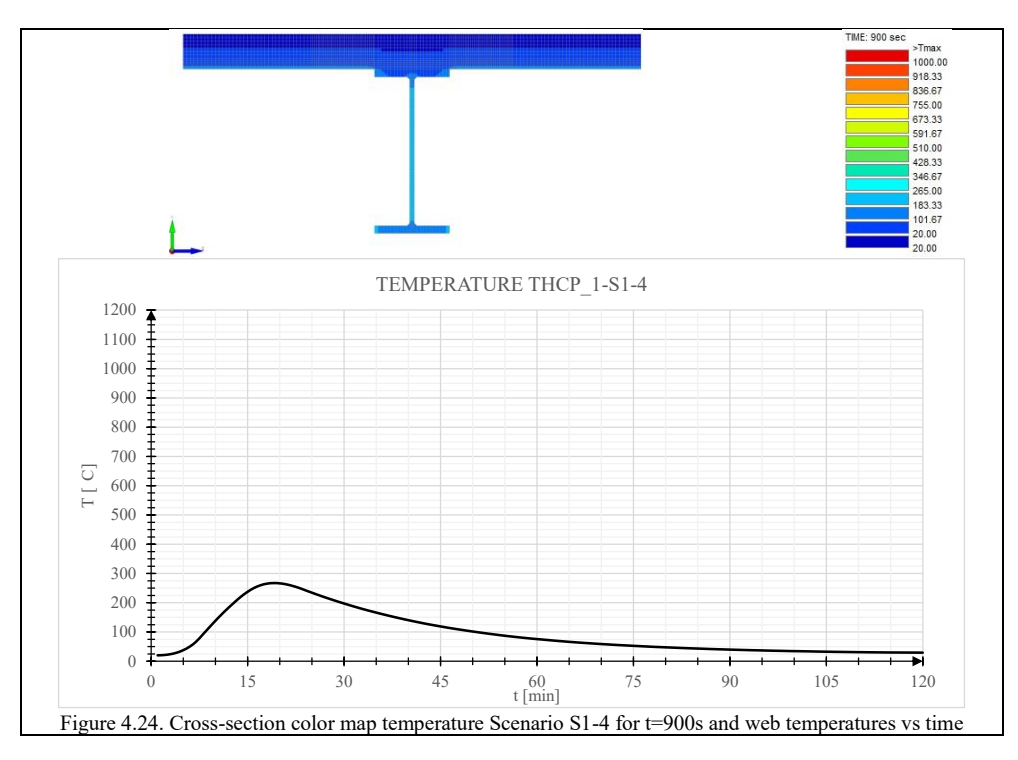
4.3.1 Thermal analyses

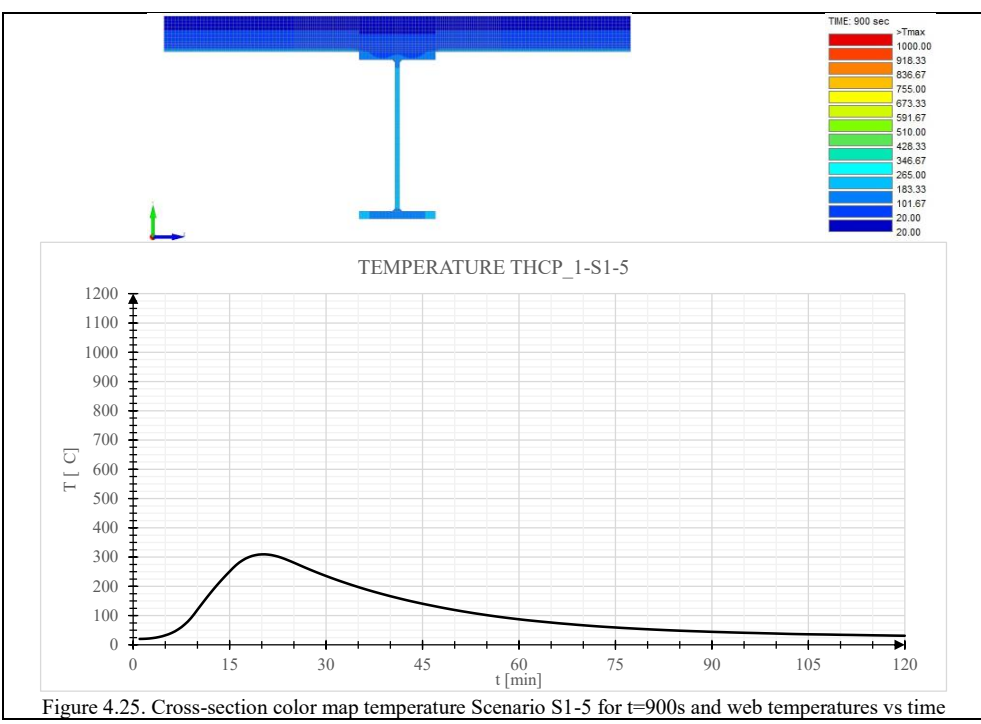
The temperatures recorded in thermocouples were then used as a thermal input in the analyses. Following is shown some thermal results in terms of temperature distribution through the cross-section and its development in time.

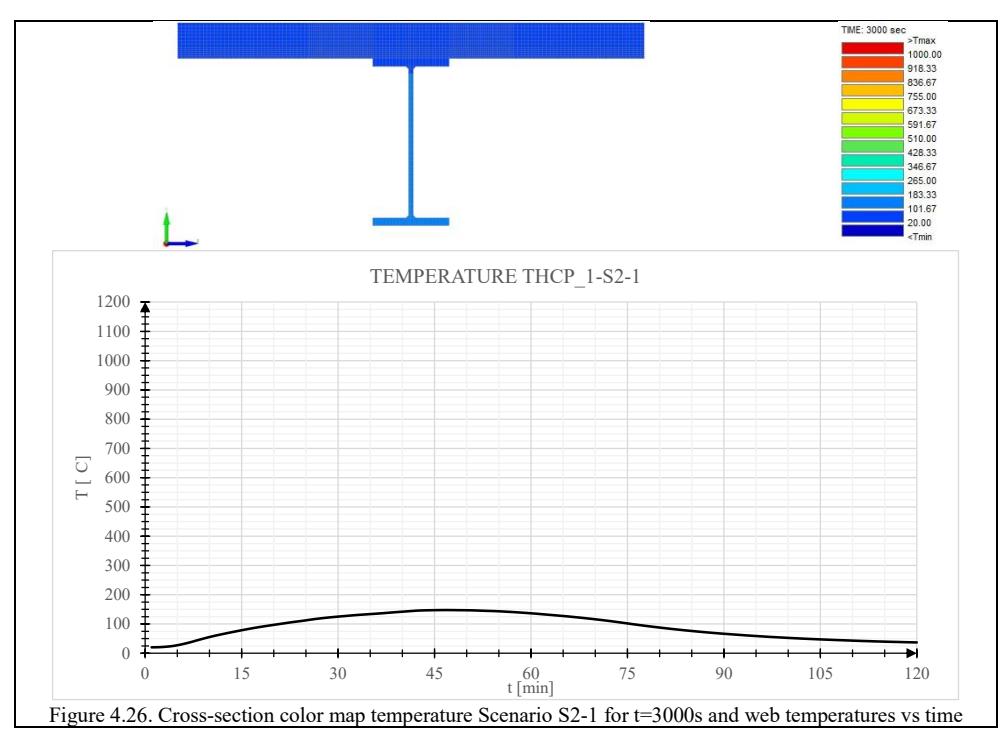


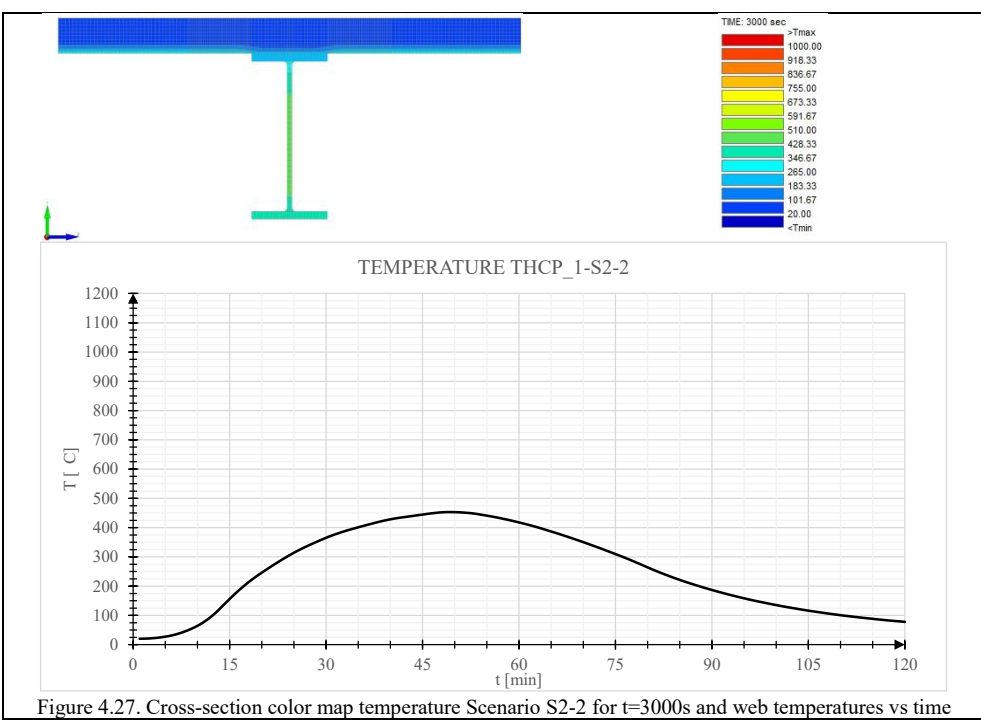


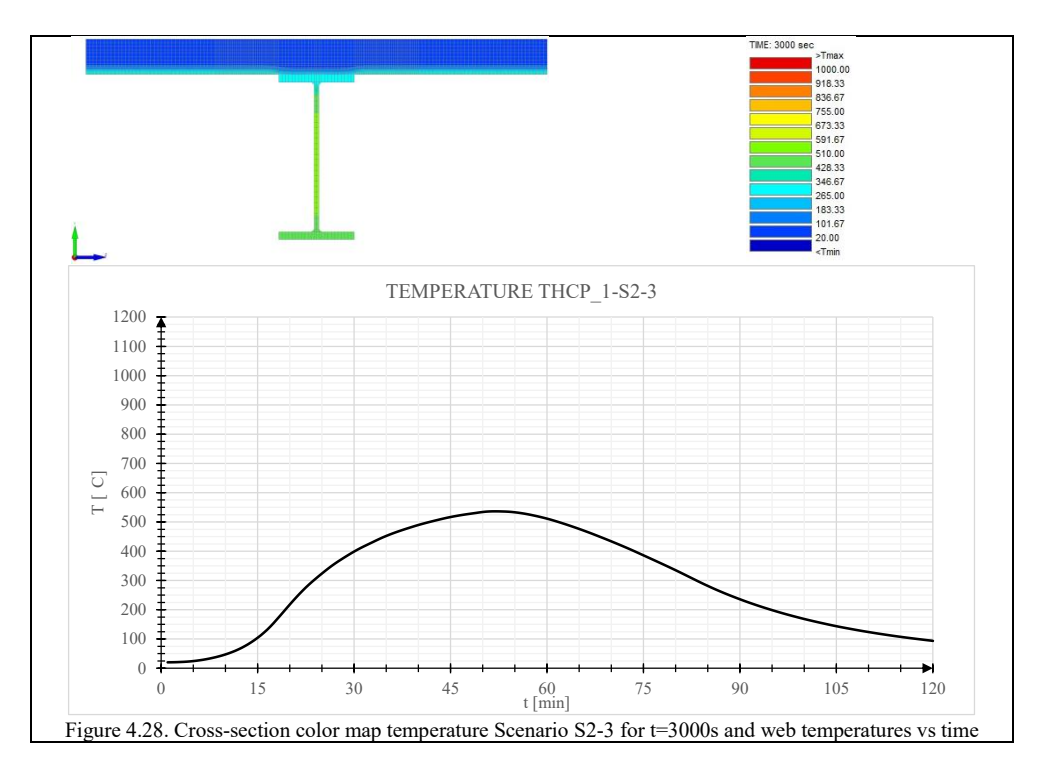


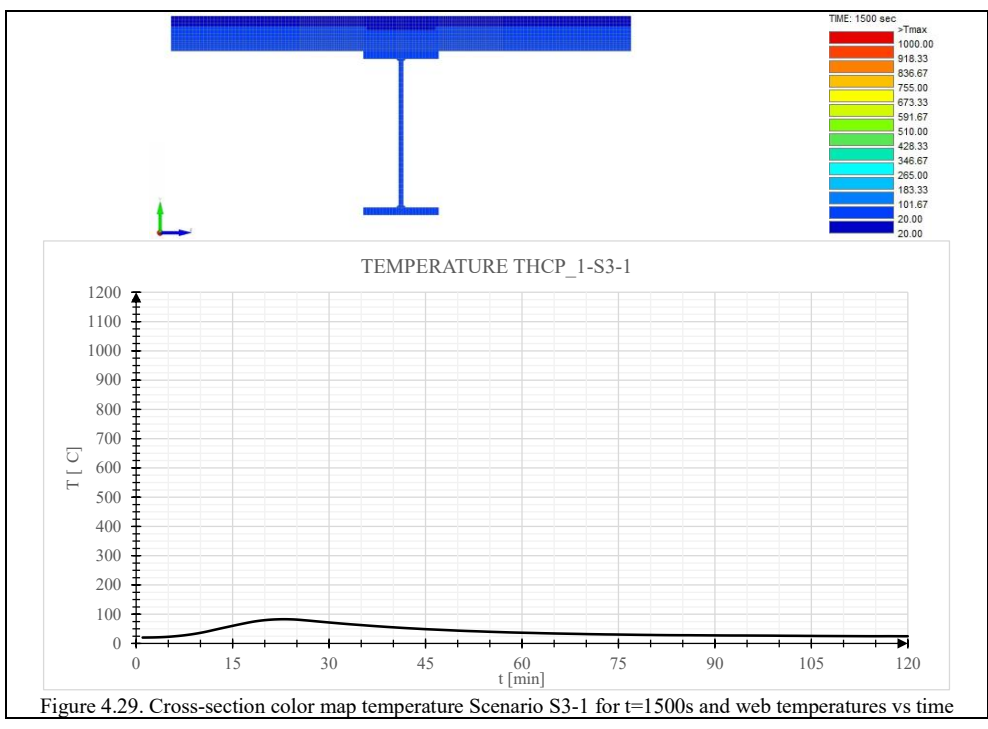


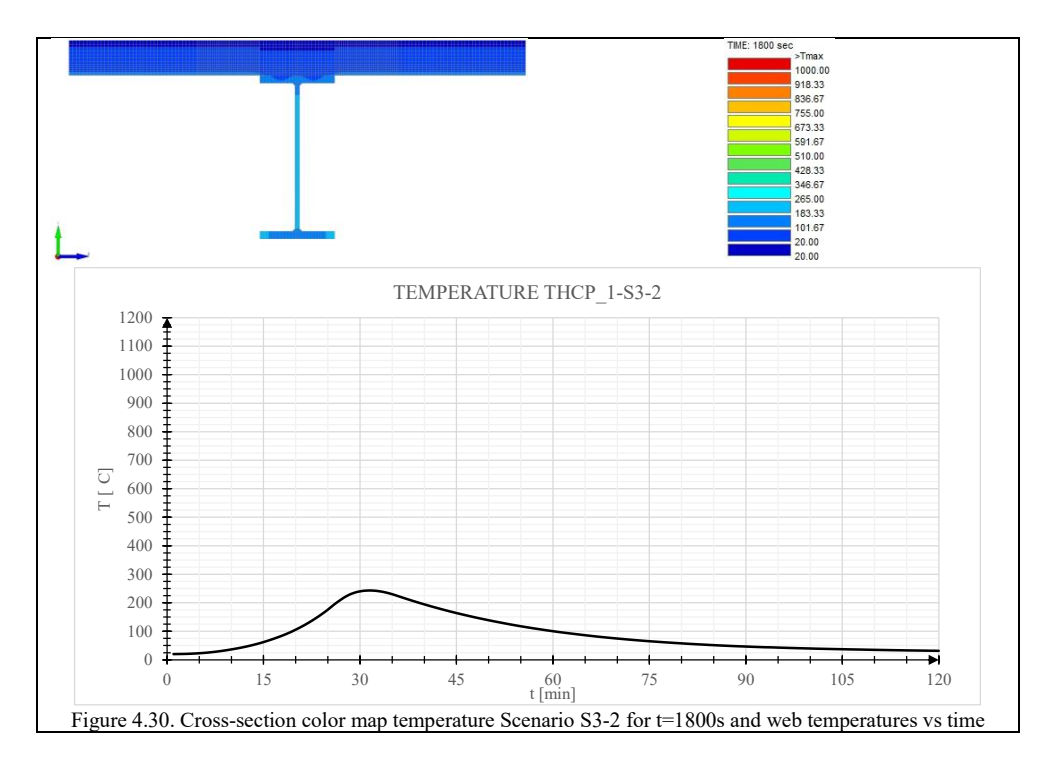


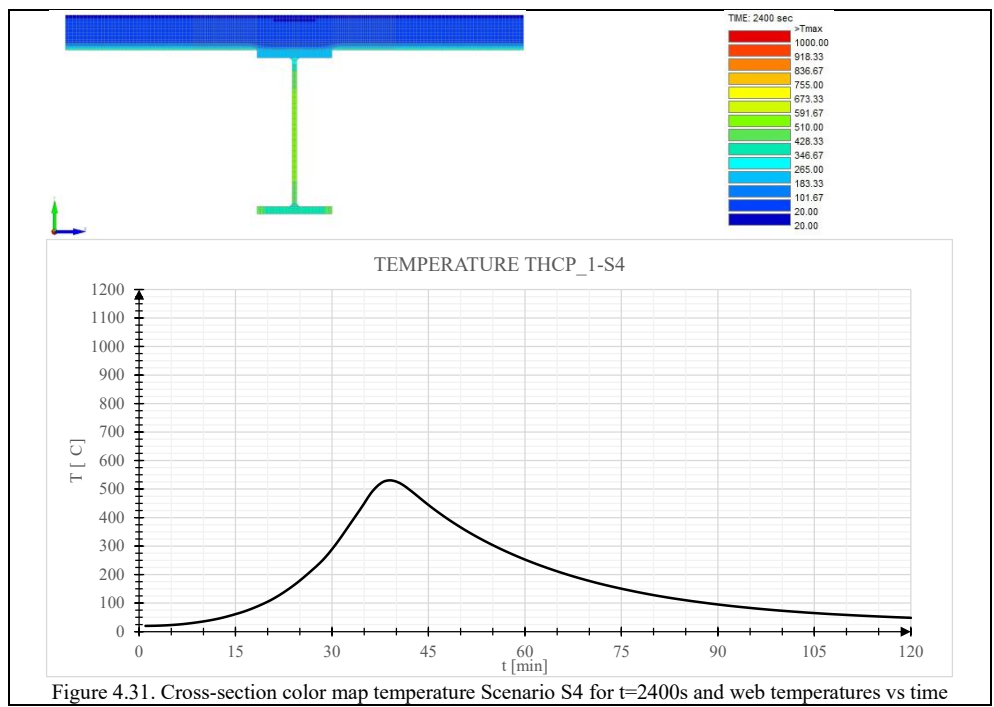


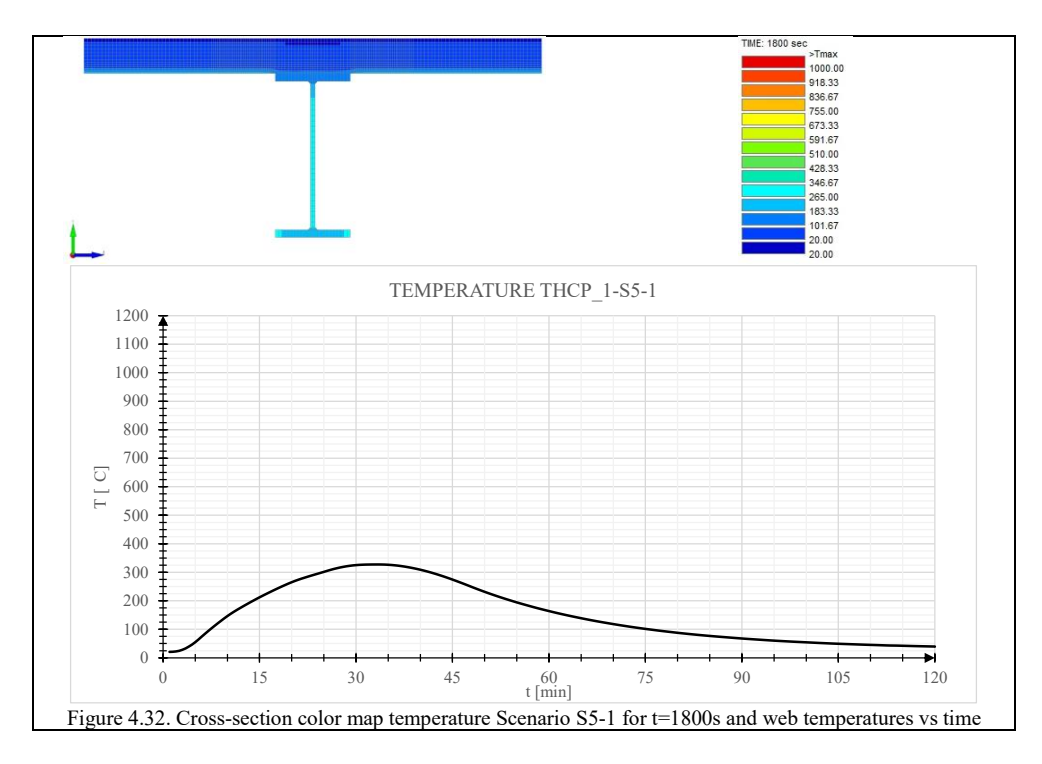


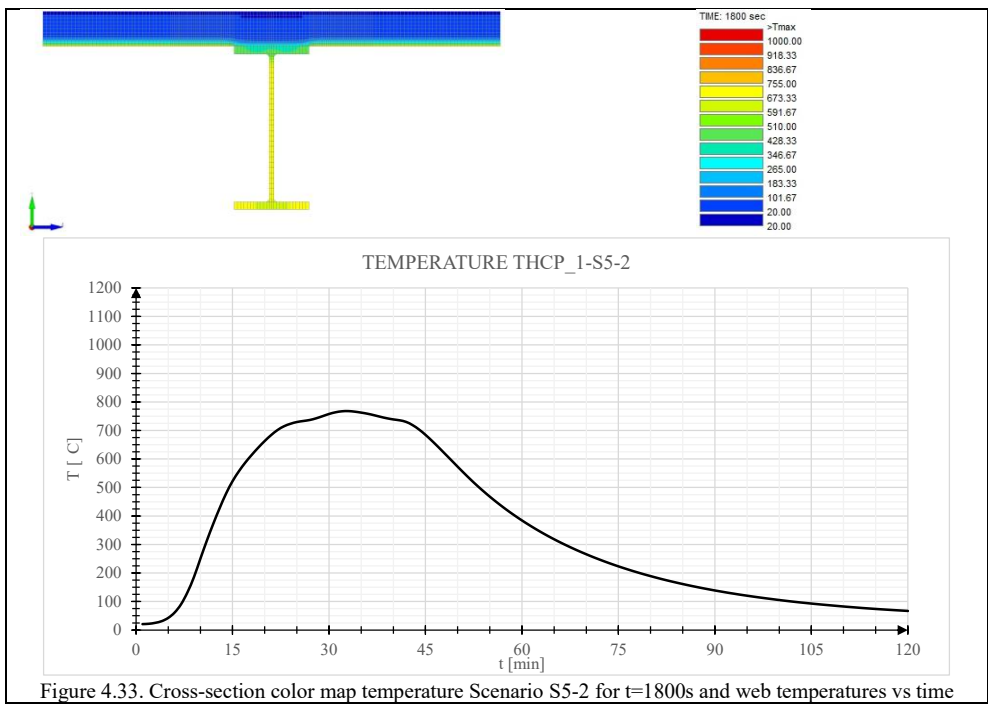


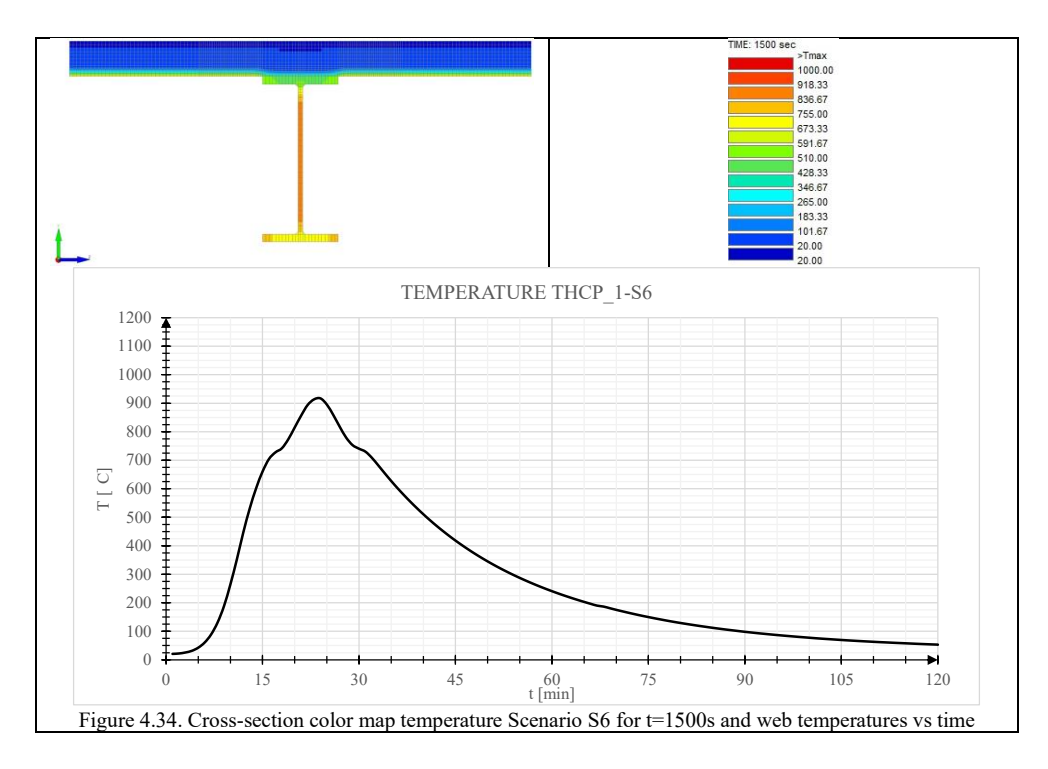












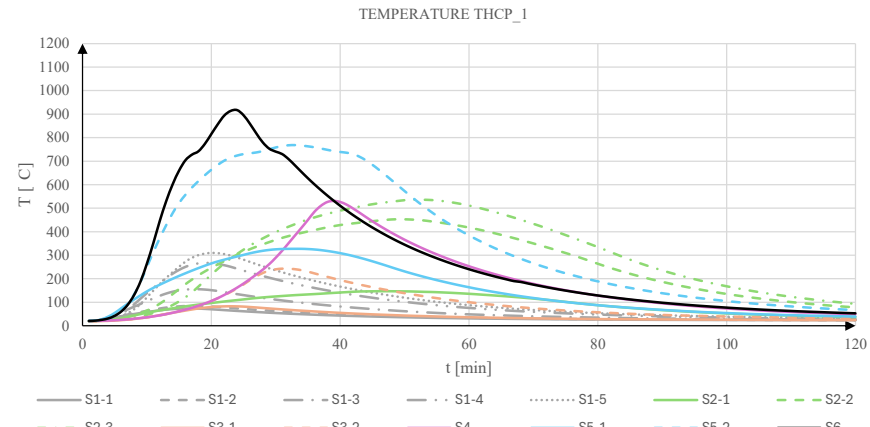


Figure 4.35. Temperature comparison for each fire scenario

4.3.2 Mechanical analyses

Mechanical analyses were performed by using as thermal input each thermal output shown in previous section. In addition, two different boundary conditions have been considered:

- simply supported beam with no hyperstatic effect throughout the thermal transient:
- simply supported beam considering the gap supports with a maximum horizontal displacement equal to 3.8 cm.

In the following sections, it has been considered three different initial degree of utilization μ_0 by increasing the vertical load applied on the girder 1.5 and 2 times with respect to the 26 kN/m applied. The three degrees of utilization are: 0.28, 0.42 and 0.56.

The following tables report the demand to capacity ratio (DCR) recorded by considering two different performance level, the PLIII and PLIV, corresponding to a displacement limit of L/100 and L/250 and the verification in terms of residual displacement as explained in the previous sections. In addition to the verification criteria in terms of maximum and residual displacement, a local verification may be carried out about the compressive of the bottom flange at support.

Indeed, the axial force transferred from the sliding support once it exhausted its free displacement is locally transferred before to the bottom flange and then in the centroid. According to EC3 - 1-8 the compression resistance of a beam flange is given by the following:

$$F_{c,fb,Rd} = \frac{M_{c,Rd}}{h - t_{fb}}$$
 Eq. 4.9

Table 4.7. DCR for isostatic model and μ_0 =0.28

Table 4.7. Dek for isostatic model and μ0–0.26								
$\mu_0 = 0.28$	Vertical Di	splacement]	PL III]	PL IV		
S	Δ _{max} [mm]	Δ _{res} [mm]	$\Delta_{\text{max}}/(\text{L}/100)$	$(\Delta_{res}\text{-}\Delta_{in})/(0.5\Delta_{in})$	$\Delta_{\text{max}}/(\text{L/250})$	$(\Delta_{res}\text{-}\Delta_{in})/(0.2\Delta_{in})$		
S1-1	44.3	36.8	0.21	0.00	0.53	0.00		
S1-2	47.9	36.8	0.23	0.00	0.57	0.00		
S1-3	58.2	36.8	0.28	0.00	0.69	0.00		
S1-4	96.8	36.8	0.46	0.00	1.15	0.00		
S1-5	120	38.1	0.57	0.07	1.43	0.18		
S2-1	61.8	38	0.29	0.07	0.74	0.16		
S2-2	162	48	0.77	0.61	1.93	1.52		
S2-3	229	58.2	1.09	1.16	2.73	2.91		
S3-1	48.2	36.9	0.23	0.01	0.57	0.01		
S3-2	85.4	36.9	0.41	0.01	1.02	0.01		
S4	237	60.4	1.13	1.28	2.82	3.21		
S5-1	84.9	36.8	0.40	0.00	1.01	0.00		
S5-2	COLLAPSE							
S6	COLLAPSE							

Table 4.8. DCR for isostatic model and μ_0 =0.42

$\mu_0 = 0.42$	Vertical Dis	splacement]	PL III]	PL IV
S	Δ _{max}	Δ _{res}	$\Delta_{\text{max}}/(L/100)$	$(\Delta_{res}\text{-}\Delta_{in})/(0.5\Delta_{in})$	$\Delta_{max}/(L/250)$	$(\Delta_{res}\text{-}\Delta_{in})/(0.2\Delta_{in})$
S1-1	65.8	58.2	0.31	0.00	0.78	0.00
S1-2	69.2	58.2	0.33	0.00	0.82	0.00
S1-3	79.6	58.2	0.38	0.00	0.95	0.00
S1-4	120	58.2	0.57	0.00	1.43	0.00
S1-5	145	61.5	0.69	0.11	1.73	0.28
S2-1	83.2	59.3	0.40	0.04	0.99	0.09
S2-2	212	90.6	1.01	1.11	2.52	2.78
S2-3	302	142	1.44	2.88	3.60	7.20
S3-1	69.5	58.2	0.33	0.00	0.83	0.00
S3-2	108	58.2	0.51	0.00	1.29	0.00
S4	314	139	1.50	2.78	3.74	6.94
S5-1	108	58.7	0.51	0.02	1.29	0.04
S5-2	COLLAPSE					
S6	COLLAPSE					

Table 4.9. DCR for isostatic model and μ_0 =0.56

$\mu_0 = 0.56$	Vertical Di	splacement	PL III		PL IV	
S	$\Delta_{ m max}$ [mm]	$\Delta_{ m res}$ [mm]	$\Delta_{\text{max}}/(L/100)$	$(\Delta_{\text{res}}\text{-}\Delta_{\text{in}})/(0.5\Delta_{\text{in}})$	$\Delta_{\text{max}}/(L/250)$	$(\Delta_{\text{res}}\text{-}\Delta_{\text{in}})/(0.2\Delta_{\text{in}})$
S1-1	81.4	73.8	0.39	0.00	0.97	0.00
S1-2	84.8	73.8	0.40	0.00	1.01	0.00
S1-3	95.2	73.8	0.45	0.00	1.13	0.00
S1-4	140	77.5	0.67	0.10	1.67	0.25
S1-5	176	91	0.84	0.47	2.10	1.17
S2-1	98.9	74.9	0.47	0.03	1.18	0.07
S2-2	256	150	1.22	2.07	3.05	5.16
S2-3	378	259	1.80	5.02	4.50	12.55
S3-1	85.1	73.8	0.41	0.00	1.01	0.00
S3-2	125	74.6	0.60	0.02	1.49	0.05
S4	387	268	1.84	5.26	4.61	13.16
S5-1	132	81.9	0.63	0.22	1.57	0.55
S5-2	COLLAPSE					
S6	COLLAPSE					

Table 4.10. DCR for hyperstatic model and μ_0 =0.28

$\mu_0 = 0.28$	Vertical Di	Vertical Displacement		PL III		PL IV	
S	$\Delta_{ m max}$	$\Delta_{ m res}$	$\Delta_{\rm max}/({\rm L}/100)$	$(\Delta_{res}\text{-}\Delta_{in})/(0.5\Delta_{in})$	$\Delta_{max}/(L/250)$	$(\Delta_{res}\text{-}\Delta_{in})/(0.2\Delta_{in})$	
Б	[mm]	[mm]	Δ_{max} (L/100)				
S1-1	44.3	36.8	0.21	0.00	0.53	0.00	
S1-2	47.9	36.8	0.23	0.00	0.57	0.00	
S1-3	58.2	36.8	0.28	0.00	0.69	0.00	
S1-4	96.8	36.8	0.46	0.00	1.15	0.00	
S1-5	84	36.8	0.40	0.00	1.00	0.00	
S2-1	61.8	38	0.29	0.07	0.74	0.16	
S2-2	81.9	36.8	0.39	0.00	0.98	0.00	
S2-3	70	36.8	0.33	0.00	0.83	0.00	
S3-1	48.2	36.9	0.23	0.01	0.57	0.01	
S3-2	85.4	36.9	0.41	0.01	1.02	0.01	
S4	COLLPASE						
S5-1	84.9	36.8	0.40	0.00	1.01	0.00	
S5-2	222	36.8	1.06	0.00	2.64	0.00	
S6	COLLAPSE						

Table 4.11. DCR for hyperstatic model and μ_0 =0.42

$\mu_0 = 0.42$	Vertical Di	splacement]	PL III]	PL IV
S	Δ _{max}	Δ _{res}	$\Delta_{\text{max}}/(L/100)$	$(\Delta_{res}$ - $\Delta_{in})/(0.5\Delta_{in})$	$\Delta_{max}/(L/250)$	$(\Delta_{res}$ - $\Delta_{in})/(0.2\Delta_{in})$
S1-1	65.8	58.2	0.31	0.00	0.78	0.00
S1-2	69.2	58.2	0.33	0.00	0.82	0.00
S1-3	79.6	58.2	0.38	0.00	0.95	0.00
S1-4	120	58.2	0.57	0.00	1.43	0.00
S1-5	86.5	58.2	0.41	0.00	1.03	0.00
S2-1	83.2	59.3	0.40	0.04	0.99	0.09
S2-2	98.1	58.2	0.47	0.00	1.17	0.00
S2-3	88	58.2	0.42	0.00	1.05	0.00
S3-1	69.5	58.2	0.33	0.00	0.83	0.00
S3-2	108	58.2	0.51	0.00	1.29	0.00
S4	113	58.2	0.54	0.00	1.35	0.00
S5-1	108	58.7	0.51	0.02	1.29	0.04
S5-2	102	58.2	0.49	0.00	1.21	0.00
S6	COLLAPSE					

Table 4.12. DCR for hyperstatic model and μ_0 =0.56

$\mu_0 = 0.56$	Vertical Di	splacement]	PL III]	PL IV
S	Δ _{max}	Δ _{res}	$\Delta_{\text{max}}/(L/100)$	$(\Delta_{\rm res}$ - $\Delta_{\rm in})/(0.5\Delta_{\rm in})$	$\Delta_{\text{max}}/(\text{L/250})$	$(\Delta_{ m res}$ - $\Delta_{ m in})/(0.2\Delta_{ m in})$
	[mm]	[mm]	0.00			
S1-1	81.4	73.8	0.39	0.00	0.97	0.00
S1-2	84.8	73.8	0.40	0.00	1.01	0.00
S1-3	95.2	73.8	0.45	0.00	1.13	0.00
S1-4	140	77.5	0.67	0.10	1.67	0.25
S1-5	118	74.1	0.56	0.01	1.40	0.02
S2-1	98.9	74.9	0.47	0.03	1.18	0.07
S2-2	160	73.8	0.76	0.00	1.90	0.00
S2-3	140	73.8	0.67	0.00	1.67	0.00
S3-1	85.1	73.8	0.41	0.00	1.01	0.00
S3-2	125	74.6	0.60	0.02	1.49	0.05
S4	163	91.3	0.78	0.47	1.94	1.19
S5-1	132	81.9	0.63	0.22	1.57	0.55
S5-2	116	86	0.55	0.33	1.38	0.83
S6	COLLAPSE					

4.4 Development of fragility curves

4.4.1 Linear regression Cloud Procedure

Herein, a regression-based probability model is used to describe the DCR_{PL} for a given IM = HRR peak (or Q). The regression probabilistic model is described in the follow:

$$E[lnDCR_{PL}|RHR_{peak}] = ln\eta_{DCR_{PL}|RHR_{peak}} = lna + blnRHR_{peak}$$
 Eq. 4.10

$$\beta_{DCR_{PL}|RHR_{peak}} = \sqrt{\frac{\sum_{i=1}^{N} \left(lnDCR_{PL,i} - ln\eta_{DCR_{PL}|RHR_{peak}}\right)^{2}}{(N-2)}}$$
 Eq. 4.11

Where a and b are the regression constants and $\beta_{DCR_{PL}|RHR_{peak}}$ and $\eta_{DCR_{PL}|RHR_{peak}}$ are the standard deviation and the mean of the gaussian distribution hypothesized for the critical $[DCR_{PL}|RHR_{peak}]$. [57] [58]

Consequently, the previous equation defining the standard deviation demonstrates that is constant with respect to IM in the Cloud method. Finally, the fragility curves obtained thanks to the Cloud analysis can be evaluated from the following equation:

$$P(DCR > 1|IM) = P(lnDCR > 0|IM) = 1 - \phi\left(-\frac{ln\eta_{DCR|IM}}{\beta_{DCR|IM}}\right)$$
 Eq. 4.12

Where $\phi(\cdot)$ is the standard normal cumulative distribution function.

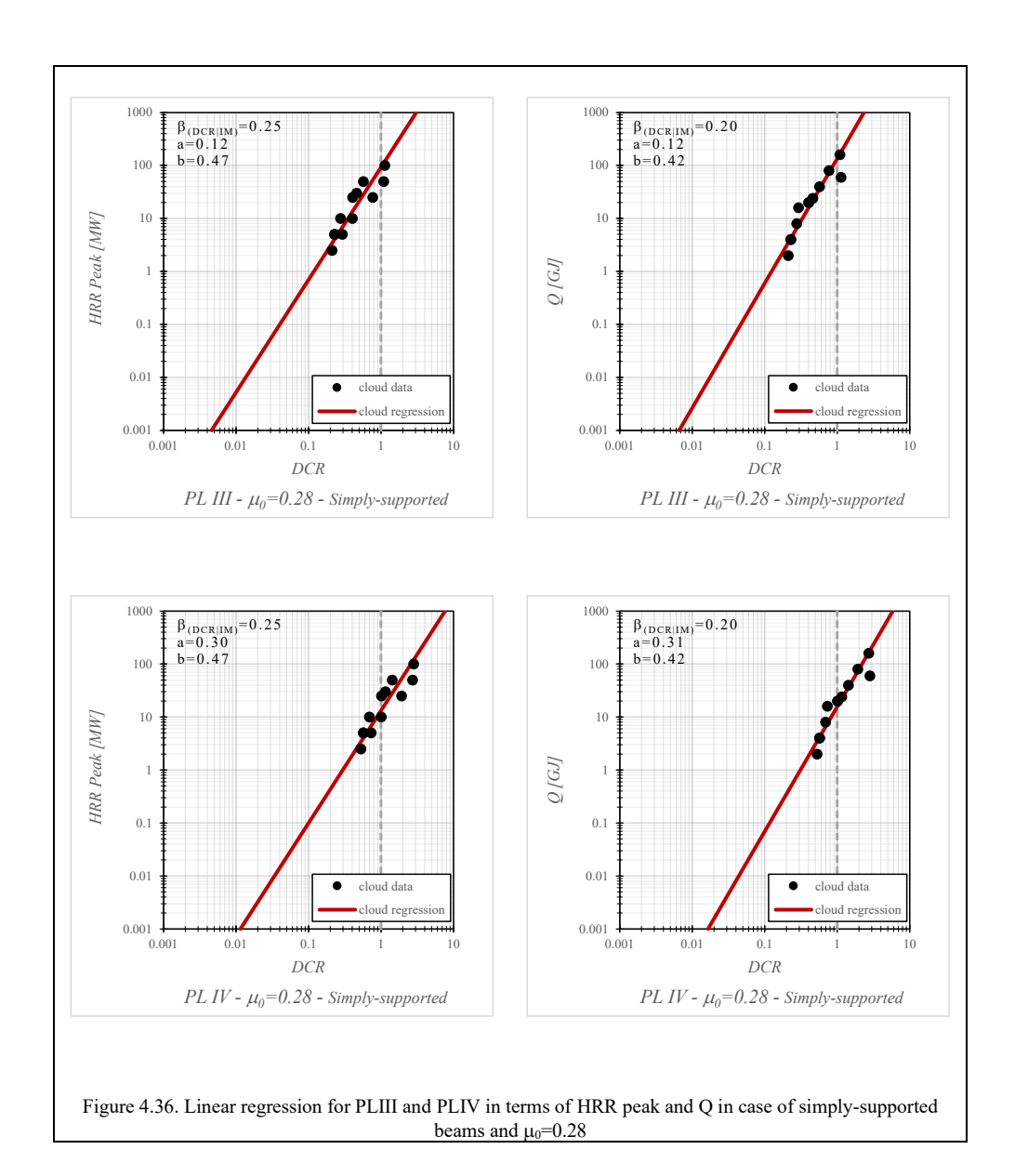
As also previously mentioned two static schemes have been considered for fragility assessment. In the following the results of the linear regression are shown for three different cases:

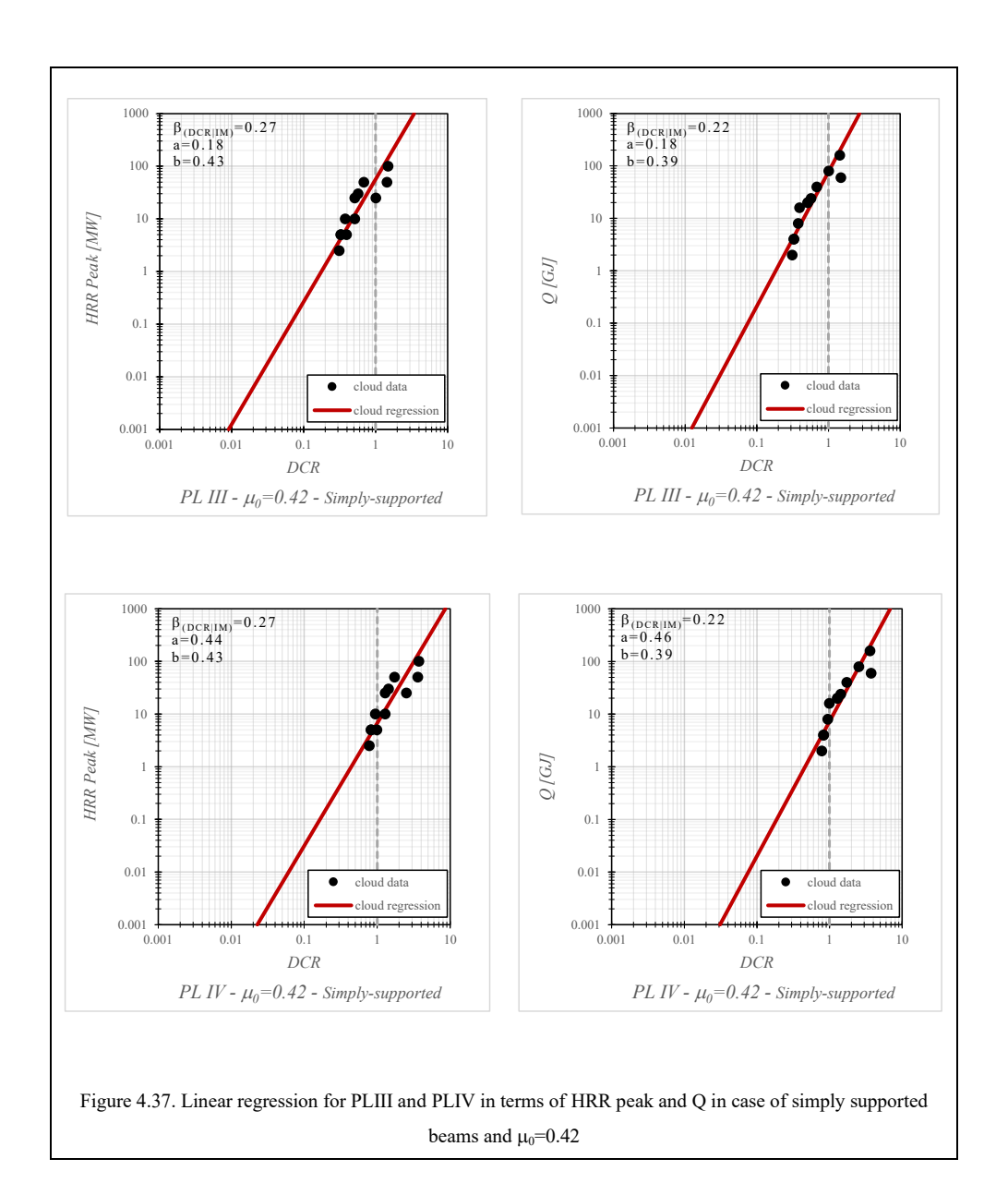
- Case 1: simply-supported beam by considering maximum displacement criteria, for PLIII and PLIV, with respect to HRR [MW] and Q [GJ] and also as a function of the initial degree of utilization.
- Case 2: simply-supported beam by considering both maximum and residual displacement criteria, for PLIII and PLIV, with respect to HRR [MW] and Q [GJ] and also as a function of the initial degree of utilization.
- Case 3: hyperstatic beam for all the criteria previously defined, for PLIII and PLIV, with respect to HRR [MW] and Q [GJ] and also as a function of the initial degree of utilization.

All the linear regressions shown below, for the different cases, are excellent, as can be understood by observing the data points' very close alignment with the interpolating line in the log-normal plane, and they are all characterized by acceptable values of the standard deviation.

CASE 1

For the first, simply supported one, the DCR considered is the one obtained as the ratio between the maximum deflection recorded during the thermal transient and the limit displacement of L/100 for PLIII and L/250 for PLIV. In the following the linear regression in these conditions are presented both for PLIII and PLIV and both for HRR Peak [MW] and fire load Q [GJ].





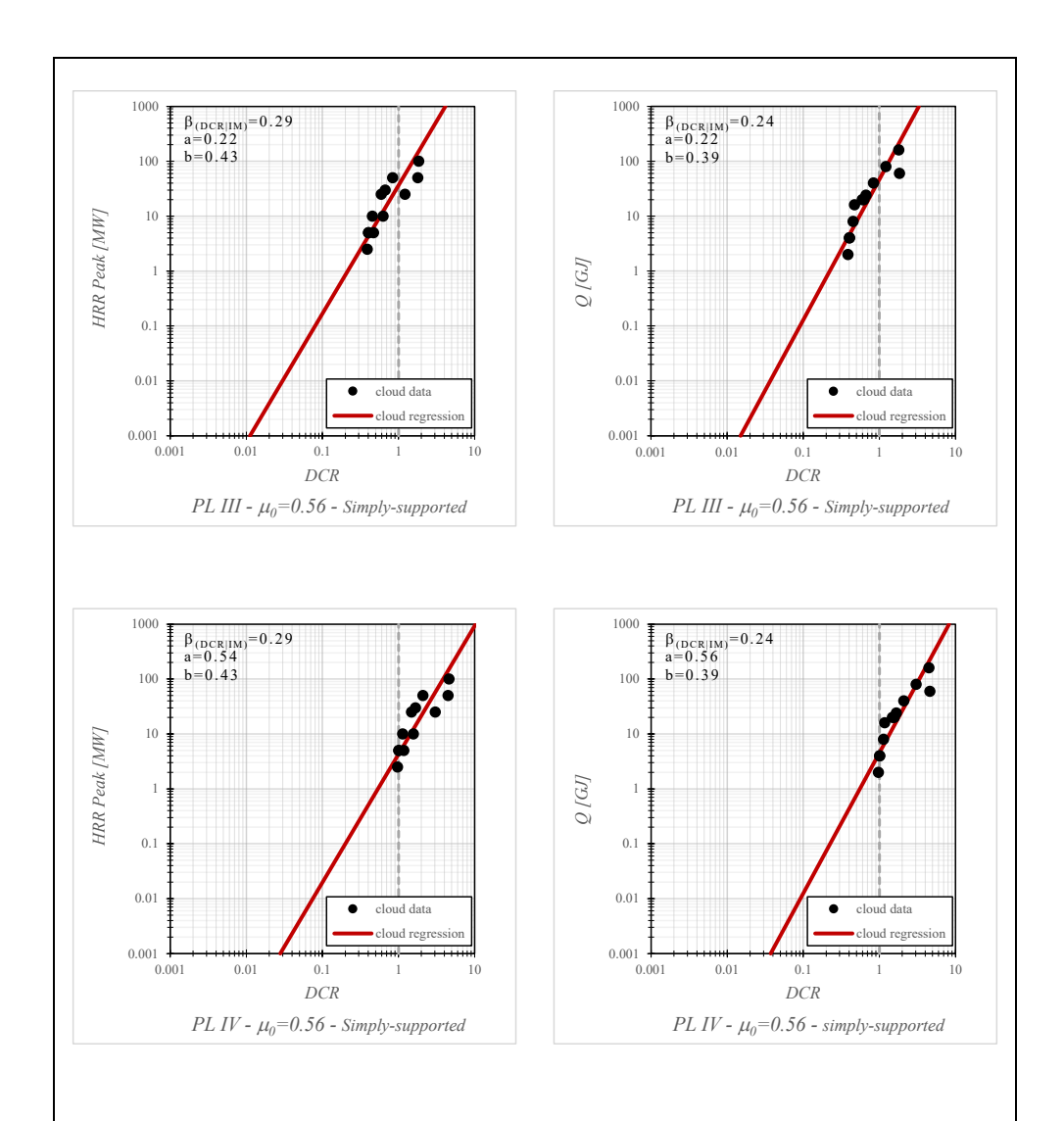
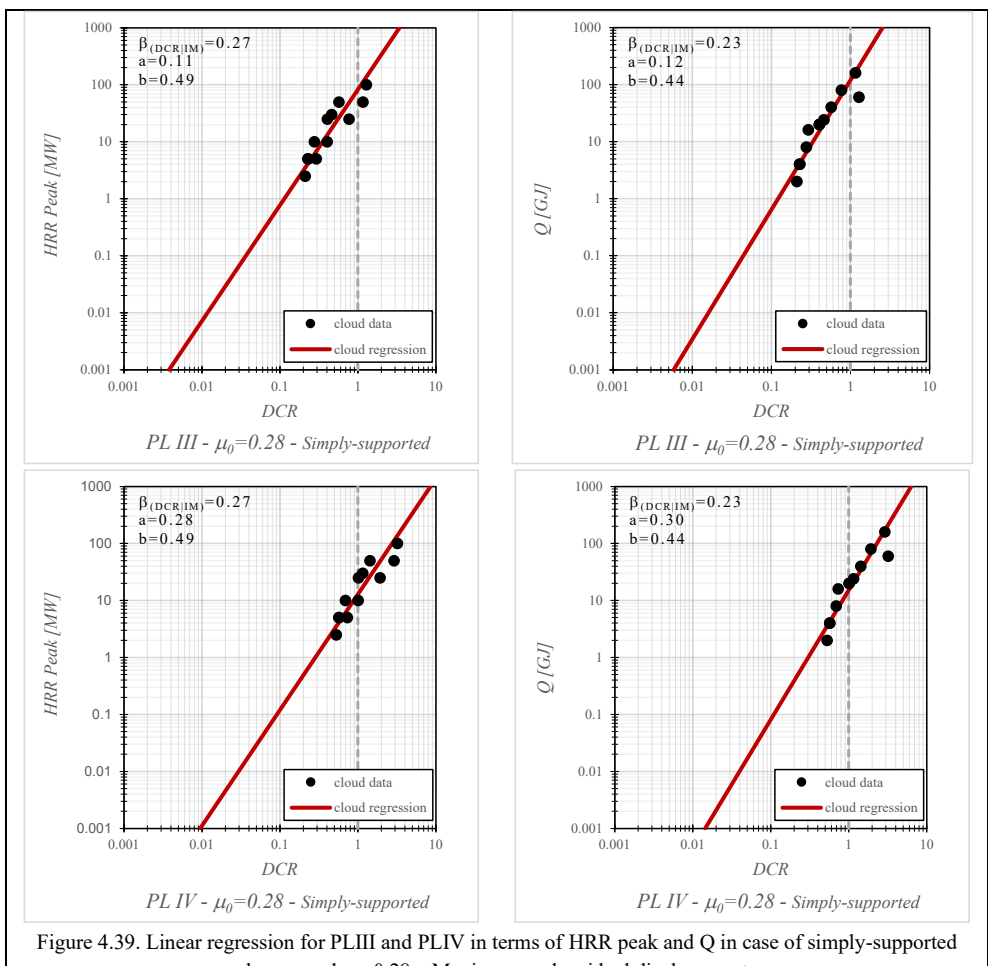


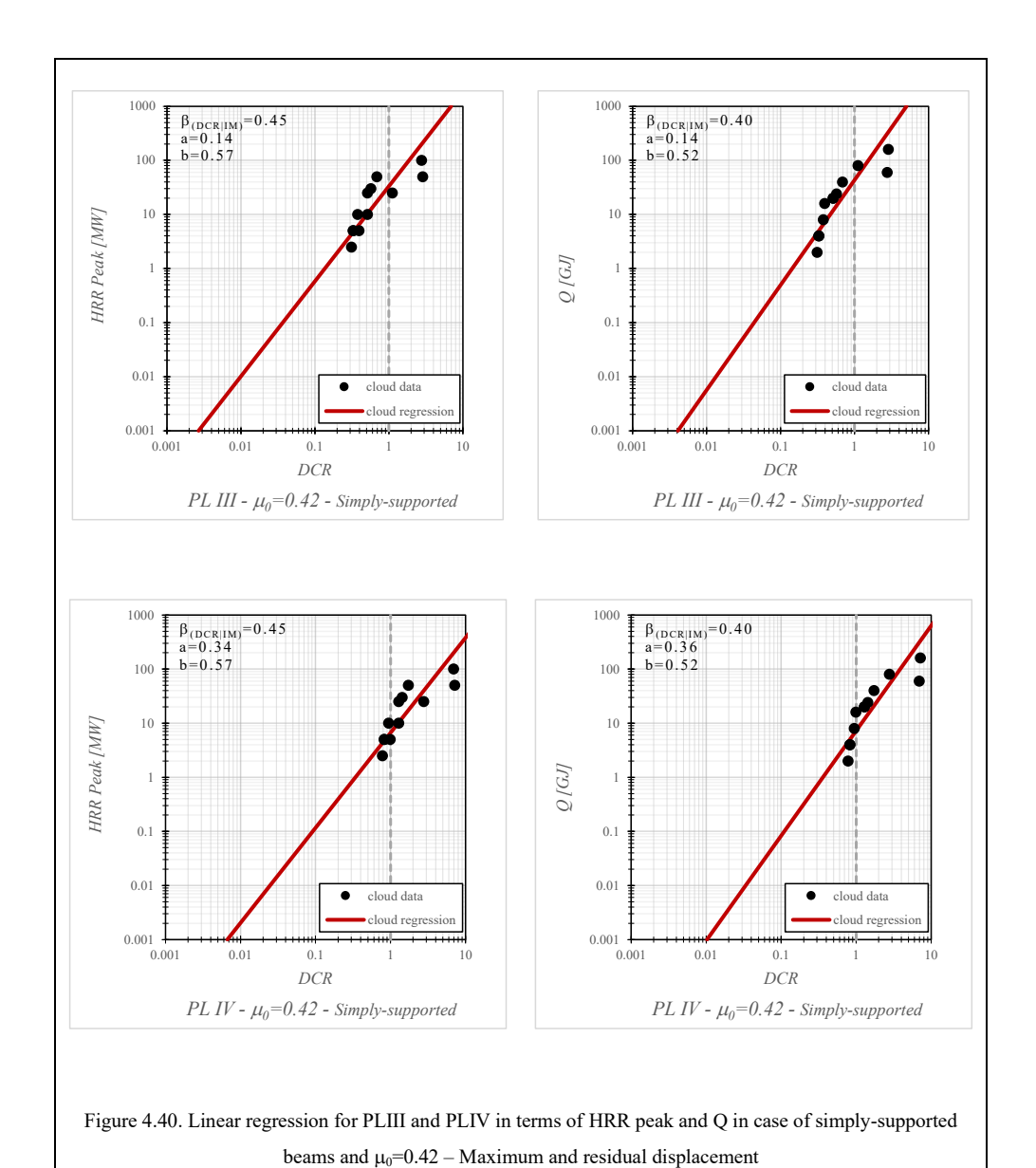
Figure 4.38. Linear regression for PLIII and PLIV in terms of HRR peak and Q in case of simply supported beams and μ_0 =0.56

CASE 2

To highlight the effect of the second PLIII and PLIV criteria about the residual displacement, the same linear regression has been done by considering as the DCR the maximum value, for each IM, between the ratio of the maximum deflection recorded during analysis and the limit displacement and the DCR obtained from the net residual displacement divided to 50% and 20 % of the initial displacement for PLIII and PLIV.



beams and μ_0 =0.28 – Maximum and residual displacement



126

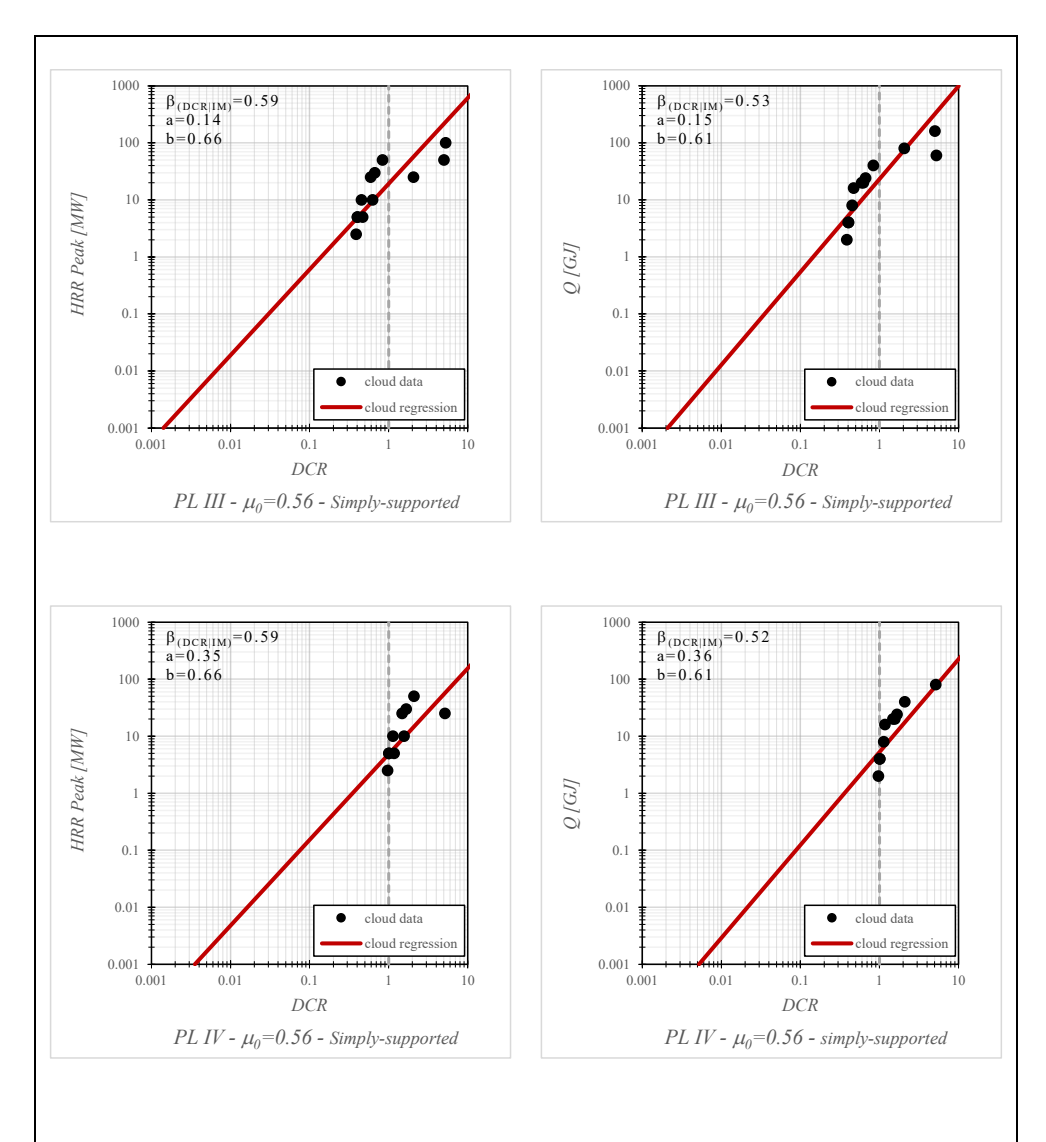


Figure 4.41. Linear regression for PLIII and PLIV in terms of HRR peak and Q in case of simply-supported beams and μ_0 =0.56 – Maximum and residual displacement

CASE 3

Finally, the second static scheme results linear regression has been done by considering DCR, for each IM, the maximum of the two criteria in terms of displacement and, in addition, it has been also taken into account the DCR of the compressive verification of the bottom flange at the support.

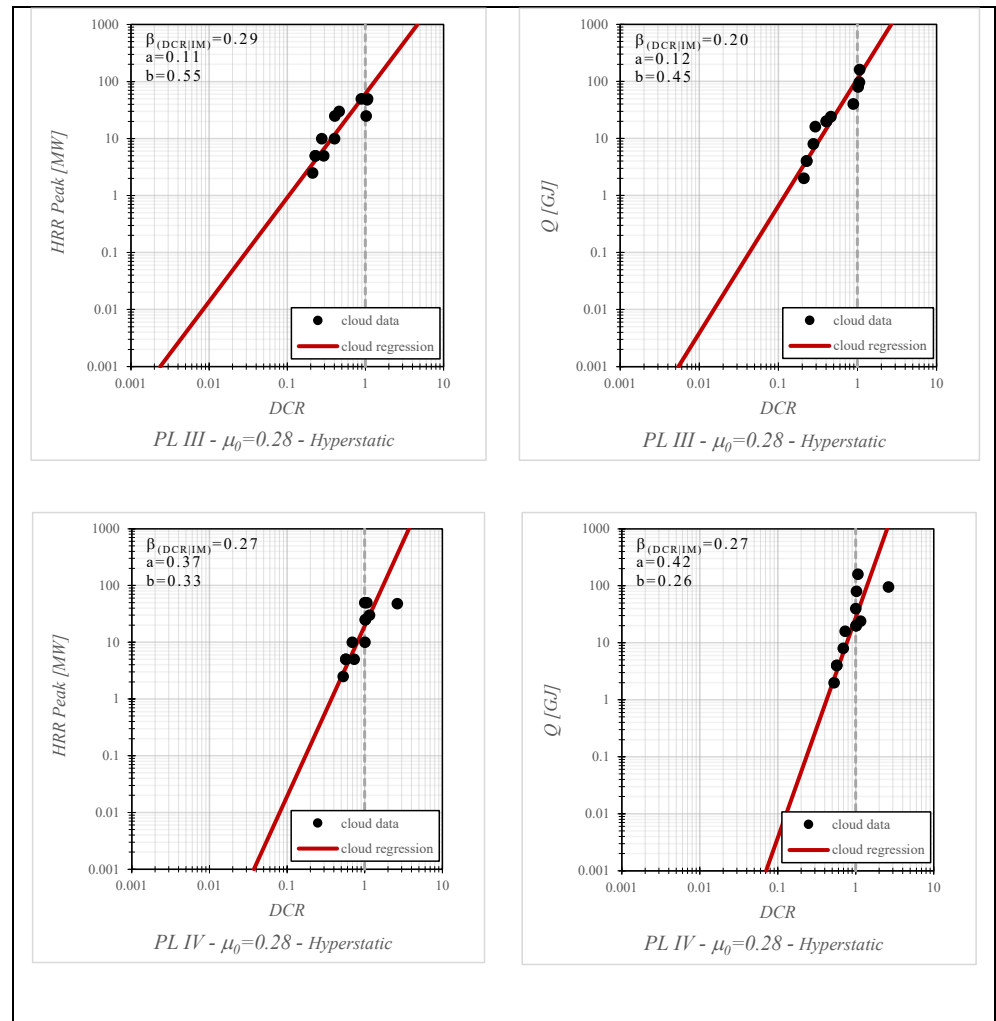


Figure 4.42. Linear regression for PLIV in terms of HRR peak and Q in case of hyperstatic beams and μ_0 =0.28

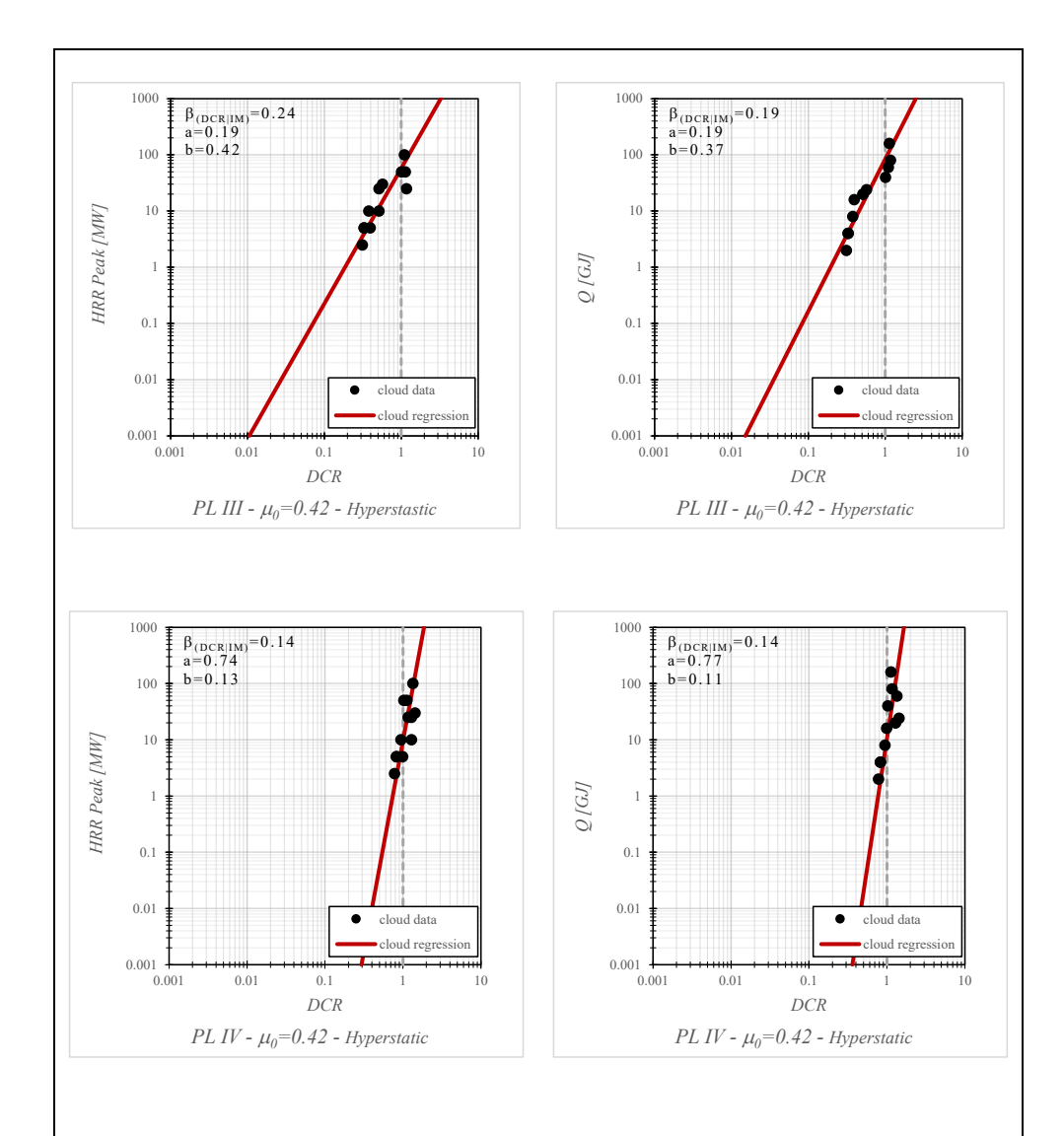


Figure 4.43. Linear regression for PLIV in terms of HRR peak and Q in case of hyperstatic beams and μ_0 =0.42

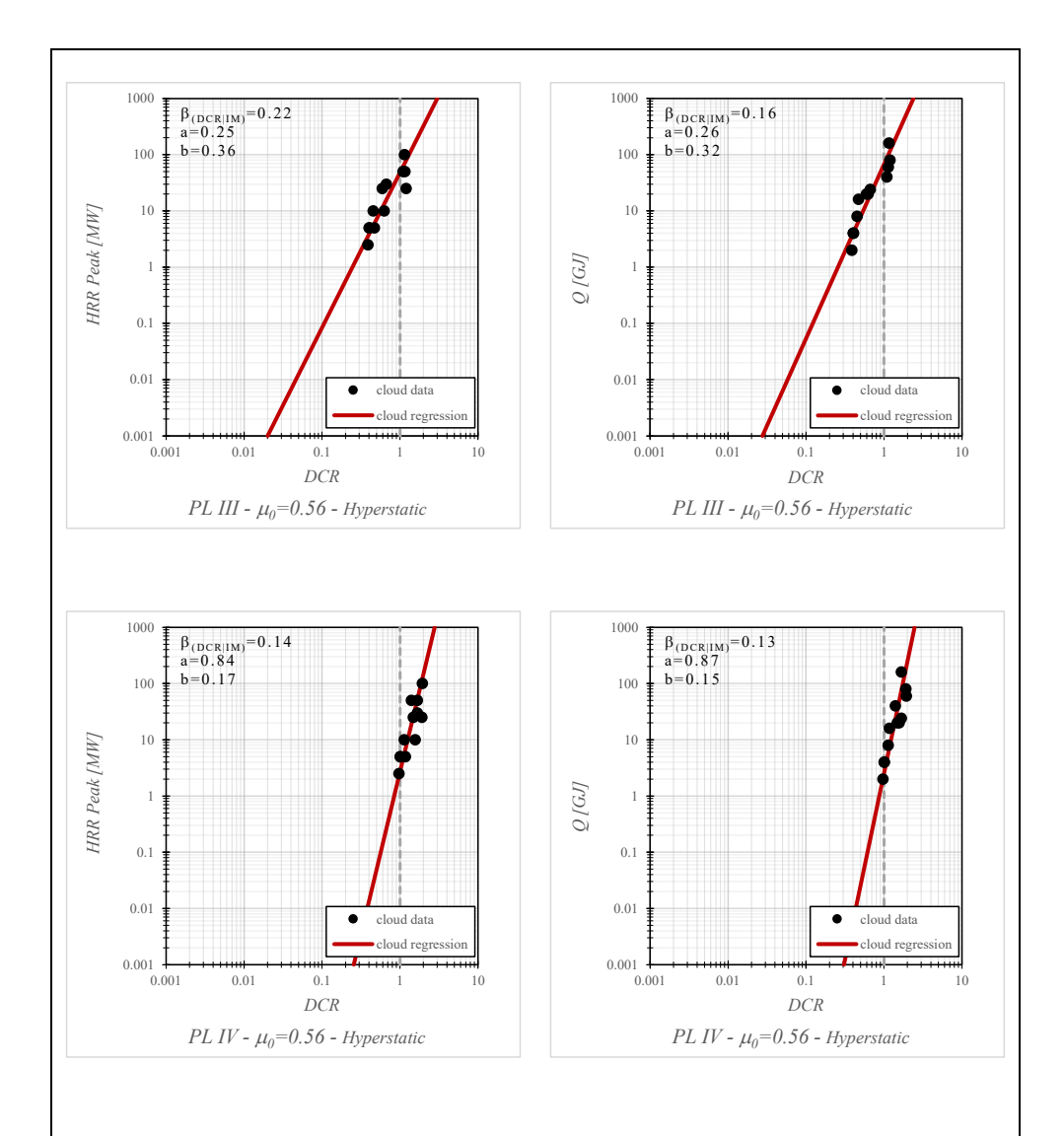


Figure 4.44. Linear regression for PLIV in terms of HRR peak and Q in case of hyperstatic beams and μ_0 =0.56

4.4.2 Fragility curves

Fragility curves are a helpful tool to understand how structures respond to fire action and to understand what the probability of exceeding predefined performance criteria or damage states is.

Fragility curves provide a graphical tool for quickly understanding how likely a structure exceeds a performance level or damage state for a given event.

Each event must be paired with a measurement intensity (IM); the choice of IM to be considered is crucial as this can strongly influence the statistical quality of the result. In the case of the present paper, the peak HRR (MW) and the fire load Q (GJ) were chosen.

These two parameters, taken as IM, lead to a very good statistical correlation as can also be seen from the results of the linear regressions reported above. In the following, various comparisons are shown between the fragility curves resulting from the previously discussed conditions.

The comparisons are made for each performance level, varying the initial degree of utilization μ_0 and as a function of the peak HRR and the fire load Q. Initially, a comparison is provided for the case of a simply supported structure for PLIII and PLIV and for different initial degrees of utilization.

The curves show excellent consistency as, for the same static scheme and required performance level PLIII, the fragility of the structure increases with the increase of the initial static degree of utilization, as the resistance reserve of the structure to withstand fire actions is lower.

This consistency is also maintained in the case of performance level PLIV and with varying static schemes.

Case 1

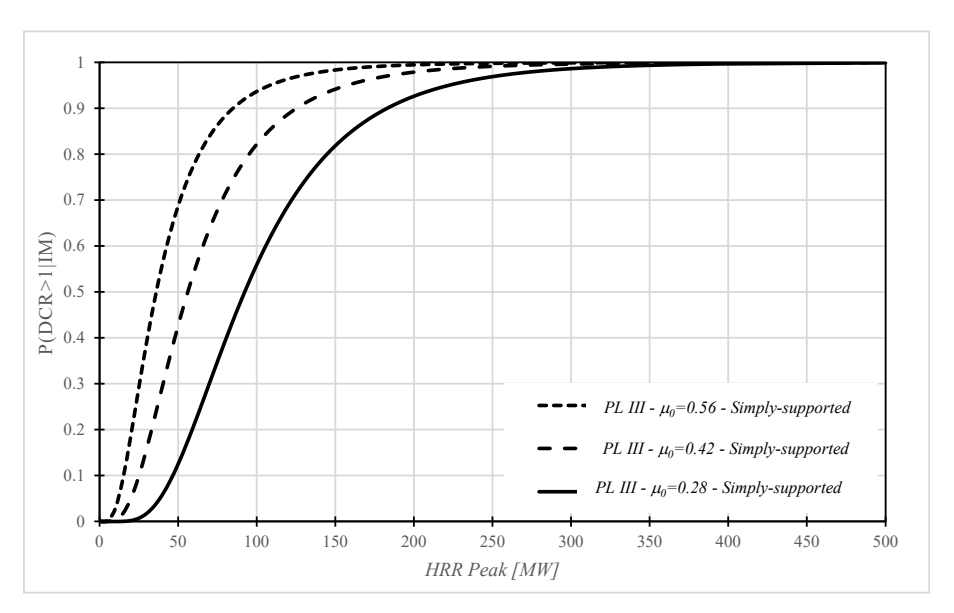


Figure 4.45. Comparison between fragility curves built for simply supported beam and PLIII verification, maximum displacement as a function of HRR peak.

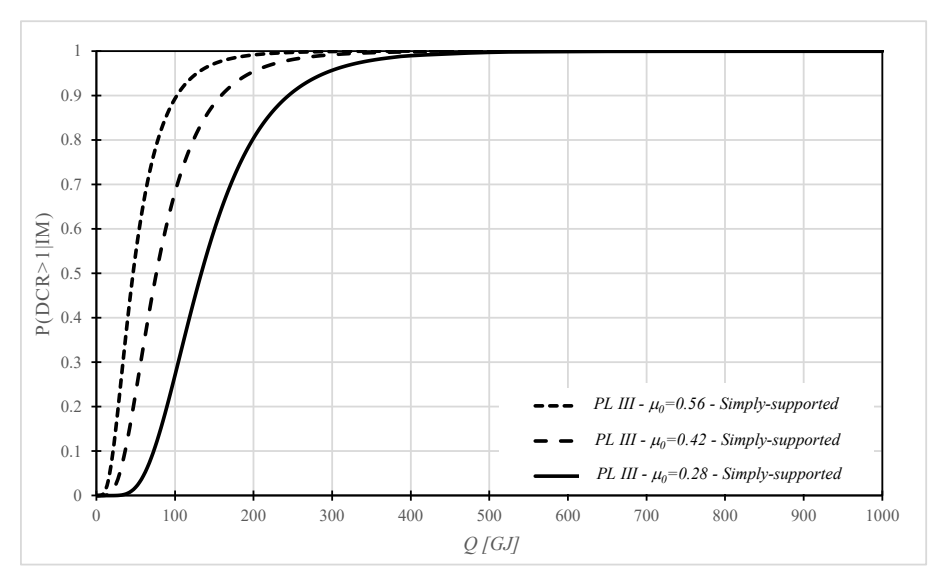


Figure 4.46. Comparison between fragility curves built for simply supported beam and PLIII verification, maximum displacement as a function of Q.

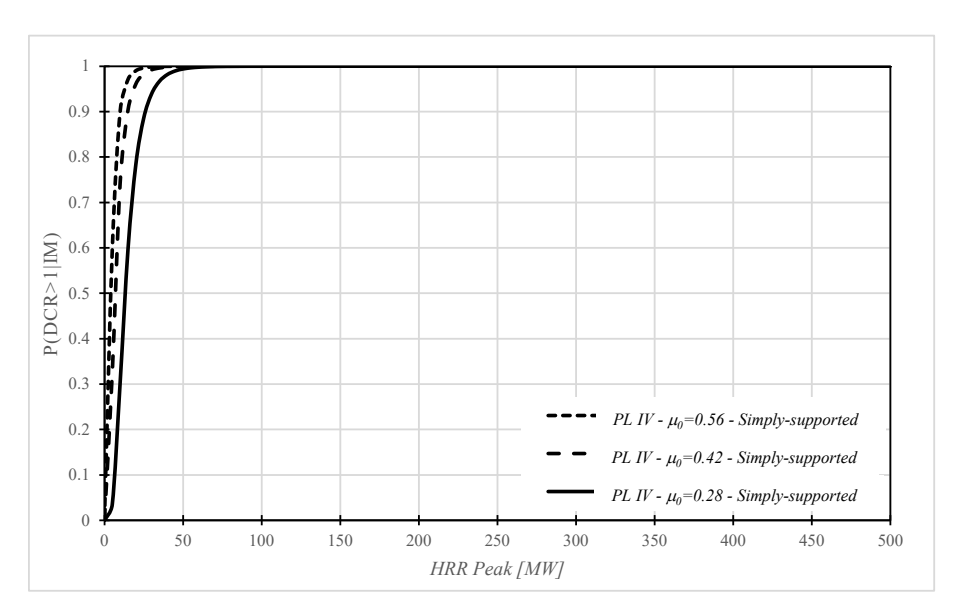


Figure 4.47. Comparison between fragility curves built for simply supported beam and PLIV verification, maximum displacement as a function of HRR peak.

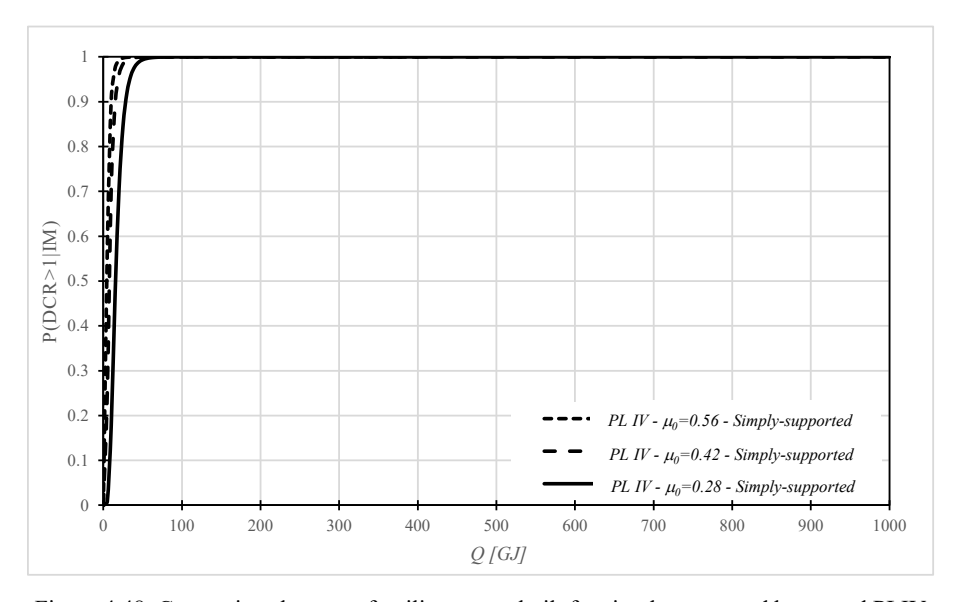


Figure 4.48. Comparison between fragility curves built for simply supported beam and PLIV verification, maximum displacement as a function of Q.

Case 2

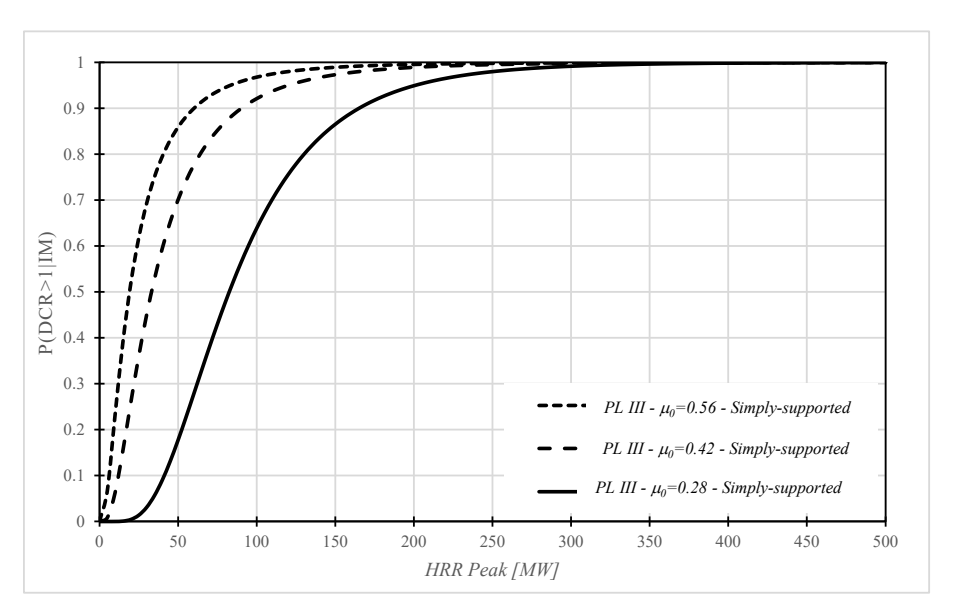


Figure 4.49. Comparison between fragility curves built for simply supported beam and PLIII verification, maximum and residual displacement as a function of HRR peak.

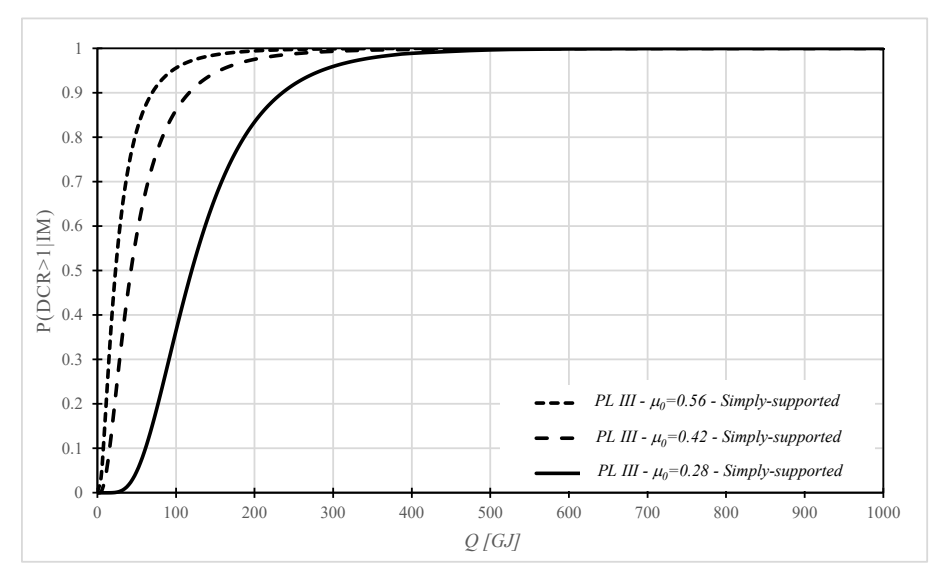


Figure 4.50. Comparison between fragility curves built for simply supported beam and PLIII verification, maximum and residual displacement as a function of Q

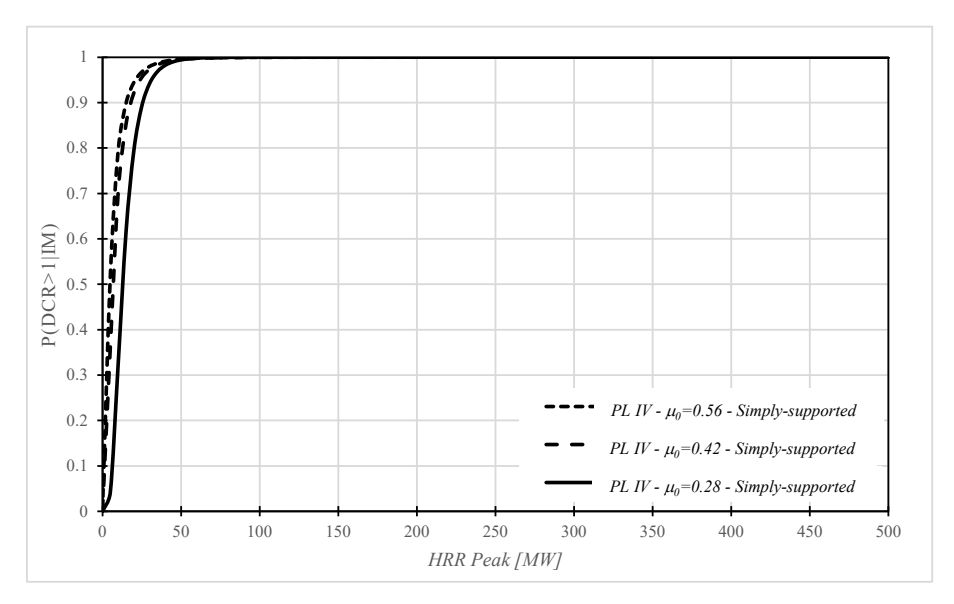


Figure 4.51. Comparison between fragility curves built for simply supported beam and PLIV verification, maximum and residual displacement as a function of HRR peak.

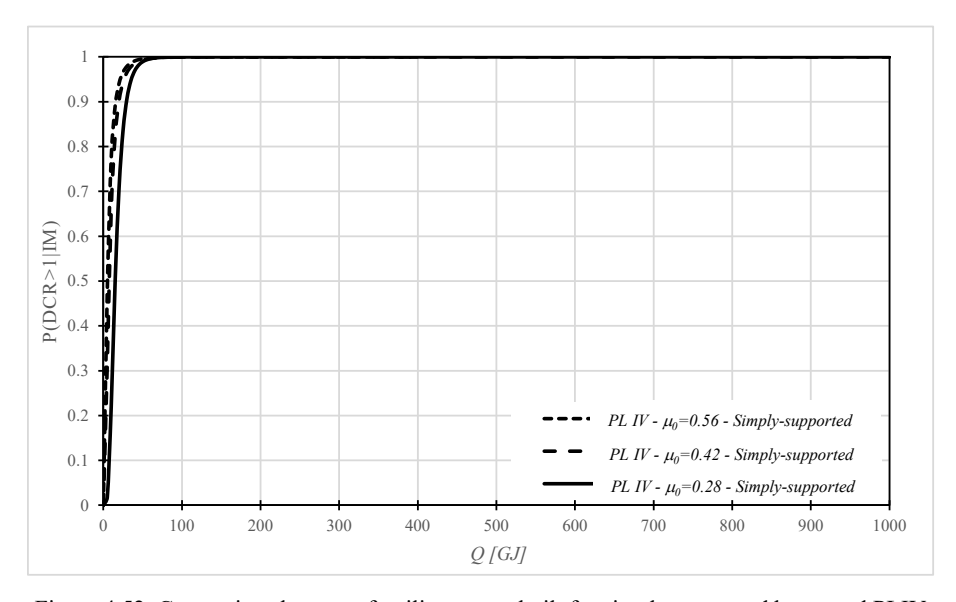


Figure 4.52. Comparison between fragility curves built for simply supported beam and PLIV verification, maximum and residual displacement as a function of Q.

Case 3

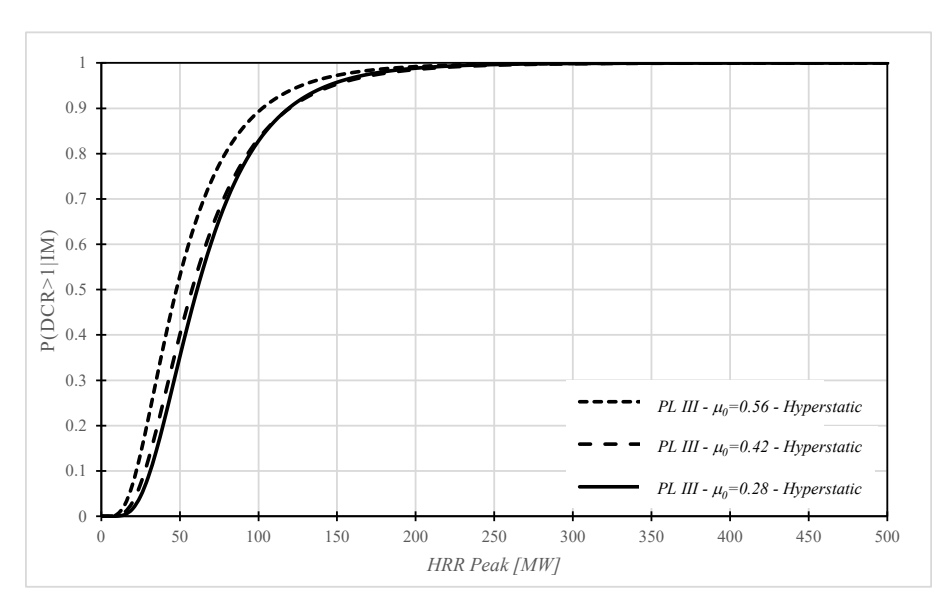


Figure 4.53. Comparison between fragility curves built for hyperstatic beam and PLIII verification, maximum and residual displacement and compressive verification of bottom flange at support as a function of HRR peak.

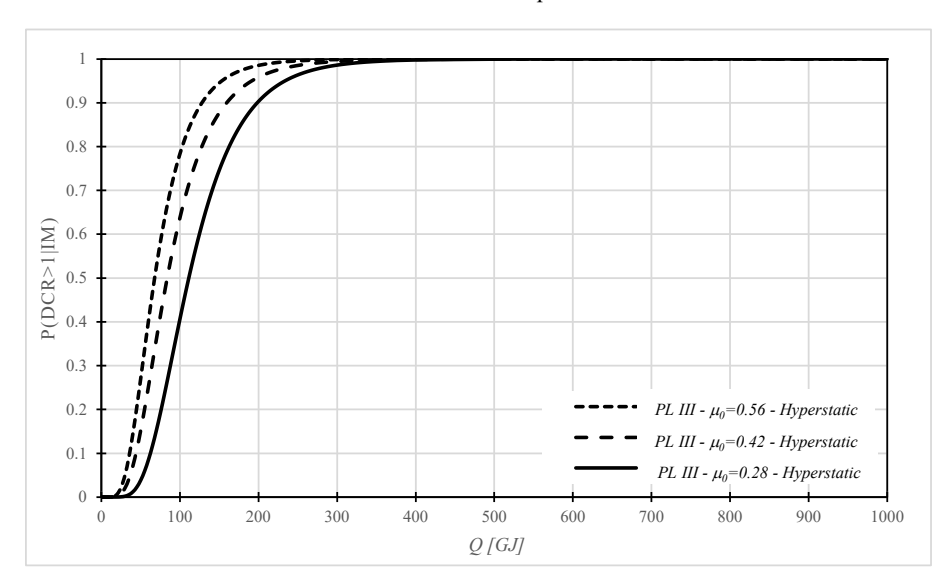


Figure 4.54. Comparison between fragility curves built for hyperstatic beam and PLIII verification, maximum and residual displacement and compressive verification of bottom flange at support as a function of Q.

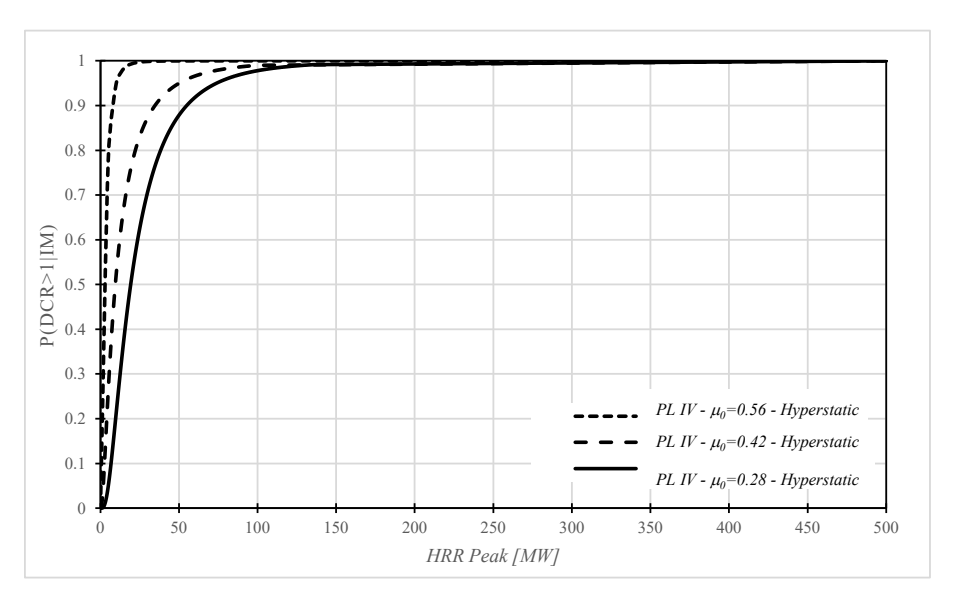


Figure 4.55. Comparison between fragility curves built for hyperstatic beam and PLIV verification, maximum and residual displacement and compressive verification of bottom flange at support as a function of HRR peak.

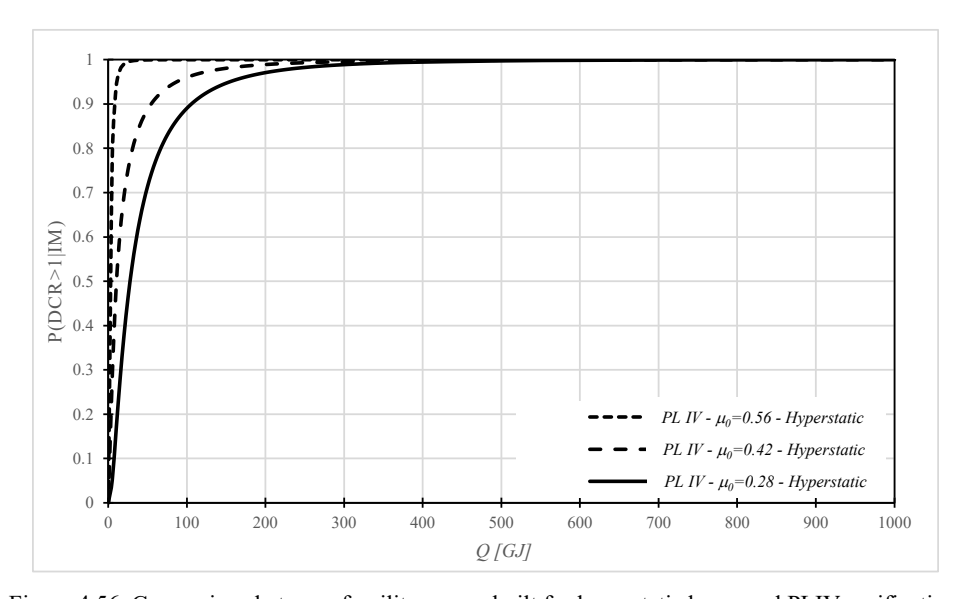


Figure 4.56. Comparison between fragility curves built for hyperstatic beam and PLIV verification, maximum and residual displacement and compressive verification of bottom flange at support as a function of Q.

Other comparisons

The fragility curves previously shown exhibit a good consistency as the fragility increases as a function of the initial degree of utilization for the same static scheme and performance level. Similarly, the same though it can be drawn by varying the performance level. Finally, a comparison is provided between the different static scheme for the same performance level and initial degree of utilization. Let the case analyzed be Case 1, Case 2 and Case 3 as also previously describe. The following two figures provide a comparison between fragility curve built in the three different cases, in order to understand the effect on the fragility for different performance level. Thus, as shown in Figure 4.57, for PLIII the fragility is increasing by taking into account progressively, only maximum displacement (Case 1) also residual displacement (Case 3) and verification for hyperstatic stresses (Case 3). On the contrary, for PLIV case the fragility is not affected from criteria on residual displacement as the fragility curves of Case 1 and 2 overlap each other, as a demonstration of the maximum displacement criteria is more severe in this case. Moreover, the Case 3 exhibits a smaller fragility, shown in Figure 4.58, as the hyperstatic effect is to basically transfer to the deck a negative bending moment which reduce the displacement (maximum and residual) at the same time the high value of axial force does not lead to a verification as severe to increase fragility.

Finally, Figure 4.59, Figure 4.60 and Figure 4.61 show the comparisons between the PLIII and PLIV fragility curve obtained for the three cases.

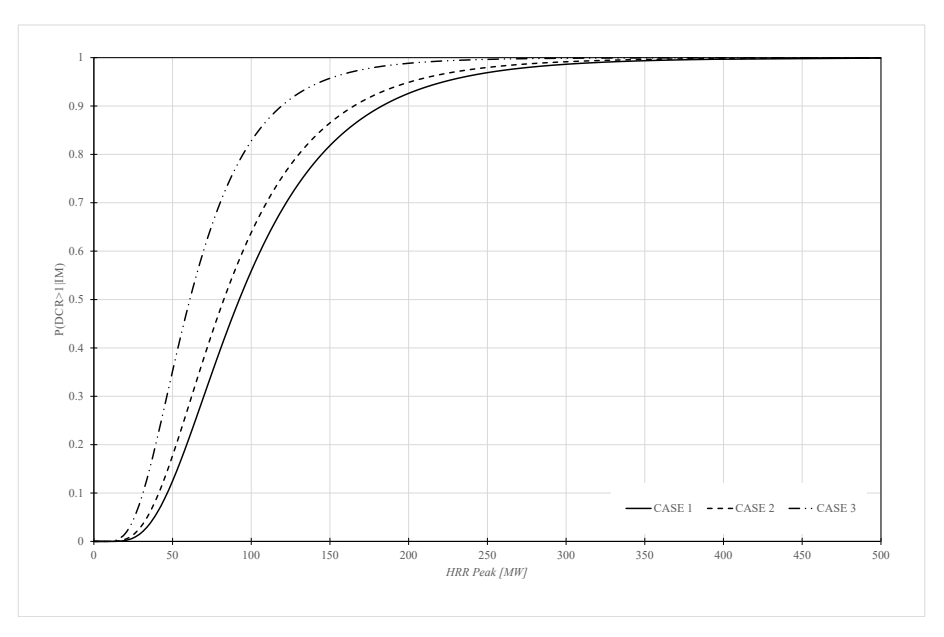


Figure 4.57. Comparison between fragility curves built for PLIII verification, maximum and residual displacement and compressive verification of bottom flange at support as a function of HRR (MW) varying the static scheme.

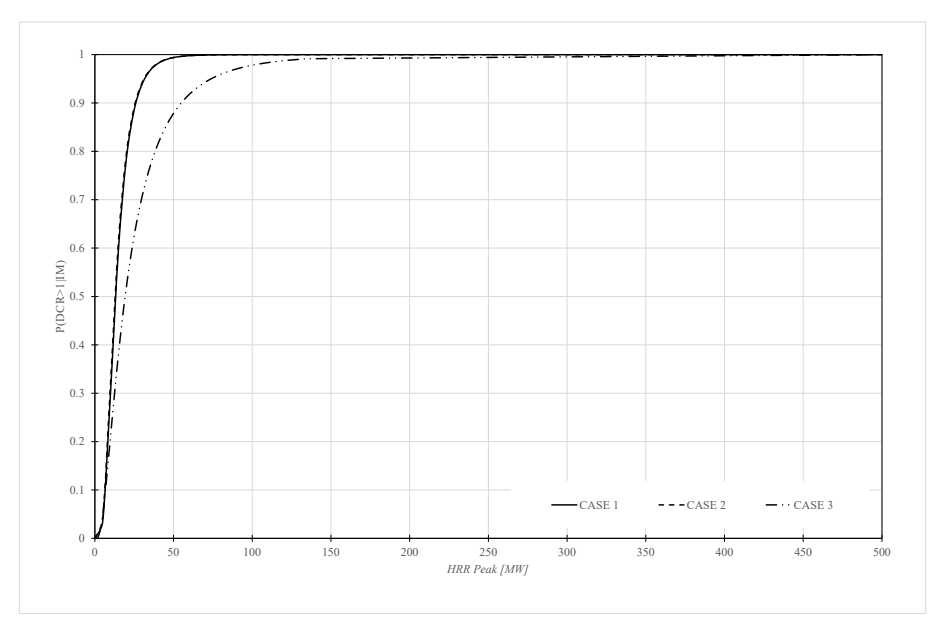


Figure 4.58. Comparison between fragility curves built for PLIV verification, maximum and residual displacement and compressive verification of bottom flange at support as a function of HRR (MW) varying the static scheme.

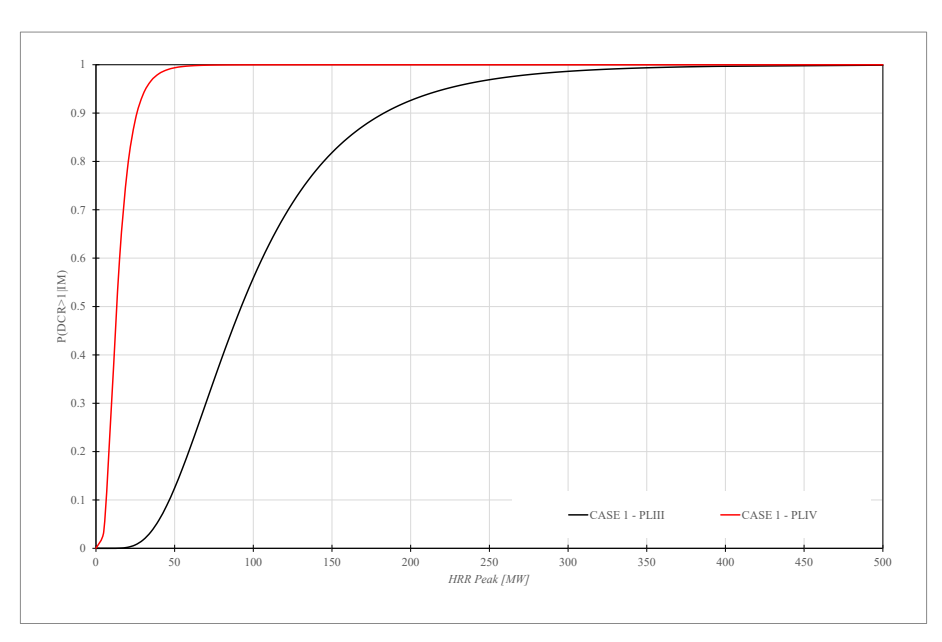
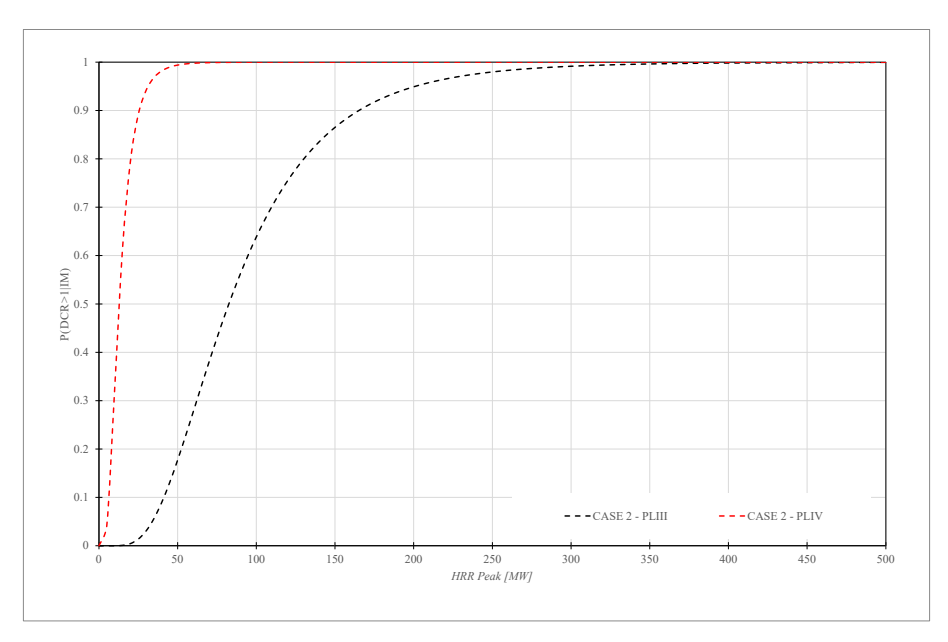


Figure 4.59. Comparison between fragility curves built for PLIII and PLIV verification, maximum displacement in Case 1 as a function of HRR (MW)



 $\label{eq:plumper} Figure~4.60.~Comparison~between~fragility~curves~built~for~PLIII~and~PLIV~verification,~maximum~and~residual~displacement~in~Case~2~as~a~function~of~HRR~(MW)$

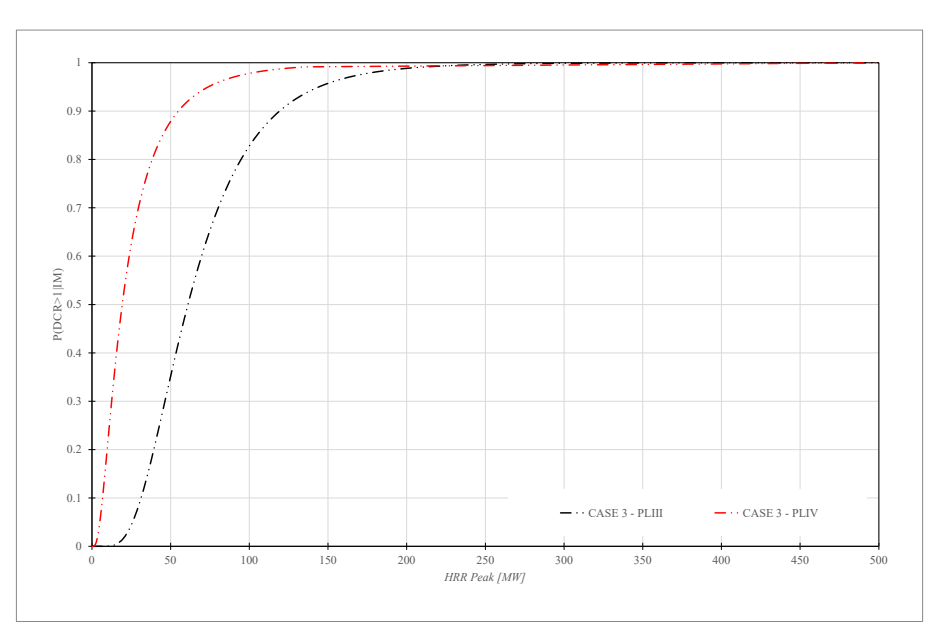
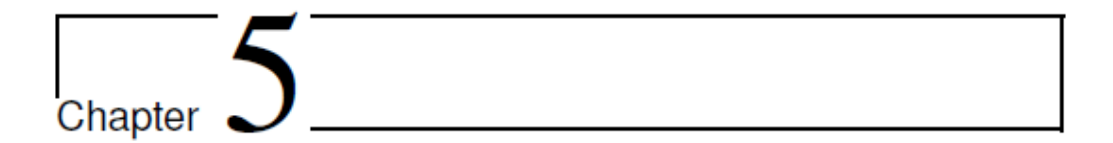


Figure 4.61. Comparison between fragility curves built for PLIII and PLIV verification, maximum and residual displacement and compressive verification of bottom flange at support in Case 3 as a function of HRR (MW)





5 Conclusions

This Ph.D. Thesis offers a comprehensive overview of the topic of fire vulnerability of infrastructures, proposing a new approach for the design and evaluation of fire fragility by defining four performance levels in the performance-based approach domain. The first part focuses on the analysis of the scientific literature and international technical standards in the field. The topic of fire vulnerability of road infrastructures is very sensitive today, as past experiences have shown that fire events in road infrastructures are not negligible in terms of probability of occurrence and, sometimes, the consequences can be significant, compromising the functionality of the structure. The infrastructural works that make up most of the road networks, especially in Italy, are sometimes old and may show a high intrinsic vulnerability to fire. For clarity, a comparison can be made with seismic actions. Many of these structures are so old that the technical standards in force at the time of their construction did not always require checks for seismic loads. However, these structures have a reserve of resistance to horizontal loads because they were designed for other horizontal actions such as wind, braking, or centrifugal forces, and thus show a non-negligible resistance to horizontal actions. In the case of fire actions, these structures were never designed for high temperatures and thus may exhibit significant vulnerability, especially in the case of steel beam viaducts.

In any case, the standards do not prescribe clear verification criteria and performance levels to be achieved, nor the fire load to be considered for thermal analysis. This is instead done for buildings with different categories of use. For these reasons, the first result was to understand the lack in the current standards for which this thesis proposes a vulnerability analysis and fire fragility assessment procedure within the performance-based approach.

Subsequently, an extensive analysis of the technical literature was carried out, from which it was evident that the main method for fire vulnerability investigation is the one proposed by Kodur. This approach, based on the definition of risk, namely that risk is the product of the probability of occurrence of an event, its magnitude, and the exposed value, defines the importance level of a given work. Four importance levels are defined, and each is associated with an IF. Based on the four defined IFs, different verification criteria are provided to achieve the minimum required performance in the context of the prescriptive approach.

This research then focuses on extending this approach by defining expected performance levels, as it is usually defined by technical standards for the performance levels of buildings. The proposed improvement is that structural performance increases with the importance of the work and, consequently, with the performance level that the given work must achieve, this is ensured by safety checks increasing in severity. In fact, with the increase in performance level, the required performance of the structure varies. For the first two levels, the resistance of the structure to collapse is verified, requiring that it does not collapse for two periods of time set equal to the evacuation time or the duration of the fire. For higher performance levels, three and four, the required performance is higher because the structure must not only avoid collapse but also ensure functionality after the fire event. This is achieved by introducing checks on the maximum displacements during the thermal transient and the residual displacements at the end of the event, and resistance check when necessary.

The proposed approach can only be used in the case of vulnerability analysis within the performance-based approach, as the fire safety engineering provides a more accurate evaluation in terms of maximum and residual displacements with respect to the results which can be obtained from a prescriptive-based approach. Consistent with an engineering approach to fire action, the analysis of the temperatures reached in the various parts of the structure is performed by using natural fire curves constructed with zone or CFD models. Additionally, a case study bridge is studied, highlighting the significant differences in the evaluated performance of the infrastructure when a prescriptive method is used compared to the proposed performance-based one. The main results of the comparative study can be summarized in the following points:

- the literature approach does not provide any serviceability or operational limit states of the bridge; in fact, for the two lower performance levels, no verification is required, and for the two higher levels, only ultimate limit state verifications for one or two hours of resistance to the standard hydrocarbon curve are required. The proposed method expands the definition of performance levels, allowing the verification of resistance in the case of less important bridges or post-fire serviceability or operational limit states in the case of strategic bridge;
- the analyses conducted demonstrate how the performance-based engineering approach allows, at the cost of a greater computational burden, to more accurately assess the vulnerability of infrastructures with even substantial differences in the evaluated collapse times.

In the final part, a complete analysis of a case study for a simply supported viaduct composed of steel beams with a non-composite slab is proposed. The complete procedure is presented, from the assessment of the initial degree of utilization to the definition of fire scenarios. The proposed scenarios involve different possible configurations of the infrastructure.

A thermo-mechanical model in SAFIR was developed for the necessary structural evaluations. The model was initially validated by comparing the results of the

analysis for a standard fire curve with those obtained from a reference work in the literature and then with manual analytical calculations. The validation process was conducted as follows:

- the mid-span displacement diagram obtained from the thermo-mechanical model in the SAFIR software was compared with the results shown in the literature obtained from a shell modelling realized in the ABAQUS software. These comparisons showed a good agreement between the results;
- a script was developed to obtain the resistance and stability domain under normal conditions and at elevated temperatures in accordance with Eurocode suggestions. It was demonstrated how the stresses in the beam at the collapse time evaluated by the SAFIR software are on the frontier of the resistance and stability domain reduced for the fire effect, demonstrating the reliability of the analysed thermo-mechanical model results.

From the validation of the thermo-mechanical model, some interesting considerations were drawn:

- the beam modelling of a single beam, assumed as a "sub-structure" of the
 entire span of the viaduct, provides similar results to a much more complex
 and onerous shell modelling of the entire span;
- particular attention was given to the modelling details, including the
 modelling of the eccentricity of the viaduct support relative to the centroid
 of the beam and the modelling of a gap constraint that made the structure
 hyperstatic after a known value of required longitudinal displacement. This
 highlighted the significant effect of hyperstatic actions on the vulnerability
 and fragility of simply supported viaducts.

Once validated, the model was used to evaluate the maximum and residual displacements for each fire scenario that did not lead to structural collapse. The

considered scenarios, for which the HRR curve was evaluated, necessary for CFD analyses, are:

- scenarios involving heavy goods vehicles (HGVs) and cars, like the normal
 operation of the space below the viaduct. In fact, these viaducts are usually
 constructed to span other roads, and for this reason, fire scenarios involving
 trucks, cars, or flammable materials transported by HGVs are commonly
 realized;
- other scenarios consider a potential change in the use of the space under the
 viaduct through a project for changing intended use. In fact, as discussed in
 the thesis, the space under viaducts is often used to create ambient with
 different purposes. For these latter, HRR curves were constructed. It is
 important to note that even in these cases, the temperatures reached are not
 negligible and can compromise the serviceability of the viaducts.

Significant importance is given to the modelling of the structure in CFD software for thermo-fluid dynamic analyses of all the fire scenarios, from which natural fire curves were obtained. The use of these advanced models was considered necessary because the zone models are too limited to the evaluation of temperature in some scenarios (i.e. when the HRR has significant peak).

These curves are useful to evaluate the temperatures in the various parts of the structure, thanks a FEM thermal analysis.

After the thermos-mechanical analyses, all results in terms of demand to capacity ratios for the checks defined at each performance level were included based on a parameter that could identify the severity of the modelled fire event. The parameters used as IM (Intensity Measure) were the peak of the HRR curve and the total fire load Q. This procedure was necessary to construct the fragility curves, obtained using the Cloud linear regression method in the final part of this work.

The fragility curves were constructed by varying these parameters:

- <u>initial degree of utilization:</u> this is a fundamental parameter to understand how much strength reserve the structure has to resist the actions induced by the fire event, both in terms of reduction of stiffness and strength of structural components at high temperatures, and in terms of any hyperstatic actions that may occur.
- <u>static scheme</u>: two static schemes were considered. The first is a simply supported beam where the sliding support has no limitations on longitudinal displacement. The second involves the modelling of a gap constraint that limits longitudinal displacement, meaning that, once the bridge's elongation induced by high temperatures exhausts the available displacement, the structure becomes hyperstatic, and an eccentric normal force is generated in the beam.
- performance level: the performance levels are considered achieved when the defined checks are met. The checks include the maximum vertical displacement recorded during the thermal transient, the residual displacement, and possibly the verification of local compression of the lower flange at the support. For PLIII and PLIV analysed in the construction of the fragility curves, resistance checks are implicitly considered satisfied as the viaduct does not collapse.

The fragility curves defined in this thesis for the typological case-study provide an important indication of the vulnerability of these types of structures to fire actions. The main results are reported below:

the effect of the different verification criteria defined in the new proposed
performance levels is captured as, in the case of a simply supported bridge
and thus in the absence of hyperstatic effects, it was noted that the criterion
on residual displacements increases fragility being a more severe check,
although it is necessary to ensure the operational conditions of the viaduct
after a fire event;

- the effect of hyperstatic actions is evident, as in the specific case examined, the negative moment, transferred from eccentric axial load, tend to reduce the maximum and residual displacements recorded during the thermal transient. However, this does not mean that the viaduct is not vulnerable as the hyperstatic stresses exceed the resistances in some cases, modifying the fragility and sometimes to the reduction of safety;
- the analysis of "b-road" fire scenarios, considering works that can be realized under the viaducts, showed that, in the event of a fire, the consequences of fire are not also related to the building or work which has been built under the viaduct but also to the latter. This places significant emphasis on regulatory prescriptions in this regard.

Therefore, the main conclusions of the PhD thesis work carried out are summarised below:

- The defined performance levels are adequate to assess vulnerability and fragility to fire actions, also depending on the importance of the structure, based on this, to perform checks that can be more or less severe depending on the required performance;
- The methodological approach used in defining the performance levels allows the verifications to be handled without losing the generality of the procedure;
- The fragility curves are a basis for calibrating new intervention strategies according to the characteristics of the bridge.

Further developments are related to the generalization of the method for infrastructures that are not necessarily simply supported viaducts. In fact, the proposed approach will be applied in fire vulnerability and fragility assessment of infrastructure characterized from different static schemes, such as continuous beam bridges or arch bridges. This will be also useful to understand if the defined criteria may not be suitable to evaluate the global performance of the structure.

Furthermore, further studies should be conducted on the analysis of the influence of fire proofing, in the case of steel and composite bridge.

This would allow the generalization of the operational tool provided in this thesis based on certain characteristic parameters of the infrastructure.



6 Bibliography

- [1] V.K.R., Kodur; M.Z., Naser, "Strategies for mitigating fire hazards in trasportation infrastructure," in *IFireSS, Second International Fire Safety Symposium*, Naples, Italy, 2017.
- [2] V.K.R., Kodur; L., Gu; M., Garlock, "Review and Assessment of Fire Hazard in Bridges," *Transportation research record: Journal of the Trasportation Research Board No. 2172*, pp. 23-29, 2009.
- [3] U.S. Department of Transportation Federal highway Administration, *Highway Statistics*, 2010.
- [4] [Online]. Available: https://www.ilriformista.it/incendio-sul-ponte-di-ferro-a-roma-crollata-parte-della-struttura-blackout-e-panico-a-ostiense-251372/.
- [5] [Online]. Available: https://www.nbcnews.com/news/us-news/bridge-collapses-atlanta-freeway-fire-during-rush-hour-n740871.
- [6] [Online]. Available: https://www.nytimes.com/2023/06/11/us/philadelphia-i-95-collapse-vehicle-fire.html.
- [7] [Online]. Available: https://www.nytimes.com/2020/07/29/us/tempe-train-bridge-fire.html.
- [8] Spera R., Stendardo L., "Below the road: Borderline cases in urban morphology," *Urbanform and Design*, vol. n.17/18, 2022.

- [9] V.K.R., Kodur; M.Z., Naser, "Effect of Local Instability on Capacity of Steel Beams Exposed to Fire," *Journal of Constructional Steel Research*, pp. 65-73, 2015.
- [10] Construction Product Directive, 89/106/EEC, 1988.
- [11] Nigro E. et al., Progettazione di strutture in acciaio e composte acciaiocalcestruzzo in caso di incendio, Editore Ulrico HOEPLI Milano, 2010.
- [12] Eurocode 2: Design of concrete structures, Part 1-2: General rules Structural fire design.
- [13] Eurocode 3: Design of steel structures, Part 1-2: General rules Structural fire design.
- [14] Eurocode 1: Actions on structures, Part 1-2: General actions- Action on structures exposed to fire.
- [15] Cook D. Robert et al., Concepts and applications of finite element analysis.
- [16] Gallo M.; Tomeo R.; Nigro E., "Safety Check of Reinforced Concrete Viaducts According to Past and Actual Design National Codes: A Real Case Study," in *ICC*, Napoli, 2022.
- [17] Gallo M.; Tomeo R.; Nigro E., "The soil-structure interaction effect on the seismic vulnerability assessment and retrofitting of existing bridges," in *ANIDIS*, Torino, 2022.
- [18] Ministero delle infrastrutture e dei trasporti , Norme tecniche per le costruzioni, 2018.
- [19] NFPA, U.S., Vehicle Fire Trends and Patterns, Batterymarch Park, Quincy, 2008.

- [20] NFPA, U.S., Guide for the Evaluation of Fire Risk Assessment, 2007.
- [21] K., Wardhana; F., Hadipriono, "Study of recent building failures in the United States," *J. Perform. Constr. Facil.*, pp. 151-158, 2003.
- [22] J., Sheer, "Failed Bridges: Case studies, Causes and Consequences," *John Wiley & Sons*.
- [23] U.S. Fire Administration Fire Estimates, U.S. Department of Homeland Security, "National Fire Data Center," 2014.
- [24] A., Eldukair; B., Ayyub, "Analysis of recent U.S. structural construction failures," *Journal of Performance of constructed Facilities*, pp. 57-73, 1991.
- [25] V.K.R., Kodur; M.Z., Naser, "Importance Factor for Design of Bridges Against Fire Hazard," *Engineering Structures*, pp. 207-220, 2013.
- [26] M., Garlock; I., Paya-Zaforteza; Kodur V.K.R., Gu L., "Fire hazard in bridges: review, assessment and repair strategies," *Engineering Structures*, pp. 89-98.
- [27] T., Elhag; Y., Wang, "Risk assessment for bridge maintenance projects; neural network versus regression techniques," *J. Comput. Civil Eng.*, 2007.
- [28] M., Dwaikat; V.K.R., Kodur, "A performance based methodology for fire design of restrained steel beams," *J. Construct. Steel Res.*, pp. 510-524, 2011.
- [29] Miano A et Al., "Updating of the seismic fragility curves for RC buildings subjected to slow-moving settlements," *Journal of Building Engineering*, 2024.
- [30] Gaetani d'Aragona M.; Polese M.; Prota A., "Seismic fragility curves for infilled RC building classes considering multiple sources of uncertainty," *Engineering Structures*, 2024.

- [31] Miano A.; Mele A.; Prota A., "Fragility curves for different classes of existing RC buildings under ground differential settlements," *Engineering Structures*, 2022.
- [32] Cantisani G.; Della Corte G., "Collapse Fragility Curves for Non-residential Older Single-Storey Steel Buildings," *BEHAVIOUR OF STEEL STRUCTURES IN SEISMIC AREAS*, 2022.
- [33] Scalvenzi M. et Al., "Progressive collapse fragility of substandard and earthquake-resistant precast RC buildings," *Engineering Structures*, 2023.
- [34] Crisci G. et Al., "Seismic vulnerability assessment of RC deck-stiffened arch bridges," *Engineering Structuers*, 2024.
- [35] Miano A. et Al., "Seismic fragility of circular piers in simply supported RC bridges: A proposal for capacity assessment," *Engineering Structures*, 2024.
- [36] Della Corte G.; Landoldo R.; Mazzolani F.M., "Post-earthquake fire resistance of moment resisting steel frames," *Fire Safety Journal*, 2003.
- [37] Gernay T.; Khorasani N.E., "Fragility analysis of a steel building in fire," *CONFAB*, 2015.
- [38] Cardellino E.; de Silva D.; Nigro E., "Estimation of Structural Fire Vulnerability Through Fragility Curves," *EUROSTRUCT*, 2021.
- [39] Ministero dell'Interno, Dipartimento dei vigili del Fuoco, del Soccorso pubblico e della Difesa civile, Direzione centrale per Prevenzione e la Sicurezza tecnica, "Norme tecniche di prevenzione incendi," 2022.
- [40] D., Schultz, "fire protection in tunnels: focus on road and rail tunnels," Technical Newsletter SCOR Global P&C, 2014.

- [41] EN 1363-1, "Fire resistance test: General requirements, European Committee for standardization," 2012.
- [42] J.M., Franssen, "A Thermal/Structural Program Modelling Structures under Fire," *Engineering Journal*, vol. 42, no. 3, 2005.
- [43] Peacock R.D. at al., "CFAST Consolidated Model of Fire Growth and Smoke Transport," *NIST Special Publication*, 2008.
- [44] M.Z., Naser; V.K.R., Kodur, "A probabilistic assessment for classification of bridges against fire hazard," *Fire Safety Journal*, 2015.
- [45] I., Paya-Zaforteza; M., Garlock, "A Numerical Investigation on the Fire Response of a Steel Girder Bridge," *Journal of Constructional Steel Research*, pp. 93-103, 2012.
- [46] D.E., Wainman; B.R., Kirthy, "Compendium of UK Standard Fire Test Data Unprotected Structural Steel," *British Steel Technical and Sweden Laboratories*, 1989.
- [47] McGrattan K.B. et al., "Fire Dynamics Simulato (Version 5) Technical Reference Guide," *NIST Special Pubblicatio*, 2010.
- [48] Wright W. et al., "Highway Bridge Fire Hazard Assessment Draft Final Report," *Virginia Polytechnic Institute and State University*, 2013.
- [49] Commissione per la Sicurezza delle Costruzioni in Acciaio in caso di Incendio, "Nomogramma Metodo Grafico di Valutazione della Resistenza al Fuoco di Strutture in Acciaio," *Fondazione Promozione Acciaio*, 2005.

- [50] Gernay T., Elhami Khorasani N., Garlock N., "Fire Fragility Curves for Industrial Steel Pipe-Racks Integrating Demand and Capacity Uncertainties," *FIRE TECHNOLOGY*, pp. 713-742, 2022.
- [51] Zhu Z., Quiel S.E., Khorasani N.E., "Bivariate Structural-Fire Fragility Curves for simple-span overpass bridges with composite steel plate girder," *Structural Safety*, 2023.
- [52] Peris-Sayol G., Payà-Zaforteza I., Moya J.A., Hospitale A., "Analysis of the Influence of Structural Models in Fire Responses of Steel Girder Bridges," *Structures Congress*, 2015.
- [53] Jean-Marc Franssen & Thomas Gernay, "A computer program for analysis of structures subjected to fire," 2023.
- [54] Patrick Covi, Nicola Tondini, Enrico Giurati, "Comparative Analysis of the Fire Performance of a steel arch Bridge," *SiF*, 2018.
- [55] Thunderhead Engineering, "PyroSim User Manual," 2024.
- [56] NIST, "Fire Dynamics Simulator User's Guide".
- [57] Jalayer F. et al., "Analytical fragility assessment using unscaled ground motion records," *Wiley*, 2017.
- [58] Jalayer F. et al., "Cloud Analysis revisited: efficient fragility calculation and uncertainty propagation using simple linear regression," *U.S. National Conference on Earthquake Engineering*, 2014.
- [59] Morgan J. Hurley, "SFPE Handbook of Fire Protection Enginnering," *Springer*.

[60] Iervolino Iunio, "Assessing uncertainty in estimation of seismic response for PBEE," *Earthquake engineering & structural dynamics*, 2017.



Author's publications

- Marco Gallo, Romeo Tomeo, Emidio Nigro. Safety Check of Reinforced Concrete Viaducts According to Past and Actual Design National Codes: A Real Case Study, Italian Concrete Conference 2022 pp. 466-480, 2023. DOI: 10.1007/978-3-03143102-9 36.
- 2. Donatella de Silva, Marco Gallo, Laura de Falco, Emidio Nigro. Fire risk assessment of bridges: from state of the art to structural vulnerability mitigation, Journal of Civil Structural Health Monitoring, 2023. DOI: 10.1007/s13349-02300670-z.
- Marco Gallo, Romeo Tomeo, Emidio Nigro. The soil-structure interaction effect on the seismic vulnerability assessment and retrofitting of existing bridges, Procedia Structural Integrity, 2023. DOI: 10.1016/j.prostr.2023.01.081.
- 4. Marco Gallo, Donatella de Silva, Laura de Falco, Emidio Nigro. Structural fire design and assessment of bridges: State of the art. Fib Symposium, 2022, pp. 459-466. DOI: 2-s2.0s85142822653.



Appendix A – Procedure for resistance and buckling domain in cold and fire conditions evaluation

Eq. A.1

$$A_{pro} = 2 \cdot b \cdot t_f + (h - 2 \cdot t_f) \cdot t_w = 565.73 \text{ cm}^2$$
 Eq. A.1
$$I_y = 2 \cdot \left(\frac{b \cdot t_f^3}{12} + b \cdot t_f \cdot \left(\frac{h - t_f}{2}\right)^2\right) + t_w \cdot \frac{(h - 2 \cdot t_f)^3}{12} = 839422.77 \text{ cm}^4$$
 Eq. A.2
$$I_z = 2 \cdot t_f \cdot \frac{b^3}{12} + (h - 2 \cdot t_f) \cdot \frac{t_w^3}{12} = 54039.22 \text{ cm}^4$$
 Eq. A.3
$$I_p := I_y + I_z = 893462.00 \text{ cm}^4$$
 Eq. A.4
$$i_y := \sqrt[2]{\frac{I_y}{A_{pro}}} = 385.2 \text{ mm}$$
 Eq. A.5
$$i_z := \sqrt[3]{\frac{I_z}{A_{pro}}} = 97.73 \text{ mm}$$
 Eq. A.6
$$W_{el.y} := I_y \cdot \frac{2}{h} = 17990.2 \text{ cm}^3$$
 Eq. A.7
$$W_{el.x} := I_z \cdot \frac{2}{b} = 2553.84 \text{ cm}^3$$
 Eq. A.8
$$J_t := \frac{1}{3} \cdot (2 \cdot b \cdot t_f^3 + (h - 2 \cdot t_f) \cdot t_w^3) = 2592.1 \text{ cm}^4$$
 Eq. A.9
$$W_{pl.y} := 2 \cdot \left(b \cdot t_f \cdot \left(\frac{h - t_f}{2}\right) + \frac{t_w}{2} \cdot \left(\frac{h}{2} - t_f\right)^2\right) = 20422.46 \text{ cm}^3$$
 Eq. A.10
$$W_{pl.x} := 2 \cdot \left(2 \cdot t_f \cdot \frac{b^2}{8} + (h - 2 \cdot t_f) \cdot \frac{t_w^2}{8}\right) = 3946.85 \text{ cm}^3$$
 Eq. A.11
$$I_w := I_y \cdot \frac{h^2}{4} = 1827553992.77 \text{ cm}^6$$
 Eq. A.12
$$CL_{uh} := \text{if } \frac{(b - t_w - 2 \cdot r_1)}{2 \cdot t_f} < 10 \cdot \varepsilon$$
 Eq. A.13
$$\begin{vmatrix} 1 \\ else \text{ if } \frac{(b - t_w - 2 \cdot r_1)}{2 \cdot t_f} < 10 \cdot \varepsilon$$
 Eq. A.13
$$\begin{vmatrix} 1 \\ else \text{ if } \frac{(b - t_w - 2 \cdot r_1)}{2 \cdot t_f} < 14 \cdot \varepsilon$$
 Eq. A.13
$$\begin{vmatrix} 1 \\ else \text{ if } \frac{(h - 2 \cdot t_f - 2 \cdot r_1)}{t_w} < 42 \cdot \varepsilon$$
 Eq. A.13
$$\begin{vmatrix} 1 \\ else \text{ if } \frac{(h - 2 \cdot t_f - 2 \cdot r_1)}{t_w} < 42 \cdot \varepsilon$$
 Eq. A.13
$$\begin{vmatrix} 1 \\ else \text{ if } \frac{(h - 2 \cdot t_f - 2 \cdot r_1)}{t_w} < 42 \cdot \varepsilon$$
 Eq. A.13
$$\begin{vmatrix} 1 \\ else \text{ if } \frac{(h - 2 \cdot t_f - 2 \cdot r_1)}{t_w} < 42 \cdot \varepsilon$$
 Eq. A.13
$$\begin{vmatrix} 1 \\ else \text{ if } \frac{(h - 2 \cdot t_f - 2 \cdot r_1)}{t_w} < 42 \cdot \varepsilon$$
 Eq. A.13
$$\begin{vmatrix} 1 \\ else \text{ if } \frac{(h - 2 \cdot t_f - 2 \cdot r_1)}{t_w} < 42 \cdot \varepsilon$$
 Eq. A.16

$$M \coloneqq \begin{bmatrix} 1 & 2 & 3 & 4 \\ 2 & 2 & 3 & 4 \\ 3 & 3 & 3 & 4 \\ 4 & 4 & 4 & 4 \end{bmatrix}$$
 Eq. A.14

$$CL_{pro} := M_{CL_{off}, CL_{origina}} = 2$$
 Eq. A.15

$$a = min\left(0.5, \frac{A_{pro} - 2 \cdot b \cdot t_f}{A_{pro}}\right) = 0.36$$
 Eq. A.16

$$N_{pl} \coloneqq A_{pro} \cdot \frac{f_y}{\gamma_{M0}} = 14143.32 \text{ kN}$$
 Eq. A.17

$$n\left(N_{app}\right) \coloneqq \frac{N_{app}}{N_{pl}}$$
 Eq. A.18

$$\begin{aligned} W_y &\coloneqq \text{if } CL_{pro} = 1 \\ &\parallel W_{pl,y} \\ &\text{else if } CL_{pro} = 2 \\ &\parallel W_{pl,y} \\ &\text{else if } CL_{pro} = 3 \\ &\parallel W_{el,y} \\ &\text{else} \\ &\parallel 0.0 \text{ } cm^3 \end{aligned} \end{aligned}$$
 Eq. A.19

$$M_{pl} = W_y \cdot \frac{f_y}{\gamma_{M0}} = 5105.62 \text{ kN} \cdot m$$
 Eq. A.20

$$\begin{split} M_{N.y.Rd}\left(N_{app}\right) \coloneqq & \text{if } M_{pl} \cdot \frac{1 - n\left(N_{app}\right)}{1 - 0.5 \cdot a} \ge M_{pl} \\ & \parallel M_{pl} \\ & \text{else} \\ & \parallel M_{pl} \cdot \frac{1 - n\left(N_{app}\right)}{1 - 0.5 \cdot a} \end{split}$$

Appendix A – Procedure for resistance and buckling domain in cold and fire conditions evaluation

$$\beta_y = 1 \beta_z = 1$$
 Eq. A.23

$$L_{0y} := \beta_y \cdot L = 21 \ m \ L_{0z} := \beta_z \cdot L = 21 \ m$$
 Eq. A.24

$$N_{cr.y}$$
:= $\pi^2 \cdot E_s \cdot \frac{I_y}{L_{0y}^2}$ = 39451.29 kN

$$N_{cr.z}\!\!\coloneqq\!\pi^2\cdot\!E_s\!\cdot\!\frac{I_z}{L_{0y}^2}\!=\!2539.74~\text{kN} \label{eq:Ncr.z}$$
 Eq. A.26

$$\lambda_{seg.y} \coloneqq \sqrt[2]{\frac{N_{pl}}{N_{cr.y}}} = 0.6$$
 Eq. A.27

$$\lambda_{seg.z} \coloneqq \sqrt[2]{\frac{N_{pl}}{N_{cr.z}}} = 2.36$$
 Eq. A.28

$$\Phi_y := 0.5 \cdot (1 + \alpha_y \cdot (\lambda_{seg,y} - 0.2) + \lambda_{seg,y}^2) = 0.72$$
 Eq. A.29

$$\Phi_z := 0.5 \cdot (1 + \alpha_z \cdot (\lambda_{seq.z} - 0.2) + \lambda_{seq.z}^2) = 3.65$$
 Eq. A.30

$$\chi_y := \frac{1}{\Phi_y + \sqrt[2]{\Phi_y^2 - \lambda_{seg,y}^2}} = 0.89$$
 Eq. A.31

$$\chi_z = \frac{1}{\Phi_z + \sqrt[2]{\Phi_z^2 - \lambda_{sea.z}^2}} = 0.16$$
 Eq. A.32

$$\chi := min(\chi_y, \chi_z) = 0.16$$
 Eq. A.33

$$lpha_{LT}$$
:= if Cur_{LT} = "a" | =0.34 Eq. A.34 | =0.34 else if Cur_{LT} = "b" | 0.34 else if Cur_{LT} = "c" | 0.49 else | 0.76

$$M_{app} = -N_{Ed} \cdot \frac{h}{2} = 0 \text{ kN} \cdot m$$
 Eq. A.35

$$M_{mezz} = M_{app} + q_{Ed} \cdot \frac{L^2}{8} = 1433.25 \text{ kN} \cdot m$$
 Eq. A.36

$$k = 1$$
 Eq. A.37

$$m := \frac{|M_{app}|}{M_{mezz}} = 0$$
 Eq. A.38

$$C_1 = 1.13 + 0.74 \cdot m = 1.13$$
 Eq. A.39

$$M_{cr} \coloneqq C_1 \frac{\pi}{k \cdot L} \cdot \sqrt[4]{\left(E_s \cdot I_y\right) \cdot \left(G \cdot J_t\right)} \cdot \sqrt[4]{1 + \frac{\pi^2 \cdot E_s \cdot I_\omega}{k^2 \cdot L^2 \cdot G \cdot J_t}} = 23198.04 \ \textit{kN} \cdot \textit{m}$$
 Eq. A.40

$$\lambda_{seg.LT} \coloneqq \sqrt[2]{W_y \cdot \frac{f_y}{\gamma_{M0} \cdot M_{cr}}} = 0.47$$
 Eq. A.41

$$\lambda_{seg,LT.0} = 0.4$$
 Eq. A.42

$$\beta_{LT}$$
:= **0.75** Eq. A.43

$$\Phi_{LT} := 0.5 \cdot \left(1 + \alpha_{LT} \cdot \left(\lambda_{seg,LT} - \lambda_{seg,LT,0}\right) + \beta_{LT} \cdot \lambda_{seg,LT}^{2}\right) = 0.59$$
 Eq. A.44

$$X_{LT} = min \left(1, \frac{1}{\lambda_{mg,LT}^2}, \frac{1}{\phi_{LT}^2 \sqrt{\psi_{LT}^2 - \beta_{LT} \cdot \lambda_{mg,LT}^2}}\right) = 0.97$$

$$Eq. A.45$$

$$N_{yk} := A_{pro} \cdot f_y = 14143.32 \text{ kN}$$

$$Eq. A.46$$

$$a = 0.36$$

$$Eq. A.47$$

$$\chi_y = 0.89$$

$$Eq. A.48$$

$$\chi_z = 0.16$$

$$Eq. A.49$$

$$\lambda_{seg,y} = 0.6$$

$$Eq. A.50$$

$$\lambda_{seg,z} = 2.36$$

$$Eq. A.51$$

$$\psi := 1$$

$$Eq. A.52$$

$$\alpha_z := \text{if } M_{app} = 0$$

$$\| 1 \\ \text{else} \\ \| min \left(\max \left(\frac{M_{mex}}{M_{app}}, -1 \right), 1 \right) \right|$$

$$C_{mg} := \text{if } \alpha_z \ge 0$$

$$\| \max \left(0.4, 0.2 + 0.8 \cdot \alpha_s \right) \\ \text{else if } \alpha_s < 0.0 \cdot \psi \ge 0$$

$$\| \max \left(0.4, 0.1 - 0.8 \cdot \alpha_s \right) \\ \text{else if } \alpha_s < 0.0 \cdot \psi \ge 0$$

$$\| \max \left(0.4, 0.1 \cdot (1 - \psi) - 0.8 \cdot \alpha_s \right) \\ \text{else if } \alpha_s < 0.0 \cdot \psi \ge 0$$

$$\| \max \left(0.4, 0.1 \cdot (1 - \psi) - 0.8 \cdot \alpha_s \right) \\ \text{else }$$

$$\| \max \left(0.4, 0.1 \cdot (1 - \psi) - 0.8 \cdot \alpha_s \right) \\ \text{else }$$

$$\| \max \left(0.4, 0.1 \cdot (1 - \psi) - 0.8 \cdot \alpha_s \right) \\ \text{else }$$

$$\| \max \left(0.4, 0.1 \cdot (1 - \psi) - 0.8 \cdot \alpha_s \right) \\ \text{else }$$

$$\| \max \left(0.4, 0.1 \cdot (1 - \psi) - 0.8 \cdot \alpha_s \right) \\ \text{else }$$

$$\| \max \left(0.4, 0.1 \cdot (1 - \psi) - 0.8 \cdot \alpha_s \right) \\ \text{else }$$

$$\| \max \left(0.4, 0.1 \cdot (1 - \psi) - 0.8 \cdot \alpha_s \right) \\ \text{else }$$

$$\| \max \left(0.4, 0.1 \cdot (1 - \psi) - 0.8 \cdot \alpha_s \right) \\ \text{else }$$

$$\| \max \left(0.4, 0.1 \cdot (1 - \psi) - 0.8 \cdot \alpha_s \right) \\ \text{else }$$

$$\| \max \left(0.4, 0.1 \cdot (1 - \psi) - 0.8 \cdot \alpha_s \right) \\ \text{else }$$

$$\| \max \left(0.4, 0.1 \cdot (1 - \psi) - 0.8 \cdot \alpha_s \right) \\ \text{else }$$

$$\| \max \left(0.4, 0.1 \cdot (1 - \psi) - 0.8 \cdot \alpha_s \right) \\ \text{else }$$

$$\| \max \left(0.4, 0.1 \cdot (1 - \psi) - 0.8 \cdot \alpha_s \right) \\ \text{else }$$

$$\| \max \left(0.4, 0.1 \cdot (1 - \psi) - 0.8 \cdot \alpha_s \right) \\ \text{else }$$

$$\| \max \left(0.4, 0.1 \cdot (1 - \psi) - 0.8 \cdot \alpha_s \right) \\ \text{else }$$

$$\| \max \left(0.4, 0.1 \cdot (1 - \psi) - 0.8 \cdot \alpha_s \right) \\ \text{else }$$

$$\| \max \left(0.4, 0.1 \cdot (1 - \psi) - 0.8 \cdot \alpha_s \right) \\ \text{else }$$

$$\| \max \left(0.4, 0.1 \cdot (1 - \psi) - 0.8 \cdot \alpha_s \right) \\ \text{else }$$

$$\| \max \left(0.4, 0.1 \cdot (1 - \psi) - 0.8 \cdot \alpha_s \right) \\ \text{else }$$

$$\| \max \left(0.4, 0.1 \cdot (1 - \psi) - 0.8 \cdot \alpha_s \right) \\ \text{else }$$

$$\| \max \left(0.4, 0.1 \cdot (1 - \psi) - 0.8 \cdot \alpha_s \right) \\ \text{else }$$

$$\| \min \left(0.4, 0.1 \cdot (1 - \psi) - 0.8 \cdot \alpha_s \right) \\ \text{else }$$

$$\| \min \left(0.4, 0.1 \cdot (1 - \psi) - 0.8 \cdot \alpha_s \right) \\ \text{else }$$

$$\| \min \left(0.4, 0.1 \cdot (1 - \psi) - 0.8 \cdot \alpha_s \right) \\ \text{else }$$

$$\| \min \left(0.4, 0.1 \cdot (1 - \psi) - 0.8 \cdot \alpha_s \right) \\ \text{else }$$

$$\| \min \left(0.4, 0.1 \cdot (1 - \psi) -$$

Appendix A – Procedure for resistance and buckling domain in cold and fire conditions evaluation

$$k_{yy}\left(N_{d}\right) \coloneqq min\left(C_{my} \cdot \left(1 + 0.8 \cdot \frac{N_{d} \cdot \gamma_{M1}}{\chi_{y} \cdot N_{yk}}\right), C_{my} \cdot \left(1 + \left(\lambda_{seg.y} - 0.2\right) \cdot \frac{N_{d} \cdot \gamma_{M1}}{\chi_{y} \cdot N_{yk}}\right)\right)$$
 Eq. A.58

$$k_{zz} \left(N_d \right) \coloneqq min \left(C_{mz} \cdot \left(1 + 1.4 \cdot \frac{N_d \cdot \gamma_{M1}}{\chi_z \cdot N_{uk}} \right), C_{mz} \cdot \left(1 + \left(2 \ \lambda_{seg.z} - 0.6 \right) \cdot \frac{N_d \cdot \gamma_{M1}}{\chi_z \cdot N_{uk}} \right) \right)$$
 Eq. A.59

$$k_{zy} \langle N_d \rangle \coloneqq \max \left(1 - \frac{0.1 \cdot \lambda_{seg.z}}{C_{mLT} - 0.25} \cdot \frac{N_d \cdot \gamma_{M1}}{\chi_z \cdot N_{yk}}, 1 - \frac{0.1}{C_{mLT} - 0.25} \cdot \frac{N_d \cdot \gamma_{M1}}{\chi_z \cdot N_{yk}} \right)$$
 Eq. A.60

$$k_{uz}(N_d) := 0.6 \cdot k_{zz}(N_d)$$
 Eq. A.61

$$N_{b.Rd} := \chi_y \cdot \frac{A_{pro} \cdot f_y}{\gamma_{Mo}} = 12594.17 \text{ kN}$$

$$M_{b,Rd}(N) := M_{pl}$$
 Eq. A.63

$$M_{inst} = 0 \ kN \cdot m$$
 Eq. A.64

$$\begin{aligned} M_{stab.y}(N_d) &\coloneqq \text{if } N_d \leq N_{b.Rd} \\ & \left\| \frac{1}{k_{yy}(N_d)} \cdot \left(1 - \frac{N_d}{N_{b.Rd}} \right) \cdot M_{b.Rd}(N_d) \right\| \\ &\text{else} \\ & \left\| M_{inst} \right| \end{aligned}$$

$$\lambda_{seg,\theta} \coloneqq \lambda_{seg,y} \cdot \left(\frac{k_{y\theta} \left(\theta_{max} \right)}{k_{E\theta} \left(\theta_{max} \right)} \right)^{0.5} = 0.72$$
 Eq. A.66

$$\alpha := 0.65 \cdot \left(\frac{235 \ MPa}{f_y}\right)^{0.5} = 0.63$$
 Eq. A.67

$$\varphi_{\theta} := \frac{1}{2} \cdot \left(1 + \alpha \cdot \lambda_{seg,\theta} + \lambda_{seg,\theta}^{2} \right) = 0.99$$
 Eq. A.68

$$\chi_{fi} := \frac{1}{\varphi_{\theta} + \sqrt[2]{\varphi_{\theta}^2 - \lambda_{seg,\theta}^2}} = 0.6$$
Eq. A.69

$$N_{\textit{fi.t.Rd}} \coloneqq A_{\textit{pro}} \cdot k_{y\theta} \left(\theta_{\textit{max}}\right) \cdot \frac{f_y}{\gamma_{\textit{M0.fi}}} = 11006.37 \text{ kN}$$
 Eq. A.70

$$N_{pl} = 14143.32 \text{ kN}$$
 Eq. A.71

$$M_{N.y.Rd}(N_{Ed.fi}) = 4914.86 \text{ kN} \cdot m$$
 Eq. A.72

$$M_{fi.t.Rd} := k_{y\theta} \left(\theta_{max}\right) \cdot \left(\frac{\gamma_{M0}}{\gamma_{M0,fi}}\right) \cdot W_y \cdot f_y = 3973.21 \text{ kN} \cdot m$$
 Eq. A.73

$$\begin{aligned} M_{fi.Rd}\left(N_{d}\right) &\coloneqq \text{if } M_{fi.t.Rd} \cdot \left(1 - \frac{N_{d}}{N_{fi.t.Rd}}\right) \leq 0 \\ & \parallel 0 \text{ kN} \cdot m \\ &\text{else} \\ & \parallel M_{fi.t.Rd} \cdot \left(1 - \frac{N_{d}}{N_{fi.t.Rd}}\right) \end{aligned}$$

$$M_{app,fi} = -N_{Ed,fi} \cdot \frac{h}{2} = -1393.73 \text{ kN} \cdot m$$
 Eq. A.75

$$M_{mezz,fi} := M_{app,fi} + q_{Ed} \cdot \frac{L^2}{8} = 39.52 \text{ kN} \cdot m$$
 Eq. A.76

$$N_{b.f.t.Rd} := \chi_{fi} \cdot A_{pro} \cdot k_{y\theta} \left(\theta_{max}\right) \cdot \frac{f_y}{\gamma_{M0.fi}} = 6602.08 \text{ kN}$$
 Eq. A.77

$$\Delta M \coloneqq \left| M_{app,fi} \right| + \left| M_{mezz,fi} \right| = 1433.25 \text{ kN} \cdot m$$
 Eq. A.78

$$\beta_{M} \coloneqq \text{if } M_{app,fi} = 0 \text{ kN} \cdot m$$

$$\parallel 1.3 \text{ else}$$

$$\parallel 1.1 + \frac{M_{mezz,fi}}{\Delta M} \cdot (1.3 - 1.1)$$

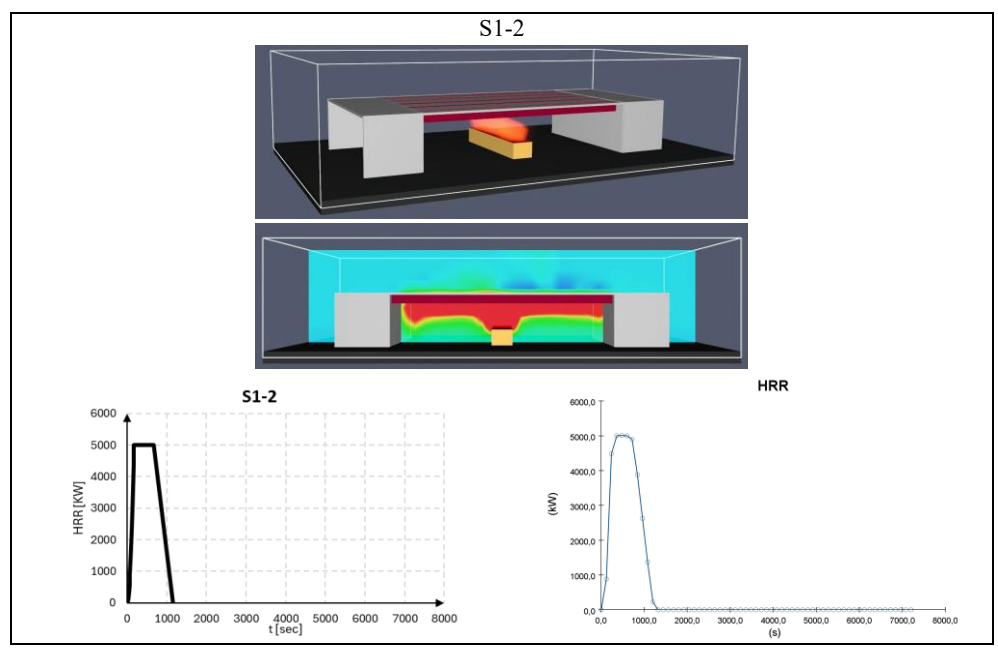
$$= 1.11$$
Eq. A.79

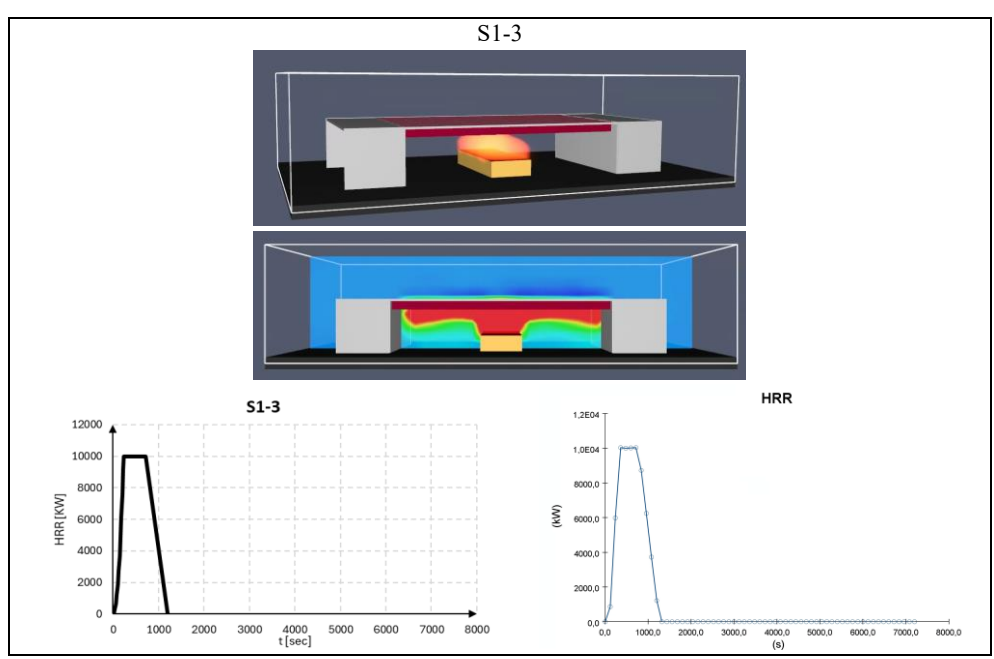
$$\mu_y\!\coloneqq\!\min\big(0.8\,,\big(2\,\boldsymbol{\cdot}\,\beta_{M}-5\big)\,\boldsymbol{\cdot}\,\lambda_{seg,\theta}+0.44\,\boldsymbol{\cdot}\,\beta_{M}+0.29\big)\!=\!-1.25 \tag{Eq. A.80}$$

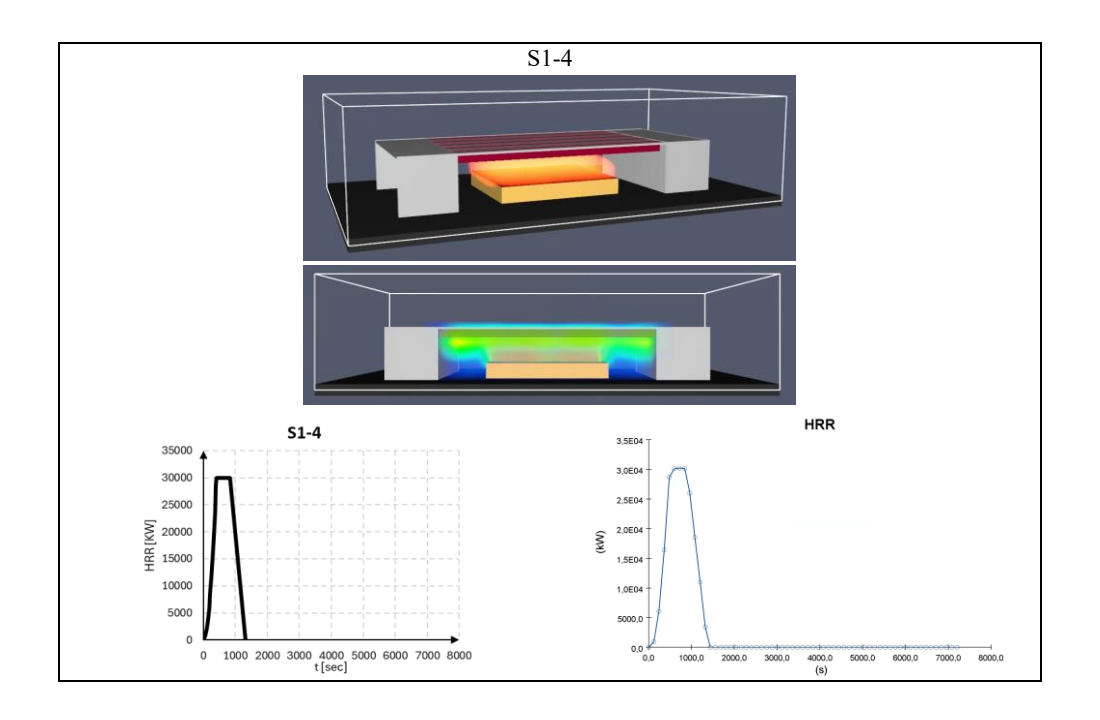
$$k_{y.fi} \left(N_d \right) \coloneqq 1 - \frac{\mu_y \cdot N_d}{\chi_{fi} \cdot A_{pro} \cdot k_{y\theta} \left(\theta_{max} \right) \cdot \frac{f_y}{\gamma_{M0.fi}}}$$
 Eq. A.81

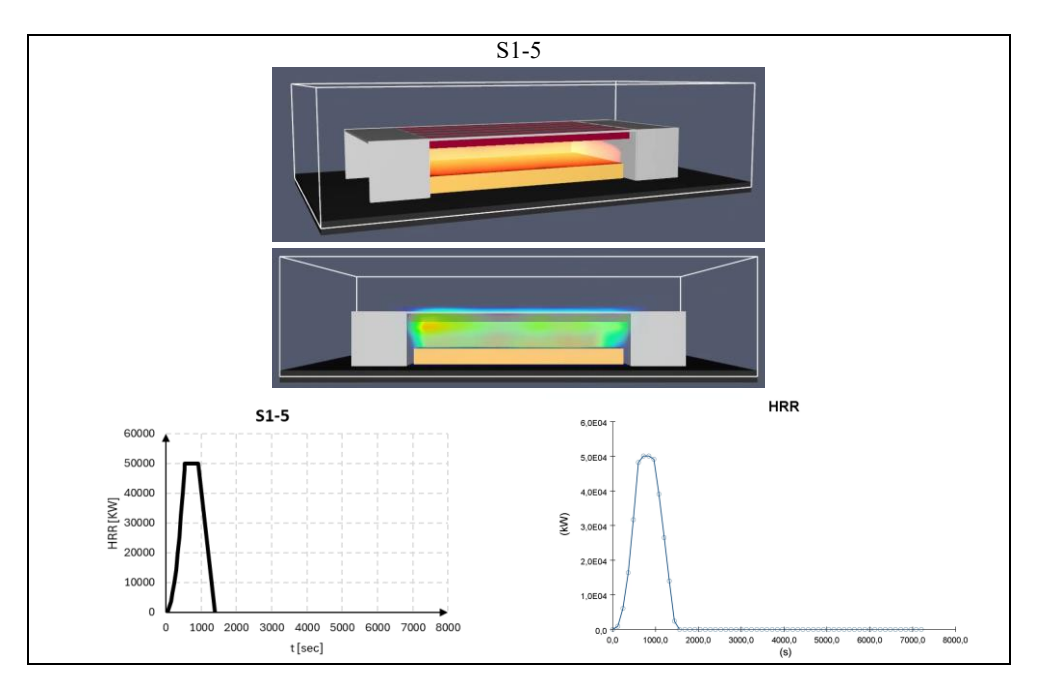
$$\begin{aligned} M_{stab,fi}\left(N_{d}\right) &\coloneqq \text{if } N_{d} \geq N_{b,fi.t.Rd} \\ &\parallel 0 \text{ } kN \cdot m \\ &\text{else} \\ &\parallel \frac{1}{k_{y,fi}\left(N_{d}\right)} \cdot M_{fi.t.Rd} \cdot \left(1 - \frac{N_{d}}{N_{b,fi.t.Rd}}\right) \end{aligned}$$

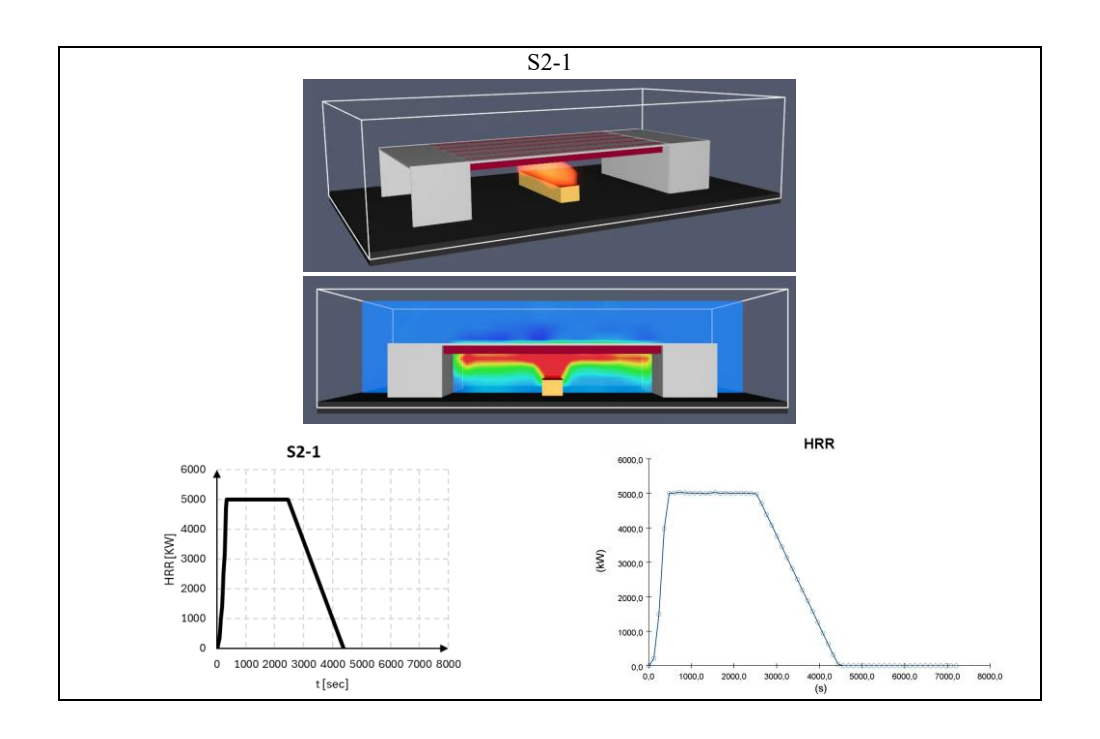
$Appendix \ B-CFD \ analyses \ results$

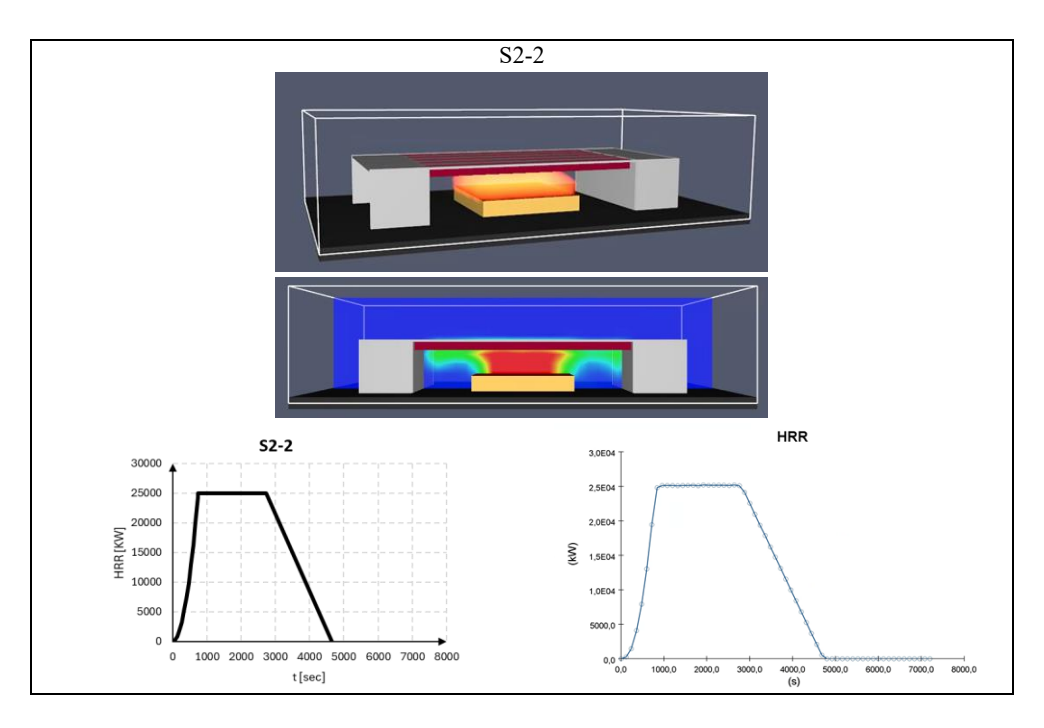


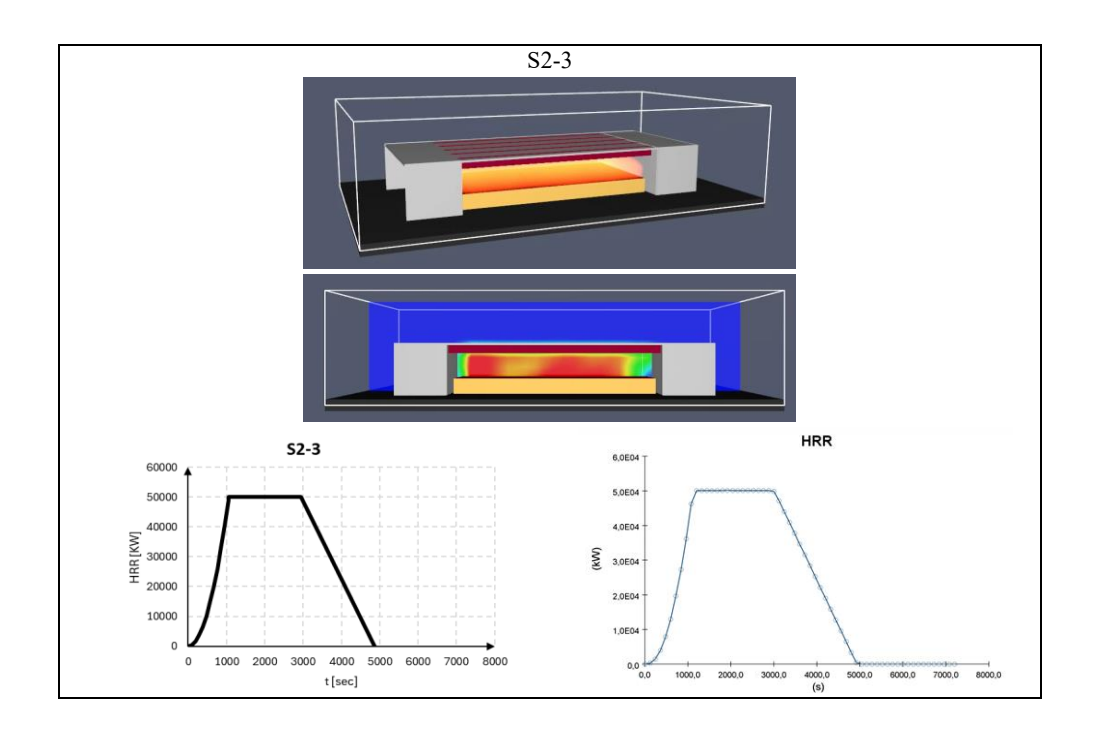


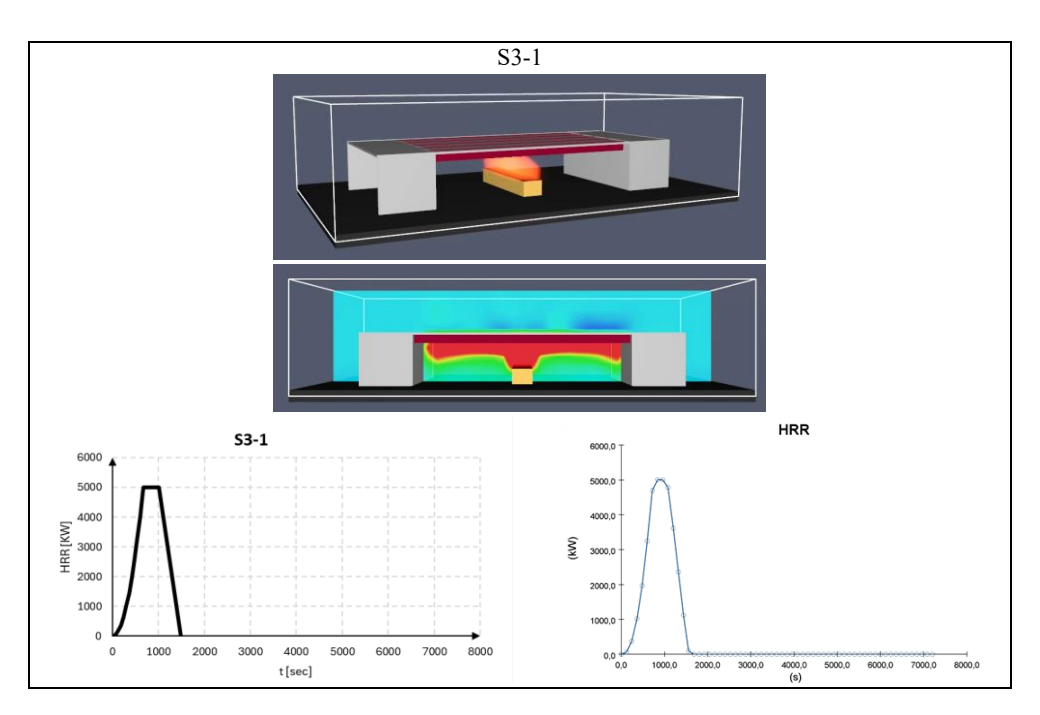


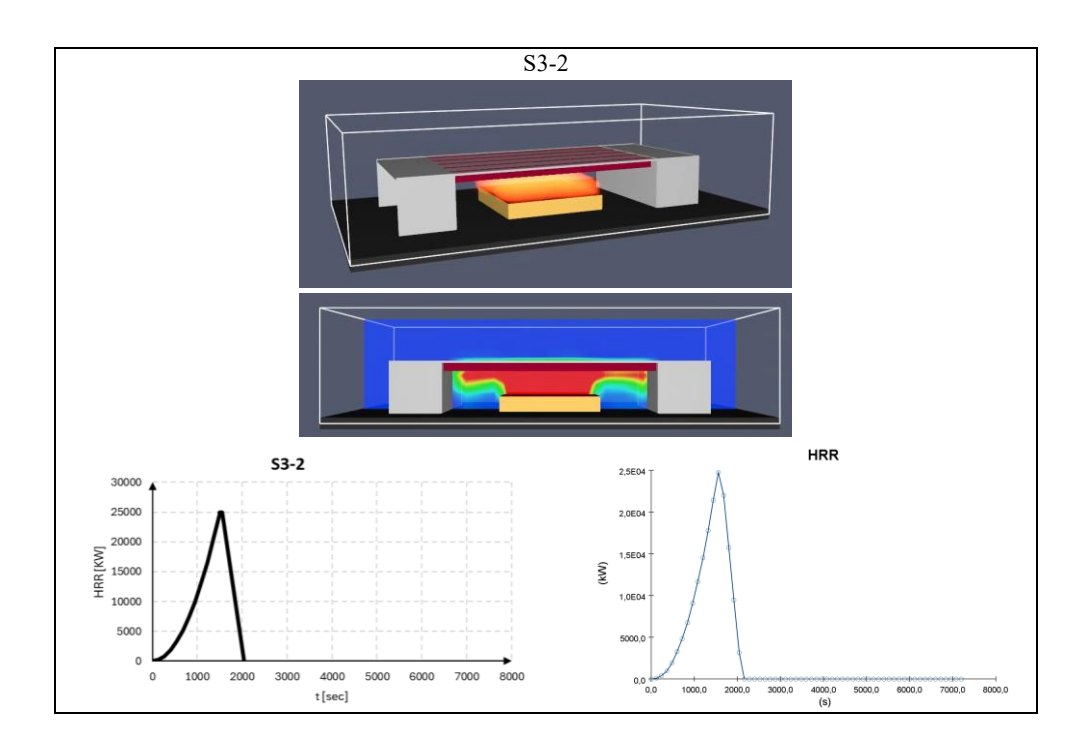


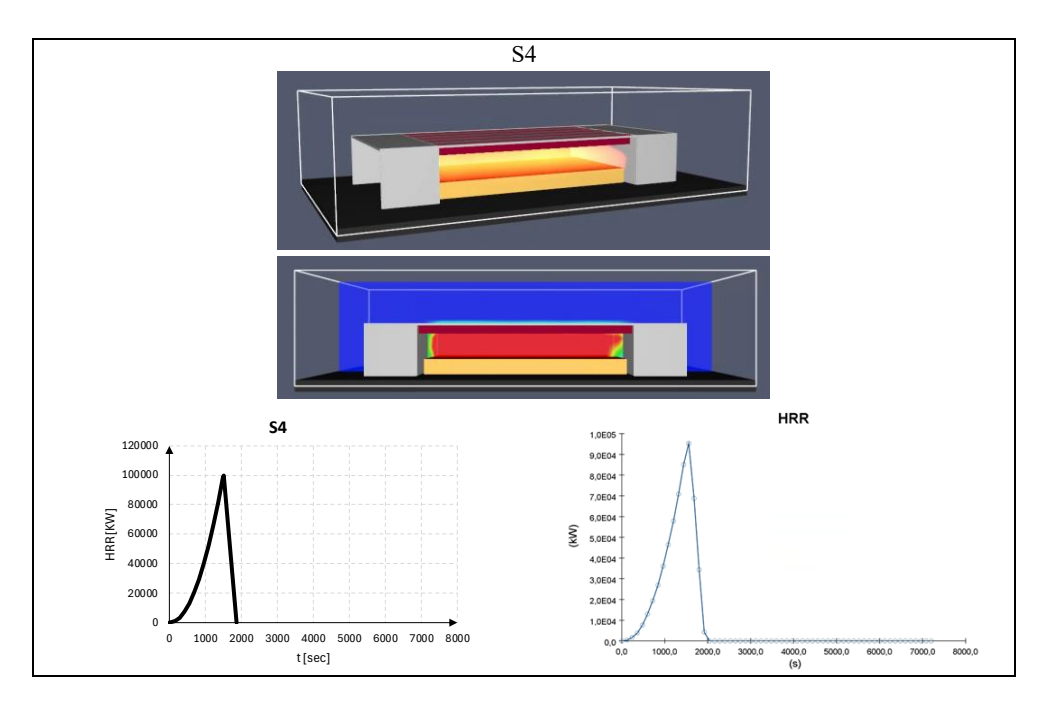


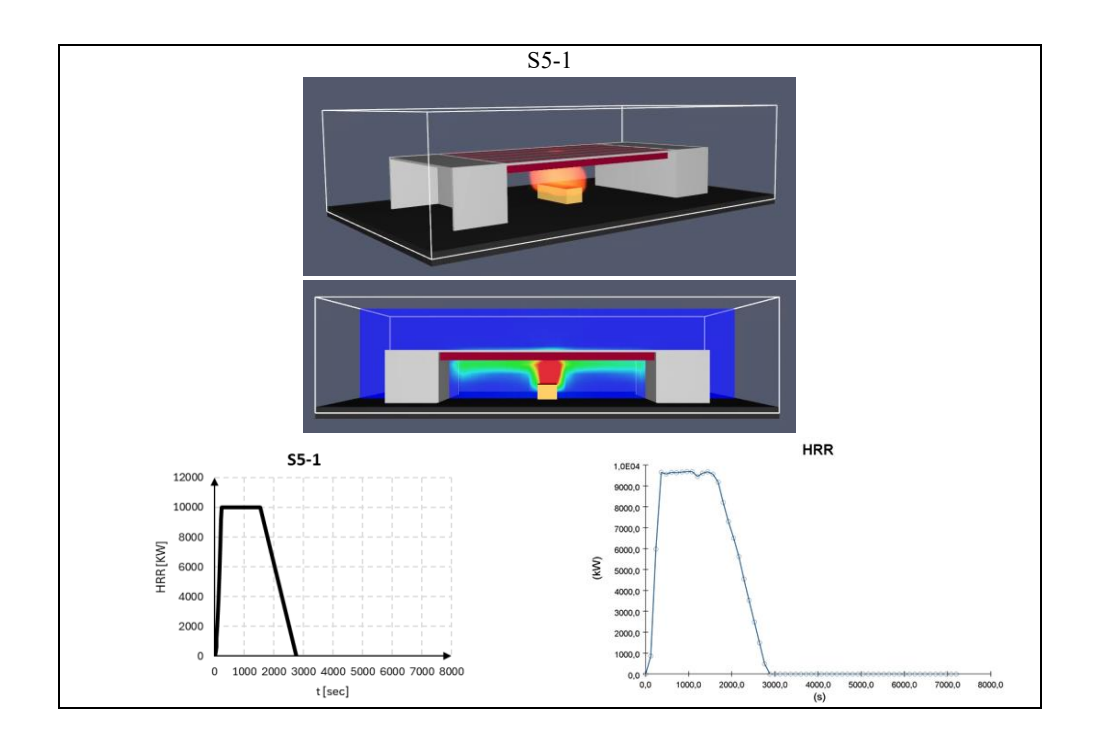


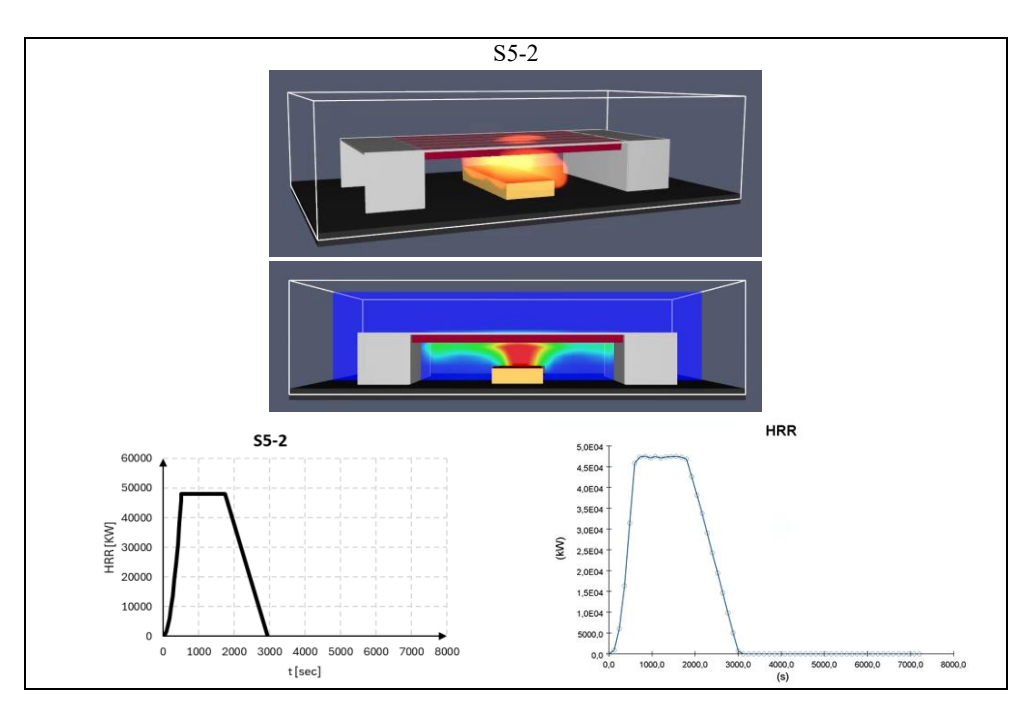


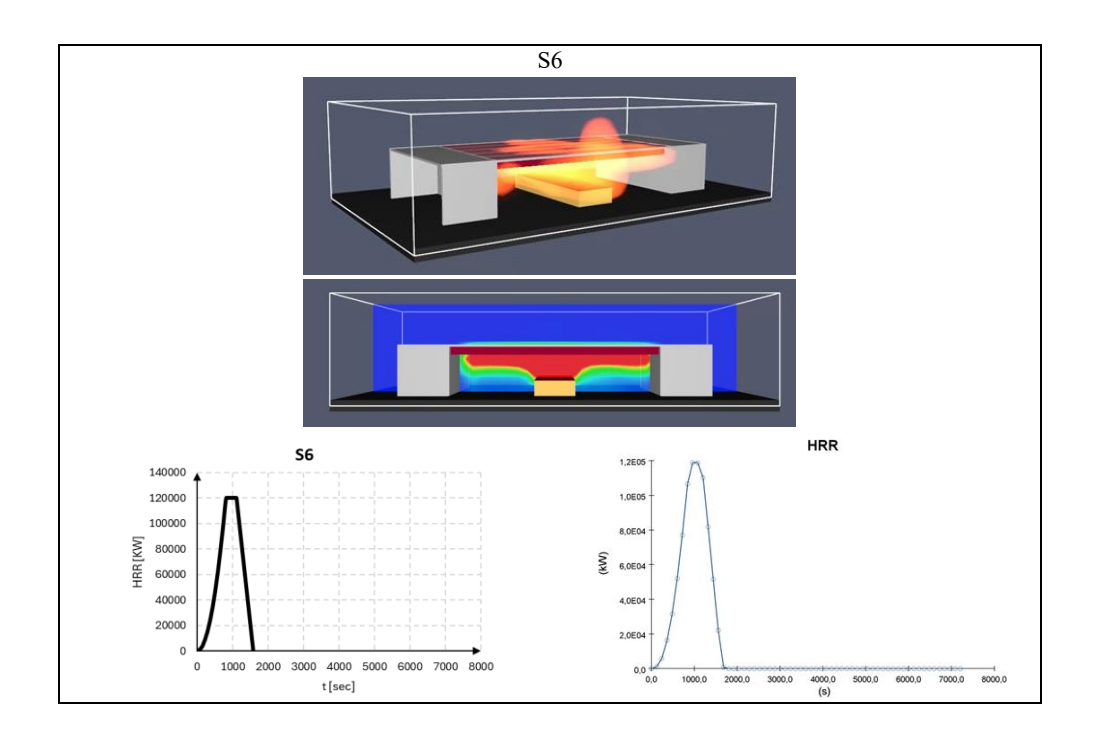












Appendix C – Fragility curves

$\underline{\textit{FRAGILITY CURVES FOR SIMPLY SUPPORTED VIADUCT FOR DCR AS A FUNCTION OF MAXIMUM DISPLACEMENT}}$

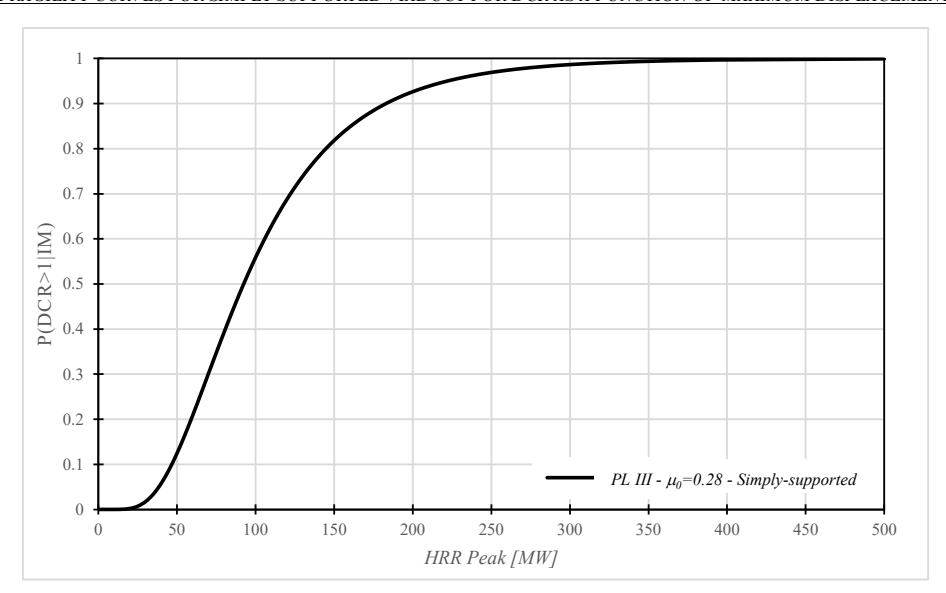


Figure C.1. Fragility curve for PLIII for HRR – $\mu_0\!\!=\!\!0.28$ – Simply-supported

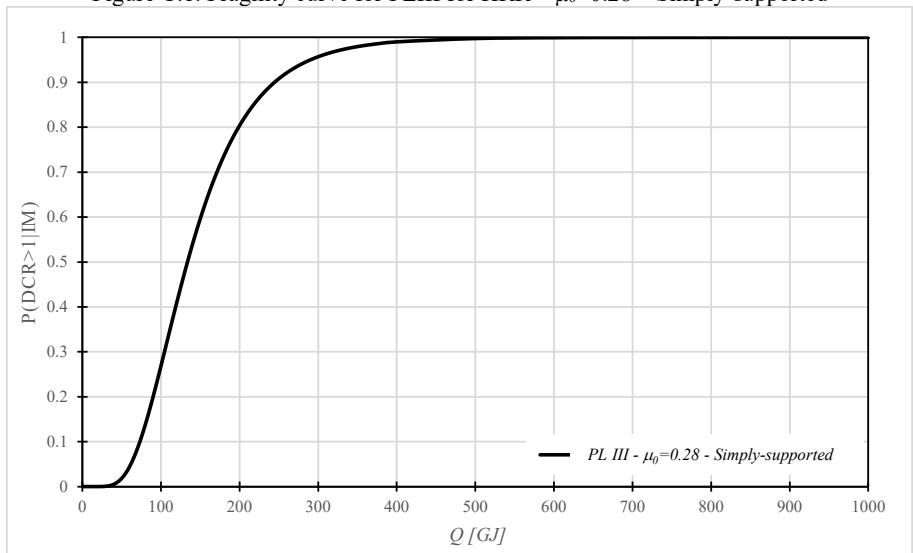


Figure C.2. Fragility curve for PLIII for Q - $\mu_0 \!\!=\!\! 0.28 -$ Simply-supported

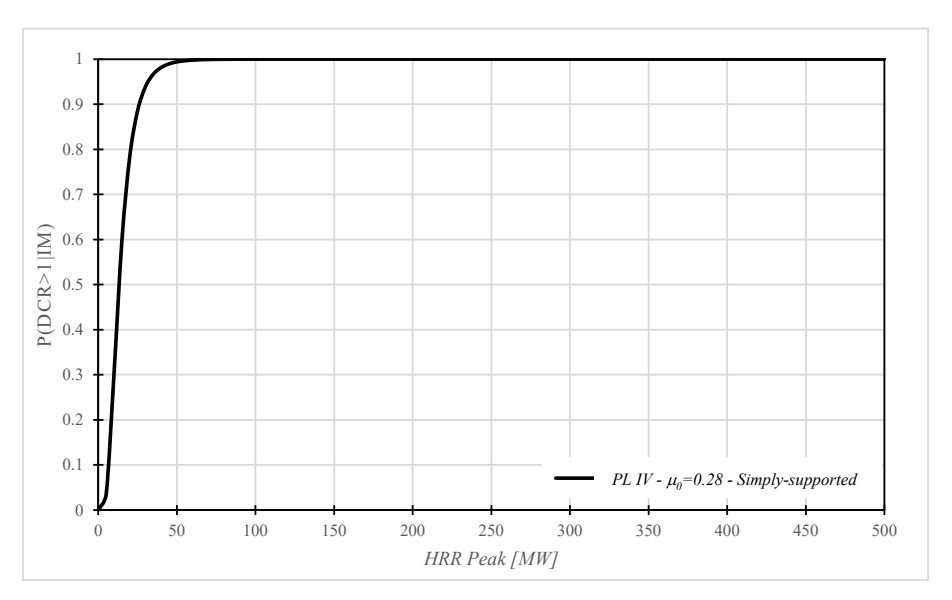


Figure C.3. Fragility curve for PLIV for HRR– $\mu_0\!\!=\!\!0.28$ – Simply-supported

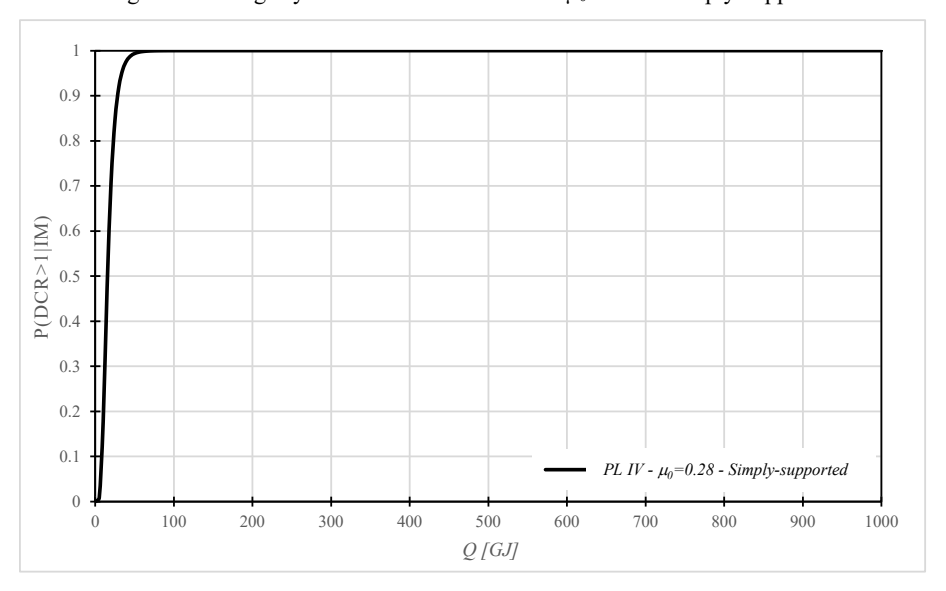


Figure C.4. Fragility curve for PLIV for $Q-\mu_0\!\!=\!\!0.28-Simply\text{-supported}$

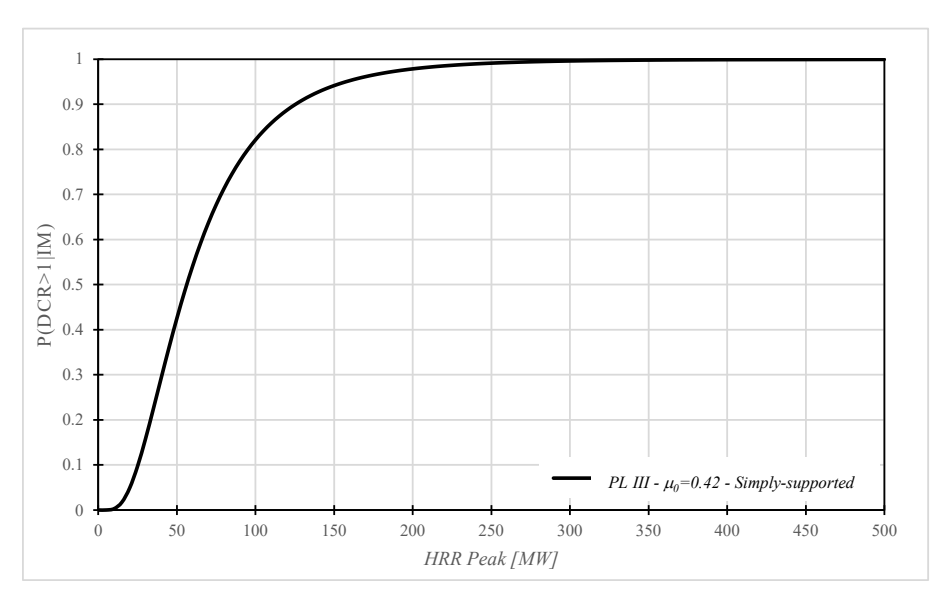


Figure C.5. Fragility curve for PLIII for HRR– $\mu_0\!\!=\!\!0.42$ – Simply-supported

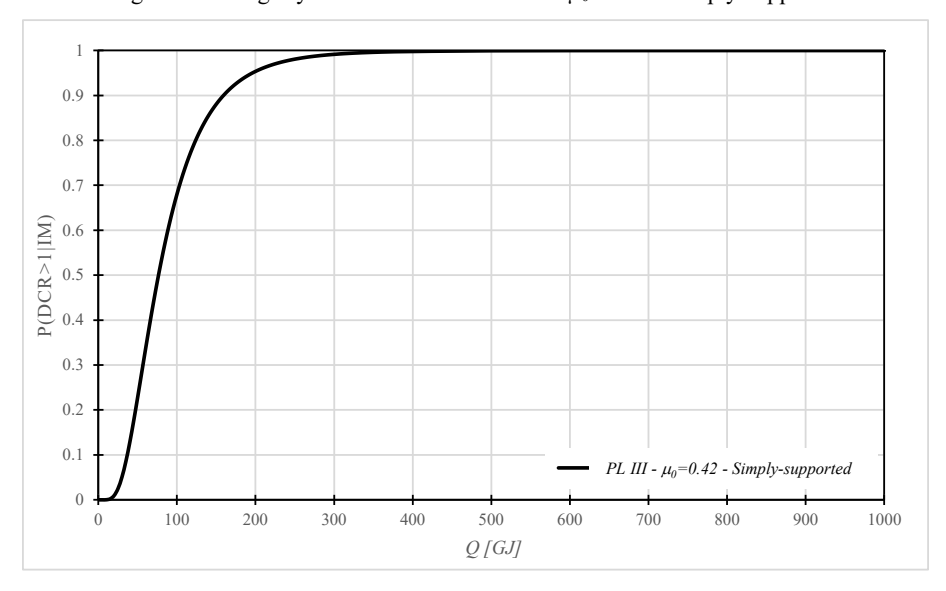


Figure C.6. Fragility curve for PLIII for $Q-\mu_0\!\!=\!\!0.42-Simply\text{-supported}$

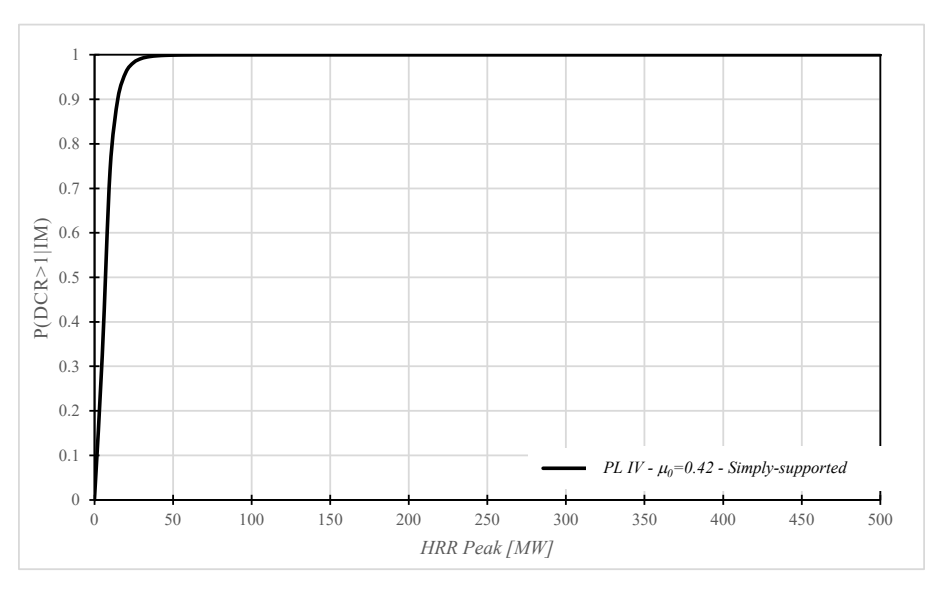


Figure C.7. Fragility curve for PLIV for HRR – $\mu_0\!\!=\!\!0.42$ – Simply-supported

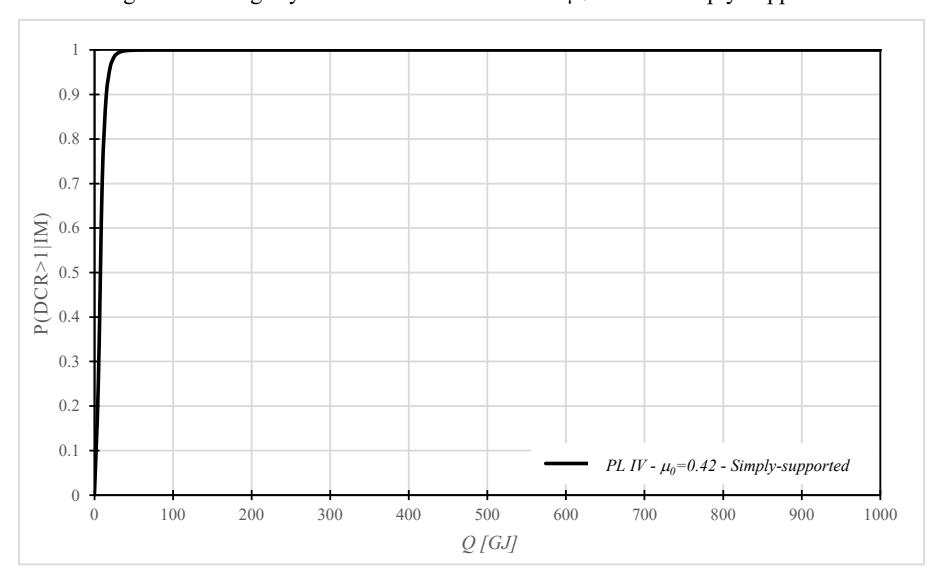


Figure C.8. Fragility curve for PLIV for Q $-\,\mu_0\!\!=\!\!0.42-Simply\text{-supported}$

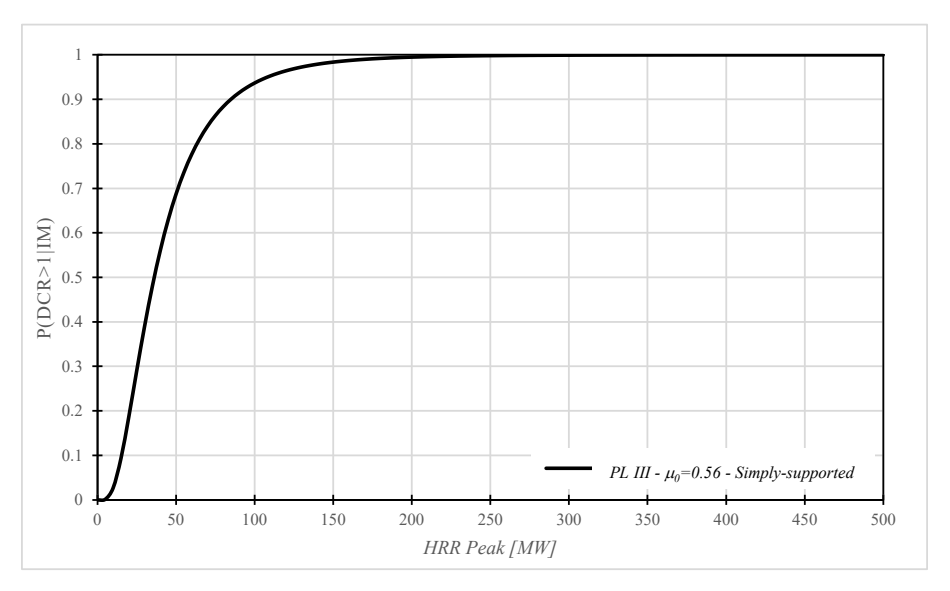


Figure C.9. Fragility curve for PLIII for HRR – μ_0 =0.56 – Simply-supported

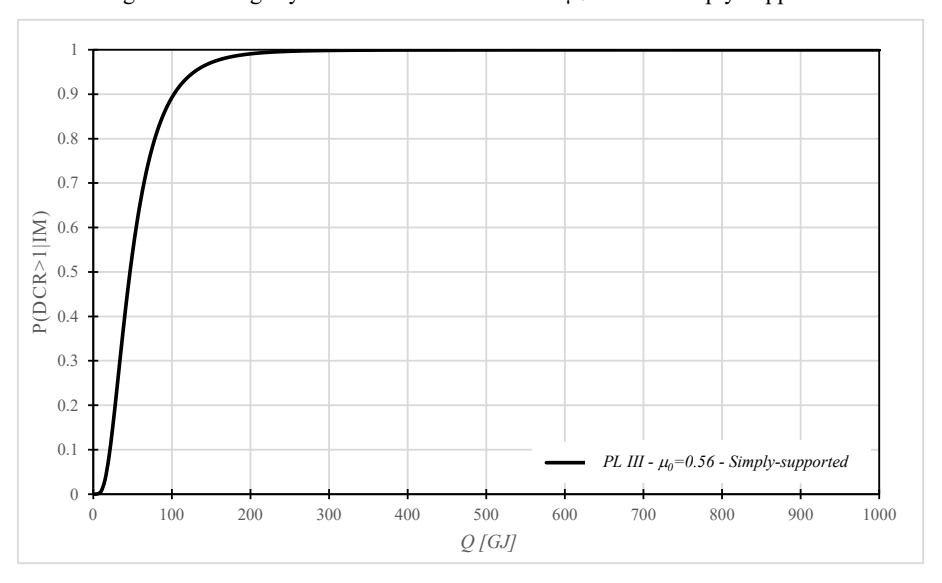


Figure C.10. Fragility curve for PLIII for Q $-\,\mu_0\!\!=\!\!0.56$ – Simply-supported

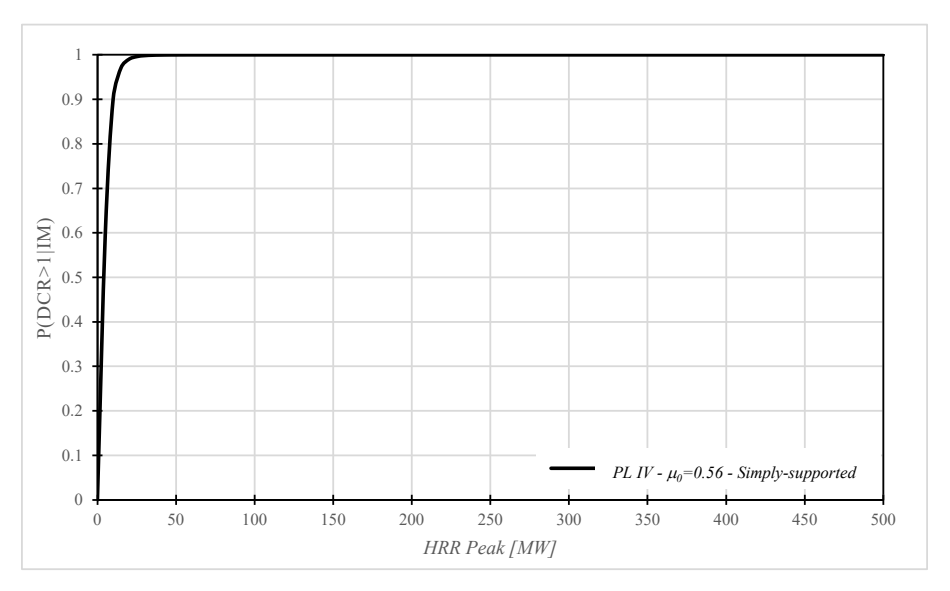


Figure C.11. Fragility curve for PLIV for HRR $-\,\mu_0 \!\!=\!\! 0.56 - Simply-supported$

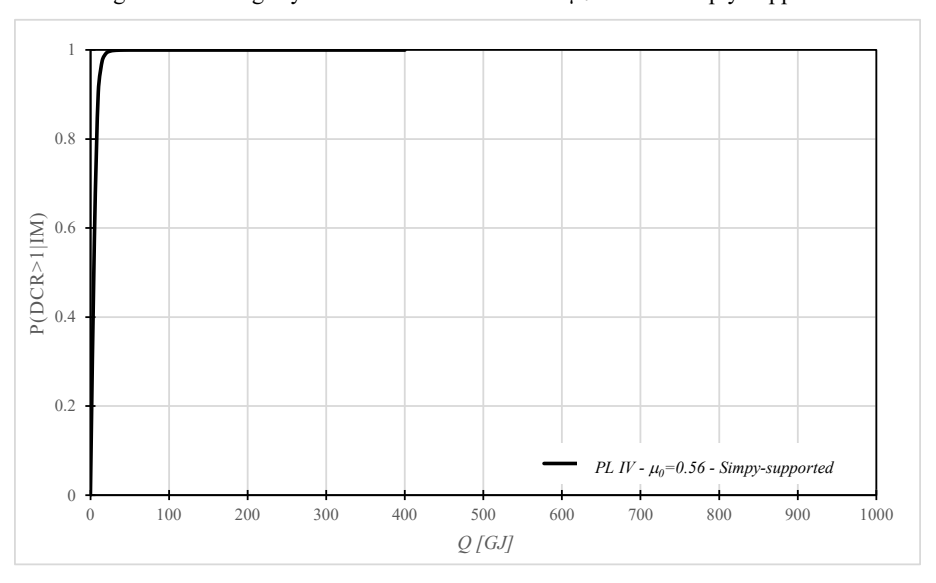


Figure C.12. Fragility curve for PLIV for Q - $\mu_0 \!\!=\!\! 0.56 - Simply-supported$

$\frac{FRAGILITY\ CURVES\ FOR\ SIMPLY\ SUPPORTED\ VIADUCT\ FOR\ DCR\ AS\ A\ FUNCTION\ OF}{MAXIMUM\ AND\ RESIDUAL\ DISPLACEMENT}$

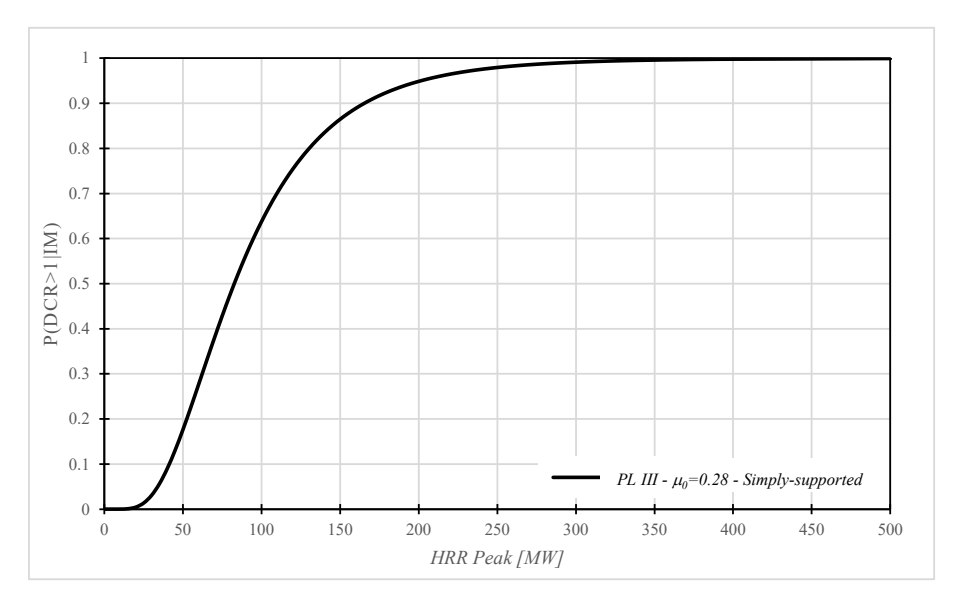


Figure C.13. Fragility curve for PLIII for HRR $-\,\mu_0\!\!=\!\!0.28-Simply\text{-supported}$

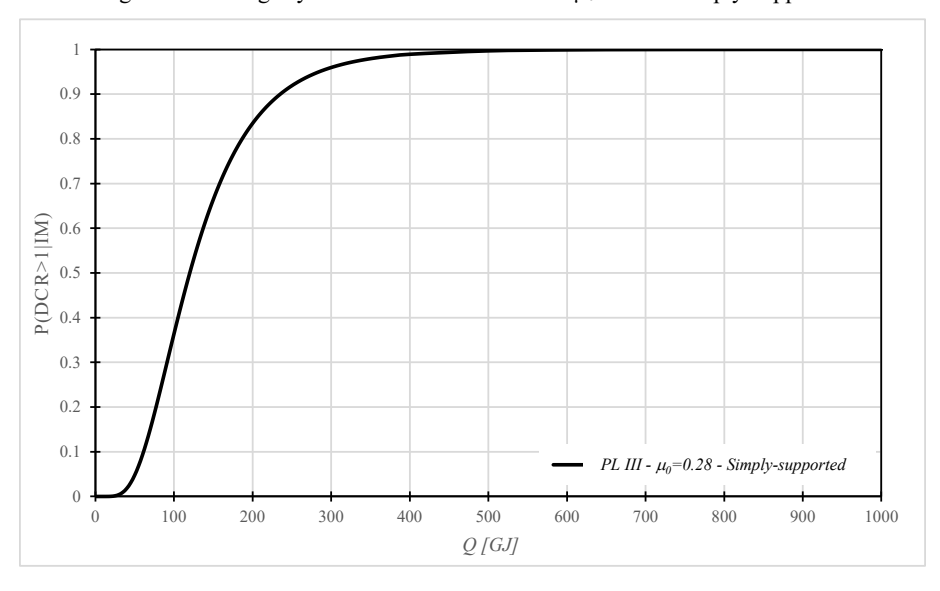


Figure C.14. Fragility curve for PLIII for Q - $\mu_0 \!\!=\!\! 0.28 - Simply-supported$

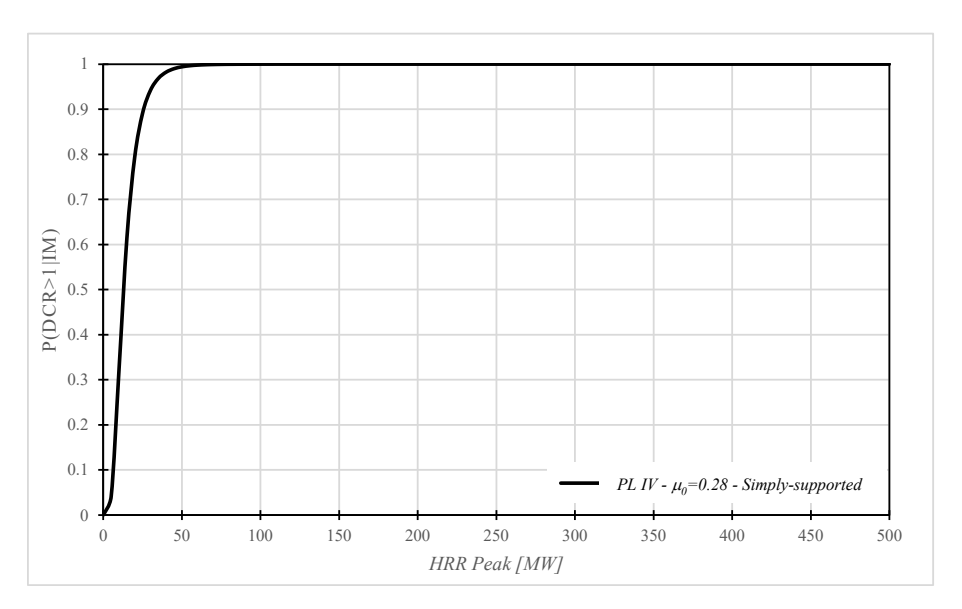


Figure C.15. Fragility curve for PLIV for HRR $-\,\mu_0\!\!=\!\!0.28-Simply\text{-supported}$

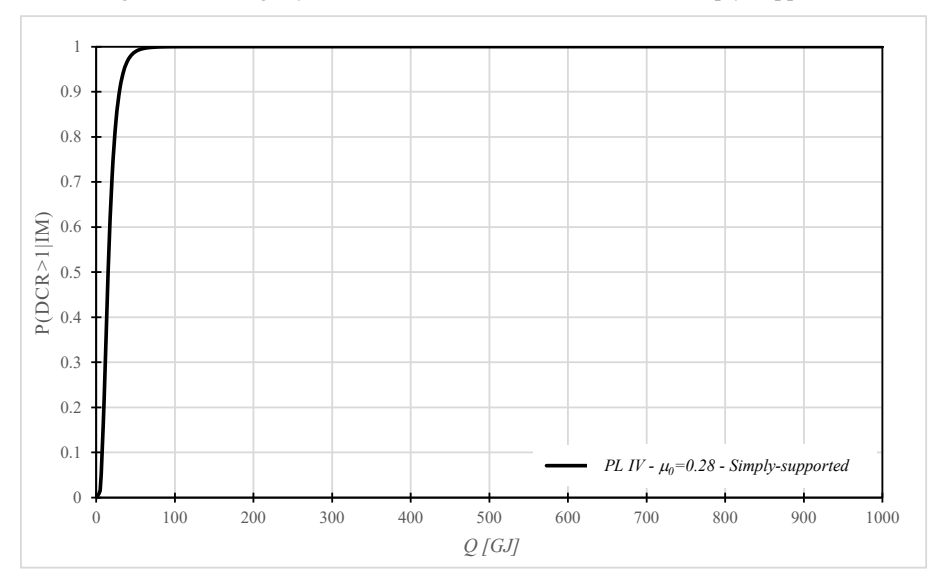


Figure C.16. Fragility curve for PLIV for Q - $\mu_0 \!\!=\!\! 0.28 -$ Simply-supported

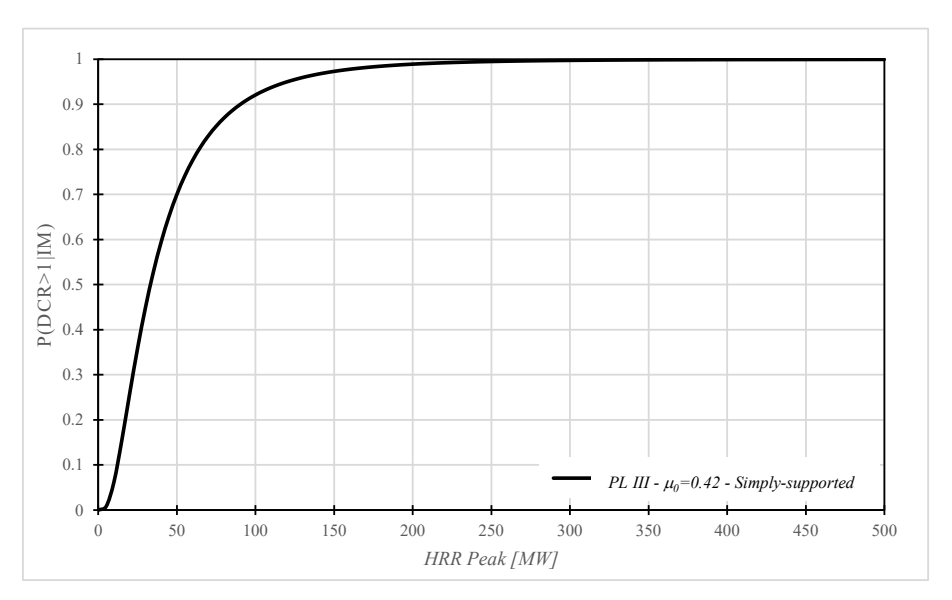


Figure C.17. Fragility curve for PLIII for HRR $-\,\mu_0 \!\!=\!\! 0.42 - Simply-supported$

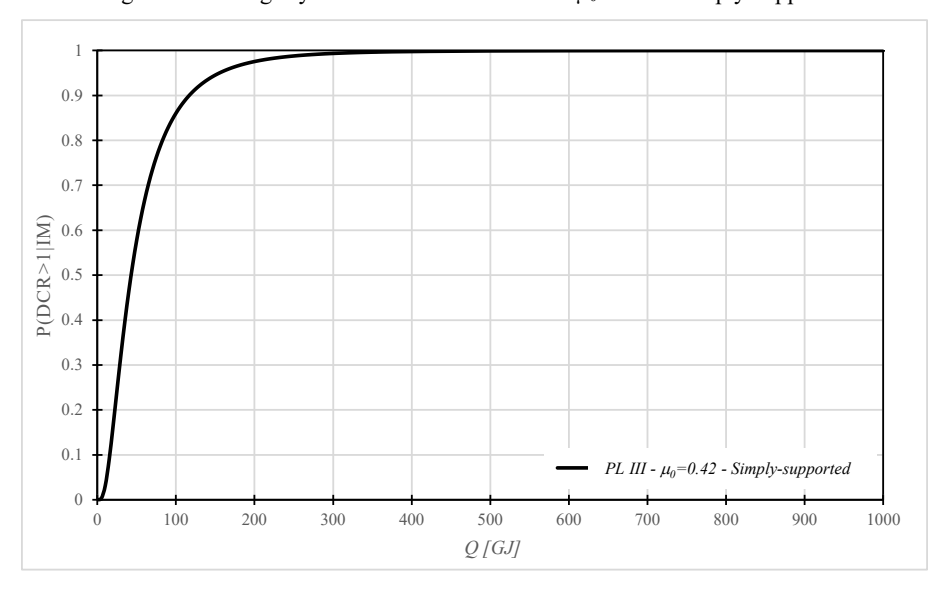


Figure C.18. Fragility curve for PLIII for Q $-\,\mu_0\!\!=\!\!0.42$ – Simply-supported

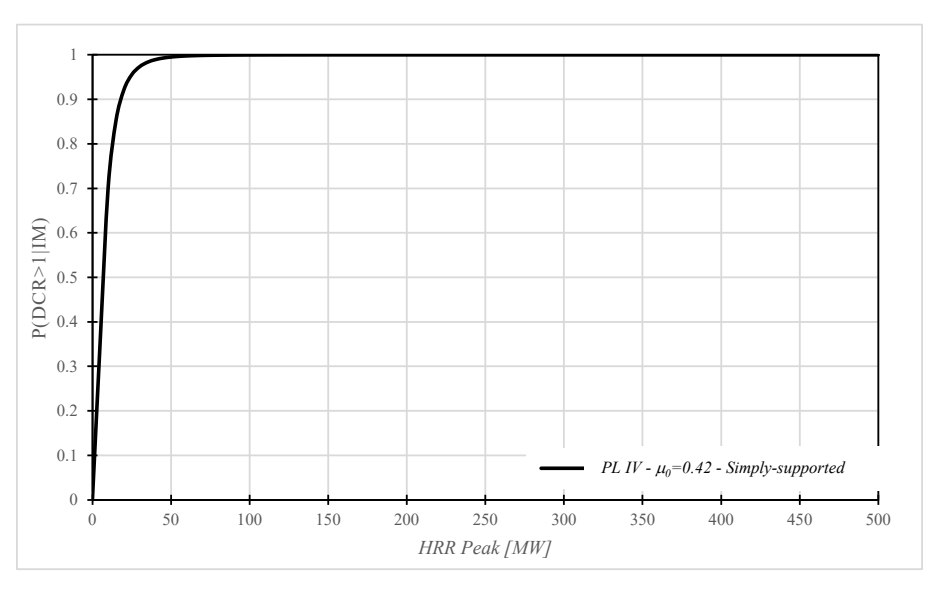


Figure C.19. Fragility curve for PLIV for HRR $-\,\mu_0\!\!=\!\!0.42-Simply\text{-supported}$

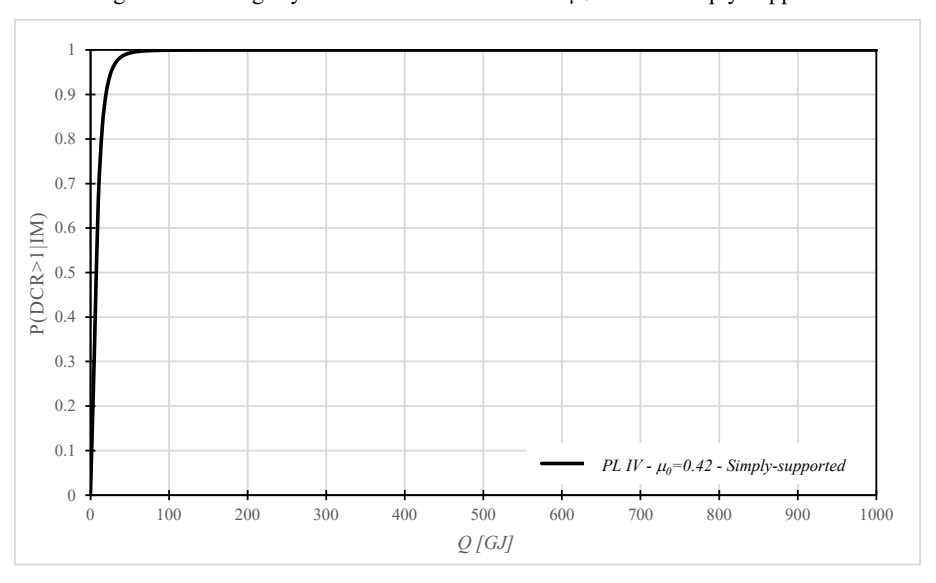


Figure C.20. Fragility curve for PLIV for Q - $\mu_0 \!\!=\!\! 0.42 - Simply-supported$

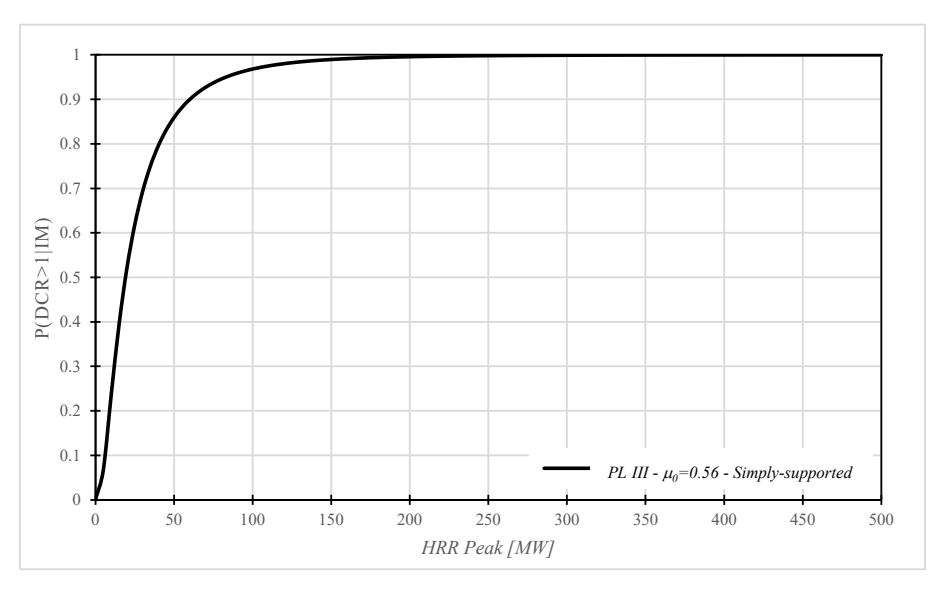


Figure C.21. Fragility curve for PLIII for HRR $-\,\mu_0\!\!=\!\!0.56-Simply\text{-supported}$

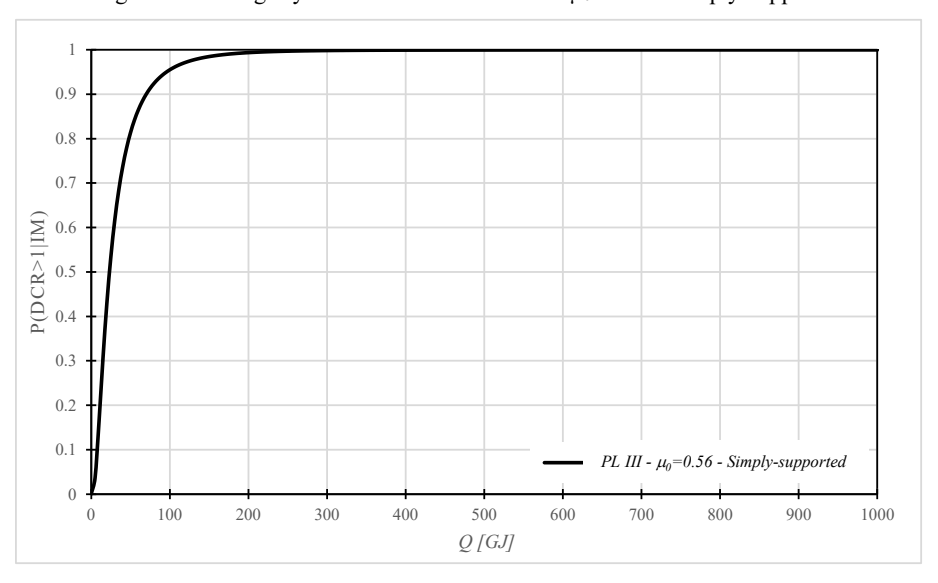


Figure C.22. Fragility curve for PLIII for Q $-\,\mu_0\!\!=\!\!0.56$ – Simply-supported

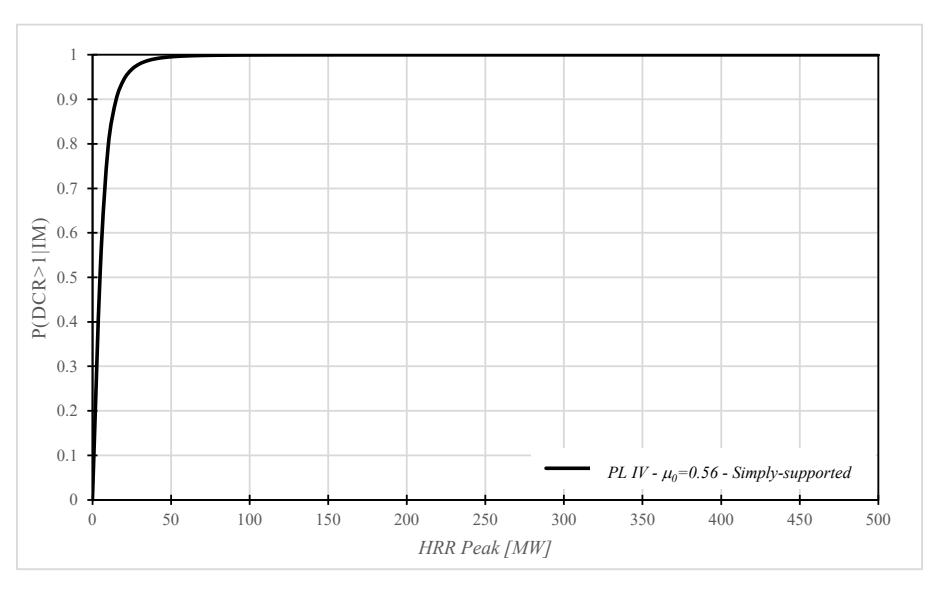


Figure C.23. Fragility curve for PLIV for HRR $-\,\mu_0\!\!=\!\!0.56-Simply\text{-supported}$

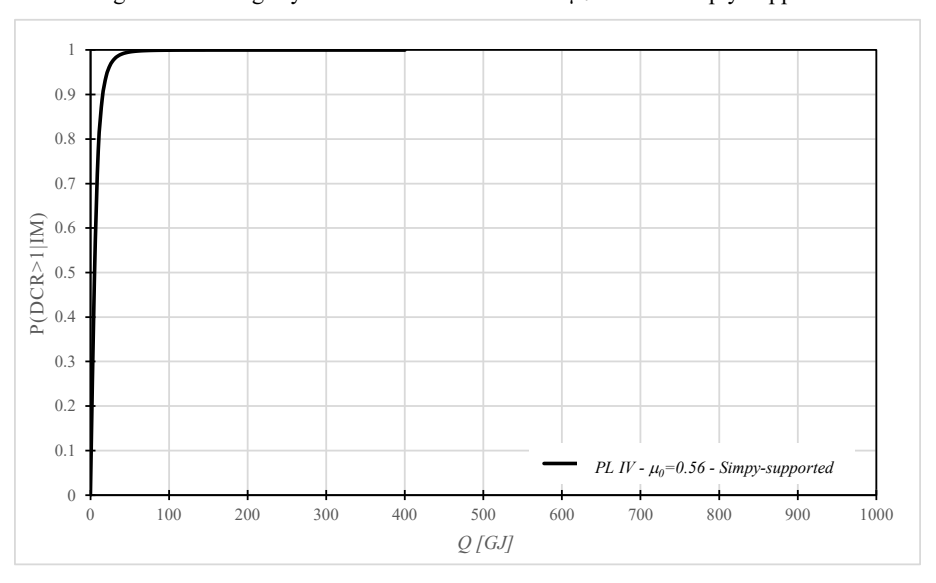


Figure C.24. Fragility curve for PLIV for Q - $\mu_0 \!\!=\!\! 0.56 - Simply-supported$

FRAGILITY CURVES FOR HYPERSTATIC VIADUCT FOR DCR AS A FUNCTION OF MAXIMUM DISPLACEMENT, RESIDUAL DISPLACEMENT AND COMPRESSIVE STRENTH OF BOTTOM FLANGE AT THE SUPPORT

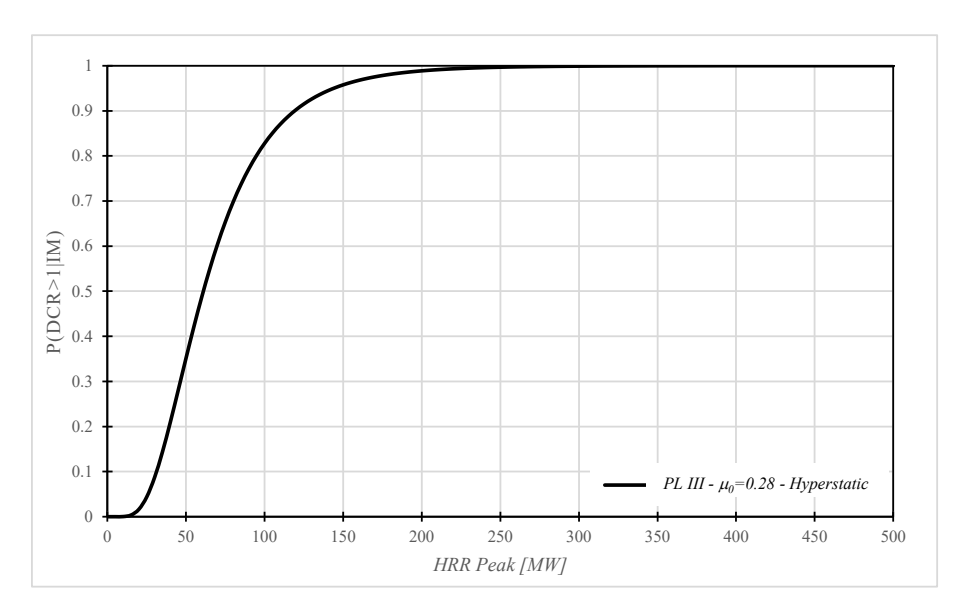


Figure C.25. Fragility curve for PLIII for HRR – $\mu_0\!\!=\!\!0.28$ – Hyperstatic

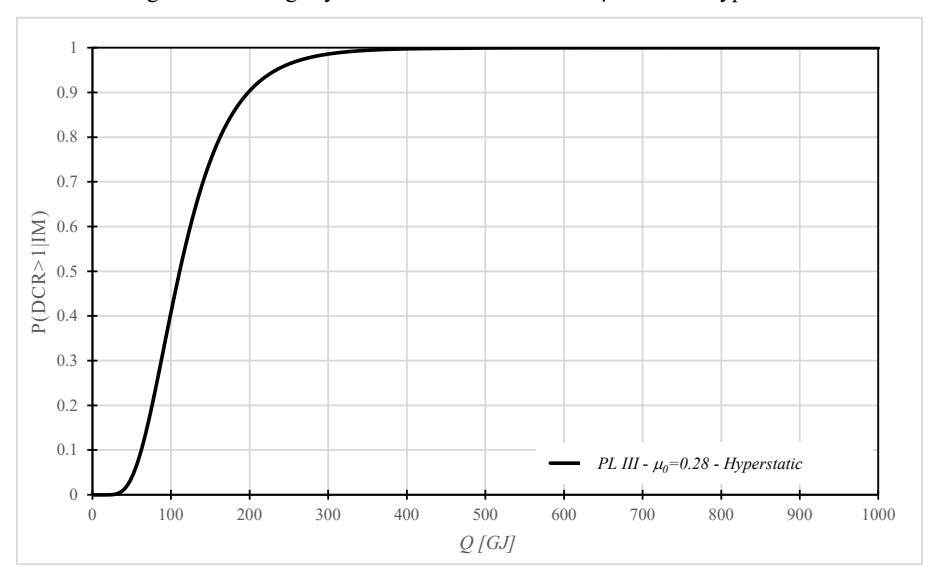


Figure C.26. Fragility curve for PLIII for Q $-\,\mu_0 \!\!=\!\! 0.28 - Hyperstatic$

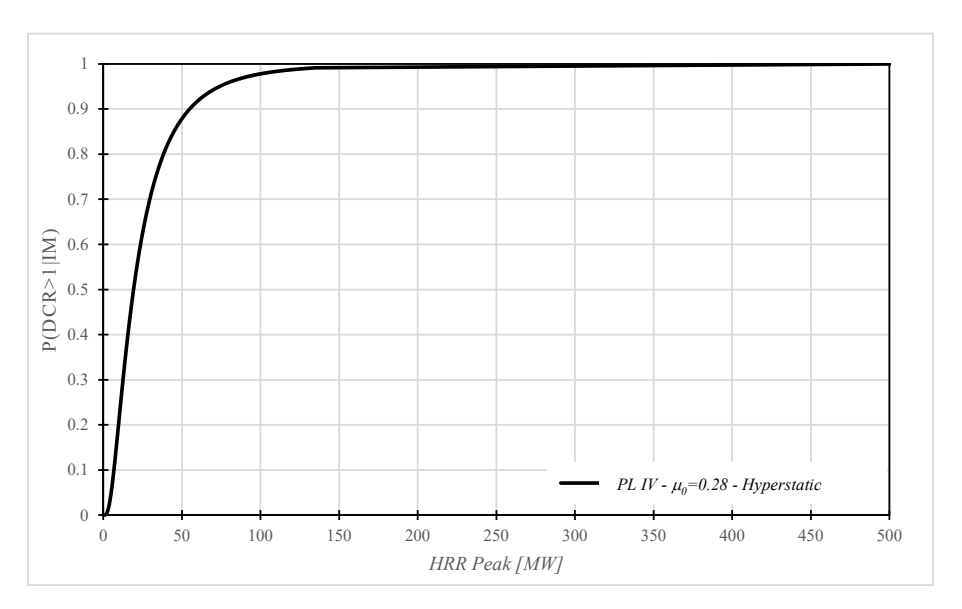


Figure C.27. Fragility curve for PLIV for HRR – μ_0 =0.28 – Hyperstatic

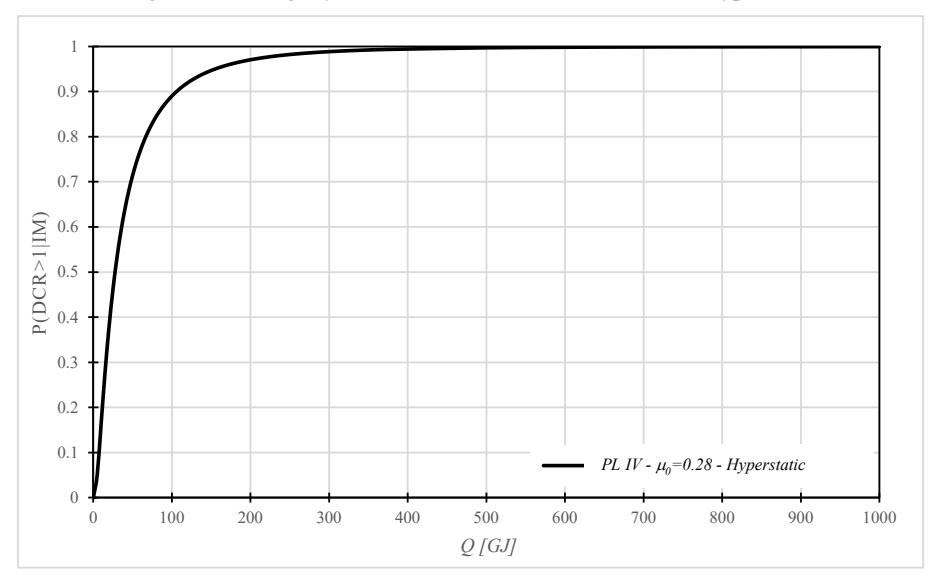


Figure C.28. Fragility curve for PLIV for Q $-\,\mu_0\!\!=\!\!0.28$ – Hyperstatic

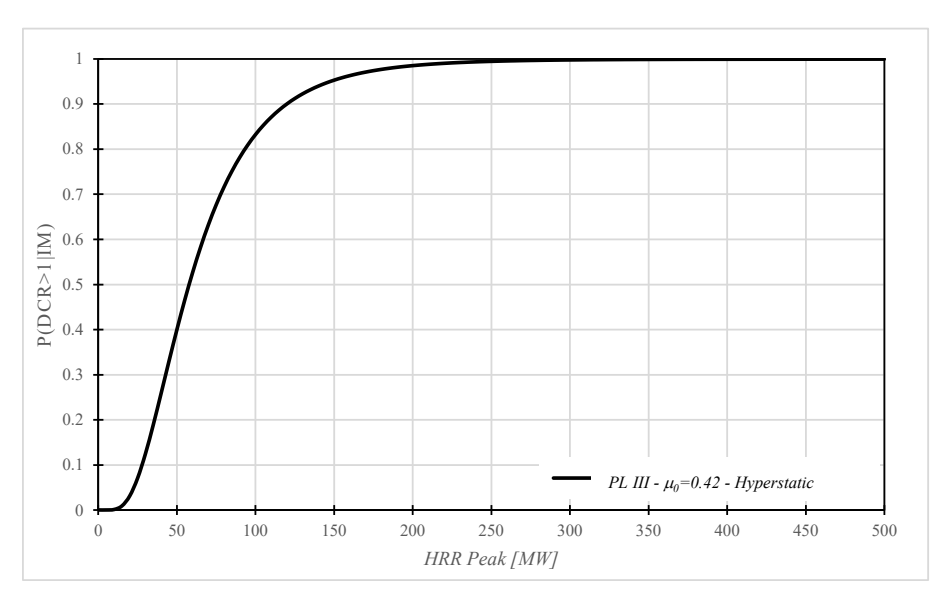


Figure C.29. Fragility curve for PLIII for HRR – $\mu_0 \!\!=\!\! 0.42$ – Hyperstatic

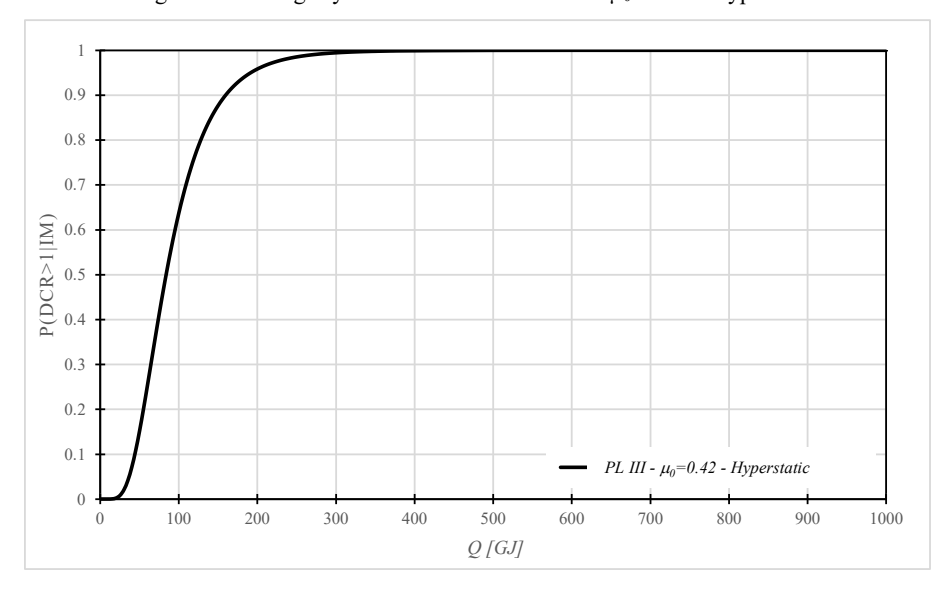


Figure C.30. Fragility curve for PLIII for Q $-\,\mu_0\!\!=\!\!0.42$ – Hyperstatic

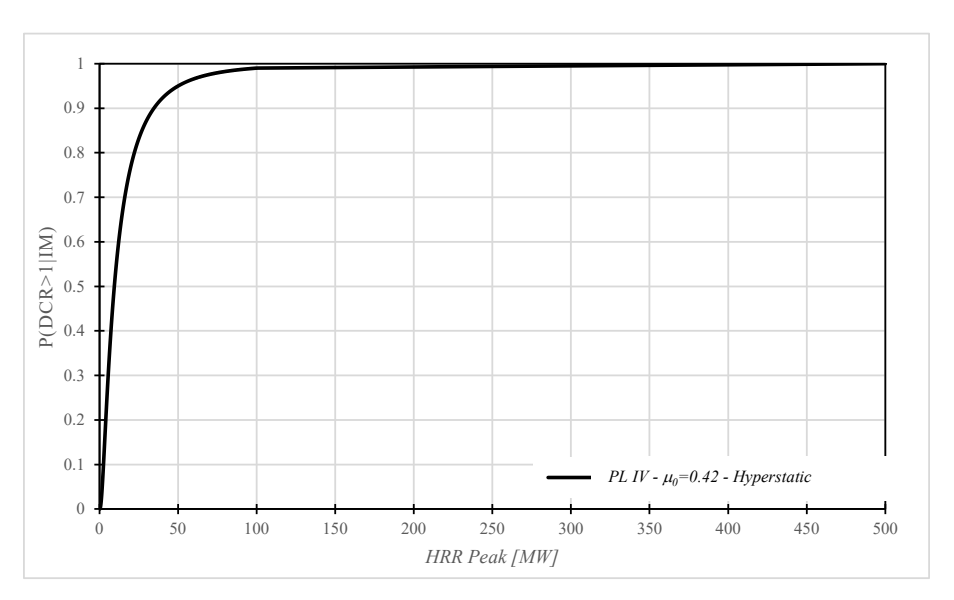


Figure C.31. Fragility curve for PLIV for HRR $-\,\mu_0\!\!=\!\!0.42-Hyperstatic$

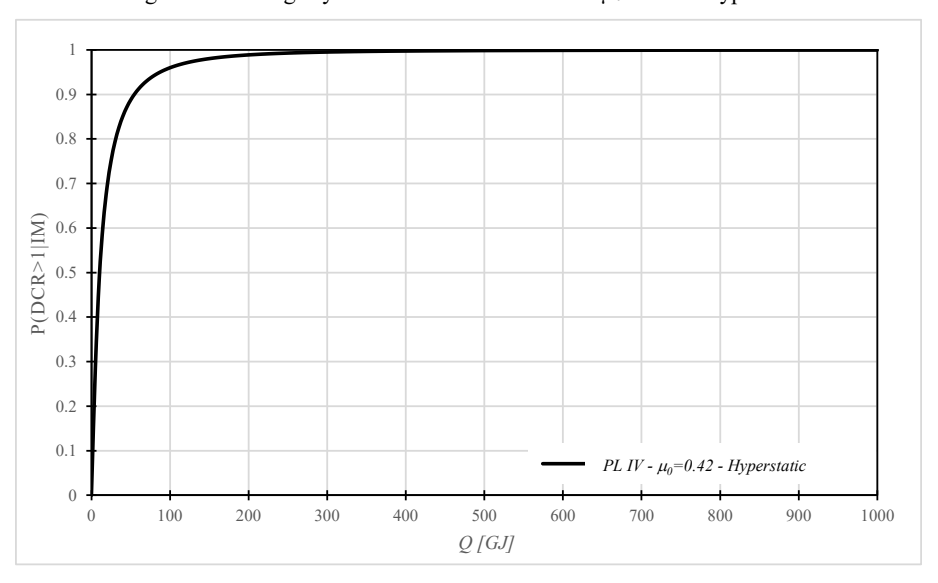


Figure C.32. Fragility curve for PLIV for Q $-\,\mu_0\!\!=\!\!0.42$ – Hyperstatic

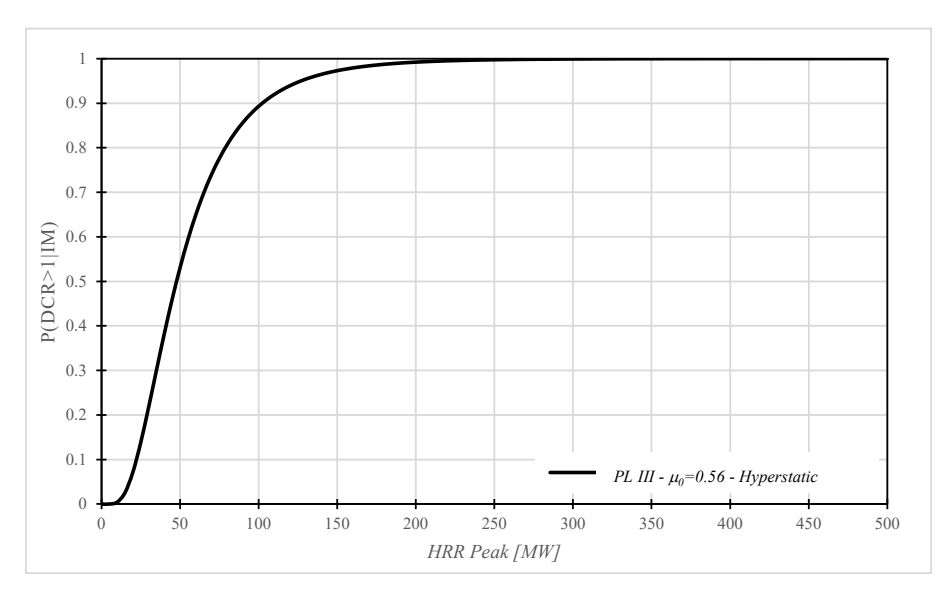


Figure C.33. Fragility curve for PLIII for HRR – $\mu_0\!\!=\!\!0.56$ – Hyperstatic

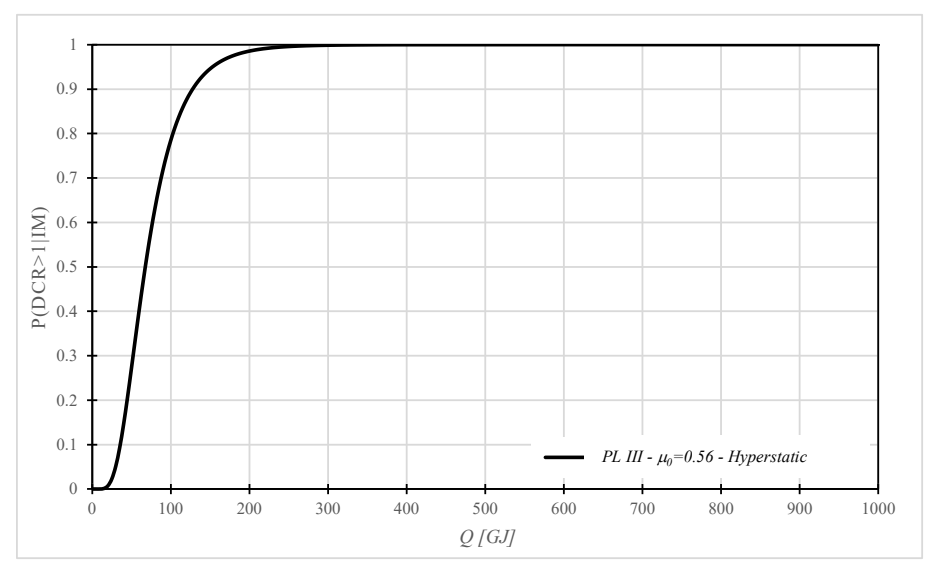


Figure C.34. Fragility curve for PLIII for Q $-\,\mu_0\!\!=\!\!0.56$ – Hyperstatic

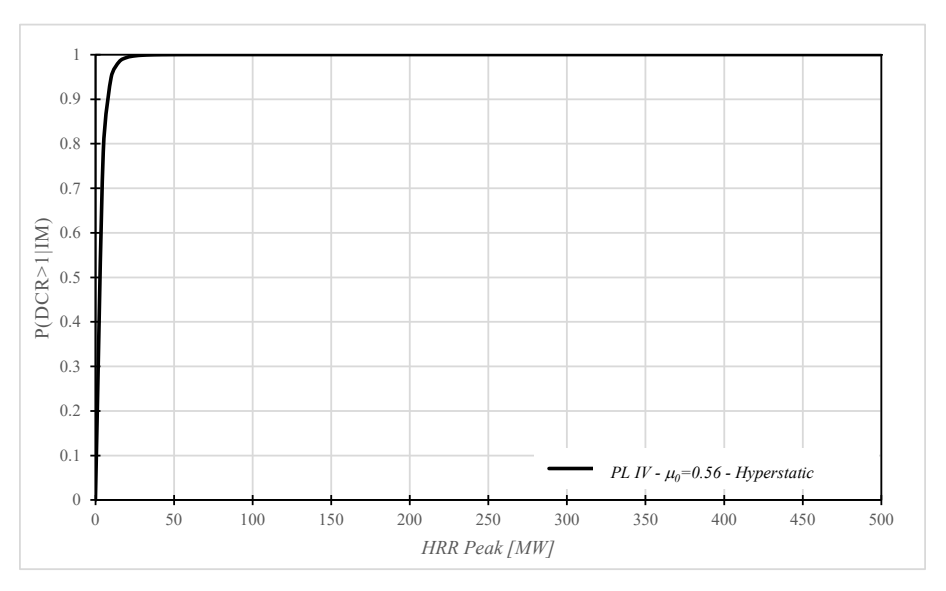


Figure C.35. Fragility curve for PLIV for HRR $-\,\mu_0\!\!=\!\!0.56-Hyperstatic$

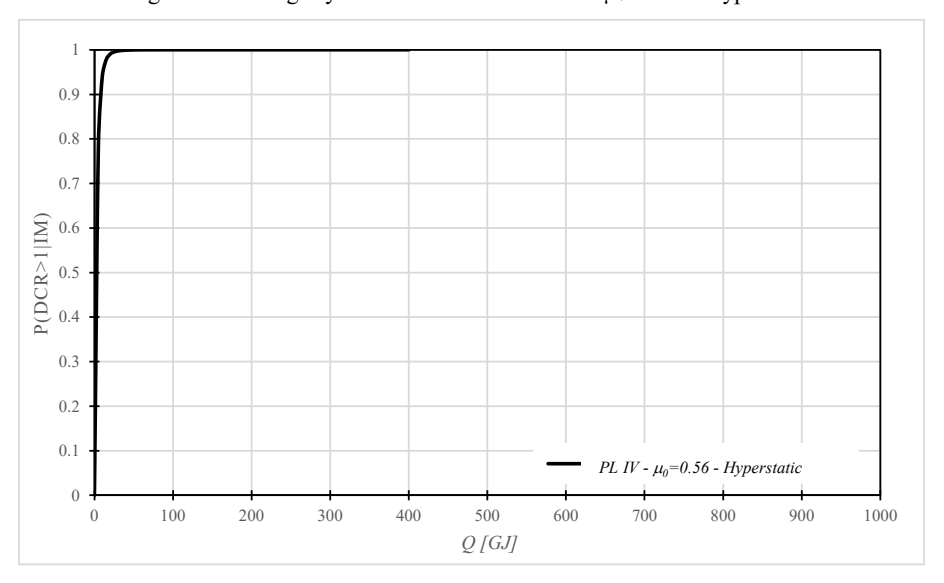


Figure C.36. Fragility curve for PLIV for Q $-\,\mu_0\!\!=\!\!0.56$ – Hyperstatic

Appendix D –Structural model code

```
InputFile created with GiD-SAFIR 2012 Interface
Safir_Static_2D_Analysis
Mesh_from_GID-Mesher
  NNODE 145
  NDIM 2
 NDOFMAX 3
 NCORES 1
 DYNAMIC PURE NR
  NLOAD
 OBLIQUE 0
COMEBACK 1.0e-5
 NORENUM
  NMAT 4
ELEMENTS
  BEAM 70 5
   NG 2
 NFIBER 2294
       TRUSS 42
END_ELEM
  NODES
         1 0.0000000E+000 0.0000000E+000 0.0000000E+000
  NODE
  NODE
         2 3.00000000E-001 0.00000000E+000 0.00000000E+000
  NODE
         3 6.0000000E-001 0.0000000E+000 0.0000000E+000
   NODE
         4 9.0000000E-001 0.0000000E+000 0.0000000E+000
   NODE 5 1.20000000E+000 0.0000000E+000 0.00000000E+000
  NODE 6 1.50000000E+000 0.0000000E+000 0.0000000E+000
         7 1.80000000E+000 0.00000000E+000 0.00000000E+000
   NODE
   NODE 8 2.10000000E+000 0.0000000E+000 0.0000000E+000
   NODE 9 2.40000000E+000 0.00000000E+000 0.00000000E+000
         10 2.70000000E+000 0.00000000E+000 0.00000000E+000
  NODE
  NODE
          11 3.00000000E+000 0.0000000E+000 0.0000000E+000
          12 3.30000000E+000 0.00000000E+000 0.00000000E+000
  NODE
```

```
NODE
        13 3.60000000E+000 0.00000000E+000 0.00000000E+000
NODE
        14 3.90000000E+000 0.00000000E+000 0.0000000E+000
NODE
        15 4.20000000E+000 0.00000000E+000 0.00000000E+000
NODE
        16 4.50000000E+000 0.00000000E+000 0.0000000E+000
NODE
        17 4.80000000E+000 0.00000000E+000 0.00000000E+000
NODE
        18 5.10000000E+000 0.0000000E+000 0.0000000E+000
        19 5.40000000E+000 0.00000000E+000 0.00000000E+000
NODE
NODE
        20 5.70000000E+000 0.00000000E+000 0.0000000E+000
NODE
       21 6.00000000E+000 0.00000000E+000 0.00000000E+000
NODE
        22 6.30000000E+000 0.00000000E+000 0.00000000E+000
NODE
        23 6.60000000E+000 0.00000000E+000 0.00000000E+000
NODE
       24 6.9000000E+000 0.0000000E+000 0.0000000E+000
NODE
       25 7.20000000E+000 0.00000000E+000 0.00000000E+000
NODE
       26 7.50000000E+000 0.00000000E+000 0.00000000E+000
        27 7.80000000E+000 0.00000000E+000 0.00000000E+000
NODE
NODE
       28 8.10000000E+000 0.00000000E+000 0.00000000E+000
NODE
       29 8.40000000E+000 0.00000000E+000 0.00000000E+000
NODE
       30 8.70000000E+000 0.00000000E+000 0.0000000E+000
NODE
        31 9.00000000E+000 0.0000000E+000 0.0000000E+000
       32 9.30000000E+000 0.00000000E+000 0.00000000E+000
NODE
NODE
       33 9.60000000E+000 0.00000000E+000 0.00000000E+000
NODE
       34 9.90000000E+000 0.00000000E+000 0.00000000E+000
NODE
        35 1.00000000E+001 0.00000000E+000 0.00000000E+000
NODE
        36 1.02000000E+001 0.00000000E+000 0.00000000E+000
NODE
        37 1.05000000E+001 0.00000000E+000 0.00000000E+000
NODE
       38 1.08000000E+001 0.00000000E+000 0.00000000E+000
        39 1.11000000E+001 0.00000000E+000 0.00000000E+000
NODE
NODE
        40 1.14000000E+001 0.00000000E+000 0.00000000E+000
NODE
       41 1.17000000E+001 0.00000000E+000 0.00000000E+000
NODE
       42 1.20000000E+001 0.00000000E+000 0.00000000E+000
NODE
       43 1.23000000E+001 0.00000000E+000 0.00000000E+000
NODE
        44 1.26000000E+001 0.00000000E+000 0.00000000E+000
NODE
       45 1.29000000E+001 0.00000000E+000 0.00000000E+000
NODE
       46 1.32000000E+001 0.00000000E+000 0.00000000E+000
NODE
        47 1.35000000E+001 0.00000000E+000 0.00000000E+000
NODE
        48 1.38000000E+001 0.00000000E+000 0.00000000E+000
```

```
NODE
        49 1.41000000E+001 0.00000000E+000 0.00000000E+000
NODE
        50 1.44000000E+001 0.00000000E+000 0.00000000E+000
NODE
       51 1.47000000E+001 0.00000000E+000 0.00000000E+000
NODE
        52 1.50000000E+001 0.0000000E+000 0.0000000E+000
NODE
       53 1.50000000E+001 4.36300000E-001 0.00000000E+000
NODE
        54 1.53000000E+001 0.00000000E+000 0.00000000E+000
       55 1.50000000E+001 4.00000000E+000 0.00000000E+000
NODE
NODE
        56 1.56000000E+001 0.00000000E+000 0.00000000E+000
NODE
       57 1.59000000E+001 0.00000000E+000 0.00000000E+000
NODE
        58 1.62000000E+001 0.00000000E+000 0.00000000E+000
NODE
        59 1.65000000E+001 0.00000000E+000 0.00000000E+000
NODE
        60 1.68000000E+001 0.00000000E+000 0.00000000E+000
NODE
       61 1.71000000E+001 0.00000000E+000 0.00000000E+000
NODE
        62 1.74000000E+001 0.00000000E+000 0.00000000E+000
        63 1.77000000E+001 0.00000000E+000 0.00000000E+000
NODE
NODE
        64 1.80000000E+001 0.00000000E+000 0.00000000E+000
NODE
       65 1.83000000E+001 0.00000000E+000 0.00000000E+000
NODE
        66 1.86000000E+001 0.00000000E+000 0.00000000E+000
NODE
        67 1.89000000E+001 0.00000000E+000 0.00000000E+000
       68 1.92000000E+001 0.00000000E+000 0.00000000E+000
NODE
NODE
        69 1.95000000E+001 0.00000000E+000 0.00000000E+000
NODE
       70 1.98000000E+001 0.00000000E+000 0.00000000E+000
NODE
        71 2.00000000E+001 0.00000000E+000 0.00000000E+000
NODE
       72 2.01000000E+001 0.00000000E+000 0.00000000E+000
       73 2.04000000E+001 0.00000000E+000 0.00000000E+000
NODE
NODE
       74 2.07000000E+001 0.00000000E+000 0.00000000E+000
       75 2.10000000E+001 0.00000000E+000 0.00000000E+000
NODE
NODE
        76 1.50000000E-001 0.00000000E+000 0.00000000E+000
NODE
       77 4.50000000E-001 0.00000000E+000 0.00000000E+000
NODE
       78 7.50000000E-001 0.00000000E+000 0.00000000E+000
NODE
       79 1.05000000E+000 0.00000000E+000 0.00000000E+000
NODE
        80 1.35000000E+000 0.00000000E+000 0.0000000E+000
NODE
       81 1.65000000E+000 0.00000000E+000 0.00000000E+000
NODE
       82 1.95000000E+000 0.00000000E+000 0.00000000E+000
NODE
        83 2.25000000E+000 0.00000000E+000 0.00000000E+000
NODE
        84 2.55000000E+000 0.00000000E+000 0.00000000E+000
```

```
NODE
       85 2.85000000E+000 0.00000000E+000 0.00000000E+000
NODE
        86 3.15000000E+000 0.00000000E+000 0.0000000E+000
NODE
       87 3.45000000E+000 0.00000000E+000 0.00000000E+000
NODE
        88 3.75000000E+000 0.00000000E+000 0.0000000E+000
NODE
       89 4.05000000E+000 0.00000000E+000 0.00000000E+000
NODE
        90 4.35000000E+000 0.00000000E+000 0.00000000E+000
        91 4.65000000E+000 0.00000000E+000 0.00000000E+000
NODE
NODE
        92 4.95000000E+000 0.00000000E+000 0.00000000E+000
NODE
       93 5.25000000E+000 0.00000000E+000 0.00000000E+000
NODE
        94 5.55000000E+000 0.00000000E+000 0.00000000E+000
NODE
        95 5.85000000E+000 0.00000000E+000 0.00000000E+000
NODE
        96 6.15000000E+000 0.00000000E+000 0.00000000E+000
NODE
       97 6.45000000E+000 0.00000000E+000 0.00000000E+000
NODE
        98 6.75000000E+000 0.00000000E+000 0.00000000E+000
        99 7.05000000E+000 0.00000000E+000 0.00000000E+000
NODE
NODE
        100 7.35000000E+000 0.00000000E+000 0.00000000E+000
NODE
        101 7.65000000E+000 0.00000000E+000 0.0000000E+000
NODE
        102 7.95000000E+000 0.00000000E+000 0.0000000E+000
NODE
        103 8.25000000E+000 0.00000000E+000 0.00000000E+000
        104 8.55000000E+000 0.0000000E+000 0.0000000E+000
NODE
NODE
        105 8.85000000E+000 0.00000000E+000 0.00000000E+000
NODE
        106 9.15000000E+000 0.0000000E+000 0.0000000E+000
NODE
        107 9.45000000E+000 0.00000000E+000 0.0000000E+000
NODE
        108 9.75000000E+000 0.00000000E+000 0.00000000E+000
        109 1.00500000E+001 0.0000000E+000 0.0000000E+000
NODE
NODE
        110 1.03500000E+001 0.00000000E+000 0.00000000E+000
        111 1.06500000E+001 0.00000000E+000 0.00000000E+000
NODE
NODE
        112 1.09500000E+001 0.00000000E+000 0.00000000E+000
NODE
        113 1.12500000E+001 0.00000000E+000 0.00000000E+000
NODE
        114 1.15500000E+001 0.00000000E+000 0.00000000E+000
NODE
        115 1.18500000E+001 0.00000000E+000 0.00000000E+000
NODE
        116 1.21500000E+001 0.00000000E+000 0.00000000E+000
NODE
        117 1.24500000E+001 0.00000000E+000 0.00000000E+000
NODE
        118 1.27500000E+001 0.00000000E+000 0.00000000E+000
NODE
        119 1.30500000E+001 0.00000000E+000 0.00000000E+000
NODE
        120 1.33500000E+001 0.00000000E+000 0.00000000E+000
```

```
NODE
          121 1.36500000E+001 0.00000000E+000 0.00000000E+000
  NODE
          122 1.39500000E+001 0.00000000E+000 0.00000000E+000
  NODE
          123 1.42500000E+001 0.00000000E+000 0.00000000E+000
          124 1.45500000E+001 0.00000000E+000 0.00000000E+000
  NODE
  NODE
          125 1.48500000E+001 0.00000000E+000 0.00000000E+000
  NODE
          126 1.51500000E+001 0.00000000E+000 0.00000000E+000
          127 1.54500000E+001 0.00000000E+000 0.00000000E+000
  NODE
  NODE
          128 1.57500000E+001 0.00000000E+000 0.00000000E+000
          129 1.60500000E+001 0.00000000E+000 0.00000000E+000
  NODE
  NODE
          130 1.63500000E+001 0.00000000E+000 0.00000000E+000
  NODE
          131 1.66500000E+001 0.00000000E+000 0.00000000E+000
          132 1.69500000E+001 0.00000000E+000 0.00000000E+000
  NODE
  NODE
          133 1.72500000E+001 0.00000000E+000 0.00000000E+000
  NODE
          134 1.75500000E+001 0.00000000E+000 0.00000000E+000
  NODE
          135 1.78500000E+001 0.00000000E+000 0.00000000E+000
  NODE
          136 1.81500000E+001 0.00000000E+000 0.00000000E+000
  NODE
          137 1.84500000E+001 0.00000000E+000 0.00000000E+000
  NODE
          138 1.87500000E+001 0.00000000E+000 0.00000000E+000
  NODE
          139 1.90500000E+001 0.00000000E+000 0.00000000E+000
          140 1.93500000E+001 0.00000000E+000 0.00000000E+000
  NODE
  NODE
          141 1.96500000E+001 0.00000000E+000 0.00000000E+000
          142 1.99500000E+001 0.00000000E+000 0.00000000E+000
  NODE
  NODE
          143 2.02500000E+001 0.00000000E+000 0.00000000E+000
  NODE
          144 2.05500000E+001 0.00000000E+000 0.00000000E+000
  NODE
          145 2.08500000E+001 0.00000000E+000 0.00000000E+000
FIXATIONS
  BLOCK 1 F0 F0 NO
  BLOCK 35 F0 F0 NO
  BLOCK 55 F0 F0 F0
  BLOCK 71 NO F0 NO
  BLOCK 75 NO F0 NO
 END FIX
NODOFBEAM
S1-1 T5.tem
TRANSLATE 1 1
TRANSLATE 2 4
```

```
END_TRANS
S1-1_T4.tem
TRANSLATE 1 1
TRANSLATE 2 4
END_TRANS
S1-1_T3.tem
TRANSLATE 1 1
TRANSLATE 2 4
END_TRANS
S1-1_T2.tem
TRANSLATE 1 1
TRANSLATE 2 4
END_TRANS
S1-1_T1.tem
TRANSLATE 1 1
TRANSLATE 2 4
END_TRANS
  ELEM 1 1 76 2 1
  ELEM 2 2 77 3 1
  ELEM 3 3 78 4 1
  ELEM 4 4 79 5 1
  ELEM 5 5 80 6 1
  ELEM 6 6 81 7 1
  ELEM 7 7 82 8 1
  ELEM 8 8 83 9 1
  ELEM 9 9 84 10 2
  ELEM 10 10 85 11 2
  ELEM 11 11 86 12 2
  ELEM 12 12 87 13 2
  ELEM 13 13 88 14 2
  ELEM 14 14 89 15 2
  ELEM 15 15 90 16 2
  ELEM 16 16 91 17 3
  ELEM 17 17 92 18 3
  ELEM 18 18 93 19 3
  ELEM 19 19 94 20 3
```

```
ELEM 20 20 95 21 3
ELEM 21 21 96 22 3
ELEM 22 22 97 23 3
ELEM 23 23 98 24 4
ELEM 24 24 99 25 4
ELEM 25 25 100 26 4
ELEM 26 26 101 27 4
ELEM 27 27 102 28 4
ELEM 28 28 103 29 4
ELEM 29 29 104 30 4
ELEM 30 30 105 31 5
ELEM 31 31 106 32 5
ELEM 32 32 107 33 5
ELEM 33 33 108 34 5
ELEM 34 34 109 36 5
ELEM 35 36 110 37 5
ELEM 36 37 111 38 5
ELEM 37 38 112 39 5
ELEM 38 39 113 40 5
ELEM 39 40 114 41 5
ELEM 40 41 115 42 5
ELEM 41 42 116 43 4
ELEM 42 43 117 44 4
ELEM 43 44 118 45 4
ELEM 44 45 119 46
ELEM 45 46 120 47 4
ELEM 46 47 121 48 4
ELEM 47 48 122 49 4
ELEM 48 49 123 50 4
ELEM 49 50 124 51 3
ELEM 50 51 125 52 3
ELEM 51 52 126 54 3
ELEM 52 54 127 56 3
ELEM 53 56 128 57 3
ELEM 54 57 129 58 3
ELEM 55 58 130 59 3
```

```
ELEM 56 59 131 60 2
ELEM 57 60 132 61 2
ELEM 58 61 133 62 2
ELEM 59 62 134 63 2
ELEM 60 63 135 64 2
ELEM 61 64 136 65 2
ELEM 62 65 137 66 2
ELEM 63 66 138 67 2
ELEM 64 67 139 68 1
ELEM 65 68 140 69 1
ELEM 66 69 141 70 1
ELEM 67 70 142 72 1
ELEM 68 72 143 73 1
ELEM 69 73 144 74 1
ELEM 70 74 145 75 1
```

NODOFTRUSS

bar.tem 314.16E-4 0. 3

bar.tem 314.16E-4 0. 2

ELEM 1 35 53 1

ELEM 2 71 53 1

ELEM 3 75 71 1

ELEM 4 53 55 2

PRECISION 1.0e-2

LOADS

FUNCTION F1

- DISTRBEAM 1 0.00e+00 -2.60e+04
- DISTRBEAM 2 0.00e+00 -2.60e+04
- DISTRBEAM 3 0.00e+00 -2.60e+04
- DISTRBEAM 4 0.00e+00 -2.60e+04
- DISTRBEAM 5 0.00e+00 -2.60e+04
- DISTRBEAM 6 0.00e+00 -2.60e+04
- DISTRBEAM 7 0.00e+00 -2.60e+04
- DISTRBEAM 8 0.00e+00 -2.60e+04
- DISTRBEAM 9 0.00e+00 -2.60e+04
- DISTRBEAM 10 0.00e+00 -2.60e+04

DISTRBEAM	11	0.00e+00	-2.60e+04
DISTRBEAM	12	0.00e+00	-2.60e+04
DISTRBEAM	13	0.00e+00	-2.60e+04
DISTRBEAM	14	0.00e+00	-2.60e+04
DISTRBEAM	15	0.00e+00	-2.60e+04
DISTRBEAM	16	0.00e+00	-2.60e+04
DISTRBEAM	17	0.00e+00	-2.60e+04
DISTRBEAM	18	0.00e+00	-2.60e+04
DISTRBEAM	19	0.00e+00	-2.60e+04
DISTRBEAM	20	0.00e+00	-2.60e+04
DISTRBEAM	21	0.00e+00	-2.60e+04
DISTRBEAM	22	0.00e+00	-2.60e+04
DISTRBEAM	23	0.00e+00	-2.60e+04
DISTRBEAM	24	0.00e+00	-2.60e+04
DISTRBEAM	25	0.00e+00	-2.60e+04
DISTRBEAM	26	0.00e+00	-2.60e+04
DISTRBEAM	27	0.00e+00	-2.60e+04
DISTRBEAM	28	0.00e+00	-2.60e+04
DISTRBEAM	29	0.00e+00	-2.60e+04
DISTRBEAM	30	0.00e+00	-2.60e+04
DISTRBEAM	31	0.00e+00	-2.60e+04
DISTRBEAM	32	0.00e+00	-2.60e+04
DISTRBEAM	33	0.00e+00	-2.60e+04
DISTRBEAM	34	0.00e+00	-2.60e+04
DISTRBEAM	35	0.00e+00	-2.60e+04
DISTRBEAM	36	0.00e+00	-2.60e+04
DISTRBEAM	37	0.00e+00	-2.60e+04
DISTRBEAM	38	0.00e+00	-2.60e+04
DISTRBEAM	39	0.00e+00	-2.60e+04
DISTRBEAM	40	0.00e+00	-2.60e+04
DISTRBEAM	41	0.00e+00	-2.60e+04
DISTRBEAM	42	0.00e+00	-2.60e+04
DISTRBEAM	43	0.00e+00	-2.60e+04
DISTRBEAM	44	0.00e+00	-2.60e+04
DISTRBEAM	45	0.00e+00	-2.60e+04
DISTRBEAM	46	0.00e+00	-2.60e+04

```
DISTRBEAM 47 0.00e+00 -2.60e+04
DISTRBEAM 48 0.00e+00 -2.60e+04
DISTRBEAM 49 0.00e+00 -2.60e+04
DISTRBEAM 50 0.00e+00 -2.60e+04
DISTRBEAM 51 0.00e+00 -2.60e+04
DISTRBEAM 52 0.00e+00 -2.60e+04
DISTRBEAM 53 0.00e+00 -2.60e+04
DISTRBEAM 54 0.00e+00 -2.60e+04
DISTRBEAM 55 0.00e+00 -2.60e+04
DISTRBEAM 56 0.00e+00 -2.60e+04
DISTRBEAM 57 0.00e+00 -2.60e+04
DISTRBEAM 58 0.00e+00 -2.60e+04
DISTRBEAM 59 0.00e+00 -2.60e+04
DISTRBEAM 60 0.00e+00 -2.60e+04
DISTRBEAM 61 0.00e+00 -2.60e+04
DISTRBEAM 62 0.00e+00 -2.60e+04
DISTRBEAM 63 0.00e+00 -2.60e+04
DISTRBEAM 64 0.00e+00 -2.60e+04
DISTRBEAM 65 0.00e+00 -2.60e+04
DISTRBEAM 66 0.00e+00 -2.60e+04
DISTRBEAM 67 0.00e+00 -2.60e+04
DISTRBEAM 68 0.00e+00 -2.60e+04
DISTRBEAM 69 0.00e+00 -2.60e+04
DISTRBEAM 70 0.00e+00 -2.60e+04
END_LOAD
  MASS
END MASS
MATERIALS
STEELEC3
    2.10e+11 3.00e-01 2.50e+8 1200. 0.
ELASTIC
     2.10e+05 3.00e-01
ELASTIC
    2.10e+13 3.00e-01
SILCONCEC2
     0.1\ 0.1\ 0.1\ 0.1\ 0.
```

TIME

60.0 7200.0 60.0

ENDTIME

LARGEDISPL

EPSTH

IMPRESSION

TIMEPRINT

 $60.0 \quad 7200.0$

END_TIMEPR

PRINTREACT

PRINTMN